

# The Use of Alternative Strategies for Enhanced Nanoparticle Delivery to Solid Tumors

Mukaddes Izci, Christy Maksoudian, Bella B. Manshian, and Stefaan J. Soenen\*




Cite This: *Chem. Rev.* 2021, 121, 1746–1803



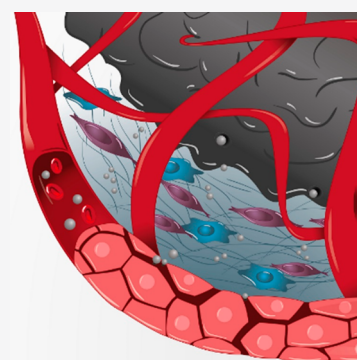
Read Online

ACCESS |

 Metrics & More

 Article Recommendations

**ABSTRACT:** Nanomaterial (NM) delivery to solid tumors has been the focus of intense research for over a decade. Classically, scientists have tried to improve NM delivery by employing passive or active targeting strategies, making use of the so-called enhanced permeability and retention (EPR) effect. This phenomenon is made possible due to the leaky tumor vasculature through which NMs can leave the bloodstream, traverse through the gaps in the endothelial lining of the vessels, and enter the tumor. Recent studies have shown that despite many efforts to employ the EPR effect, this process remains very poor. Furthermore, the role of the EPR effect has been called into question, where it has been suggested that NMs enter the tumor *via* active mechanisms and not through the endothelial gaps. In this review, we provide a short overview of the EPR and mechanisms to enhance it, after which we focus on alternative delivery strategies that do not solely rely on EPR in itself but can offer interesting pharmacological, physical, and biological solutions for enhanced delivery. We discuss the strengths and shortcomings of these different strategies and suggest combinatorial approaches as the ideal path forward.



## CONTENTS

1. Introduction	1747	3.1.1. Indirect and Direct EPR Imaging	1757
1.1. The Use of Nanomaterials for Cancer Therapy and Diagnosis	1747	3.1.2. Companion/Nanodiagnostics	1757
1.2. NM Delivery to the Tumor: Active and Passive Targeting	1749	3.2. Maximizing NM Delivery to Solid Tumors	1757
1.3. Difficulties in Delivering NMs to solid Tumors	1750	3.2.1. Advantages and Limitations of EPR-Mediated NM Delivery	1757
2. Modulating the Tumor Microenvironment (TME)	1751	3.2.2. Potential Bottlenecks Related to NM Delivery	1758
2.1. Pharmacological Methods to Increase Blood Flow and Associated NM Delivery	1752	4. Use of Peptides to Improve NM Delivery to Solid Tumors	1759
2.1.1. Vascular Permeabilization	1752	4.1. Transcytosis with iRGD	1759
2.1.2. Vascular Normalization	1752	4.1.1. iRGD in Breast Cancer	1759
2.1.3. Vascular Disruption	1752	4.1.2. iRGD in Other Tumor Models	1761
2.2. Physical Treatments That Improve Blood Flow	1753	4.1.3. Treating Pregnancy Complications	1768
2.2.1. Hyperthermia	1753	4.1.4. iRGD for Imaging and Theranostic Applications	1768
2.2.2. Radiotherapy	1753	4.1.5. Debate	1769
2.2.3. Sonoporation	1753	4.2. Multiple Peptides: Finely Tuning NM Functionalization for Targeted Delivery	1769
2.2.4. Phototherapy	1753	4.2.1. Dual-Ligand Targeting in Breast Cancer	1769
2.3. Modulating Physiological Parameters, Such as Hypoxia, Acidosis, and Elevated IFP	1753	4.2.2. Dual-Targeting of Brain Glioma	1769
2.4. ECM	1754		
2.5. Stromal Cells	1755		
2.6. Immunosuppression	1755		
2.7. Conclusion	1756		
3. EPR-Mediated NM Delivery and Quantification	1756		
3.1. Personalized Medicine	1756		

Received: July 25, 2020

Published: January 14, 2021



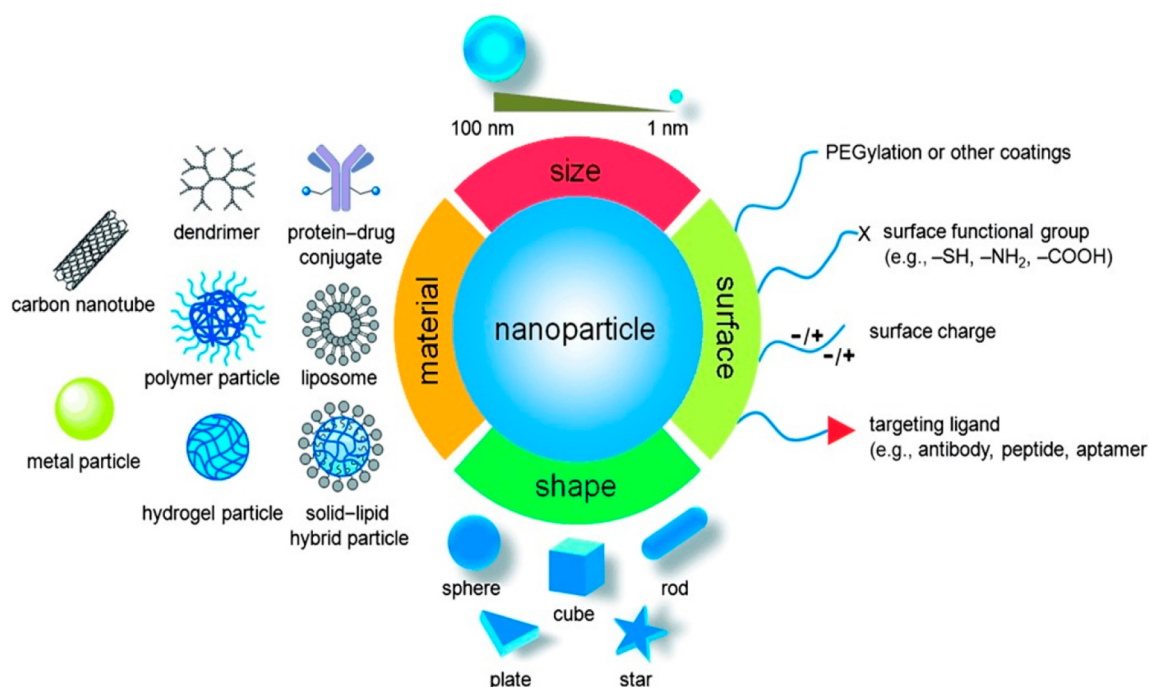


**Figure 1.** Nanomaterials as carrier for drug delivery in cancer therapy. The biophysicochemical properties are also shown. Reproduced with permission from ref 15. Copyright 2014 Wiley VCH.

4.2.3. Use of Dual Ligands in Other Tumor Models	1770
4.2.4. Multiple Ligands	1771
4.2.5. Conclusion	1771
5. Magnetic Guidance of Magnetic Particles	1771
6. Biological Methods to Improve NM Delivery to Tumors	1773
6.1. Cell-Mediated Delivery	1774
6.1.1. Red Blood Cells	1774
6.1.2. Monocytes and Macrophages	1775
6.1.3. Lymphocytes	1777
6.1.4. Neutrophils	1777
6.1.5. Stem Cells	1777
6.1.6. Cell-Surface-Binding vs Encapsulation of NPs	1779
6.2. Biomimetic Cell Membrane-Coated NPs (MCNPs)	1779
6.2.1. Membranes from Normal Circulatory Cells	1780
6.2.2. Use of Cancer Cell Membranes	1781
6.3. Use of Extracellular Vesicles	1781
6.4. Use of Attenuated (Nonimmunogenic) Bacteria	1782
7. Translational Value	1783
7.1. Difficulties Concerning Bionano Interaction Studies	1783
7.2. <i>In Vivo</i> Translation of <i>In Vitro</i> Results	1784
7.3. Clinical Translation	1785
8. Conclusion	1785
Author Information	1786
Corresponding Author	1786
Authors	1786
Author Contributions	1786
Notes	1786
Biographies	1786
Acknowledgments	1786

Abbreviations	1786
References	1788

## 1. INTRODUCTION

### 1.1. The Use of Nanomaterials for Cancer Therapy and Diagnosis

The application of nanotechnology for medical purposes, also known as nanomedicine, is a relatively novel field that has been gaining increasing interest over the years. It owes its success to the highly multidisciplinary nature of the field itself, bridging physics and chemistry expertise in nanomaterial (NM) synthesis and characterization with expertise in biology and medicine for functional applications.<sup>1</sup> While NMs have been mostly investigated within the electronic and industrial fields, the unique properties of NMs render them ideally suited to be explored in a wide variety of biomedical applications. As a result, various studies have focused on the interactions of NMs with their biological environment, aiming at elucidating which particular aspects of the NMs trigger which exact biological response.<sup>2</sup> Through our increased understanding of bionano interactions in combination with the rapid developments and in-depth knowledge gained in several medical fields such as oncology, research groups have been able to exploit the various unique properties of NMs to enhance therapeutic and diagnostic outcomes in cancer research and clinical use.<sup>2</sup>

The unique properties of NMs stem from a variety of characteristics, including their high surface area over volume ratio, easy tunable size, and the availability of a wide range of different materials, of which some possess even further unique properties such as the superparamagnetism and surface plasmon resonance (SPR) of magnetic and gold NMs, respectively. The surface of the NMs can also be easily functionalized in a wide range of manners, significantly impacting their biodistribution and clearance from the

Chart 1. A Description of Common Factors Involved in NM Delivery to Solid Tumors

Once a NM is administered into the blood stream, it would ideally immediately go from the blood into the tumor cells. There are however a number of mechanisms that make this process very inefficient. Here, we will shortly indicate the behaviour of a NM upon administration and define some key terms that play an important role in this process.

Upon administration, the NMs will typically be rapidly covered by serum proteins that will form an additional layer that nearly completely surrounds the NM (**protein corona**). This typically consists of an inner layer of tightly bound proteins (**hard corona**) and an outer layer of more loosely bound, interchangeable proteins (**soft corona**). These proteins can affect colloidal stability and will influence biodistribution. Depending on the surface chemistry of the NM, any targeting ligands may be covered by this corona and hence become inaccessible for targeting purposes. Furthermore, these proteins may include so-called opsonins, which are essential components of the immune system, and hereby induce **opsonisation**. The bound opsonins can then be recognized by antibodies or receptors present on cells of the RES (phagocytic cells, predominantly present in the liver, that clear out any foreign or antigenic substances from the blood) and result in rapid clearance of the NMs from the blood stream.

To reduce opsonisation and/or corona formation, surface passivation is used, which often involves **PEGylation**. The flexible nature of the PEG chains slow down the kinetics of protein binding, but do not stop it completely. It hereby extend blood circulation times, allowing the particles to pass through the tumor-associated vessels multiple times. This increases the chance of **extravasation** at the tumor, in which the NM leave the blood circulation and end up at the tumor. As tumor growth is linked with adequate blood supply, new vessels are formed rapidly (**angiogenesis**), and tumor-associated vessels can, but are not always, immature, resulting in gaps between endothelial cells and reduced coverage of blood vessels by pericytes. It has been long proposed that NMs mainly extravasate at the tumor through these openings between endothelial cells in a process called **EPR**. It had been suggested that NMs should therefore be smaller than these endothelial gaps. Once crossing the endothelial lining, the NMs still need to circumvent the **tumor microenvironment**, which consist of a dense **extracellular matrix** which can cause steric hindrance, and various cell types, including macrophages of fibroblasts that can internalize the NMs before they reach the actual tumor cells. Recent studies have questioned the validity of the EPR mechanism and have looked at other means to stimulate targeted NM delivery, which are discussed in detail in this review.

bloodstream. Finally, different functionalities can be incorporated into a single entity (*i.e.*, fluorescent probe, drug, or antibody coupled onto a magnetic carrier), allowing the engineering of a nanocarrier with multiple properties and functions.<sup>2</sup>

For cancer therapy and diagnosis, various NMs have already been approved for clinical use, and many more are currently undergoing clinical trials.<sup>3</sup> The therapeutic and diagnostic NMs can generally be classified into two categories: organic NMs (*i.e.*, liposomes, polymeric, micelles, *etc.*) and inorganic NMs (*i.e.*, iron oxide, gold, silica, *etc.*) (Figure 1). Because of their high biocompatibility and reduced long-term side effects, organic NMs have been most successful in their translation into the clinic and are mainly being developed for applications like vaccination, long-lasting depot delivery systems, hemostasis, and topical agents for systemic delivery through the skin.<sup>3–7</sup> Intravenously delivered organic NMs are mainly aimed at two specific applications: the delivery of small molecule drugs for cancer treatment (*i.e.*, breast, melanoma, head and neck, *etc.*) and gene therapy.<sup>8–11</sup> Translation of inorganic NMs into the clinic has been more limited, despite major successes on a preclinical level,<sup>12</sup> due to their lower biocompatibility and lack of knowledge and consensus pertaining to their safety and long-term deposition in different organs such as the liver and spleen. Inorganic NMs are thus mainly used as contrast agents for magnetic resonance imaging (MRI) and are currently undergoing clinical trials for different applications such as thermal ablation of tumors and intraoperative sentinel lymph node imaging.<sup>13,14</sup>

Organic NMs are mainly being explored for drug or gene delivery purposes as they enhance drug/gene protection, extend circulation in the blood, and provide controlled release of their encapsulated content while improving targeting to diseased tissues compared to their free drug counterparts.<sup>11,16</sup> Inorganic NMs, can, depending on their properties, offer the same advantages as the organic NMs while simultaneously providing further functional benefits associated with the chemical composition of their core. For example, magnetic NMs can be used for MRI or magnetic targeting, and the SPR present on noble metals such as gold and silver can be used for imaging or thermal heating during direct therapy or triggered drug release, which other molecules and individual drugs do not offer without profound additional chemical functionalization.<sup>5,17</sup>

Both organic and inorganic NMs have thus the potential to work as promising delivery systems with different design features such as drug encapsulation, targeting antibodies, and control over how/when the diseased site interacts with this drug in a “plug-and-play” format for the treatment of other or additional diseases. While the main application of both types of NMs is their sole use as carriers for more common chemotherapeutic agents,<sup>1,3</sup> the intrinsic properties of NMs can be further exploited as direct therapeutic or diagnostic agents, particularly in the case of inorganic NMs.<sup>12,18–20</sup> In this review, both organic and inorganic NMs will be discussed. A short overview of the mechanisms involved in NM delivery to solid tumors is described in Chart 1 and more extensively described in sections 1.2 and 1.3.



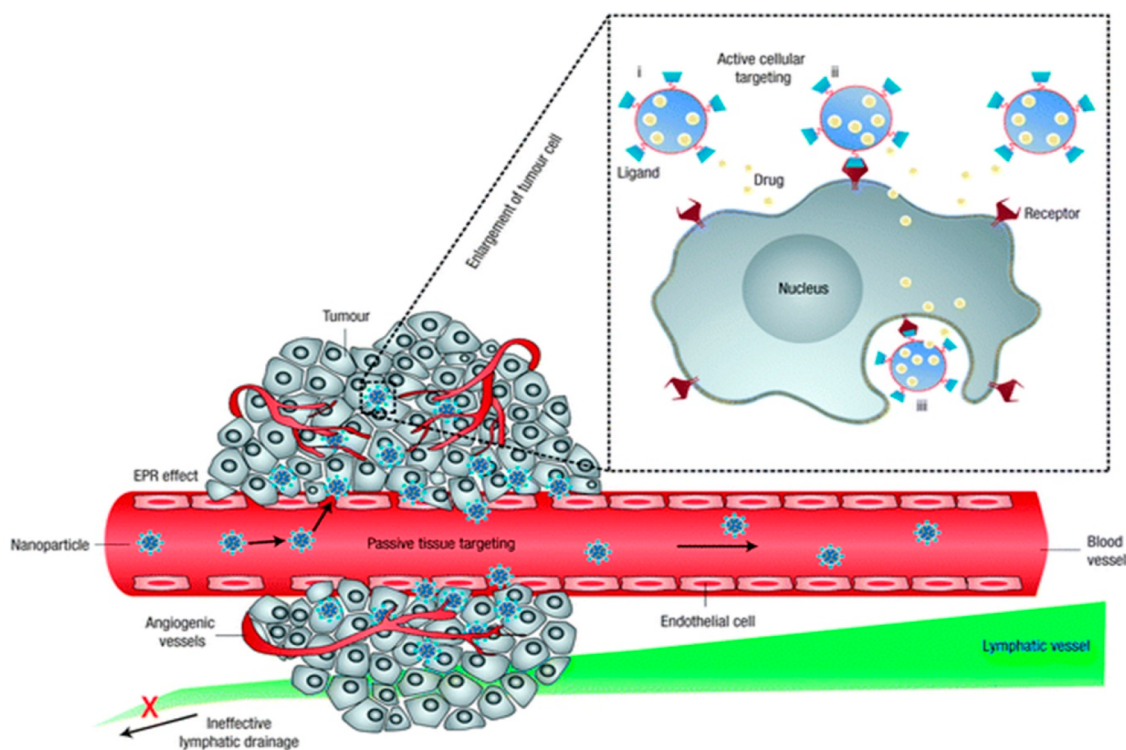


**Figure 2.** Passive and active tumor targeting. Passive tumor targeting is the extravasation of NM due the increased permeability of the tumor vessel together with a lower lymphatic drainage. This is also known as the EPR effect. Active cellular targeting is the surface functionalizing of NM with ligands to induce cell-specific recognition and binding. The contents of the NMs can be released close to the target cells (i), act as an extracellular release drug depot by attaching to the cell membrane (ii) or can also internalize into the cell (iii). Reproduced with permission from ref 11. Copyright 2007 Nature Publishing Group.

## 1.2. NM Delivery to the Tumor: Active and Passive Targeting

Owing to their physicochemical properties, (in)organic NMs can enhance the specific delivery of pharmaceutical agents to the tumor, either passively or by stimulated (externally triggered) release.<sup>1</sup> Passive delivery of NMs to the tumor site is normally achieved in a process known as the enhanced permeability and retention (EPR) effect, the idea being that NMs are able to passively accumulate within the tumor interstitium due to the increased leakiness of the tumor vasculature compared to its normal counterpart, in combination with its poor lymphatic drainage that allows NMs to remain in the tumor tissue for longer.<sup>21</sup> The increased permeability of tumor-associated blood vessels is due to the high metabolism of tumors and tumor-associated endothelial cells, which drive angiogenesis (the growth of novel vessels) at high rates and prevent adequate vessel maturation. The fenestrations of these newly formed blood vessels have a cutoff size that will determine the maximal dimensions of the NM that allows extravasation. Specifically, NMs with the size of 6–8 nm are typically cleared very rapidly from the bloodstream by the kidneys and therefore often fail to achieve high tumor-specific uptake levels. At the same time, sizes of around 200 nm are too big and are for this reason unlikely to extravasate from the blood vessels into the tumor site.<sup>22</sup>

Most bare NMs will eventually get cleared from the bloodstream by the immune and reticulo-endothelial systems (RES). To prevent NM recognition by immune cells and complement factors such as opsonins,<sup>23,24</sup> NMs have been optimized for reduced agglomeration and improved long-term circulation (*i.e.*, by coating with polyethylene-glycol, PEG),

enhancing their extravasation through the leaky tumor endothelium.<sup>25</sup> Specifically, the longer the NMs circulate in the bloodstream by avoiding clearance by the RES, the higher the chance for tumor delivery because the NMs will flow multiple times through the tumor-associated blood vessels, and with every passage, there is a chance of extravasation.<sup>26</sup> Besides PEG, various other antifouling agents, such as synthetic coatings (*i.e.*, polyvinylpyrrolidone, PVP; polyphosphoesters, PPEs; polyelectrolytes; zwitterionic polymers, *etc.*) and natural polymeric coatings (*i.e.*, polynucleotides, polypeptides, dextrans, chitosan, *etc.*) have been developed with the aim of maintaining the physicochemical properties and functional integrity of NMs upon their exposure to biological systems and fighting against the RES, NM agglomeration, protein corona formation, and other bionano interactions that serve as barriers for effective NM delivery.<sup>27,28</sup> The translation of NMs from *in vitro* to *in vivo* settings, including the effect of protein corona formation on NMs, will be discussed in more detail in section 7.2. For more information on the various types of biocompatible coatings, a thorough review by Schubert and Chanana can be consulted.<sup>27</sup>

The sole reliance on EPR for NM delivery typically results in low levels of NM accumulation at the tumor site (Figure 2; delivery by EPR will be discussed in great detail in section 3). Accordingly, most studies make use of active targeting ligands (*i.e.*, antibodies, peptides, or membranes from host cells) to improve tumor targeting in a variety of ways.<sup>29</sup> For endothelial targets such as RGD peptides against  $\alpha_v\beta_3$  integrin present on neovessels, this can result in an enhanced accumulation of the NMs within close proximity to the tumor cells, which would enhance tumor cell uptake of drugs that are locally released.



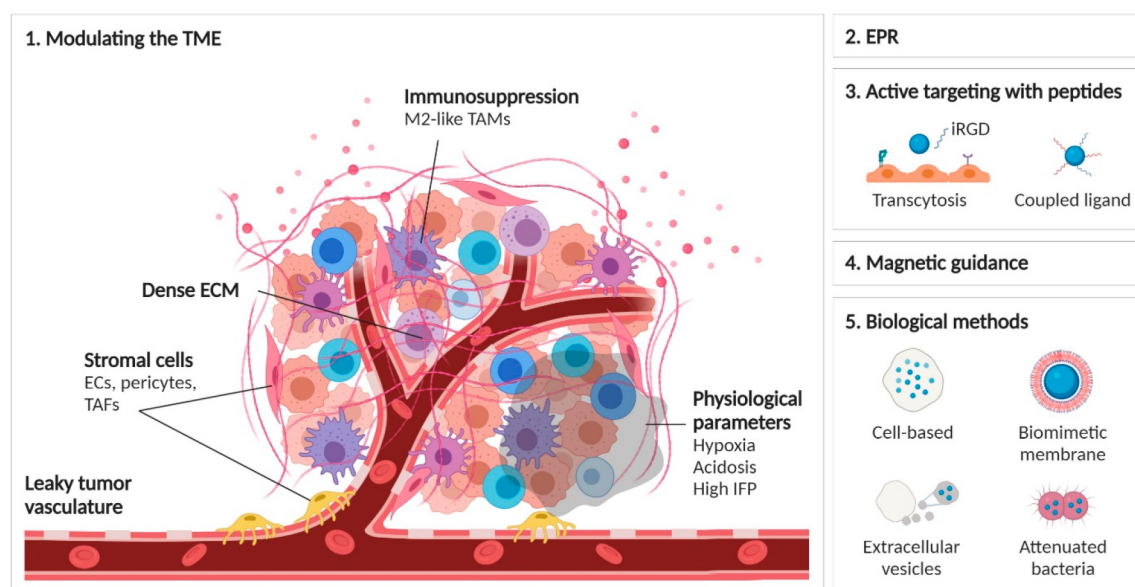


**Figure 3.** Schematic overview of the different methods used to enhance NM delivery to solid tumors. (1) Modulation of the tumor microenvironment and associated factors including stromal cells, immunomodulation, physiological parameters, or extracellular matrix density, as discussed in section 2 of this review. (2) The principle of enhanced permeability and retention and how to enhance or exploit it as discussed in section 3. (3) The use of multiple peptides or peptides aiming at enhancing transcytosis, as discussed in section 4. (4) The concept of magnetic targeting for enhanced tumor delivery as discussed in section 5. (5) The use of biological methods, including cellular hitchhiking of NMs, use of cell-based membranes for biomimetic coatings, the use of extracellular vesicles or attenuated bacteria to specifically guide NMs to the tumors, as discussed in section 6.

Alternatively, targeting tumor cells themselves still requires the NMs to extravasate *via* the EPR effect, similar to passive delivery. However, as solid tumors have high interstitial fluid pressure (IFP), this impedes the retention of NMs that would have managed to traverse the endothelial barrier (and extracellular matrix) into the solid tumor mass, as they will effectively be pushed outward again. Any ligand that can facilitate binding of the NMs to tumor cells would in turn prevent the removal of the NMs from the tumor by anchoring it onto the tumor cell membrane or even promote tumor cell internalization.

Another alternative active strategy to improve NM delivery to solid tumors is to use biological methods such as extracellular vesicles and attenuated bacteria, as well as encapsulate NMs in cells that naturally home toward tumors in a Trojan Horse-like mechanism or functionalize them onto the surface of such cells (section 6). Various cell types have been used for cell-based delivery of NMs or have had their membranes isolated and coated onto NMs including erythrocytes, macrophages, leukocytes, stem cells, tumor cells, among others. For instance, Cao *et al.*<sup>29</sup> used macrophage membranes as an active targeting method, given that macrophages are present as some of the most abundant cells in the tumor microenvironment (TME) and can bind to metastatic cancer cells *via* the  $\alpha 4$  integrins of the macrophage and the vascular cell adhesion molecule-1 (VCAM-1) of cancer cells. In this study, cytotoxic anticancer drug Emtansine was encapsulated into pH-sensitive organic liposomes, which were then coated with isolated macrophage membranes. These nanoformulations were intravenously injected in mice bearing lung metastasis models of breast cancer, and their delivery to metastatic sites was considerably improved *via* the  $\alpha 4$  integrin–VCAM-1 interactions compared to the uncoated liposomes, significantly inhibiting metastasis.<sup>29</sup>

### 1.3. Difficulties in Delivering NMs to solid Tumors

Despite all the efforts made in optimizing NM design to promote active or passive targeting, a slightly controversial meta-analysis of Chan and his group published in 2016 showed that in preclinical models only 0.7% of the intravenously administered dose of either organic and inorganic NMs accumulates in solid tumors irrespective of whether this has occurred *via* passive or active targeting.<sup>30</sup> The analysis itself studies the percentage of NMs that reach the tumor after intravenous injection without taking into account the size of the tumor itself nor the injected dose. For therapeutic applications, 0.7% of a given substance in a small-sized tumor (only a few cells) could be more than sufficient, while this may not be the case for a much larger tumor, as the number of existing cancer cells could influence the success rate of NMs reaching the tumor site. Additionally, therapeutic efficacy is not solely determined by effective NM targeting but also on the efficiency of the drug release. Although 0.7% may not seem very convincing, this value in itself is much higher than the values obtained for many conventional drugs not associated with a nanoformulation.<sup>31</sup> The authors also do not discuss the heterogeneity of the EPR and do not consider that 0.7% delivery may be sufficient for full anticancer therapy and patient benefit. Lastly, the meta-analysis was focused on the percentage of the injected dose, hereby ignoring the level present in blood or relative differences in tumor size between studies. A recent reanalysis of these data using classical pharmacokinetic metrics revealed a far greater relative tumor delivery of NMs.<sup>32</sup> In a more recent study published by Warren Chan and his group, they suggest that a minimum dose threshold of 1 trillion nanoparticles (NPs) is required to achieve a 12% tumor delivery efficiency to 93% of all cells within the tumor and attribute this successful delivery to the

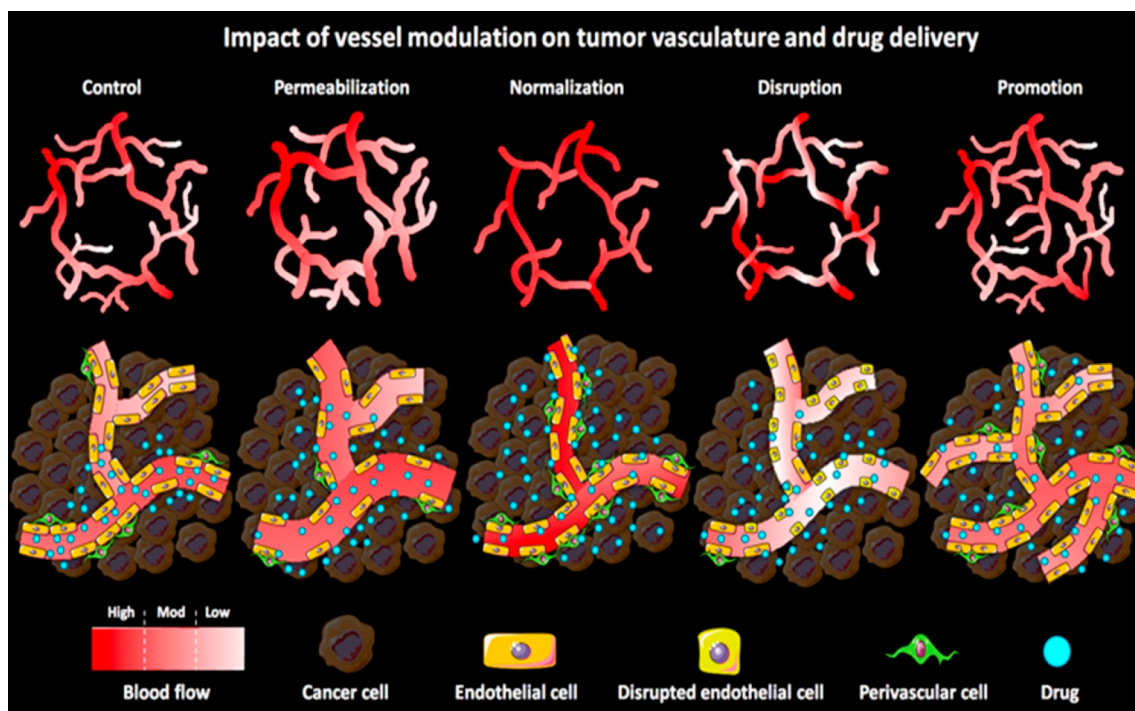


**Figure 4.** The impact of pharmaceutical vessel modulation on macro- and microtumor vasculature and on tumor-targeted drug delivery. During vessel permeabilization, the gaps between the endothelial cells are widened due to the vasodilatation and increased gaps between endothelial and perivascular cells. Vessel normalization restores the morphology and functionality of the tumor vasculature by improving vascular perfusion and promoting vascular maturity. Vascular disruption tampers with the endothelial lining and reduces the perfusion (of immature vasculature), which enhances the vascular permeability. Vascular promotion increases vessel density and distribution leading to an enhanced relative blood volume in tumors. On the basis of the vascular characteristics of tumors, many pharmaceutical strategies could be used that have different effects on the penetration and accumulation of the drugs and drug delivery systems. Reproduced with permission from ref 36. Copyright 2017 Elsevier Publishing.

overwhelming of Kupffer cell uptake rates, reduced liver clearance, and enhanced circulation.<sup>33</sup>

Nanoformulations have been shown to dramatically enhance the time frame of tumor exposure by significantly reducing the clearance rate of the agent.<sup>31</sup> They have therefore been shown to have great clinical potential but also a large window of opportunity for further improvement, which can be achieved by boosting delivery efficacies.<sup>34</sup> To do so, treatment regimens need to incorporate various strategies aimed at overcoming different biological barriers. While the NMs themselves can be engineered in a way that exploits the inherent differences in microenvironments of healthy and tumor tissues for specific tumor targeting, the various obstacles within the TME can be simultaneously modulated through pharmacological and physical means to facilitate NM transport across the different stages. Among the barriers of the TME are the pro-tumorigenic stromal cells and highly dense cell masses associated with elevated IFP, hindering the diffusion of NMs from the blood into the tumor against this pressure difference. In fact, another study by Warren Chan and his group has shown that the size of gold NMs plays a pivotal role in the delivery efficacy mainly due to the thickness and permeability of the stromal barrier.<sup>35</sup> Accordingly, as thickness and compactness of the stromal barrier was related to tumor size, delivery efficacy could be optimized by tuning gold NM diameter in function of tumor size. The authors varied tumor volume to determine whether cancer pathophysiology could possibly influence tumor accumulation and penetration of differently sized gold NMs and found that changes in pathophysiology were associated with tumor volume, which could selectively change tumor

uptake of gold NMs of varying sizes. Their results suggest that NMs could be personalized according to a patient's disease state to achieve an optimal diagnostic and therapeutic outcome.<sup>35</sup>

Another issue lies in the biological differences between different tumors, even of the same type. Both in patients and animals, two tumors are not fully identical. For (in)organic NMs to extravasate from the bloodstream into the tumor mass, there should be ample perfusion of the tumor (sufficient number of blood vessels) and the vessels should be permeable to the NMs. The process of angiogenesis is highly complex, involves many different factors and signaling pathways, and is influenced by the growth rate of the tumor, any signaling mediated by tumor-associated immune cells, the presence of hypoxic regions, among others. All these factors will differ between individuals, and thus the ability for a given formulation to reach a certain tumor cannot be predicted without knowledge of these factors.<sup>31</sup> In this review, we will discuss the various pharmacological, physical, and biological strategies aimed at enhancing NM delivery to solid tumors, including the modulation of the TME, the EPR effect, increased transcytosis across endothelial barriers, and the use of cell-based therapy (Figure 3).

## 2. MODULATING THE TUMOR MICROENVIRONMENT (TME)

Upon their administration into the body, NMs need to go through several stages in order to reach cancer cells from blood circulation and exert their therapeutic effect, starting with their

vascular navigation toward various regions of the tumor, followed by their transvascular passage through the vessel walls, and finally their transport across the interstitium to reach the cancer cells. Compared to normal tissue, the TME is characterized by leaky blood vessels and poor lymphatic drainage that significantly affect blood flow, as well as altered physiological parameters (*i.e.*, acidosis, hypoxia, and elevated IFP) and a dense ECM containing stromal cells that have developed pro-tumorigenic properties. In this section, we briefly discuss the various barriers existing within the TME, how they affect efficient NM delivery, and some of the numerous strategies that have been developed over the years to modulate the TME and facilitate on-target NM delivery.

### 2.1. Pharmacological Methods to Increase Blood Flow and Associated NM Delivery

The EPR effect for (in)organic NM delivery and thereby NM accumulation is variable due to the heterogeneity of the tumor vasculature, which is differentiated according to various characteristics, such as vessel maturity, perfusion, density, and pore size. Given that NM and drug delivery to tumors is significantly affected by blood flow, the tumor vasculature is an important target for the modulation of EPR-mediated targeted delivery. To enhance the EPR effect and overcome EPR heterogeneity, numerous physical and pharmacological strategies have been developed, many of which have been discussed in depth by Ojha *et al.*<sup>36</sup> Here, we provide only a short overview of these methods and refer the interested readers to the review by Ojha *et al.* for more detailed information (Figure 4).<sup>36</sup> We also touch upon potential shortcomings associated with each of these methods.

**2.1.1. Vascular Permeabilization.** One method of increasing blood flow to the tumor area is vascular permeabilization, which is the widening of the endothelial pores by inflammatory cytokines and other vasomodulators (neuronal regulators of blood flow) such as bradykinin, histamine, tumor necrosis factor- $\alpha$  (TNF- $\alpha$ ), and serotonin, or using external mechanical forces. Vasoconstrictive endothelin-1 (ET-1) and its receptor ETA are both significantly overexpressed in tumor vessels to maintain vascular contractility, at 13-fold and 5-fold higher than in their normal counterparts, respectively.<sup>37</sup> Despite the ability of vasodilators to increase blood flow and enhance the accumulation and efficacy of NMs and anticancer drugs,<sup>36</sup> their systemic administration has been associated with several side effects, such as lethal shock, tissue injury, among others.<sup>38,39</sup> With the aim of overcoming systemic toxicity, Eggermont *et al.* used isolated limb perfusion (ILP) to deliver TNF- $\alpha$  (a potent pro-inflammatory agent), interferon gamma (IFN $\gamma$ , a cytokine important for innate and adaptive immunity), and cancer chemotherapeutic melphalan to treat patients with soft tissue sarcomas.<sup>40</sup> Given that this treatment regimen was well-tolerated and a vast antitumor response was detected in 87% of the patients, it has now become a standard treatment for melanomas and sarcomas.<sup>40,41</sup> In a more recent study, the hypotensor captopril was able to dilate tumor blood vessels by upregulating bradykinin, resulting in enhanced vascular permeability and delivery of paclitaxel-loaded PEG-poly(lactic acid) (PLA) nanoparticles (NPs) to glioma tumor xenograft models, which in turn led to increased tumor shrinkage and necrosis.<sup>42</sup>

**2.1.2. Vascular Normalization.** Another effective approach for enhancing NM delivery to solid tumors is vascular

normalization. The tumor vascular network is chaotic, with several functional and structural abnormalities that are caused by an imbalance between pro- and antiangiogenic factors, hampering NM delivery and efficacy. During vascular normalization, low doses of antiangiogenic agents are used to correct these vascular abnormalities by reducing the levels of vascular endothelial, fibroblast, and platelet-derived growth factors (VEGF, FGF, and PGDF, respectively). Restoring the balance between pro- and antiangiogenic factors has shown to correct these structural abnormalities, partially restore functionality of the tumor vasculature, and reduce IFP.<sup>43</sup> For instance, Batchelor *et al.* combined chemoradiation together with cediranib (a pan-VEGF receptor tyrosine kinase inhibitor) to shed light on mechanisms of newly diagnosed glioblastoma patients (nGBM) and showed that the resulting increased blood perfusion was able to significantly improve tumor oxygenation and patient survival.<sup>44</sup>

While normalization has been found to promote the delivery of free chemotherapeutics and very small mainly inorganic NMs,<sup>45,46</sup> it may impede the permeability of larger organic NMs due to the reduced amount and size of endothelial fenestrations associated with the resulting decreased leakiness of the tumor blood vessels. For example, upon normalization of the abnormal vasculature in orthotopic E0771 murine breast cancer models using the anti-VEGFR2 antibody DC101, the delivery of 10 nm albumin-based nanocarriers (Abraxane) was significantly improved, while the normalization did not have any considerable effect on the accumulation of 100 nm liposomal nanomedicines, such as Doxil (PEGylated liposomal doxorubicin), at the tumor site.<sup>46</sup> Despite these promising results, more research into this method is required as normalization is, for example, short-lived and highly dependent on dosing and timing, rendering it difficult to predict therapeutic outcomes, schedule for normalization therapy, and optimally combine normalization with chemo and/or radiotherapy.<sup>47</sup> Additionally, the dense tumor ECM may affect the penetration and extravasation of NMs even postvascular normalization.<sup>36,48</sup> Modulating the ECM and other barriers of the TME will be discussed in more detail in the remainder of section 2.

**2.1.3. Vascular Disruption.** Vascular disruption is the breakdown of the endothelial lining that can be caused by either vascular disrupting agents, such as combretastatin A4 phosphate (CA4P, a tubulin-binding agent that inhibits tubulin polymerization) or by certain mechanical stimuli, allowing anticancer agents and NMs to easily accumulate at the target site. For instance, Satterlee *et al.* used CA4P as a pretreatment to improve the accumulation and efficacy of lutetium-loaded lipid-calcium-phosphate NPs (Lu-LCP) in subcutaneous UMUC3/3T3 ovarian, orthotopic 4T1 breast, and B16 melanoma tumors.<sup>49</sup> The combination therapy of CA4P and Lu-LCP showed a significant inhibition of tumor growth compared to CA4P and Lu-LCP treatment alone. In addition, the accumulation of Lu-LCP was significantly higher in CA4P-pretreated tumors than those treated with Lu-LCP alone. Despite the potential for vessel disruption to enhance the target site accumulation of NMs and anticancer agents, the systemic administration of these disrupting agents are associated with severe side effects, calling for more on-site vascular disruption strategies to be incorporated into treatment regimen.<sup>49,50</sup>



## 2.2. Physical Treatments That Improve Blood Flow

**2.2.1. Hyperthermia.** Hyperthermia is the application of microwaves, radiofrequency, and ultrasound (US) to locally heat the tumor to temperatures up to  $\sim 70$  °C as an anticancer treatment. Even mild hyperthermia (39–42 °C) makes the tumor more sensitive to chemo- and radiotherapy by dilating the blood vessels, enhancing oxygenation and promoting perfusion and improving the efficacy and clinical performance of (in)organic NM formulations.<sup>36,51–55</sup> Sato *et al.* investigated the effect of combined hyperthermia-chemotherapy using  $\mu$ -oxo *N,N'*-bis(salicylidene)ethylenediamine iron (Fe(Salen)) NPs, which are specifically delivered to the tumor site with magnetic guidance as a new strategy for cancer treatment. Because Fe(Salen) NPs need to be rapidly heated up in an alternating magnetic field (AMF), the authors hypothesized that these single-drug NPs would be effective for combined hyperthermia-chemotherapy, as opposed to conventional hyperthermic particles that are mainly composed of iron oxide and thus are not associated with anticancer activity in the absence of an AMF. They found that Fe(Salen) NPs induced apoptosis in cultured cancer cells together with an enhanced apoptotic effect due to AMP exposure. Further, they evaluated the combined 3-fold strategy in a rabbit model of tongue cancer, *i.e.*, chemotherapy with Fe(Salen) NPs, magnetically guided delivery of the NPs to the tumor, and AMF-induced heating of the NPs to induce local hyperthermia. After intravenous administration of the NPs, the tumor volume ratio was reduced almost by half, even before the other two modalities were applied, each of which then inhibited tumor growth even further.<sup>56</sup>

**2.2.2. Radiotherapy.** About half of the solid tumor patients are treated with radiotherapy. While radiotherapy can exert direct antitumor effects, it can also enhance the accumulation and penetration of drugs and NMs into the tumor.<sup>57–59</sup> This is mainly due to increased tumor vessel permeability resulting from the induction of endothelial cell apoptosis and enhanced expression of vasoactive mediators (*i.e.*, VEGF), which reduce cellular density and IFP in treated tumors.<sup>36</sup> In a recent study by Erel-Akbaba *et al.*, radiotherapy was applied to orthotopic glioblastoma xenograft murine models to improve the delivery of iRGD-mediated solid lipid NPs loaded with epidermal growth factor receptor (EGFR) and programmed cell-death ligand-1 (PD-L1) siRNAs.<sup>60</sup> This combination of radio-, targeted-, and immunotherapy showed significant inhibition in glioblastoma growth and extension of mouse survival, with the radiotherapy-treated group exhibiting considerable down-regulation of EGFR and PD-L1 compared to the other groups as a result of increased NP uptake within the brain tumor regions. Improved NM delivery *via* transcytosis using iRGD will be further elaborated on in section 4.

**2.2.3. Sonoporation.** Sonoporation is the permeabilization of the cell membranes or endothelial barriers by inducing high intensity-focused US after fast expansion and compression of gas-filled microbubbles (MB), which initially cavitate and finally implode, thereby physically damaging any biological membrane in their immediate vicinity.<sup>61</sup> Theek B *et al.* evaluated the impact of sonoporation on the PEGylated double-fluophore-labeled liposome accumulation in two tumor models with low EPR baseline levels, *i.e.*, highly cellular A431 epidermoid xenografts and highly stromal BxPC-3 pancreatic carcinoma xenografts. The MBs and liposomes were coinjected intravenously, and the MBs were then locally destroyed in the tumor region using US. Using *in vivo* computed tomography-

fluorescence molecular tomography (CT-FMT) imaging and *ex vivo* multiphoton-photon microscopy, the authors found that sonoporation was able to significantly enhance the accumulation and penetration of liposomes in both tumor models.<sup>62</sup>

**2.2.4. Phototherapy.** During photodynamic therapy (PDT), photosensitizers are locally or systemically administered and the tumor is then locally irradiated with a laser light with a specific wavelength. Light exposure leads to the absorption of photons by the photosensitizers, causing elevated energy levels from a grounded singlet state to an excited state. The subsequent relaxation of the photosensitizers to the ground state generates a singlet oxygen and a reactive oxygen species (ROS), which is an unstable molecule that easily reacts with other biological molecules. The resulting elevated ROS levels then lead to cell damage and induce apoptosis.<sup>63</sup> Similar to radiotherapy, the enhanced (in)organic NM delivery by PDT is mainly driven by the loss of cell numbers and reduced IFP. This PDT method is gaining interest as an anticancer treatment because it also causes toxic effects on endothelial cells, which are able to cause higher vascular leakiness and/or vascular shutdown in tumor tissues.<sup>64–68</sup> The pro-tumorigenic effects of endothelial cells will be further discussed in section 2.3.

A recent study by Paris *et al.* used NPs as drug delivery systems (DDS) for multimodal antivascular therapeutics that incorporates dual drug release, photothermal, and photodynamic therapy.<sup>69</sup> This proof-of-concept DDS was based on mesoporous silica NPs, in which four therapeutic modalities were formulated: (1) the gold nanorod core provided photothermal therapy (PPT, generating local heat) upon near-infrared (NIR) irradiation, (2) the coupled photosensitizer indocyanine green (ICG) enabled PDT and generated toxic ROS under the same stimulus as PTT, (3) the two drugs of interest, AAD (doxycycline or DOXY) and CA4P were loaded into the NP design for antiangiogenic and vascular disruption activities, respectively, and (4) the surface-functionalized iRGD enabled the NPs to reach and interact with the overexpressed integrins on the surface of tumor endothelial cells, facilitating uptake. These four therapeutic modalities were evaluated in an *ex vivo* fibrosarcoma xenograft model, which showed a significant decrease in the number of blood vessels within the tumors upon NP delivery and after which the remaining blood vessels were destroyed with NIR irradiation.<sup>69</sup>

## 2.3. Modulating Physiological Parameters, Such as Hypoxia, Acidosis, and Elevated IFP

Hypoxia is a prominent physiological feature found in 50–60% of solid tumors that results from the inability of the abnormal vasculature to supply the rapidly developing and highly energy-consuming tumor with sufficient oxygen levels.<sup>70</sup> As a result, hypoxic TMEs have been shown to contain up to a 96% decrease in oxygen levels compared to their normoxic counterparts, such as from 8.5 to 1.5% in breast and from 7.5 to 0.3% in pancreatic tissues.<sup>71</sup> Hypoxia has been found to play a key role in the alteration of gene expression profiles (*i.e.*, upregulation of hypoxia-induced factors, HIFs), leading to the development of the invasive and metastatic characteristics of tumors, as well as their induction of epithelial-mesenchymal transitions (EMTs), angiogenesis, and resistance to various conventional therapies. One way of mitigating tumor hypoxia is improving blood flow by one of the aforementioned means.

Another method is to increase oxygen delivery to these targeted areas using hemoglobin and perfluorocarbon, although the amounts of oxygen delivered with these alone are often insufficient.<sup>72</sup> Alternative strategies include the delivery of MnO<sub>2</sub>, CaO<sub>2</sub>, and catalase, which are able to induce *in situ* production of oxygen, often in the form of nanocarrier systems to the tumor site.<sup>73–75</sup> For instance, polyelectrolyte-albumin-containing MnO<sub>2</sub> NPs have been shown to increase tumor oxygen levels by 45%,<sup>76</sup> while Ce6-loaded PEG-coated MnO<sub>2</sub> NPs reduced hypoxic-positive areas by 35% in orthotopic and subcutaneous breast cancer tumors, respectively,<sup>77</sup> significantly inhibiting tumor growth in combination with either ionizing radiation or PDT. Lastly, reducing oxygen consumption by delivering agents such as metformin, atovaquone, tamoxifen, or NO to tumors has also proven to mitigate hypoxic levels through interference with the mitochondrial electron transport chain.<sup>78–81</sup> Given that PDT is able to significantly contribute to tumor hypoxia by consuming oxygen and decreasing vascular perfusion, incorporating hypoxia regulators into PDT regimen significantly improves therapeutic outcomes.<sup>82,83</sup> It is important to note that extensive efforts have also been made to develop nano-complexes that harness the differences in oxygen levels between healthy and tumor tissues to specifically target tumor cells.<sup>84</sup>

Another effect of hypoxia on the TME is acidosis, which simultaneously results from the large concentration of acidic byproducts of glycolysis.<sup>85</sup> Upon delivery to the tumor site and subsequent internalization into cells by endocytosis, NMs experience a range of pH from 7.4 in healthy tissue to 5.7–7.8 in tumor regions and 4.5–5.5 within the lysosomal compartments of cells.<sup>86</sup> These changes in pH may significantly affect the structural and thereby functional integrity of NMs, such as etching of coatings as well as catalyze the degradation of NMs prior to reaching their destination.<sup>87</sup> While the design of pH-sensitive NMs is one strategy of overcoming the effects of tumor acidosis, modulating tumor acidosis itself can also significantly improve NM efficiency, for instance by acid neutralization. Such strategies include the use of buffers (*i.e.*, bicarbonate, imidazoles, lysine), proton-pump inhibitors (*i.e.*, omeprazole and esomeprazole), MCT inhibitors (*i.e.*,  $\alpha$ -cyano-4-hydroxycinnamate, CHC), and CAIX inhibitors (*i.e.*, sulphonamide-based, glycosylcoumarins, acetazolamide).<sup>88,89</sup> Similarly to the case with hypoxia, NMs have also been designed to exploit the differences in pH levels between healthy and tumor tissues to specifically target tumor cells.<sup>90</sup>

Interstitial fluid pressure (IFP) is another physiological outcome inherent to most solid tumors, where it can reach 75–130 mmHg in pancreatic tumors, for instance, compared to 8–13 mmHg in the healthy pancreas.<sup>91</sup> Such elevated pressure results from aberrant blood flow along the tumor vessels as well as the extravasation of excessive fluid from the leaky tumor vessels into the tumor interstitium, where the poor lymphatic drainage is not able to restore normal pressure levels. Hydraulic conductivity in desmoplastic tumors also contributes to IFP and is dependent on the characteristics and organization of fibers in the ECM. For example, increasing amounts of tumor collagen significantly reduces hydraulic conductivity while anionic glycosaminoglycans increase flow resistance by the trapping of water.<sup>92</sup> The elevated IFP reduces the convection of NM delivery as it redirects the blood from the center of the tumor to the periphery through compression of the vessel walls and even leak into healthy tissue while

containing not only NMs but also growth factors and tumor cells, which may lead to metastasis.<sup>93</sup> At the same time, higher IFP enhances the EPR effect and can thus be beneficial for NM delivery as long as the IFP remains lower than the microvascular pressure.<sup>94</sup> Strategies that have shown to reduce tumor IFP include the aforementioned pharmacological and physical methods that aim to regulate blood flow, including PDT and targeting of VEGF, PDGF, and TNF, as well as modulating the ECM, which will be discussed in further detail below.

## 2.4. ECM

Under normal physiological conditions, the ECM consists of a myriad of macromolecules that can be classified as either fibrous proteins (*i.e.*, collagens, fibronectin, integrins, laminins) or proteoglycans (*i.e.*, hyaluronan), the combination of which varies among different tissues, and serves as a natural barrier for cell proliferation and differentiation along the basement membrane and interstitial space.<sup>95,96</sup> However, during tumor progression, the ECM becomes highly unregulated and disorganized and has been shown to either excessively produce the aforementioned macromolecules in desmoplastic tumors (leading to fibrosis) or downregulate production in highly vascularized tumors, such as gliomas and melanomas.<sup>97,98</sup> Collagens, which provide tissue tensile strength, and integrins, which are the main cell adhesion receptors in the ECM, have been associated with tumor progression in their dysregulated forms in various studies.<sup>99</sup> During tumor fibrosis, the high collagen turnover thickens and eventually stiffens the epithelial structures, such as through its cross-linking with elastin fibers *via* lysyl oxidase (LOX), while the individual collagen fibers interact with various tumor-associated proteins, and their catabolins (*i.e.*, matrix metalloproteinases, MMPs) expose their binding sites, facilitating tumor invasion.<sup>100–102</sup> At the same time, dysregulated bindings and transformations of integrins lead to the induction of EMTs and tumor invasion.<sup>103</sup> Other components of the ECM that are highly upregulated in various tumors are hyaluronan and fibrin. Hyaluronan provides the ECM with its gel-like phenotype, which increases IFP and hinders the penetration of external fluids and NMs.<sup>104</sup> Fibrin has been found to be abundant in highly vascularized tumors due to the continuous leakage of coagulation factors from circulation to the tumors, and it mainly resides in the vicinity of the vessels where it causes vessel compression, thereby reducing blood flow and NM delivery.<sup>105,106</sup>

Thus, while the strengthening of the ECM is able to hinder tumor metastasis at early stages, it also significantly interferes with NM delivery in desmoplastic tumors by creating a dense matrix mesh that reduces blood flow and NM convection and diffusion while also elongating the diffusion paths by enlarging the interstitial spaces.<sup>107,108</sup> As such, one of the main strategies for modulating the ECM is the degradation of its various components. This can be achieved through physical methods (*i.e.*, photothermal, ultrasound), or the delivery of biochemical enzymes (*i.e.*, hyaluronidases, collagenases, tissue plasminogen activators) or chemical agents (*i.e.*, cyclopamine, relaxin, NO).<sup>91,109–115</sup> For instance, treatment of pancreatic cancer xenograft-bearing mouse models with cyclopamine has shown to disrupt ECM fibronectins, improving tumor perfusion rate of PEG–PLA NPs and thereby significantly inhibiting tumor growth.<sup>97</sup> With the aim of improving the tumor-specific disruption of the ECM and reducing damage to healthy tissue, NMs coated with various ECM enzymes have been shown to

provide more effective NM diffusion and associated therapeutic outcomes compared to the separate and systemic administration of these agents.<sup>112,116</sup> A similar strategy for regulating the ECM is to interfere with the native ECM assembly by blocking specific stages of the process, such as LOX, MMPs and growth factors involved in tumor-associated fibroblast (TAF) stimulation (*i.e.*, TGF, Hedgehog, PDGF using angiotensin II receptor antagonists), which have been shown to also encode for ECM components.<sup>117–119</sup> In cases where the aim is to enhance the barriers for metastasis, particularly in early stages of tumor progression, then the opposite strategy is implemented wherein the ECM is strengthened to minimize cancer cell leakage by using artificial materials, such as laminin-mimicking peptides (LMPs).<sup>120</sup> These LMPs are self-assembled into NPs that are capable of transforming into nanofibers upon binding to integrins and laminin receptors on the surface of tumor cells and have been shown to stabilize in the tumor for over 72 h, inhibiting lung metastasis by 82% in breast and 50% in melanoma tumor models.

## 2.5. Stromal Cells

Growth factors secreted by tumor and tumor-associated cells may cause functional changes in stromal cells of solid tumors, including endothelial cells (ECs), pericytes, and fibroblasts, that give rise to their tumorigenic properties. Specifically, tumor-associated ECs tend to be more proliferative, upregulate various angiogenesis-related markers and genes, such as aminopeptidase N and tumor endothelial marker 8, and contribute to the immunosuppressive TME that interferes with successful NM delivery.<sup>121,122</sup> Pericytes, which reside in the perivascular space, tend to contribute to blood vessel growth and maturation and promote EC survival.<sup>123,124</sup> In highly desmoplastic tumors, pericytes have been shown to cover up to 70% of the endothelium, limiting the transport of NMs through endothelial gaps, and may even become phagocytic, internalizing NMs along their way.<sup>125–127</sup> While antiangiogenic agents have proven to successfully target ECs, these treatments have led to increased pericyte growth.<sup>128</sup> As such, efforts have been made to target pericytes using drug-loaded NMs functionalized with different peptides, such as CPRECES and TH10, which target the aminopeptidase A protein and NG2 proteoglycan, respectively, on the surface of pericytes.<sup>129,130</sup> It is important to note that, as is the case with ECM degradation, late-stage targeting and destruction of pericytes may affect blood vessel permeability and facilitate leakage of tumor cells, leading to metastasis.

Another type of stromal cell that is highly abundant in desmoplastic tumors are TAFs, which are distinct from healthy tissue-resident fibroblasts and overexpress fibroblast activation proteins (FAPs) and fibroblast-specific proteins.<sup>131</sup> It is claimed that TAFs originate from a variety of sources, including epithelial and endothelial cells through mesenchymal transitions, and bone marrow-derived mesenchymal and hematopoietic stem cells. Another theory is that TAFs differentiate from normal fibroblasts that have been activated by growth factors such as EGF and TGF- $\beta$ , and these cells are characterized by the expression of  $\alpha$ -smooth muscle actin (SMA) and exhibit enhanced migratory abilities compared to TAFs originating elsewhere.<sup>132</sup> TAFs contribute to tumor progression and hinder efficient NM delivery in a number of ways.<sup>132</sup> First, they contribute significantly to the densening and stiffening of the ECM by producing large amounts of

collagen and proteoglycans as well as MMPs, disintegrins, and plasmin to disrupt and remodel the ECM. Second, they produce and secrete high amounts of VEGF, TNF, IL-6, PDGF, and TGF- $\beta$ , providing tumors with their chemoresistant properties and promoting their growth. As such, disrupting or targeting TAFs through the use of FAP antibodies, antifibrotic angiotensin receptor II (AR2) antagonists, or cyclooxygenase-2 inhibitors, for example, have been shown to significantly improve the therapeutic efficacy of NMs.<sup>133–137</sup> For instance, AR2 antagonist (losartan)-loaded peptides capable of self-assembling into long filaments to form a hydrogel were able to remain in the tumor for at least nine days, gradually and sustainably releasing losartan to destroy TAFs in breast tumor-bearing mice.<sup>134</sup> Other groups have targeted the wntless-type MMTV integration site (Wnt) that is overexpressed in cisplatin-treated TAFs using anti-Wnt16 siRNAs loaded in lipid-calcium-phosphate (LCP) liposomes in combination with cisplatin, reducing resistance to cisplatin and improving its therapeutic efficiency.<sup>138</sup>

## 2.6. Immunosuppression

Another prominent feature of solid tumors is their immunosuppressive environment, which arises due to a variety of events including the downregulation of MHC and recruitment of anti-inflammatory immune cells by tumor cells, reducing the immune system's capacity for defense. Various immunosuppressive molecules are also released, such as PDL1, immune-checkpoint molecules (*i.e.*, CD47), natural killer cell ligands (*i.e.*, FASL),<sup>139</sup> among many others. One type of immune cell that has gained significant attention within the field of cancer immunotherapy over the years is the macrophage, which is capable of developing either an anti- or pro-tumorigenic phenotype (M1 or M2, respectively) depending on the activation conditions. Within the hypoxic TME, macrophages tend to exhibit M2-like genetic expression profiles such as lower IL12 and elevated IL10, indoleamine, NO, arginase, PGE2, and TGF- $\beta$  levels and further hinder M1 activation.<sup>139</sup> Tumor-associated macrophages (TAMs) have been shown to originate from monocytes and healthy tissue-resident macrophages that have gained the ability to promote angiogenesis, tumor invasion, and immune evasion.<sup>140,141</sup> Other negatively immunomodulating cells involved in tumor progression include regulatory T cells (Tregs) and myeloid-derived suppressor cells (MDSCs) that are triggered in response to tumor-released cytokines (*i.e.*, macrophage colony-stimulating factor MCSF and IL6).<sup>142,143</sup> Together, they interfere significantly with T-cell function and activation by secreting large amounts of arginase-1, NO, IL10, and TGF- $\beta$  and suppressing dendritic cells (DCs).<sup>144,145</sup> Tregs also secrete perforin and granzymes to disrupt effector T cells and are further triggered by the presence of indoleamine-2,3-dioxygenase (IDO) to activate the suppressive MDSCs.<sup>146</sup> In combination with the lack of immune activation in the TME, the downregulation of NK cells and adhesion molecules ICAM-1 and VCAM-1 as well as CD62L on the surface of CD8+ T cells hinders effective antitumor immune response.<sup>147,148</sup>

Given the variety of existing immunosuppressive elements within tumors, numerous strategies have been developed to boost the immune system's ability to fight against cancer cells, with immune checkpoint inhibitors (*i.e.*, anti-PD1 and -PDL1 antibodies and small molecules) exhibiting some of the most significant therapeutic benefits and making their way to the



clinic.<sup>149</sup> Other immunosuppressive molecules that have been targeted include IDO, MMPs, and TGF- $\beta$ .<sup>150</sup> Depleting TAMs has also been widely explored by the administration of colony-stimulating factor 1 receptor (CSF-1R) and bisphosphonates, although such treatments tend to result in the simultaneous destruction of M1-like macrophages.<sup>151,152</sup> More targeted strategies involve inhibiting the specific recruitment and survival of M2-type TAMs through M2pep and anti-CD204 ligand modifications, for instance, or repolarizing them to an M1 phenotype using agents such as chloroquine, celecoxib, and TLR agonists.<sup>153–156</sup> In relation to tumor cytotoxic-NM delivery, however, the depletion of TAMs and other phagocytic inflammatory cells could reduce NM uptake by these cells and thus off-target delivery, improving the therapeutic efficiency of the NMs. In fact, Roode *et al.* have shown that in melanoma xenograft tumor models, NP uptake was 4-fold greater in TAMs than in cancer cells.<sup>157</sup> At the same time, the phagocytic properties of these cells can be exploited to facilitate the on-target delivery of NMs that have been specifically developed to target TAMs and other negatively modulating immune cells rather than tumor cells. Other strategies have aimed at depleting Tregs through PDT or modulating them using CTL4 and STAT3/5 pathway inhibitors, while MDSCs have been targeted using derivatives of oleanolic acid and gemcitabine, for example, potentiating cancer therapy.<sup>158–162</sup> As such, the combination of NMs with immunotherapeutic agents has been extensively explored over the recent years to modulate the TME and maximize the therapeutic efficacy of treatment regimen.

## 2.7. Conclusion

Most of the methods described above rely on disrupting the barriers that are present within the TME to improve NM delivery. While the permeability of tumor blood vessels and the various components of the ECM are, from a practical point of view, interesting to exploit in view of targeted delivery of (in)organic NMs to solid tumors, the resulting fenestrae within the endothelial barrier do pose some dangers. Solid tumors themselves are, depending on their nature, sometimes hard to treat, but one of the major issues with cancer lies in the dissemination of cancer cells from the original tumor into remote metastases. Tumor cells that can find their way from the main tumor mass into the bloodstream can then be further transported to other organs and locations into the body. The endothelial barrier is one of the major obstacles that impede tumor cells from accessing the blood and vessel normalization, whereby fenestrae in the vessels are inhibited, is one of the major clinical applications in a variety of tumor treatments including ovarian cancer.<sup>163</sup> Any effect on the integrity of the endothelial barrier by promoting blood flow may therefore result in higher levels of metastasis. In particular, for less controlled methods, such as radiotherapy, phototherapy, or sonoporation, endothelial cell death or damage can open doors for promoting tumor malignancy.

## 3. EPR-MEDIATED NM DELIVERY AND QUANTIFICATION

While the EPR effect is significantly influenced by various features of the TME, it is also affected by the physicochemical properties of the NMs, including composition, size, stability, and surface properties, which determine the nature of the bionano interactions and thereby NP half-life and behavior in circulation and transvascular transport to the tumor. For

instance, as a result of the leaky tumor vasculature, organic NMs of sizes <500 nm can easily penetrate through the vascular gaps (depending on the gap size in the vessel wall) and into the tumor tissue, while smaller NMs of (<30 nm) can also easily diffuse back into circulation and are thus associated with poor tumor retention.<sup>164</sup> This low retention at the tumor site can, however, be significantly enhanced by active targeting.<sup>165</sup> At the same time, the longer the half-life of the NM in circulation, the more likely it is to experience the EPR effect. In an early study by Liu *et al.*, the biodistribution of liposomes of varying sizes was evaluated 4 h after their intravenous administration, and it was found that 60% of the NPs ranging from 100 to 200 nm in size were still found in circulation compared to only 20% of those with sizes <50 and >250 nm.<sup>166</sup> Similar observations were made for tumor uptake data wherein 100–200 nm liposomes exhibited a 4-fold higher uptake rate in the tumor compared to those with sizes <50 and >300 nm.

The surface characteristics of NMs is another prominent factor that influences the EPR effect as it is associated with the solubility, aggregation, biocompatibility, and the ability of NMs to transport themselves across biological barriers. In general, NMs with neutral surface charge have been shown to be more shielded from uptake by the mononuclear phagocytic system (MPS) and thus remain in circulation for longer than their charged counterparts.<sup>167</sup> Specifically, cationic NMs tend to interact with anionic serum proteins *in vivo*, forming large aggregates that can cause transient embolism in the lung, and these aggregates are better detected by the MPS for clearance.<sup>168</sup> At the same time, while cationic NMs bind more easily to cell membranes and may thus be better taken up by cells, they also bind more easily to the negatively charged vascular endothelial surface which leads to a decreased NM concentration in the plasma that is available to experience EPR.<sup>169</sup> Improving the *in vivo* stability and biodistribution of NMs *via* the reduction of MPS recognition and protein corona and aggregate formation can thus be achieved by coating the NMs with PEG and other antifouling agents that reduce surface charge.<sup>170–172</sup> Similarly, the biocompatibility and stability of organic NMs render them less susceptible to aggregation and MPS clearance compared to inorganic NMs, whose reactive sites can easily interact with the various elements in the biological environment. Besides PEGylation, cell-based therapy has evolved as a relatively novel strategy to enhance NM circulation time, wherein for instance, NMs can be loaded into or functionalized on the surface of various circulatory cells or even coated with isolated cell membranes, shielding them from potential recognition by the MPS and significantly improving their half-life and delivery to solid tumors. Cell-based therapy will be discussed in great detail in section 6.

### 3.1. Personalized Medicine

Various efforts have recently been undertaken to try and boost the delivery of (in)organic NMs to solid tumors. One trend that has emerged is the need for personalized medicine, where depending on the physiology of the tumor of a particular individual, this tumor would be more or less susceptible for NM therapy.<sup>21</sup> Where most studies to date do not classify different tumors based on their vascular properties (total blood flow and tumor vessel permeability), they frequently will observe a broad distribution in the tumor-targeting ability of any administered NM.

Individual patients have a high heterogeneity in EPR effect among them. Because of this heterogeneity, the clinical translation of NMs has been marginal. Patients with high vs low levels of EPR effect in a clinical trial can possibly cause different therapeutic results, which may also show some superiority compared to gold-standard treatments when the patients with high levels of EPR-mediated accumulation are preselected. Patient preselection using protocols and probes are for this reason needed for NM therapies, during which factors such as vascular leakiness, perfusion, ECM density and macrophage content need to be considered. EPR level assessment using imaging methods can possibly predict a correlation between a high tumor accumulation of a given nanomedicine and an increased antitumor response. At the same time, low levels of EPR are likely to show a poor antitumor response. The visualization and quantification of EPR-mediated tumor targeting and the evolution of EPR during therapy could be done using noninvasive direct or indirect imaging techniques.<sup>21</sup>

**3.1.1. Indirect and Direct EPR Imaging.** Indirect EPR imaging is the visualization and quantification of tumor characteristics in a noninvasive way. These tumor characteristics correlate with the level of NM accumulation in the tumor itself. Some preclinical studies focus on key EPR-determining parameters of the tumor vasculature, which are correlated with the accumulation and/or efficacy of NMs.<sup>173</sup> In one preclinical study, assessment of the relative blood volume (rBV) in tumors was done *via* contrast-enhanced ultrasound imaging. They observed a correlation between rBV values and the tumor accumulation of *N*-(2-hydroxypropyl) methacrylamide (HPMA)-based organic polymeric drug carriers, highlighting the usefulness of imaging vascular parameters in predicting EPR-mediated tumor targeting.<sup>174</sup> Coll and colleague (2016) performed MRI scans for the characterization of tumor models, which further correlated rBV and vessel permeability with fluorophore-labeled nanocarrier accumulation. This method was used for the detection of biomarkers for EPR-based NM accumulation.<sup>175</sup> Accordingly, indirect imaging of biomarkers depends on the correlation of tumor vascularization with NM accumulation, which in turn is correlated with treatment response.<sup>21</sup> Direct EPR imaging is for this reason preferred, during which the tumor accumulation of nanodiagnosics or nanotheranostics (coloaded of nanocarriers with an imaging agent and a drug) can be visualized and quantified directly.<sup>176–178</sup>

Recent studies have shown that by using an imaging contrast agent along with the therapeutic NM, a better understanding of the vascular properties of every particular individual can be obtained, based on which the decision of whether or not this particular individual would be susceptible to NM-based therapy can be made.<sup>179</sup> A study performed by Merrimack Pharmaceuticals used <sup>64</sup>Cu-labeled human epidermal growth factor receptor (HER2)-targeted organic PEGylated liposomes loaded with doxorubicin (DOX) for the evaluation of the EPR effect in patients with primary and metastatic breast cancer tumors.<sup>180</sup> Quantitative PET imaging was used to analyze liposome accumulation in different lesions, and biopsies were taken to determine the DOX concentration within tumors and metastatic sites to be correlated with the therapeutic outcomes.<sup>180</sup> They found that the treatment response is highly influenced by the amount of drug accumulation at a target site, which was shown to be highly heterogeneous between patients and within the same patient, as well as by other aspects such as

drug release, sensitivity to the drug, cellular uptake, and intratumoral distribution.<sup>180</sup>

Despite its effectiveness, EPR effect quantification using direct imaging, wherein NMs are labeled and imaged themselves and their uptake in tumors is directly quantified, is almost never done in clinical practice due to cost challenges and regulatory legislation.<sup>179</sup> Indirect imaging is more likely to be used and employs nanosized imaging agents that behave similarly to NMs to predict NM localization using imaging techniques. For instance, Ferumoxytol (FMX, Feraheme), a clinically approved inorganic magnetic 30 nm NM, can predict colocalization (delivery and efficacy) of NMs by MRI. FMX-MRI correlates well with NM uptake, cellular response, and inhibition of tumor growth in mouse xenograft models. Thus, FMX can be used as a generic diagnostic NM companion for multiple therapeutic NM formulations to select the patients that are more likely to benefit from EPR-mediated treatment.<sup>179</sup>

**3.1.2. Companion/Nanodiagnosics.** Companion diagnostics is an intermediate option between indirect vascular imaging and the direct nanotheranostic imaging. One preclinical study by Perez-Medina *et al.*<sup>181</sup> introduced a PET nanoreporter that serves as a companion diagnostic for organic PEGylated liposomes loaded with chemotherapeutics such as Doxil. Liposomes with physicochemical properties similar to Doxil were loaded with chelators to allow <sup>89</sup>Zr-labeling and PET imaging, allowing the prediction of the therapeutic outcome in individual tumors based on the accumulation of nanoformulations. Doxorubicin and nanoreporter concentrations in tumors were found to be correlated with therapeutic efficacy, suggesting that PET nanoreporters can be used as effective tools for the preidentification of tumors with good therapeutic response.<sup>181</sup> The prediction of the tumor accumulation of drug-containing organic liposomes in different solid mouse tumor models was also investigated more recently by Lee *et al.*, where diagnostic PEGylated liposomes were labeled with <sup>64</sup>Cu.<sup>182</sup> Accumulation of the <sup>64</sup>Cu-containing companion diagnostic liposomes matched well with three different therapeutic liposomes target site depositions. The classification of tumors into high vs low levels accumulation of liposomes was enough for the prediction of the tumor response to NM therapy.<sup>182</sup>

## 3.2. Maximizing NM Delivery to Solid Tumors

**3.2.1. Advantages and Limitations of EPR-Mediated NM Delivery.** Various direct and indirect imaging tools and technologies have been developed to determine the heterogeneity in EPR-based tumor targeting, each of which are associated with advantages and limitations based on clinical translatability, versatility, and predictive power.<sup>21</sup> Although indirect imaging approaches are less accurate, they have the ability to be versatile and have a straightforward clinical translation. For this reason, some clinically approved inorganic NMs with pronounced imaging contrast such as ferumoxytol can fasten the use of companion nanodiagnosics for patient preselection.<sup>21</sup> At the same time, while direct nanotheranostic agents can be powerful tools for the accurate prediction of a NM formulation performance, a new chemical entity (such as chelators that can bind tightly to metal ions) must be incorporated into every formulation for further radiolabeling. This means that every formulation has to face a new full set of preclinical and clinical toxicology experiments for the safety evaluation of the new chemical.<sup>21</sup>

In conclusion, additional studies are needed to determine the required level of accuracy and specificity for EPR-mediated drug targeting assessment. The useful parameters to predict patient responses to EPR-based NM therapies should also be taken into consideration.<sup>21</sup> While personalized medicine and characterization of EPR efficacy can be very useful, they do not improve NM delivery to tumors on their own. For this purpose, these image-based methods should be combined with alternative strategies that can enhance (in)organic NM delivery to solid tumors while taking into account the dangers associated with these physical, chemical, and biological strategies discussed in this review.

An important remark concerning the use of these methods to enhance NM delivery to solid tumors is that the EPR effect has been proposed quite some time ago as the major mechanism by which NMs can be efficiently targeted to cancerous tissues. This paradigm has now been challenged in a recent study by Warren Chan's group, in which they demonstrated that most NMs reach solid tumors through active transcytosis pathways across the endothelial barriers.<sup>183</sup> The gaps between endothelial cells, which are essential for EPR-based strategies did not seem to be the major factors in enabling NMs to reach the tumor cells. Instead, using a combination of detailed intravital microscopy studies and mathematical modeling, the authors observed that up to 97% of injected NMs arrived in tumors through active transport mechanisms rather than passive EPR. For these studies, so-called zombie mice were used, being paraformaldehyde-fixed and which were completely devoid of active transport mechanisms. The authors noted that NM delivery into tumors in these zombie mice was largely reduced. This paradigm shift has elicited major responses from the scientific community,<sup>184</sup> and more research work should be done to confirm these findings and enhance our understanding of how NMs can efficiently reach tumors. A wide range of different strategies have already been investigated and will be discussed in detail in the sections below. It is important to note that while the EPR effect may not be the major contributing factor to NM deposition in the tumor, it should not be completely ignored. Optimal results will therefore likely stem from a combination of the methods listed above along with methods described below. A personalized approach, in which the perfusion and vessel density of the tumor is well-characterized, in combination with various physical, pharmacological, and biological NM-based strategies described in this review, may constitute a big step forward in cancer therapy.

### 3.2.2. Potential Bottlenecks Related to NM Delivery.

Numerous attempts have been and are continuously being made to improve NM delivery to solid tumors, in particular, by physical or chemical means, including blood vessel disintegration, sonoporation, radiotherapy, or thermal therapy, all of which aim to break the endothelial barrier and reduce interstitial pressure in the dense tumor mass.<sup>21</sup> Recent work by the group of Warren Chan and colleagues has demonstrated that blood clearance levels of NMs are limited and tumor delivery can be significantly enhanced by exceeding this saturation threshold of approximately 1 trillion NM per mouse.<sup>33</sup> For drug-loaded NMs, this can be achieved by initially administering high levels of empty NMs, followed by a second administration of loaded NMs, resulting in nearly 12% tumor targeting efficacy.<sup>33</sup> While for inorganic NMs this can indeed be an excellent opportunity, the high levels of NMs to be used need to be considered carefully in view of their

toxicity. Similarly, for all strategies relating to disruption of the blood vessels, it needs to be carefully validated whether this does not bring any issues in themselves. Recent work by Peng and colleagues<sup>185</sup> revealed that inorganic (titanium dioxide, silica, and gold) NMs themselves can damage the endothelial barrier, which in turn can increase intravasation and extravasation of tumor cells, resulting in potentially higher levels of metastasis.<sup>185</sup> NMs have also been found to elicit inflammation and result in elevated levels of TGF- $\beta$ , a key cytokine that among its many roles also induces cancer cell migration and invasiveness, thereby promoting metastasis.<sup>186</sup> Hence, the understanding that (inorganic titanium dioxide) NMs by themselves can disturb the tight junctions that hold together the endothelial barrier<sup>187</sup> surely raises concerns of significant risks in view of cancer progression and malignancy.<sup>188</sup> The deliberate breakdown of the barrier by physical or chemical means would clearly add to this risk. One might ask, albeit, whether the added efficiency in NM delivery outweighs the increased concerns about the potential risk in metastasis formation. After all, surgical removal of a tumor tissue is also, to a certain level, associated with potential increase in the risk of metastasis at a later stage.

The matter of fact is that the actual impact of these findings is yet unclear and warrants further research. It is true that the major threat in cancer lies in the dissemination of cancer cells from the primary tumor to secondary metastatic sites. The process of intravasation is very common and can be increased by a wide range of factors, for example, by the activation state of nearby macrophages.<sup>189</sup> However, the formation of metastatic nodes is a very inefficient process, where less than 0.01% of circulating tumor cells lead to tumor formation at secondary sites.<sup>189</sup>

The formation of metastases is not completely understood but is often explained in view of the seed and soil theory, where circulating tumor cells will only be able to form secondary tumors in organs where the microenvironment is favorable to the tumor cells.<sup>190</sup> For this, the "soil" is thought to be prepared by extracellular vesicles released by the primary tumor,<sup>191</sup> where the genetic transfer of material from the primary tumor to the new target organ by the exosomes facilitates any circulating tumor cells to nestle in. But, even then, the tumor cell will still have to adapt to its new environment, quite often undergoing changes in its metabolism to adapt to local nutrient availability.<sup>192</sup> All these processes are quite complex and require all conditions to be near-optimal for the migrating cell before any metastasis can occur.

In view of the increased intravasation or extravasation of cancer cells owing to NMs themselves or by physical or chemical means, some considerations must be taken into account before forming conclusions. For example, as mentioned above, first, the complex process of metastasis requires quite some time for all conditions to be met for the metastatic tumor to start growing. For *in situ* metastasis, the cells will have to first intravasate, migrate, and then extravasate, requiring them to pass the endothelial barrier twice. The study by Peng and colleagues revealed a clear effect of the inorganic NMs on extravasation when the cells were injected intravenously, but this was less clear in their *in situ* tumor experiments where cells had to first migrate from the primary tumor.<sup>185</sup> At this point, it also remains unclear whether the disturbances are long-term or short-lived. NMs themselves are normally only in circulation for a few hours, after which they



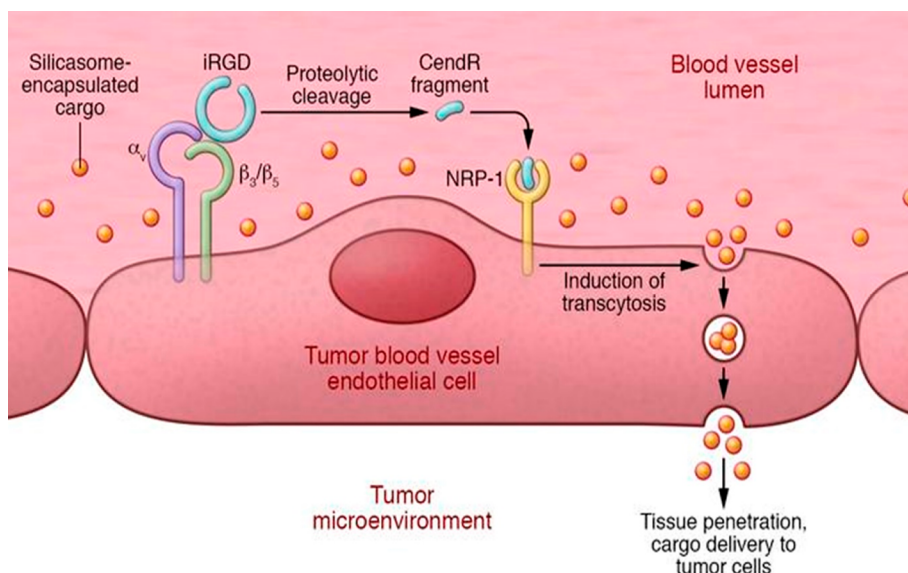


**Figure 5.** The three-step process of iRGD-enhanced tumor accumulation of silicasome-encapsulated drugs. iRGD binds first to  $\alpha_v$  integrins, followed by a protease cleavage of bound iRGD. This cleavage leads at the tumor site to a C-terminus CendR-containing fragment of iRGD. Finally, this CendR fragment binds to NRP-1 receptor, which further induces transcytosis through the vessel endothelium and promotes thus the uptake of the silicasome. Cargo is delivered directly to the target tumor. Reproduced with permission from ref 197. Copyright 2017 American Society for Clinical Investigation.

are often cleared out by the body and can no longer harm the endothelial barriers.

A study that would be worth reading would be on the subject of the fate of these endothelial barriers over time. Can these barriers repair themselves, and how long would this process require? At this point, an actual increase in the level of intravasation or extravasation due to the endothelial barrier disruption also remains unclear, where in-depth studies utilizing intravital microscopy recordings would be ideally suited to try and quantify the extent of cellular motion across endothelial barriers. As some of the inorganic particles tested in the study by Peng and colleagues<sup>185</sup> have also been shown to induce metastasis formation by TGF- $\beta$  generation,<sup>186</sup> it could be that changes in the TME caused by this specific set of NMs contributed to the observed effects. The use of alternative targeting strategies by means of biomimicry, in which the (in)organic NMs are coated by biological membranes to avoid recognition by immune cells, could help reduce endothelial disruptions or inflammatory responses. In addition, the use of clinically approved vessel normalization strategies, often a first line response in clinical settings to avoid tumor spreading.<sup>193</sup>

Therefore, we would like to highlight the importance of not generalizing NM behavior until the above-mentioned points are taken into account and the questions raised in this review are answered sufficiently. Additionally, it would be imperative to conduct a comparative, comprehensive study to clarify as to exactly which NM properties contribute to the barrier leakiness.<sup>189</sup> Together, the data presented by Peng and colleagues<sup>185</sup> sheds essential light on the future direction of nanomedicine and the importance of treading carefully when proposing to use NMs for cancer treatment. Conversely, at this stage, the impact of these findings are too premature to develop an unenthusiastic attitude that could hinder the development and the testing of NMs for such applications.

## 4. USE OF PEPTIDES TO IMPROVE NM DELIVERY TO SOLID TUMORS

### 4.1. Transcytosis with iRGD

Among the major factors limiting the therapeutic efficacy of NMs and anticancer drugs are their poor penetration into tumors and their off-target deposition and adverse effects on healthy cells, requiring additional doses (beyond safety thresholds) to be administered for effective anticancer activity and priming the tumor tissue for drug resistance. An alternative method to the previously mentioned strategies for enhancing NM uptake into the tumor tissue is *via* transcytosis using iRGD.<sup>194</sup>

iRGD (CRGDK/RGPD/EC) is a tumor-penetrating peptide that can be chemically conjugated to the NM and facilitates its transportation deep into the extravascular tumor tissue. Specifically, iRGD binds to  $\alpha_v$  integrins that are expressed on the tumor vessel endothelium, which in turn proteolytically cleave the peptide in the tumor into CRGDK/R. The resulting cleaved peptide has been found to trigger transcytosis *via* neuropilin-1 (NRP-1), a transmembrane glycoprotein that is highly expressed in tumor-associated endothelial cells and cancer cells and is involved in angiogenesis (Figure 5).<sup>195,196</sup> Upon its gained affinity for NRP-1, iRGD loses its integrin binding, leading to tissue penetration alongside its cargo. This NRP-1 and iRGD binding is tumor specific because the cleavage of the peptide requires the binding of the peptide to the integrins.<sup>194</sup> An overview of studies using iRGD for enhanced NP delivery is provided in Table 1.

**4.1.1. iRGD in Breast Cancer.** Various studies have investigated the efficacy of iRGD to improve tumor uptake of drug-loaded nanocarriers, particularly in breast cancer models. Sugahara and colleagues showed that NMs do not need to be chemically conjugated to the iRGD peptide but can simply be provided by means of coadministration for effective tumor uptake.<sup>194</sup> They showed that the systemic administration of iRGD with different modalities including organic NMs (nab-

Table 1. Overview of Studies Employing iRGD for Enhanced Tumor Delivery of Nanoparticles

cancer type	NM composition	material	hydrodynamic diameter (nm)	iRGD administration	ref
human breast cancer (BT474) and human prostate cancer (22Rv1)	iRGD-ABX (conjugated)  iRGD+ABX (combination) DOX liposomes+iRGD (combination)	albumin and doxorubicin liposomes	130/120 nm	conjugated or coadministration	194
pancreatic ductal adenocarcinoma (PDAC)	irinotecan-loaded silicasome	silicasome	130 nm	coadministration	201
murine breast cancer (4T1)	IDDHN, hyaluronic acid (HN) shell +dendri-graft-L-lysine conjugated with doxorubicin and indocyanine (IDD)	dendrimer	35–150 nm	coadministration	198
murine breast cancer (4T1)	iRGD/AuNPs-A&C	gold		coadministration	413
murine breast cancer (4T1)	iNP/IT  (iRGD-conjugated NP loaded with ICG and TPZ)	lipid-polymer hybrid	112 nm	conjugated	199
human liver cancer (HepG2)	DOX+SOR/iRGD NPs	lipid-polymer hybrid	126 nm	conjugated	202
murine colon cancer (colon-26)	iRGD-PEG-NPs (CPT-loaded)	polymeric	280 nm	conjugated	203
human colon cancer (Iovo-6-luc-1) /human gastric cancer (MKN45)/ human ovarian cancer (IGROV-1)	iRGD/DOX	liposomes	not reported	coadministration	204
human ovarian cancer (OVCAR-8) /human schwannoma (HEI-193)	iRGD-transportan-siRNA	peptides/siRNA	80 nm	conjugated	205
human breast cancer (MCF10CA1a) /pancreatic ductal adenocarcinoma (KRAS-Ink) /human prostate cancer (PC-3)	ZHA-QDs	quantum dots	12 nm	coadministration	207
human prostate cancer (PC3-MM2)	Psi-NPs	silicon	202 nm	conjugated	209
murine breast cancer (4T1)	iRGD-NDs iRGD-NPs	carbon	ND = 10 nm NP = 70 nm	conjugated	200
pregnancy complications	FAM-iRGD	iron oxide nanoworms	180 nm	conjugated	206
pregnancy complications	liposome-iRGD	liposomes	146 nm	conjugated	206

paclitaxel and DOX liposomes), small molecules (DOX), and a monoclonal antibody (trastuzumab) enhances the tumor-specific delivery and therapeutic index of these drug compositions in mice bearing orthotopic breast and pancreatic tumor models, thereby reducing off-target deposition and associated side effects on healthy tissue.<sup>194</sup> In another study, the coadministration of iRGD with multistage-responsive organic dendrimer NMs loaded with DOX and photothermal agent ICG resulted in an efficient therapeutic distribution deep inside the tumor, causing the primary tumor growth to be nearly fully eradicated.<sup>198</sup> In a similar cancer model, iRGD-modified organic poly(lactic acid/glycolic acid) (PLGA)/lipid hybrid NMs were developed and administered *in vivo* to

achieve simultaneous tumor-specific delivery of ICG and hypoxia-activated prodrug tirapazamine (TPZ). While the primary tumor growth was significantly reduced, metastasis was also inhibited and minimal side effects were detected. Co-delivering ICG and TPZ in one single NM formulation had more anticancer benefits than a mixture of NMs loaded with individual drugs.<sup>199</sup> Similar delivery and therapeutic efficiencies have been observed for combinations of iRGD with inorganic NMs, including legumain responsive aggregable gold NPs.<sup>197</sup>

Ni *et al.*<sup>200</sup> used a droplet-confined/cryodesiccation-driven crystallization approach to design nanocrystallites of the poorly soluble chemotherapeutic drug paclitaxel (PTX) with considerably high drug loading capacity, in the form of nanodots

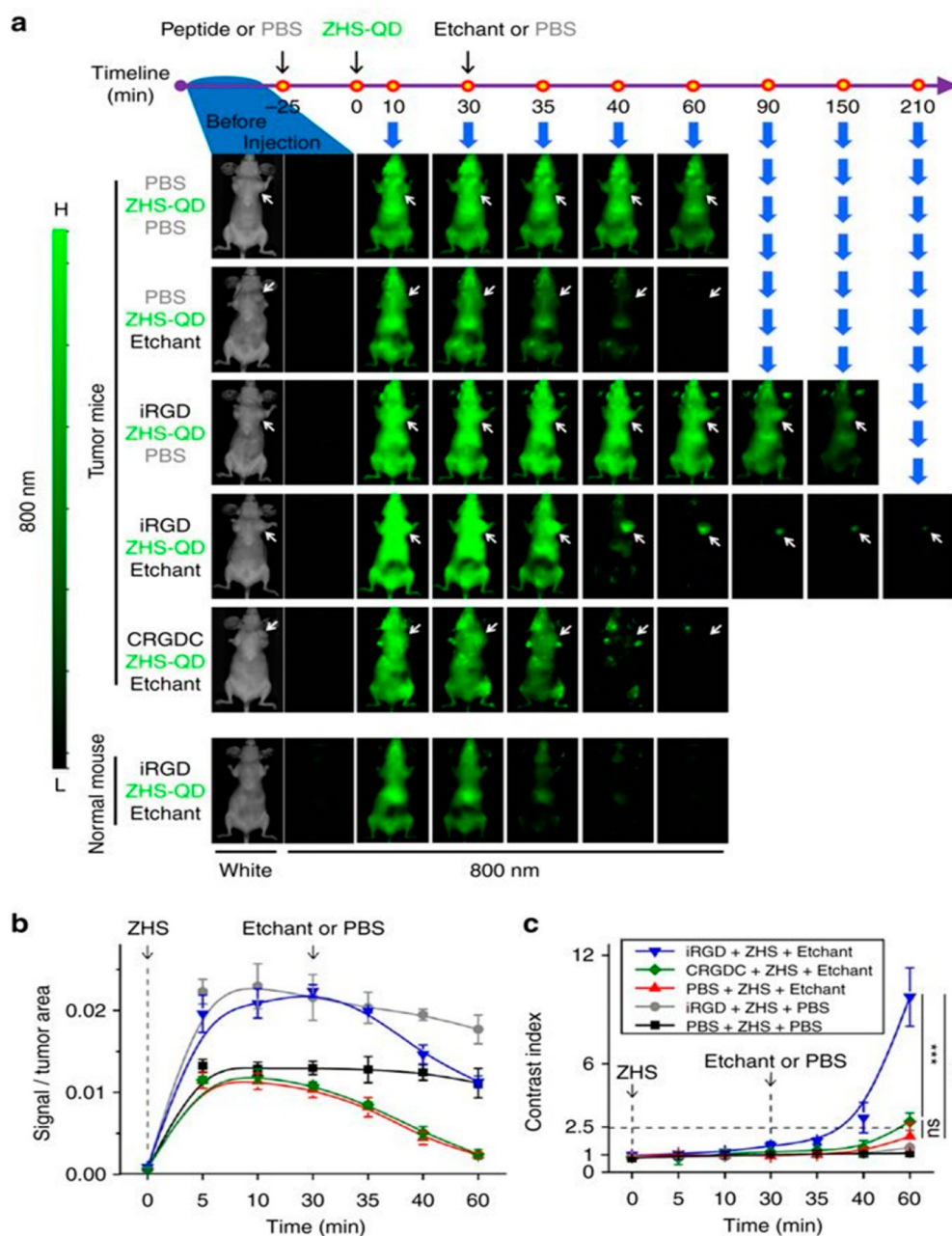


**Figure 6.** Time-dependent *in vivo* breast tumor imaging with etchable ZHS-QDs. Normal mice and mice bearing orthotopic MCF10CA1a human breast tumors received an intravenous injection of iRGD, CRGDC, or PBS before intravenous ZHS-QD injection. Ag-TS or PBS was given intraperitoneally.  $n = 4$  per group. (a) The mice were anesthetized and imaged from the ventral side with a Li-Cor Pearl imager under 800 nm channel at the indicated time points. Arrows, tumors. (b) NIR signals in the tumor per unit area plotted against time. (c) Time-dependent changes of CI in the tumor area. Statistics, two-way analysis of variance; error bars, SEM; ns, not significant; \*\*\* $P < 0.001$ . Reproduced with permission from ref 207. Copyright 2017 Nature Publishing group.

(NDs  $\approx 10$  nm) and NMs (NMs  $\approx 70$  nm). These NDs and NMs were coated with iRGD, which was shown to enhance the tumor cell uptake in an indiscriminative way in a monolayer cell culture model. However, clearly improved inward penetration and ensuing elimination of 3D multicellular tumor spheroids were obtained to a greater extent by iRGD-NDs than iRGD-NMs, highlighting the significance of particle size variation where smaller-sized NMs seemingly benefited more from iRGD delivery enhancement. Only iRGD-coated nanocrystallites of ultranano size (NDs) were able to be delivered intratumorally, reach the cancer stem cells inside the

tumor core, and exert antimetastatic activity in orthotopic breast cancer murine models.<sup>200</sup>

**4.1.2. iRGD in Other Tumor Models.** The group of André Nel demonstrated that coadministration with iRGD can trigger transcytosis of large inorganic silicasome NMs (130 nm diameter), resulting in their specific delivery to pancreatic cancer cells.<sup>201</sup> The resulting ultrastructural images showed that in the iRGD coadministered tumors, a vesicular transport pathway was induced, which carried the silicasomes from the blood vessel lumen to the perinuclear site in the cancer cells. The silicasome-encapsulated drugs were thus able to breach the tumor barrier, although the large silicasome size (130 nm)



Table 2. Tumor Delivery Efficiency of Peptide (or Common Antibody)-Targeted Nanomaterials<sup>a</sup>

cancer type	material	shape	hydrodynamic diameter (nm)	peptide on surface	peptide target	tumor uptake (%id/g)	np composition	year	ref
Breast Cancer									
murine breast cancer (4T1)	silica	spherical	194	TRC105	CD105	9.9 (4 h)	hollow MSN HMSN-ZW800-TRC105	2014	414
murine breast cancer (4T1)	silica	spherical	175	TRC105	CD105	5.4 (4 h)	multifunctional MSN <sup>64</sup> Cu-MSN-800CW-TRC105(Fab) (dual ligand)	2014	415
murine breast cancer (4T1)	silica	spherical	168	TRC105	CD105	5.9 (5 h)	DOX-loaded	2013	416
murine breast cancer (4T1)	CuS NP encapsulated in mesoporous silica shells	spherical	155	TRC105	CD105	6.0 (24 h)	<sup>64</sup> Cu-NOTA-mSiO <sub>2</sub> -PEG-TRC105 <sup>64</sup> Cu-CuS@MSN-TRC105	2015	417
murine breast cancer (4T1)	zinc oxide	spherical	101	TRC105	CD105	6.4 (0.5 h)	( <sup>64</sup> Cu)-NOTA-ZnO-PEG-TRC105	2015	418
murine breast cancer (4T1)	polymeric	spherical	37	TRC105	CD105	5.7 (5 h)	PAMAM-PLA- <i>b</i> -PEG-TRC105	2013	419
murine breast cancer (4T1)	graphene oxide	flake	37	TRC105	CD105	5.7 (6 h)	<sup>64</sup> Cu-NOTA-RGO-TRC105	2013	420
murine breast cancer (4T1)	graphene oxide	flake	27	TRC105	CD105	5.8 (0.5 h)	NOTA-GO-TRC105	2012	421
murine breast cancer (4T1)	graphene	flake	27	TRC105	CD105	5.8 (7 h)	<sup>66</sup> Ga-NOTA-GO-TRC105	2012	422
murine breast cancer (4T1)	hyaluronic hydrogel	spherical	226	hyaluronic acid	CD44 receptor	1.3	HA-HPCD/ADA-PEG	2015	423
murine breast cancer (4T1)	polymeric	spherical	71	folic acid	folate receptor	13.9 (6 h)	FA-functionalized DOX-conjugated micelles (FA-PEG- <i>b</i> -PCL-hyd-DOX)	2013	424
murine breast cancer (4T1)	quantum dots	spherical	14	CGKRRK	p32 (gC1qR or HABP)	7.3 (24 h)	QD-CGKRRK ( <sup>64</sup> Cu-QD-OCH <sub>3</sub> )	2019	425
murine breast cancer (4T1)	iron oxide	spherical	51	human serum albumine	gp60 receptor (albondin) and SPARC	3.25 (1 h)	D-HINPs (DOX-loaded HINPs)	2011	426
murine breast cancer (CI-66)	polymeric	spherical	23	cRGD	integrin $\alpha(v)\beta_3$	6.0	cyclic RGD-DOX-nanoparticle (NP)	2005	427
human breast cancer (MDA-MB-231)	liposomes	spherical	121	hyaluronic acid	CD44 receptor	2.0 (24 h)	HA-liposomes-PEG	2014	428
human breast cancer (MDA-MB-231)	polymeric	spherical	91	F3	cellular nucleolin	6.1 (24 h)	PAMAM-DOX-F3	2018	429
human breast cancer (MDA-MB-231)	polymeric	spherical	274	folic acid	folate receptor	0.1	ICG loaded FA-PLGA and mPEG-PLGA (dual modified NP)	2012	430
human breast cancer (MDA-MB-231)	gold	star	68	aptamer AS1411	NCL (shuttle protein nucleolin)	3.1	Apt-AuNS	2015	431
human breast cancer (MDA-MB-435)	gold	spherical	60	transferrin	transferrin receptor (CD71)	20.0	AuNP	2014	432
human breast cancer (MDA-MB-435)	iron oxide	nanoworm	70 length and 30 thickness	CREKA	clotted plasma proteins in the blood vessels and stroma of tumors	5.3 (24 h)	NW-C (NW-P175-C)	2009	433
human breast cancer (MCF-7/ADR)	hydrogel	spherical	152–219	hyaluronic acid	CD44 receptor	12.5 (10 h)	DOX-loaded HA-Lys-LA X-NP	2015	434
human breast cancer (MCF-7)	polymeric	spherical	72–80	hyaluronic acid	CD44 receptor	8.6 (6 h)	DOX-loaded cross-linked HA-PBLG-LA NP (CLNPs)	2016	435

Table 2. continued

cancer type	material	shape	hydrodynamic diameter (nm)	peptide on surface	peptide target	tumor uptake (%id/g)	np composition	year	ref
Breast Cancer									
human breast cancer (MSA-MB-468)	polymeric	spherical	25 and 60	EGF	EGFR	4.1 (MDA 25 nm), 5.1 (MDA 60 nm), 1.6 (MCF-7 25 nm), 3.7 (MCF-7 60 nm) (48 h)	<sup>111</sup> In-labeled T-BCM-25/60	2010	436
human breast cancer (MCF-7)									
human breast cancer (MDA-MB-468)	liposomes	spherical	80–100	cetuximab (C225 mAb)	EGFR	15.4 (72 h)	anti-EGFR immunoliposomes-DOX	2005	437
human breast cancer (MDA-MB-361)	gold	spherical	54.2	trastuzumab antibody	HER2 receptor	29.6 (48 h)	<sup>111</sup> In-Au-T	2012	438
human breast cancer (BT474-M3)	liposomes	spherical	101	scFv F5	HER2 receptor	6.7 (24 h)	<sup>64</sup> Cu <sub>4</sub> -DEAP-ATSC loaded into PEGylated liposomal DOX (PLD) and HER2-targeted PLD (MM-302)	2015	439
human breast cancer (BT-474)	gold	spherical	15	herceptin	HER2 receptor	8.3 (20 h)	herceptin-AuNPs	2011	440
human breast cancer (BT-474)	liposomes	spherical	90	anti-HER Mab fragments	HER2 receptor	2.8 (24 h)	anti-HER2 immunoliposomes	2006	441
human breast cancer (SUM190)	protein-based	spherical	not reported	biotinylated herceptin	HER2 receptor	21 (40 h)	Cys <sub>5</sub> S/Herceptin/DOTA- <sup>111</sup> In NP	2010	442
human breast cancer (SKBr3)	iron oxide	spherical	(16) TEM	trastuzumab antibody	HER2 receptor	12.6 (48 h)	trastuzumab functionalized, DOX-conjugated, <sup>111</sup> In labeled, APTES-PEG coated SPION	2015	443
human breast cancer (NIH3T6.7)	Mn-doped MnFe <sub>2</sub> O <sub>4</sub>	spherical	69,12	herceptin	HER2 receptor	3.4 (24 h)	<sup>111</sup> In-labeled Mn/MeIO-herceptin	2007	444
human breast cancer (HBT 3477)	Iron oxide	spherical	40	ChL6 mAb	integral membrane glycoprotein	13.5 (48 h)	immunoreactive <sup>111</sup> In-ChL6bioprobe	2005	445
human breast cancer (HBT 3477)	Hydrogel iron oxide hybrid	spherical	20 (core size TEM)	ChL6 mAb	membrane glycoprotein	13.3 (2 days)	<sup>111</sup> In-DOTA-ChL6	2007	446
Glio- and Neuroblastoma									
human glioblastoma (U-87MG)	iron oxide	spherical	161	biotin	avidin/streptavidin	0.6	MNP-APS-biotin	2013	447
human glioblastoma (U-87MG)	gold	tripod	24	RGD	integrin $\alpha(v)\beta_3$	7.9 (24 h)	RGD-Au-tripods	2014	448
human glioblastoma (U-87MG)	iron oxide	spherical	not reported	RGD	integrin $\alpha(v)\beta_3$	5.6 (6 h)	cRGD-conjugated SPIO nanocarriers	2011	449
human glioblastoma (U-87MG)	silica	spherical	226	cRGDyK	integrin $\alpha(v)\beta_3$	8.1 (3 h)	<sup>64</sup> Cu-NOTA-HMSN-PEG-cRGDyK	2015	450
human glioblastoma (U-87MG)	NaGdF <sub>4</sub>	spherical	32	cRGDyK	integrin $\alpha(v)\beta_3$	2.8 (4.5 h)	(cRGDyK)(2)-UCNPs	2013	451
human glioblastoma (U-87MG)	quantum dots	spherical	20	RGD	integrin $\alpha(v)\beta_3$	4.0 (25 h)	DOTA-QD-RGD	2007	452
human glioblastoma (U-87MG)	single-walled carbon nanotubes	AR 67 rods	200 × 3 nm <sup>2</sup> (AFM)	RGD	integrin $\alpha(v)\beta_3$	12.1	PEG-RGD-SWNTs	2007	453
human glioblastoma (U-87MG)	dendrimer-entrapped gold NP	spherical	72	RGD	integrin $\alpha(v)\beta_3$	0.9	Gd-Au DENPs-RGD	2015	454

Table 2. continued

cancer type	material	shape	hydrodynamic diameter (nm)	peptide on surface	peptide target	tumor uptake (%id/g)	np composition	year	ref
Glio- and Neuroblastoma									
human glioblastoma (U-87MG)	quantum dots	spherical	19.6	RGD	integrin $\alpha(v)\beta_3$	10.0 (4 h)	QD800-RGD	2010	455
human glioblastoma (U-87MG)	iron oxide	spherical	40	RGD	integrin $\alpha(v)\beta_3$	6.75 (6 h)	$^{125}\text{I}$ -RGD-PEG-MNPs ( $^{125}\text{I}$ -c(RGDyK) peptide PEGylated Fe@Fe <sub>3</sub> O <sub>4</sub> NP)	2016	456
human glioblastoma (U-87MG)	polymeric	spherical	50	RGD	integrin $\alpha(v)\beta_3$	7.7 (8 h)	DOX-loaded (cRGD30-RCCM) micelle	2017	457
human glioblastoma (U-87MG)	copper sulfide	spherical	49.7	cRGDK	integrin $\alpha(v)\beta_3$	10.3 (24 h)	( $^{64}\text{Cu}$ )CuS-PEG-c(RGDfK)	2018	458
human glioblastoma (U-87MG)	dendrimers	spherical	15.6	cRGD and angiopep-2	integrin $\alpha(v)\beta_3$ and LRP (low-density lipoprotein receptor-related protein) receptor	0.5 (24 h)	Den-RGD-Angio	2012	459
human glioblastoma (U-87MG)	liposomes	spherical	131.3	RGD and substance P	integrin $\alpha(v)\beta_3$ and neurokinin-1 receptors	1.0 (1 h), 1.2 (4 h)	$^{111}\text{In}$ -Hybrid-LP	2013	460
human glioblastoma (U-87MG)	polymeric	spherical	300	anti- $\beta$ -HcG mAb	somatostatin receptor (SSR)	4.3	PEG-Ltd-NP (PEG-coated- $^{177}\text{Lu}$ -DOTATATE-PLGA)	2016	461
human glioblastoma (U-87MG)	silica	spherical	129	VEGF	VEGFR	7.8 (3 h)	$^{64}\text{Cu}$ -NOTA-MSN(SUN)-VEGF <sub>121</sub>	2014	462
human glioblastoma (U-87MG)	quantum dots	spherical	23	VEGF	VEGFR	4.16 (24 h)	DOTA-QD-VEGF	2008	463
human glioblastoma (U-87MG)	graphene oxide	flake	33	VEGF <sub>121</sub>	VEGFR	8.2 (3 h)	( $^{64}\text{Cu}$ )-GO-VEGF <sub>121</sub>	2015	464
rat glioma (9L-E29)	gold	spherical	42	EGF peptide	EGFR	6.0 (24 h)	EGF <sub>600</sub> -Au NP-Pc4	2015	465
murine neuroblastoma (Neuro 2A)	liposomes	spherical	130	RGD	integrin $\alpha(v)\beta_3$	5.2 (1 h)	siRNS RGD-PEG-PEI	2007	466
murine glioma (GL261)	carbon nanotubes	tubular	8–24	angiopep-2	LRP-1	2 (in brain) (5 min)	ANG-targeted chemically functionalized multiwalled carbon nanotubes (f-MWNTs)	2016	467
murine neuroblastoma (Neuro 2A)	gold	spherical	70	transferrin	transferrin receptor	2.4 (24 h)	TF-PEG-AuNP	2010	468
Skin Cancer									
human epidermoid carcinoma (A431)	polymeric	spherical	100	C225 antibody (cetuximab)	EGFR	<0.1	MMPU (multifunctional multiblock polyurethanes) nanocarrier	2013	469
human epidermoid carcinoma (A431)	gold	spherical	37	C225 antibody	EGFR	7.4 (24 h)	$^{111}\text{In}$ -labeled DTPA-C225-HAuNS	2008	470
human epidermoid carcinoma (A431)	gold iron oxide heterostructure	spherical	24	affibody protein (Ac-Cys-ZEGFR:1907)	EGFR	4.6 (48 h)	Au-IONPs ( $^{64}\text{Cu}$ -NOTA-Au-IONP-affibody)	2013	471
human epidermoid carcinoma (A431)	nanobody	nanobody	15 kDa	$^{99m}\text{Tc}$ -7C12 and $^{99m}\text{Tc}$ -7D12	EGFR	7–12 for $^{99m}\text{Tc}$ -7C12 and 4–8 for $^{99m}\text{Tc}$ -7D12 (1.5 h)	$^{99m}\text{Tc}$ -7C12 and $^{99m}\text{Tc}$ -7D12	2008	472
human epidermoid carcinoma (A431)	gold	spherical	31	cetuximab	EGFR	3.7 (48 h)	AuNPs-PPAA-cetuximab- $^{89}\text{Zr}$	2013	473
human melanoma (M21)	liposomes	spherical	131.3	RGD and substance P	integrin $\alpha(v)\beta_3$ and neurokinin-1 receptors	0.6 (1 h)	$^{111}\text{In}$ -hybrid-LP (M21)	2013	460
human melanoma (M21)	silica	spherical	7	cRGDY	integrin $\alpha(v)\beta_3$	2.0 (4 h)	cRGDY-PEG-dots	2011	474
murine melanoma (B16/F10)	gold	spherical	43	NDP-MSH	melanocortin type-1 receptor	12.6 (4 h)	NDP-MSH-PEG-HAuNS	2009	475



Table 2. continued

cancer type	material	shape	hydrodynamic diameter (nm)	peptide on surface	peptide target	tumor uptake (%id/g)	np composition	year	ref
Skin Cancer murine melanoma (B16F10)	gold	spherical	12.5	cRGD	integrin $\alpha(v)\beta_3$	8.7 (4 h)	$^{199}\text{AuNP}$ -RGD	2019	476
murine melanoma (B16)	polymeric	spherical	150–155	cRGD	integrin $\alpha(v)\beta_3$	6.13 (6 h)	cRGD20/DOX-SCID-Ms	2016	477
murine skin melanoma (B16-F1)	liposomes	spherical	356 (p39-Flt-1), 125 (p24-NRP-1 and p47-Lyp-1)	p39-Flt-1, p24-NRP-1, p47-Lyp-1	VEGFR-1, neuropilin-1, mitochondrial protein p32 (gC1qR)	3.6 (p39-Flt-1, PE-PEG750), 7.2 (p24-NRP-1, PE-PEG750), 5.0 (p47-Lyp-1; PE-PEG750/2000) (24 h)	DOX-loaded radiolabeled liposomes engrafted with peptides (p39-Flt-1, p24-NRP-1, p47-Lyp-1)	2011	478
canine hemangiosarcoma (CHSA)	polymeric	spherical	<100	A10 aptamer	PSMA	8.5 (24 h)	A10 (IR783) doxo-PLA NCs	2015	479
Lung Cancer human non-small cell lung cancer (A549)	hyaluronic acid hydrogel	spherical	200	hyaluronic acid	CD44 receptor	1.5 (6 h)	HA-ODA/HA-PEG	2013	480
human non-small cell lung cancer (A549)	MnO	spherical	100	cRGD	integrin $\alpha(v)\beta_3$	45.8	mPEG&cRGD-g-Pasp@MnO	2015	481
human non-small cell lung cancer (A549)	polymeric	spherical	70	cRGD	integrin $\alpha(v)\beta_3$	1.2 (1 h)	cRGD-encoded SPPM	2009	482
human lung cancer (H1299 and A549)	magnetite nano-cluster	spherical	85	RGD	integrin $\alpha(v)\beta_3$	4.7 big and 6.1 nascent tumors (12 h)	RGD-MNC	2012	483
human non-small lung carcinoma (A549)	gold	rod shaped	50–80	ScFv, ATF (amino terminal fragment), cRGD	ScFv against EGFR, ATF against uPAR, cRGD against avb3 integrin receptor	1.8 (ScFv), 1.9 (uPAR), 0.5 (avb3) (24 h)	Au NRs	2010	484
human lung cancer (NCI-H460)	protein-based	spherical	100–125	RGD	integrin $\alpha(v)\beta_3$	39.49 (24 h), 6.97 (72 h)	RGD-BSA-PCL	2017	485
human lung cancer (NCI-H460)	liposomes	spherical	120–150	anisamide	sigma receptor	76.7 (4 h)	siRNA in targeted NP	2008	486
human non-small cell lung cancer (H1975)	solid lipid NP	spherical	160	cetuximab	EGFR	5.06 (24 h)	PtSLNs (PEG-modified surface targeted solid lipid nanoparticles)	2015	487
Ovarian Cancer human ovarian cancer (SKOV3)	polymeric	spherical	105–134	NR7 peptide	EGFR	11.1 (24 h)	DOX-loaded peptide-conjugated PLGA-PEG NP	2012	488
human ovarian cancer (SKOV3)	quantum dots	spherical	19	anti-HER2 antibody	HER2 receptor	15 (4 h)	nanoparticle–antibody conjugates (QD800-PEG)	2011	489
human ovarian cancer (SKOV3)	quantum dots	spherical	12	RGD	integrin $\alpha(v)\beta_3$	19.7 (4 h)	QD710-tetrandom-RGD2	2012	490
Liver Cancer murine hepatocellular carcinoma (H22)	chitosan hydrogel	spherical	133	B $_1$ -BPP-9a peptide	B2 receptors	5.0 (12 h)	Pt-CS-BPP	2014	491
murine hepatocellular carcinoma (H22)	hyaluronic acid hydrogel	spherical	50	hyaluronic acid	CD44 receptor	4.0 (4 h)	DOX-loaded HA nanogels	2015	492
murine hepatocellular carcinoma (H22)	protein-based	spherical	45.7	RGD	integrin $\alpha(v)\beta_3$	15 0.1 (24)	RGD-sNPs	2019	493

Table 2. continued

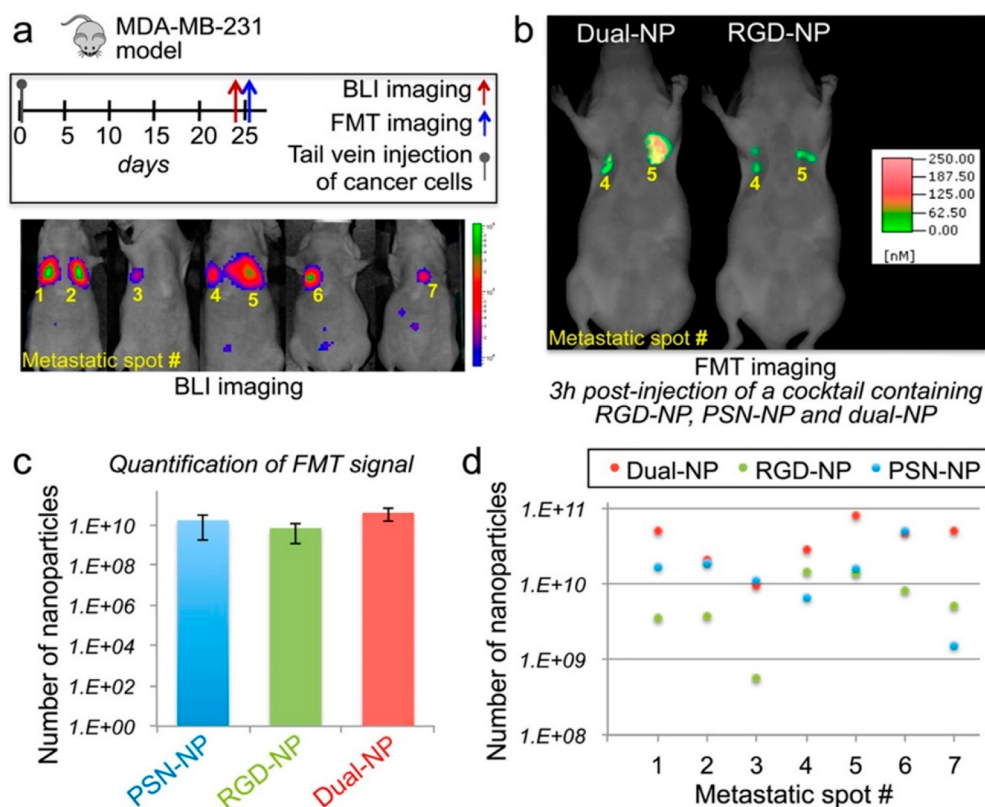
cancer type	material	shape	hydrodynamic diameter (nm)	peptide on surface	peptide target	tumor uptake (%id/g)	np composition	year	ref
Liver Cancer									
human hepatocellular carcinoma (HuH7)	polymeric	linear and round	107.1	B6	transferrin receptor	8 (4 h)	LPEI-PEG-B6/NIS	2017	494
human liver carcinoma (HepG2)	albumin	spherical	170	glycyrrhetic acid (GA)	GA-receptor	13.6 (1 h)	DOX/GA-HSA NPs	2015	495
rat hepatocellular carcinoma (HeDe)	polymeric	spherical	124	folic acid	folate receptor	9.62 (2 h)	radiolabeled self-assembled NPs <sup>90m</sup> Tc-CH/γ-PGA-FA-NP	2013	496
Prostate Cancer									
human prostate cancer (PC-3)	PhMV-like NPs (Physalis motile virus)	spherical	35.7	DGEA	integrin $\alpha 2 \beta 1$	5.5 (10 days)	Gd-Cys-5-PhMV-DGEA	2019	497
human prostate cancer (PC-3)	iron oxide	spherical	140	PSMA inhibitor	PSMA	4.3 (48 h)	PSMA-targeted BNF NP	2015	498
human prostate cancer (LnCAP)	lipid/polymeric	spherical	30	cys-DB (anti-PSMA cysteine-diabody)	PSMA	15 (19 h)	DOTA-cys-DB-PEG-LNP + DOX-PEG-LNP	2017	499
human prostate cancer (Pca)	polymeric	spherical	160	A10 aptamer	PSMA	1.6 (24 h)	PLGA- <i>b</i> -PEG- <i>b</i> -Apt (NP-Apt-5%)	2008	500
human prostate cancer (DUT45)	gold	AR 4.0 rods	61 × 15 (TEM)	RGDFk	integrin $\alpha (v) \beta 3$	1.3 (48 h)	RGDFk-GNRs	2011	501
human prostate cancer (PC-3M)	polymeric	spherical	23	TNYL-RAW (EphB4-binding peptide)	EphB4	2.9 (24 h)	TNYL-RAW-CCPM	2011	502
Cervical Carcinoma									
human cervical carcinoma (HeLa)	gold	AR 3.8 Rods	26	folic acid	folate receptor	17.1 (24 h)	FA-AuNRs	2015	503
human cervical carcinoma (HeLa)	gold	spherical	40–50	folic acid	folate receptor	5.1 (6 h)	F-PEG-HAuNs-siRNA	2010	504
human cervical carcinoma (HeLa)	polymeric	spherical	56	folate	folate receptor	1.1 (6 h)	PEG-PnBA-PDMAEMA	2011	505
human cervical carcinoma (HeLa)	copper sulfide	spherical	88.5	RGD	integrin $\alpha (v) \beta 3$	16.8 (4 h)	RGD@HCuS(VA)	2017	506
human cervical carcinoma (HeLa)	silica coated Mn <sub>3</sub> O <sub>4</sub>	Spherical	53	AS411 aptamer	folate receptor	6.3 (12 h)	Mn <sub>3</sub> O <sub>4</sub> @SiO <sub>2</sub> (RB)-PEG-Apt	2013	507
murine sarcoma (S-180)	polymeric	spherical	101.4	transferrin	transferrin receptor	0.6 (6 h)	actively targetable nanoparticles (ATN)	2005	508
murine sarcoma (S-180)	fullerene	spherical	94	transferrin	transferrin receptor	0.7 (1 h)	HA-C60-Tf/AS	2015	509
human carcinoma (KB)	polymeric	spherical	71	folic acid	folate receptor	15.1 (1 h)	dendrimer (PAMPAM)-polymer hybrid NPs: PEG-PLA NPs	2014	510
human carcinoma (KB)	liposomes	spherical	76	folic acid	folate receptor	2.4 (24 h)	folate-modified gadolinium lipid-based NPs (F(S000)-Nps)	2014	511
human carcinoma (KB)	iron oxide	spherical	54	folic acid	folate receptor	0.6 (4 h)	folate acid modified maghemite NPs	2013	512
human carcinoma (KB)	polymeric	spherical	77	folate acid (PEG and 50% FA)	folate receptor	6.5	fol-PEG-p(Asp-Hyd-ADR)	2007	513
human carcinoma (KB)	polymeric	spherical	not reported	folic acid	folate receptor	5.9 (4 h)	<sup>64</sup> Cu-TETA-SCK-folate	2005	514
human carcinoma (KB)	dendrimer	spherical	not reported	folic acid	folate receptor	6.9 (4 days)	tritiated GS-3H-FA	2005	515

Table 2. continued

cancer type	material	shape	hydrodynamic diameter (nm)	peptide on surface	peptide target	tumor uptake (%id/g)	np composition	year	ref
Kidney Cancer	dendrimers	spherical	not reported	RGD	integrin $\alpha(v)\beta_3$	7.27 (2 h)	$^{111m}$ -labeled tetrameric RGD-dendrimers	2007	516
human renal cell carcinoma (SK-RC-52)	liposomes	spherical	300	NGR motif peptide	CD13	1.4 (24 h)	R4/NGR-PEG-LP (dual-ligand)	2012	517
renal cell carcinoma (OS-RC-2)	liposomes	spherical	225	transferrin	transferrin receptor	2.8	(Tf(+))-PEG-CL liposomes	2006	518
Colon Cancer									
murine colon adenocarcinoma (C-26)									
Gastric Cancer									
human gastric cancer (MKN45)	copper sulfide	spherical	61	cRGD	integrin $\alpha(v)\beta_3$	23.4 (12 h)	T-MAN (Gd-doped CuS micellar NPs with cRGD and MMP-2-cleavable fluorescent substrate	2019	519
human gastric cancer (MGC-803)	gold	spherical	6	folic acid	folate receptor	<0.1	Ce6@GNCs-PEG2K-FA	2015	520
Pancreatic Cancer									
human pancreatic carcinoma (PANC-1)	gelatin hydrogel	spherical	231	EGFR peptide	EGFR	23.2 (2 h)	SH-Gel PEG peptide	2013	521
Laryngeal Cancer									
human laryngeal squamous cell carcinoma (Tu686)	gold	spherical	80	ScFv antibody	EGFR	8.0 (5 h)	SERS NPs	2008	522
Other									
human fibrosarcoma cells (HT1080)	iron oxide	nanoworm	70 length and 30 thickness	CREKA	clotted plasma proteins in the blood vessels and stroma of tumors	5.3 (24 h)	NW-C (NW-PI75-C)	2009	433
murine fibroblasts (16-17)	iron oxide	spherical	33-35	Her2 affinity peptide (3.5), LDS affinity peptide (1.3), RGD (1.5)	HER2 receptor, HSP47, avb3 integrin receptor	1-3.5 (24 h)	SPION	2014	523
Ehrlich ascites tumor (EAT)	liposomes	spherical	386	hyaluronic acid	CD44 receptor	2.4 (2 h)	HA-NLC	2014	524

<sup>a</sup>Nanomaterial delivery efficiency to solid tumors with targeted peptide coating of the NM, from studies published in 2005–2020. Please note that for this table, only those studies are taken into account where the delivery efficacy of the nanomaterials to the tumors has been determined (*i.e.* %ID/g). ID/g = injected dose per gram of tissue. The value between brackets indicates the time after injection at which the analysis was performed.





**Figure 7.** Evaluation of the ability of the dual-ligand nanoparticles to target metastasis *in vivo* in the MDA-MB-231 mouse model. (a) The synopsis shows the timeline and schedule of the *in vivo* imaging studies. After 25 days from systemic injection of MDA-MB-231 cells *via* the tail vein, bioluminescence imaging (BLI) showed the development of metastasis in the lungs. Each metastatic site was numbered, which is indicated on the BLI images. (b) Representative fluorescence molecular tomography (FMT) images of the mouse with metastatic spots 4 and 5. FMT imaging was performed 3 h after injection of a cocktail of RGD-NP, PSN-NP, and dual-ligand-NP. (c) Using the different NIR fluorophores on each nanoparticle variant, the fluorescence signal in the thoracic region of the FMT images was quantified for each formulation ( $n = 5$  mice). On the basis of phantom measurements of each formulation using the FMT system, the fluorescence signal was converted to nanoparticle concentration (mean  $\pm$  SD; y-axis is in logarithmic scale). (d) Total number of nanoparticles for PSN-NP, RGD-NP, and dual-ligand-NP is shown for each metastatic spot (y-axis is in logarithmic scale). Reproduced with permission from ref 211. Copyright 2015 American Chemical Society.

can hamper their internal tumor access.<sup>197</sup> This iRGD-mediated NM codelivery combination therapy was also used for the treatment of hepatocellular carcinoma (HCC). While DOX combined with sorafenib (SOR) is an effective strategy as an anti-HCC treatment, each of these two drugs have different pharmacokinetic and endocytosis capacities which hamper their current application. For this reason, iRGD was coupled to an organic lipid-polymer hybrid NM with a shell-core structure to make the DOX and SOR codelivery possible (DOX+SOR/iRGD NMs).<sup>202</sup> In a separate colon cancer study by Ma *et al.*, iRGD was introduced on PEGylated camptothecin (CPT, topoisomerase poison)-loaded organic PLGA NMs, which improved the accumulation of the NMs in tumor-bearing mice and increased tumor cell apoptosis.<sup>203</sup> iRGD has also been used to improve intraperitoneal chemotherapy (IPC) of ovarian cancer, which is often associated with poor penetration<sup>204</sup> as well as NM-mediated gene therapy.<sup>205</sup>

**4.1.3. Treating Pregnancy Complications.** Besides tumor targeting, iRGD has also been investigated as a tool for targeted delivery of payloads to the placenta given the lack of therapeutics for pregnancy complications as a result of the high risk of causing damage to the fetus. King A *et al.* used the tumor-homing peptide sequences CGKRK and iRGD which bind selectively to the placental surface of humans and mice and do not interfere with normal development.<sup>206</sup> When the

iRGD-coated inorganic iron oxide nanoworms and organic liposomes were injected intravenously into pregnant mice, these NMs accumulated inside the mouse placenta more efficiently than control groups without iRGD administration, in which a reduced binding and fetal transfer were detected.<sup>206</sup>

**4.1.4. iRGD for Imaging and Theranostic Applications.** iRGD has also been used in tumor imaging to improve the poor tumor specificity of nanoprobe.<sup>207,208</sup> In 2017, Liu *et al.* developed a nanosystem composed of NIR inorganic quantum dots (QDs) and a membrane-impermeable etchant (cation donor) to apply selective background quenching and obtain tumor-specific signals.<sup>207</sup> Specifically, upon the intravenous administration of the QDs in combination with iRGD in mice bearing orthotopic breast and pancreatic tumors, the QDs are quenched by the etchant through cation exchange, which facilitates the renal clearance of metal ions from the QDs. This leads to a high tumor-specific signal provided by the intact QDs remaining in the extravascular tumor cells and fibroblasts (Figure 6).<sup>207</sup>

Theranostic NM systems in which therapeutic payloads are combined with diagnostic imaging modalities in a single probe have also been studied upon coadministration with iRGD. Wang *et al.* developed dual-labeled iRGD-modified multifunctional porous inorganic silicon NMs (Psi NMs) and loaded them with sorafenib (a hydrophobic antiangiogenic drug) to

enhance drug dissolution rate and improve cancer therapy.<sup>209</sup> These NMs were further radiolabeled with <sup>111</sup>In to monitor their *in vivo* biodistribution by single photon emission computed tomography (SPECT) in metastatic prostate cancer mouse xenograft models, and their long-term biodistribution were studied by fluorescent labeling *ex vivo*. They found that iRGD-conjugated NMs were associated with enhanced tumor uptake and thereby increased tumor growth suppression.<sup>209</sup>

**4.1.5. Debate.** Co-administration of iRGD with NMs is associated with several added advantages over their chemical conjugation. First, the transport capacity of the carrier system is mostly based on the available number of NRP-1 receptors on the endothelial cells. The transport of conjugated NM is for this reason limited by the relatively low number of target receptors on the endothelial cells that can be reached by the peptide-bound NMs. Co-administered iRGD on the other hand leads to a bulk transfer of NM to the tumor site. Second, free iRGD has an antimetastatic activity due its regulation of the integrin function, and finally, free iRGD is more practical for clinical use because the conjugation step can be complex and expensive.<sup>201</sup>

Despite the high potency demonstrated by the use of iRGD for the enhanced tumor delivery of NMs, this transcytosis strategy has remained somewhat controversial, mainly due to the discrepancy between the reproduction study performed by Mantis *et al.*<sup>210</sup> and the original report by Sugahara *et al.*<sup>194</sup> In contrast to the original data that showed enhanced DOX penetrance, coadministration of the iRGD peptide did not have an impact on the permeability of free DOX in a xenograft model of prostate cancer.<sup>210</sup> In other studies, however, an impact on permeability was clearly observed.<sup>194,201–205,207</sup> The apparent discrepancy among these different reports can be explained by the fact that the replication study used free DOX instead of DOX combined with NMs, suggesting that the iRGD system may be most effective for NM delivery rather than the delivery of free drugs. Additionally, the purity and quality of the iRGD peptide which was used in the replication study is not clearly stated, which could also have a clear impact on the contradictive results of their data. Lastly, the level of  $\alpha_v\beta_3$  integrins and NRP1 on tumor-associated blood vessels is linked with differences in tumor growth, angiogenesis, and hypoxia and can therefore differ for the same tumor type between different studies, significantly impacting the extent of on-target NM delivery.

#### 4.2. Multiple Peptides: Finely Tuning NM Functionalization for Targeted Delivery

The classical method of active targeting involves the functionalization of NMs with one particular type of ligand against a cancer-related epitope. Table 2 highlights various studies performed between 2005 and 2020 that used peptide/antibody coating for active targeting and in which the tumor targeting efficiency was properly evaluated. It shows that three targeting moieties (folate, Fa; transferrin, Tf; hyaluronic acid, HA; EGF; HER2) that are very frequently used, without any moieties proving to be clearly superior in terms of targeting efficiency. As most epitopes are not unique to the cancer cells but are rather overexpressed, and cancer-related epitopes are not easily found by blood-bound NMs, this one-ligand targeting strategy typically results in a poor targeting efficacy. To overcome this issue, several groups have looked into optimizing targeted delivery by means of multiple ligands. In this section, we discuss several recent studies that have used

dual-targeting for improved tumor-specific NM delivery, namely in breast and brain glioma tumor models, some of which have also incorporated iRGD into their delivery strategies.

##### 4.2.1. Dual-Ligand Targeting in Breast Cancer.

Doolittle and colleagues investigated the effect of organic liposomes loaded with peptides targeting P-selectin (cell adhesion molecule on surfaces of activated endothelial cells) and  $\alpha_v\beta_3$  integrin receptors on the spatiotemporal changes of the expression patterns of these receptors in breast and triple negative breast (TNB) mouse tumor models (Figure 7).<sup>211</sup> P-selectin and  $\alpha_v\beta_3$  integrin are functionally linked to different stages of development of metastatic disease, and as such, the authors found that these dual-ligand liposomes had the ability to capture different metastatic sites in the same animal which had an overexpression of both receptors.<sup>211</sup> In a study pertaining to gene delivery in TNB cancer, lipid-coated and siRNA-loaded calcium phosphate (LCP) NMs were further conjugated with folic acid and/or EGFR-specific antibodies to enhance therapeutic siRNA cellular uptake and transfection efficiency both *in vitro* and *in vivo*.<sup>212</sup>

The potential of a dual-targeted pH-sensitive DOX pro-drug (DP) organic microbubble complex (DPMC) in US-assisted antitumor therapy was studied by Luo and colleagues.<sup>213</sup> The DP was composed of a succinylated-heparin carrier conjugated with DOX *via* hydrazine linkage and was further linked with dual targeting ligands Fa and iRGD and with a microbubble (MB) *via* an avidin–biotin bridge. The subsequent sonoporation and cavitation using US disrupted aggregates and resulted in a uniform size distribution of the NMs, which then led to an improved DPMC intracellular accumulation and therapeutic efficiency. These US-exposed DPMCs were able to target angiogenic endothelial cells in the tumor region using  $\alpha_v\beta_3$ -mediated recognition, which further facilitated the specific binding to tumor cells by the Fa receptor recognition. DPMC in combination with US exhibited increased tumor specificity and toxicity against breast cancer cells *in vitro* compared to free DOX and DP and resulted in higher tumor inhibition rates in breast cancer xenograft-bearing mice by inducing apoptosis and inhibiting cell proliferation and angiogenesis.<sup>213</sup>

**4.2.2. Dual-Targeting of Brain Glioma.** One of the most difficult challenges in oncology is the treatment of brain glioma as drugs must be transported through the blood–brain barrier (BBB) to specifically reach the brain and reduce off-target delivery and side effects on normal tissue. These drugs must also target brain cancer cells because most of the antitumor drugs are also toxic to normal brain tissue. Glioblastoma multiforme (GBM) is known to be the most malignant brain tumor in the central nervous system with extensive cell proliferation and angiogenic properties. One of the strategies aimed at overcoming this poor drug penetration and accumulation is the use of functionalized nanocarriers with different targeting ligands. To date, there only exists a few studies that investigate effect of dual-targeting of NMs on BBB crossing and brain tumor targeting by mainly using organic lipid and polymeric NMs and liposomes.<sup>214,215</sup> Gao and colleagues used a phage-displayed TGN peptide and an AS1411 aptamer against the BBB and cancer cells, respectively.<sup>215</sup> These ligands were conjugated to organic PEG-poly(*ε*-caprolactone) NMs to form a brain glioma cascade delivery system (AsTNP) loaded with docetaxel, significantly improving tumor growth inhibition and survival of glioma-bearing mice.<sup>215</sup> A few years later, the authors

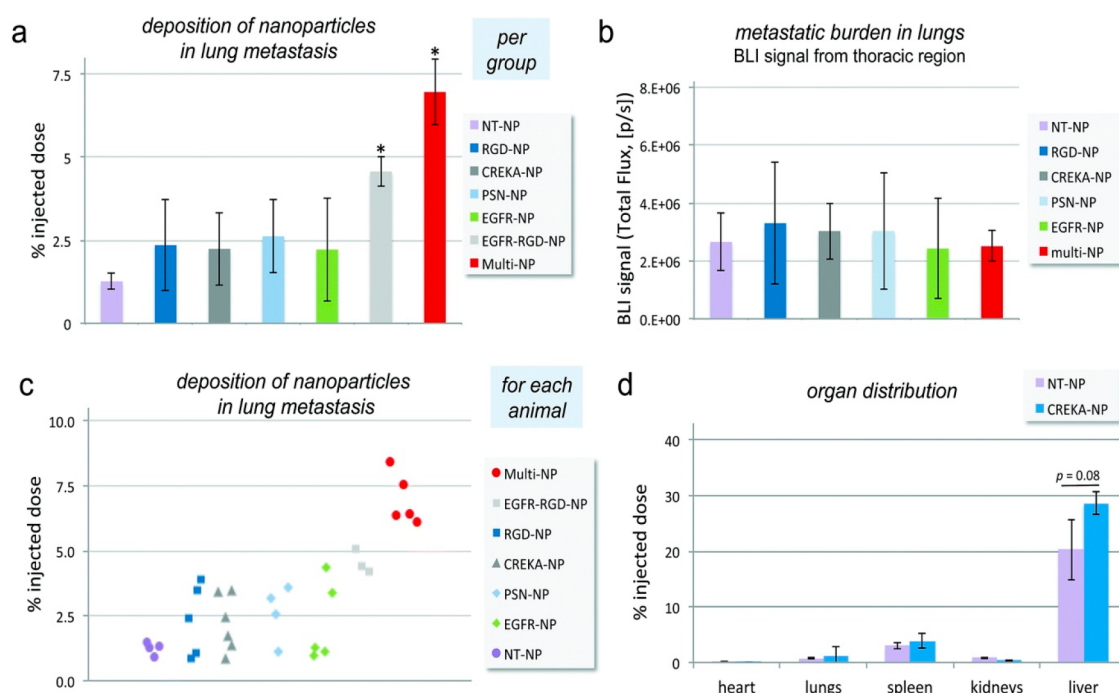


**Figure 8.** Quantitative evaluation of the ability of the nanoparticle targeting variants to target metastasis in the 4T1 mouse model. (a) Each formulation was systemically administered *via* a tail vein injection at the same dose (NT-NP indicates the nontargeted nanoparticle). The fluorescence signal of the fluorescence images of the lung sections was quantified for each formulation at 3 h after injection ( $n = 5$  mice). On the basis of phantom measurements of each formulation using the IVIS imaging system, the fluorescence signal was converted to nanoparticle concentration (mean  $\pm$  SD; \* indicates  $p < 0.05$  by Student's *t* test;  $n = 4$ –6 mice per group). (b) Bioluminescence signal from the thoracic region of each animal was quantified and summarized for each group, representing the metastatic burden of the different groups used in the targeting studies. Data are presented as mean  $\pm$  SD. (c) Nanoparticle deposition of the nanoparticle targeting variants in lung metastasis is presented separately for each animal. (d) Organ distribution of NT-NP and CREKA-NP was evaluated in the 4T1 mouse model ( $n = 5$ ). Reproduced with permission from ref 227. Copyright 2018 Royal Society of Chemistry.

developed organic polymeric NMs functionalized with iRGD and IL-13 to target  $\alpha v \beta 3$  on neovasculature and IL13R $\alpha 2$  on GBM cells, respectively.<sup>216</sup> Another dual-targeting liposomal system was modified with T7 and cell-penetrating peptide (CPP) TAT that enhanced the targeting of the brain glioma tumor and transport across the BBB, respectively.<sup>217</sup>

Several other groups have also used iRGD as part of a dual-targeting mechanism. Chen *et al.* screened organic liposomes containing one of six peptide-based ligands that are widely used for brain delivery (Pep-1, D-SP5, Angiopep-2, T7, Peptide-22, and iRGD) for optimal targeting ability across the BBB and into the tumor tissue.<sup>218</sup> On the basis of this screening, iRGD and Peptide-22 dual-modified liposomes were selected for further *in vivo* testing and showed significant inhibition of glioma growth.<sup>218</sup> Co-modified lactoferrin- and iRGD dual-ligand, Temozolomide and vincristine-co-loaded nanostructured organic lipid carriers (L/RT/V-NLCs) were also developed as combination therapy for GBM. These nanosystems exhibited sustained-release behaviors, high synergy, and cytotoxicity effects, increased drug accumulation in the tumor tissue and cellular uptake and significant tumor inhibition with low systemic toxicity, and thus serve as promising delivery systems for glioblastoma chemotherapy.<sup>214</sup>

**4.2.3. Use of Dual Ligands in Other Tumor Models.** Levine and colleagues<sup>219</sup> developed dual-targeted heteromultivalent PEGylated liposomes conjugated with different ratios of fibronectin-mimetic peptide (PR<sub>b</sub>) and AG86, which in turn bind cancer biomarkers  $\alpha 5 \beta 1$  and  $\alpha 6 \beta 4$  integrin, respectively, and investigated their delivery to cancer cells with different

integrin concentrations. On 20 different cell lines, the expression of these cancer biomarkers were quantified to determine the appropriate *in vitro* model system, and the results showed that liposomes with equal ligand valencies showed an improved selectivity and binding for cancer cells with equal and high levels of receptor expression, such as the human ovarian cancer SKOV3 cell line, and thereby increased internalization of encapsulated DNA.<sup>219</sup> In another gene delivery study, organic PEG-phosphatidylethanolamine (PE) NMs were linked with Tf and Fa separately to form Tf-PEG-PE and Fa-PEG-PE ligands to improve gene delivery to the liver in hepatocellular carcinoma-bearing mice, and found a 30% increase in transfection efficiency compared to single and nontargeted NMs.<sup>220</sup>

In 2013, Cheng *et al.* have also aimed to improve targeting to the liver by incorporating chitosan into organic polymeric NMs composed of lactic acid and glycyrrhetic acid (GCGA), as chitosan has been shown to possess liver-targeting abilities *via* the interaction between galactose and asialoglycoprotein receptor on healthy and cancerous liver tissue. These NMs were further conjugated with the thymidylate synthase inhibitor 5-fluorouracil (5-FU), which has been commonly used as an anticancer agent for various solid tumors, although in the absence of targeted delivery, its systemic administration has been associated with numerous toxic effects including bone marrow suppression, mucositis, diarrhea, among others.<sup>221</sup> GCGA/5-FU NMs were shown to enhance NM accumulation in the liver and gradually release 5-FU, successfully suppressing tumor growth in orthotopic liver transplantation mouse



models and improving survival.<sup>222</sup> In another study, Chen *et al.* tested the targeting of both osteosarcoma and cancer stem cells (CSC) with salinomycin-entrapped organic lipid-polymer NMs, which were labeled with CD133 and EGFR aptamers (CESP), and found that CESP had a significantly higher cytotoxicity to both cell types than single targeting or nontargeted NMs. *In vivo* administration of this dual-targeted NM resulted in improved efficacy of tumor growth inhibition in osteosarcoma-bearing mice.<sup>223</sup> For the *in vitro* and *in vivo* evaluation of the treatment of lung cancer, NMs were loaded with Fa and Tf modified cisplatin (CDDP) to improve the delivery of cisplatin to tumors. These FA/Tf-CDDP-NMs resulted in enhanced tumor inhibition and increased accumulation in tumor tissue *in vivo* and *in vitro* compared to free drugs, as well as a near-full suppression of tumor growth without any significant changes in animal body weight.<sup>224</sup>

Several research groups have also incorporated iRGD into their dual-targeting strategies, such as Jang and colleagues,<sup>225</sup> who developed inorganic nanographene oxide (nGO) NMs conjugated with Fa and iRGD using noncovalent interactions that allow for the precise control of ligand numbers on the nGO surface as well as ensure stability under physiological conditions. KB cells (HeLa subline) which overexpress folate and integrin  $\alpha v \beta 3$  receptors were used to evaluate the *in vitro* tumor targeting abilities of single- and dual-ligand coated nGOs and exhibited a double increase in the uptake of dual-ligand nGO compared to single targeted nRGD-nGO or FA-nGO. Subsequent *in vivo* biodistribution experiments in mouse xenograft models showed a significantly higher tumor accumulation of iRGD-FA-nGO compared to single targeting, leading to the total ablation of the tumor tissue when combined with NIR laser irradiation for photothermal therapy.<sup>225</sup> In an earlier study, Xu *et al.*<sup>226</sup> designed organic hyperbranched amphiphilic polymeric peptides (HPAE-co-PLA/DPPE) surface-functionalized with iRGD and Tf and loaded with paclitaxel. The presence of iRGD and Tf improved the cytotoxic efficiency of the NMs by 10-fold and 2-fold in  $\alpha v \beta 3$ -overexpressed human umbilical vein endothelial cells and Tf receptor-overexpressed human cervical carcinoma cells, respectively, *in vitro*.<sup>226</sup>

**4.2.4. Multiple Ligands.** Metastasis consists of a heterogeneous, continuously evolving cell population, and because of the change in expression of the targetable biomarkers on these cancer cells, single-ligand NMs are not effective in this context and instead require multiple ligands to be incorporated into the formulation. Peiris *et al.*<sup>227</sup> used multiligand liposomal NMs that target metastatic disease biomarkers including EGFR, fibronectin, P-selectin, and  $\alpha v \beta 3$  integrin on the endothelium. *In vivo* and terminal imaging studies were performed to detect the targeting performance of single- and dual-ligand NMs compared to these multiligand NMs in breast cancer tumor mouse models. Dual-ligand NMs showed 2-fold higher deposition into the lung metastases compared to single-ligand NMs, while the multiligand NMs achieved about 7% deposition of the injected NMs to lung metastases (Figure 8).<sup>227</sup>

Many of the drug target sites are located within intracellular organelles or in the cytosol, and only after reaching their target site of action, these drugs can exert their pharmacological effect. Maximum therapeutic efficacy and minimum side effects can be achieved when the drug is delivered specific to these organelles. As such, Chen *et al.* designed mitochondrial-targeted multifunctional NMs (MNM) based on chitosan

derivatives possessing different functions such as hepatocyte targeting, stealth, multistage pH-response, mitochondrial targeting, and lysosomal escape.<sup>228</sup> These formulations were loaded with brucine (natural anticancer drug) and surface-modified with glycyrrhetic acid (GA) to boost cellular internalization. Once inside the cell, these NMs are able to escape the endosomes due to a proton influx facilitated by the imidogen on the MNM surface. Lastly, the highly positive charge of these MNMs causes them to aggregate at the mitochondria *via* electrostatic interactions. As such, the shedding of each of these factors results in targeted drug release, efficient intracellular delivery and mitochondrial localization, inhibition of tumor growth, enhancement of antitumor efficacy, and reduction of anticancer drug toxicity.<sup>228</sup>

**4.2.5. Conclusion.** Given the improvement in NM delivery observed in the various studies wherein NMs are conjugated with ligands that target different elements along the NM journey to the tumor, this targeting strategy has proven to be promising in the advancement of cancer therapy and nanomedicine. The physicochemical characteristics and effect of surface distribution of dual ligands on the cellular uptake of (in)organic NMs has also been investigated using dissipative particle dynamics simulations, and the results suggest that cellular uptake of the NMs is improved by the spontaneous rearrangement (from a random pattern to an organized pattern) of the dual-ligand on the surface of the NMs. Interestingly, study analyses show that the ligand rearrangements are restricted by their short length and that NMs coated with short dual ligands are not able to wrap the cell membranes fully, except if these ligands are separated from the beginning on the NM surface. At the same time, the enhancement of the uptake efficiency by dual-ligand targeting is not possible if there is a nonspecific interaction or a length mismatch between the dual ligands.<sup>229</sup>

Colombo and colleagues further demonstrated the significance of controlling the amount of antibodies attached to the NM surface, as these can significantly interfere with NM surface properties and size.<sup>230</sup> In other words, increasing the number of surface-functionalized ligands does not necessarily entail improved targeting and therapeutic efficacy. In their study, inorganic gold NMs conjugated with two trastuzumab antibodies (antineoplastic agent) exhibited improved targeting *in vitro*, whereas NMs with a single ligand showed better targeting in a subcutaneous MCF-7 breast cancer mouse model.<sup>230</sup> As such, dual-ligand targeting is somehow controversial because of the complex interplay among multiple factors such as the densities of the dual ligands, ratios, length matching, type of ligands, among others, all of which significantly affect NM behavior.<sup>231</sup>

## 5. MAGNETIC GUIDANCE OF MAGNETIC PARTICLES

Targeted NM delivery can also be performed by magnetically guiding magnetic NMs to specific tissues within the human body while still exploiting the EPR effect and thereby the passive accumulation of NMs in solid tumors. As previously explained, this passive NM accumulation varies according to different tumor vascularization and tissues, which could influence magnetic targeting.

In 2016, a series of studies were performed by Bai *et al.*, wherein they developed oil-cored polymeric nanocapsules (m-NCs) encapsulating inorganic SPIONs and NIR dye ICG for negative magnetic resonance (MR) contrast and fluorescence imaging, respectively.<sup>232</sup> The oil core allowed for the high

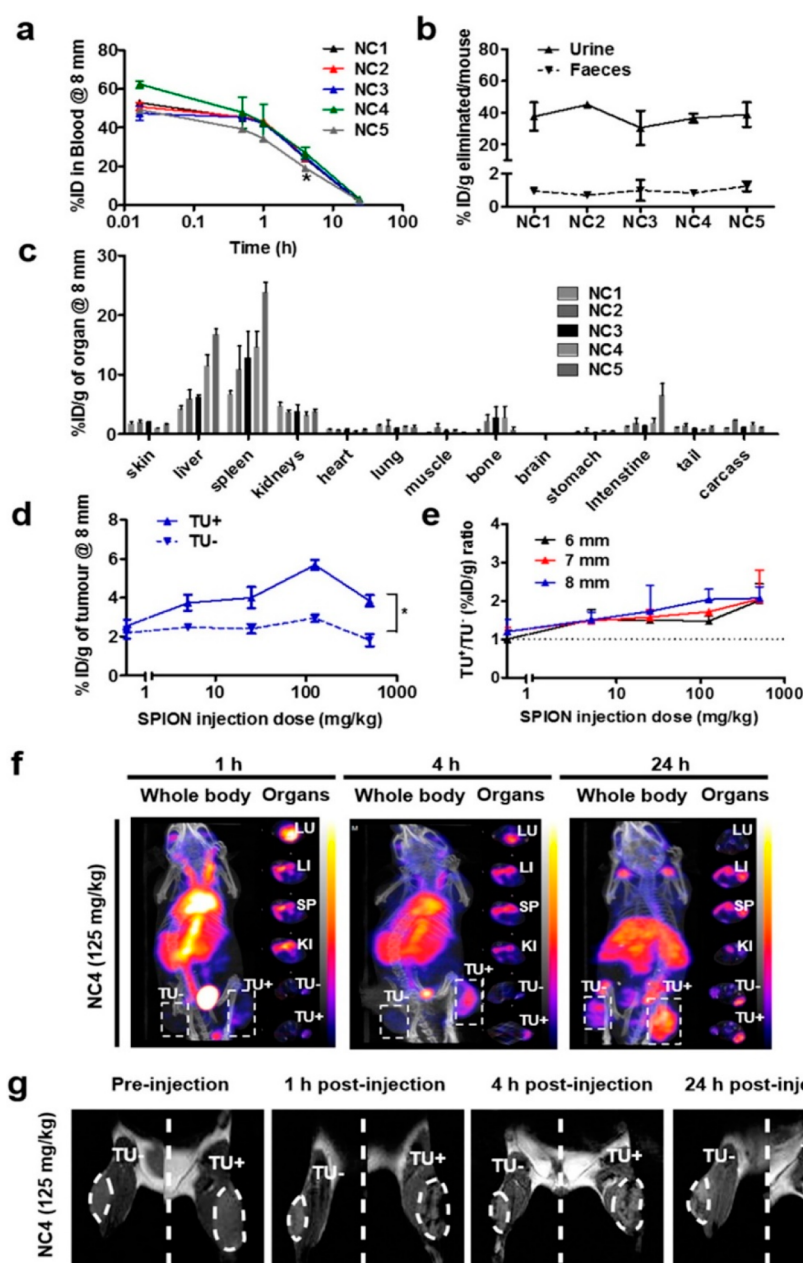


**Figure 9.** *In vivo* magnetic targeting assessment of m-NC-111In with increasing amounts of SPION in CT26 tumor-bearing BALB/c mice under the influence of an 8 mm diameter magnet (0.43 T). Mice were iv injected with indium-111 labeled NC 1–5. A permanent magnet (0.43 T, 8 mm in diameter) was applied at one tumor site (TU+) for 1 h, and organs were excised at 24 h postinjection. (a) Blood clearance profiles. (b) Excretion profiles. (c) Organ biodistribution profile. (d) Tumor accumulation profiles. (e) Magnetic targeting efficacy. (f) *In vivo* single-photon emission computed tomography-computed tomography (SPECT-CT) imaging of m-NC 4–111In. (g) *In vivo* T2-weighted MR imaging of m-NC 4–111In. Cross sections in (f) were from lung (LU), liver (LI), spleen (SP), kidney (KI), nonmagnetically targeted tumor (TU-), and magnetically targeted tumor (TU+) at equivalent time points. Tumors in (f) and (g) are marked in dashed lines. Results are expressed as % ID/g of organ as mean  $\pm$  SEM ( $n = 3$ ). One-way ANOVA was performed using IBM SPSS Statistics software followed by Tukey's multiple comparison test (\*,  $p < 0.05$ ; \*\*,  $p < 0.01$ ). Reproduced with permission from ref 233. Copyright 2016 American Chemical Society.

hydrophobic SPION loading. These NMs were then radio-labeled with indium-111 for nuclear imaging, resulting in a triple-modal *in vivo* imaging system. To test the efficiency of their NMs, the authors administered them intravenously in colon carcinoma-bearing mice and found a 3- and 2-fold increase in tumor uptake after 1 and 24 h, respectively, compared to passively targeted NMs.<sup>232</sup> In a follow-up study, the authors aimed at determining the key parameters affecting the efficacy of magnetic targeting using mathematical modeling and computation of the magnetic, viscoelastic, convective, and

diffusive forces influencing m-NC behavior and extrapolating this murine data to human contexts. In similar colon carcinoma-bearing mice, they found that magnetic targeting efficiency was directly correlated with SPION loading and strength of the magnetic field, although extremely high SPION loading resulted in lowered blood circulation and static targeting efficiency. On the basis of their calculations, they concluded that the parameters applied to these murine models is sufficient for efficient targeting in humans. An *in vivo* murine tumor growth delay study was also performed with docetaxel

(DTX)-encapsulated m-NCs, which showed enhanced therapeutic efficacy and improved mouse survival due to magnetic targeting (Figure 9).<sup>233</sup> In a parallel study, the behavior of these m-NCs inside blood vessels and tumor tissues were investigated and visualized using fibered confocal fluorescence microscopy (FCFM) before, during, and after magnetic field exposure. Their results show that the m-NC distribution within the tumor vasculature significantly differed in the presence and absence of the magnetic field. Specifically, when the tumors were exposed to the magnetic field, the m-NCs concentrated as clusters near the blood vessel walls without causing any vascular disruptions. By using the FCFM imaging technique, it was possible to detect the real-time, *in vivo in situ* microvascular behavior of m-NCs during magnetic targeting using high spatial resolution in a minimally invasive manner.<sup>234</sup> Lastly, the authors investigated whether tumor and thereby vascular heterogeneity affects the magnetic guiding and targeting of m-NCs by administering these NMs in different murine tumor models, including breast, lung, colon, and melanoma. Gamma counting was used to assess the passively and magnetically driven tumor accumulation of these radio-labeled m-NCs. They showed that tumor permeability and microvessel density and diameter significantly affected passive and magnetic tumor targeting and accumulation. However, these vascular parameters played different roles when the m-NCs were targeted to the tumor with different strategies. While tumor permeability was seen to be rate-limiting in both methods, microvessel diameter mainly influenced passive targeting, and its density mainly influenced magnetic targeting.<sup>235</sup>

Many other research groups have also exploited the magnetic properties of iron oxide-based NMs to improve NM delivery to solid tumors. Nigam *et al.* used DOX-loaded inorganic dendritic Fe<sub>3</sub>O<sub>4</sub> NMs to study their magnetically guided delivery to tumor sites and potential to cause an impairment of melanoma growth *in vivo*. They detected in the tumor-bearing mice higher NM localization in the tumor due to magnetic guidance compared to passive localization. High concentrations of iron and DOX were detected in the tumor, which caused significant tumor regression and tumor growth arrest. Furthermore, 20 days post-treatment, the tumor was fully eradicated and about 100% survival rate was detected.<sup>236</sup> The group of Yang synthesized inorganic magnetic-fluorescent Fe<sub>3</sub>O<sub>4</sub>/SiO<sub>2</sub> NMs with a radioisotope rhenium-188-labeled graphene oxide (GO)-modified core-shell as nanocarriers for gambogic acid (GA), a potent anticancer agent.<sup>237</sup> Their results show a pH-dependent GA release from the NMs, with higher release rates in acidic environments, as well as varying *in vivo* biodistributions between peanut-shaped and spherical NMs, where peanut-like NMs tended to accumulate in the spleen, lung, and liver. Compared to nontargeted therapy, targeted therapy showed higher efficacy in the inhibition of tumor cell growth.<sup>237</sup>

Alev and colleagues investigated *in vitro* whether encapsulating mitoxantrone (MTO) within SPIONs diminishes its antitumor activity as an immunogenic cell-death (ICD) inducer, which, when systemically administered *in vivo*, impairs the immune system of the patient.<sup>238</sup> The results showed that these MTO-loaded SPIONs indeed caused ICD and the maturation of dendritic cells to the same extent as the free drug. The magnetic targeting efficiency of these constructs was confirmed in dynamic flow systems that mimic blood circulation. They conclude that magnetically targeting MTO

to the tumor site can lead to the successful modulation of the TME by locally activating the immune response and minimizing off-target cytotoxicity.<sup>238</sup> These results confirm earlier reports of unaffected MTO antitumor activity as a result of their encapsulation within SPIONs. These earlier studies also showed reduced MTO uptake in circulating leukocytes *in vivo*,<sup>239</sup> improved accumulation to the tumor by more than 50% of the injected dose as well as animal survival,<sup>240</sup> and significant tumor size reduction<sup>241</sup> due to the improved tumor targeting resulting from the application of an external magnetic field.

Alternating magnetic fields have also been used to produce heat for hyperthermia or to release thermosensitive-bound drugs, but this method has mainly been applicable to treat superficial tumors. Accordingly, Roeth and colleagues aimed at translating this strategy to an endoscopic setting and reach tumors deep within the body.<sup>242</sup> They built a biophysical model to find the ideal endoscopic magnetic field trap that accumulates the most SPION. By simulation, they were able to enhance the efficiency of the magnetic field traps by 38-fold in prostate and 8-fold in esophageal cancer models. Their method was able to reach tumors inside the body in a minimal-invasive way.<sup>242</sup> In another study, the group of Zhang<sup>243</sup> developed a novel real-time imaging-based guidance system with the aim of improving SPION transport across the BBB and into brain tumor regions.<sup>243</sup> They used an electromagnetic actuator and low-amplitude-excitation-field magnetic particle imaging (MPI) for the simultaneous noninvasive NM guiding and tracking inside a tube.<sup>243</sup> Both of these proposed systems are yet to be applied to *in vivo* tumor models for confirmed efficiency.

Finally, it is important to consider that for magnetic targeting, the magnetic properties and external field strength must be sufficiently strong to achieve the desired effects. The exact numbers will depend on the size of the region to be targeted and entire individual, as well as the chemical composition of the materials themselves. Other important factors are also the shape, surface coating, and size of the NMs, which all affect the saturation magnetization, magnetic anisotropy, magnetic structure, and magnetic behavior of the NMs. At the same time, these parameters also influence general biodistribution and blood clearance rates, and more detailed studies are required that look into the delicate fine-tuning of optimal NM parameters for enhanced tumor delivery by magnetic guidance.

## 6. BIOLOGICAL METHODS TO IMPROVE NM DELIVERY TO TUMORS

Although the previously discussed methods such as the EPR effect and the use of active targeting ligands and polymeric NMs have been shown to exhibit some improvement in NM delivery, a large proportion of these particles are still cleared by the reticuloendothelial system (RES), while only a small subset of NPs are able to reach the TME, limiting the clinical translation of these materials. Thus, the ability to evade the RES is a key element in designing a delivery system that is capable of remaining in blood circulation for a long period of time to allow the proper application of the EPR effect and the efficient NP accumulation within solid tumors. One transpiring approach is to exploit the natural ability of circulatory cells to evade the immune system and transport themselves to specific, vascular, or systemic locations around the body and cross biological barriers that are otherwise nearly impermeable.<sup>244</sup>



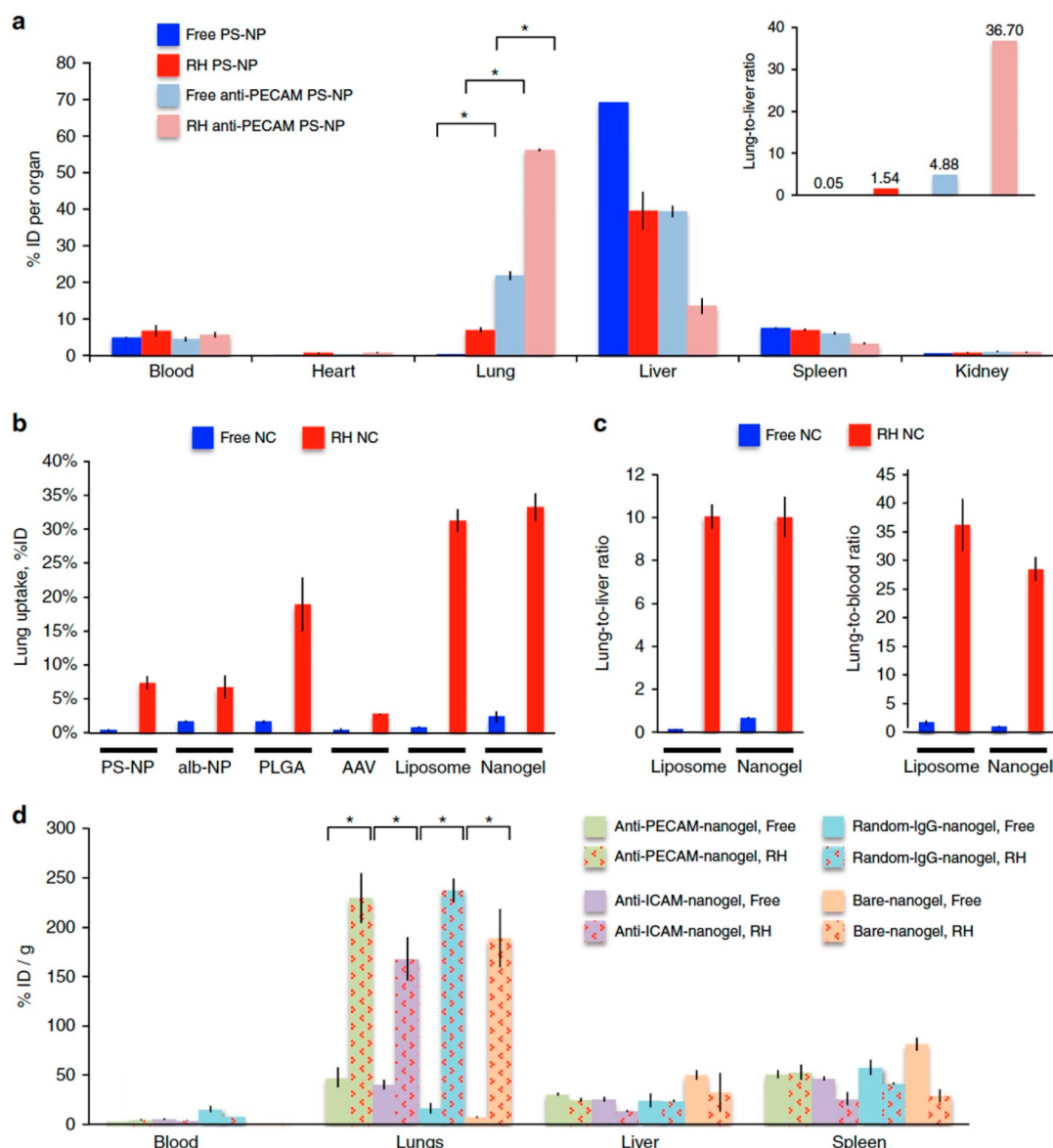


**Figure 10.** (a) Polystyrene NPs (PS-NPs) were covalently coated with either IgG or anti-PECAM lung affinity moieties, labeled with trace amounts of I-125-IgG and IV injected into mice either alone or hitchhiked onto RBCs (R-H). Shown is the percent injected I-125 dose (%ID) for each organ, as well as the lung-to-liver %ID ratios for each group. (b) %ID in the lungs for the different types of nanocarriers (NCs) either freely administered or adsorbed onto RBCs. (c) Lung-to-liver and lung-to-blood ratios for the RH NCs that displayed the highest lung uptake (liposomes and nanogels). (d) %ID per organ for mice injected with free or RH nanogels that were either bare or coated with random rat IgG, anti-PECAM, or anti-ICAM. Reproduced with permission from ref 253 Copyright 2018 Nature Publishing Group.

Besides their stealth properties, these circulatory cells possess unique structures and surface ligands that provide them with tumortropic properties, further improving the reach of cell-associated NPs to tumors. They also have the capacity to hold a large number of NPs and any associated drugs, thereby increasing the concentration of therapeutic agents at the target sites. In this section, we provide an overview of the various biological methods that use cell-based therapy for improved NP delivery, including hitchhiking of NPs on a wide variety of cell types, coating the NPs with cell membranes, loading NPs into extracellular vesicles, and the use of attenuated non-immunogenic bacteria.

### 6.1. Cell-Mediated Delivery

One method of improving NP homing to tumors is through a cellular “hitchhiking” process, in which NPs are conjugated

onto the surfaces of circulatory cells or encapsulated within them, a mechanism also known as “Trojan Horse” as a result of the triggered NP release from the intracellular environment at the tumor site. There exist advantages and disadvantages to both forms of NP delivery, which will be discussed in this section. Understanding the structure, surface properties, and the resulting distinct cellular functions associated with each circulatory cell type is key in designing an effective tumortropic “supercarrier”-NP formulation.

**6.1.1. Red Blood Cells.** RBCs are produced in the bone marrow and function as natural transporters of nutrients and oxygen throughout the body *via* hemoglobin. They are one of the most researched biological drug delivery systems due to their clinical safety of transfusion,<sup>245</sup> abundance in the blood (~20 trillion), lengthy circulation time (~3 months),<sup>246</sup>

biconcave shape that provides a large surface area for the carriage of various compounds, and flexibility that allows them to reversibly deform while navigating through smaller blood vessels. Their surface self-marker CD47 allows them to remain cloaked from the immune system, providing them with their stealth properties.<sup>247,248</sup> Additionally, RBC membranes are slightly negatively charged and host a wide variety of proteins that allow easy surface modifications and functionalizations to be made.<sup>249</sup> As such, conjugating NPs onto the surface of RBCs or encapsulating them within the cells results in the circumvention of several issues inherent to NPs, such as their short circulation time and rapid clearance by the RES.<sup>250</sup> In fact, polystyrene NPs attached to the surface of RBCs have been shown to remain in blood circulation for over 10 h in rats compared to the 5 min circulation exhibited by the free NPs<sup>251</sup> and to avoid homing to the liver and spleen in a follow-up study in mice.<sup>252</sup> At the same time, Brenner *et al.* reported the significantly increased accumulation of RBC-hitchhiked NMs (particularly liposomes and nanogels) in different organs compared to freely administered NMs (Figure 10) and showed that an intracarotid artery injection of an RBC-hitchhiking regimen delivers a 10-fold higher number of polymeric NPs to the brain compared to affinity moieties such as transferrin.<sup>253</sup>

The ability of RBCs to modify the pharmacokinetic properties of hitchhiking NPs and improve their distribution in the blood and tissues has led to the development of a wide variety of RBC engineering strategies to improve tumor homing of various NMs. For instance, functionalizing PEGylated and Ce6-grafted (photodynamic agent) poly-(allylamine hydrochloride) (PAH)-coated magnetic iron oxide NPs (IONPs) onto the surface of RBCs has shown to improve not only the circulation time of the NPs *in vivo* but also their tumor-homing abilities under a certain magnetic field, significantly improving their efficacy as theranostic agents.<sup>254</sup> The resulting synergistic effect of the photodynamic and chemotherapy of the 4T1 murine tumor model led to a significant inhibition in tumor growth compared to either therapy alone. Magnetic IONPs have also been encapsulated within RBCs, where the resulting magnetization due to the asymmetric distribution of the NPs within the cells has been exploited to magnetically guide the cells throughout the body using acoustic propulsion.<sup>255</sup> The ability of the RBCs to shield the IONPs from the etching ions in the blood and from being uptaken by macrophages renders them a promising hitchhiking tool for delivery to tumors. Besides IONPs, other inorganic NPs that have been used in the context of RBC-based therapy include upconversion NPs (UCNPs), which are being widely explored for their potential use in *in vivo* fluorescence imaging due to their ability to convert NIR light to the visible range. For instance, lanthanide-doped UCNPs that have been conjugated onto the surface of RBCs were able to significantly inhibit tumor volumes by 90% over 3 weeks compared to other control groups.<sup>256</sup> RBCs harboring magnetic NPs and tumor-targeting folic acid on their surfaces were able to capture circulating tumor cells (CTCs) with high efficiency (~93%) and purity (>75%) compared to MACS beads (80% and 20%, respectively), with the resulting CTC-RBC complexes being isolated using a magnetic field.<sup>257</sup>

Various studies have also used organic NPs as RBC hitchhikers. Sun *et al.* developed a smart RBC system containing doxorubicin and bovine serum albumin nano-complexes for the chemo- and photothermal therapy of glioblastoma cells, respectively.<sup>258</sup> These RBCs were further

functionalized with the active ligand RGD to target the integrins of the tumor angiogenic endothelium. Although this system was only tested in an *in vitro* setting as a proof-of-concept for the light-controlled release of NPs from the RBCs, a synergistic effect of the combination therapy could be observed, highlighting its potential anticancer efficacy *in vivo*. In another study, the surfaces of RBCs were functionalized with doxorubicin-loaded PLGA NPs, and the resulting RBC-NP complexes not only exhibited a 10-fold increase in circulation time compared to free NPs in mice bearing melanoma lung metastasis, but they also led to the significant inhibition of tumor growth and improved animal survival.<sup>259</sup> Interestingly, in another metastatic model of melanoma, Zelepukin *et al.* revealed that the improved lifetime circulation that is usually observed in the RBC-hitchhiking of large submicrometer agents is not seen for anionic sub-200 nm polymeric particles with various coatings.<sup>260</sup> However, they also show that even for such NPs with no extended circulation time, RBC-hitchhiking significantly improves their distribution throughout the body, with reduced accumulation in the liver and an increased homing to the lungs reaching a record high of 120-fold and resulting in a decrease of tumor nodes and slowed tumor growth. While the incorporation of RBCs into the therapeutic regimen provides the NPs with improved behaviors in biological systems, it is also important to understand the effects of NPs on the RBCs themselves to obtain a holistic overview of the bidirectional relationship between carrier and hiker and optimize the parameters accordingly. For instance, at similar loading concentrations of polystyrene NPs (PSNPs) and lysozyme-dextran nanogels (LDNGs) on the surfaces of mouse and human RBCs, PSNP-RBCs exhibited agglutination, stiffening, increased sensitivity toward osmotic, mechanical and oxidative stress, as well as increased surface exposure of phosphatidylserine (which enhances RBC clearance *in vivo*), whereas LDNG-RBCs did not exhibit any of the aforementioned behaviors.<sup>261</sup> Therefore, it is imperative to select the optimal RBC-NM combination for the successful translation of such constructs to the clinic.

**6.1.2. Monocytes and Macrophages.** Similar to RBCs, leukocytes are found in abundance in the blood (4–10 billion) and have long circulation times (20 days). They comprise the body's adaptive and innate immunity and are also being widely investigated as NP carriers due to their natural ability to overcome endothelial barriers and home specifically to the sites of disease and into hypoxic TMEs.<sup>262,263</sup>

Monocytes are produced in the bone marrow, circulate in the bloodstream, and penetrate deep within each organ in the body in the process of differentiating into tissue-resident phagocytic macrophages. In these tissues, macrophages detect and phagocytose apoptotic/necrotic cells, pathogens, and other foreign particles *via* specialized membrane receptors, and upon stimulation, are able to travel through inflammatory and hypoxic regions<sup>264,265</sup> as well as across the blood–brain barrier *via* diapedesis and chemotaxis.<sup>266</sup> As free NPs are mostly unable to reach these areas and TAMs may comprise up to 70% of tumor masses,<sup>267</sup> the natural ability of monocytes to be recruited to solid tumors can be exploited for NP delivery. One method that does not require any membrane modifications and prevents nonspecific interaction of NPs with nontarget tissue is the natural phagocytosis of NPs by monocytes, which, upon homing to the tumor site and differentiating into macrophages, are able to serve as “Trojan Horses” and release their cargoes deep within the hypoxic tumor regions in a controlled manner.

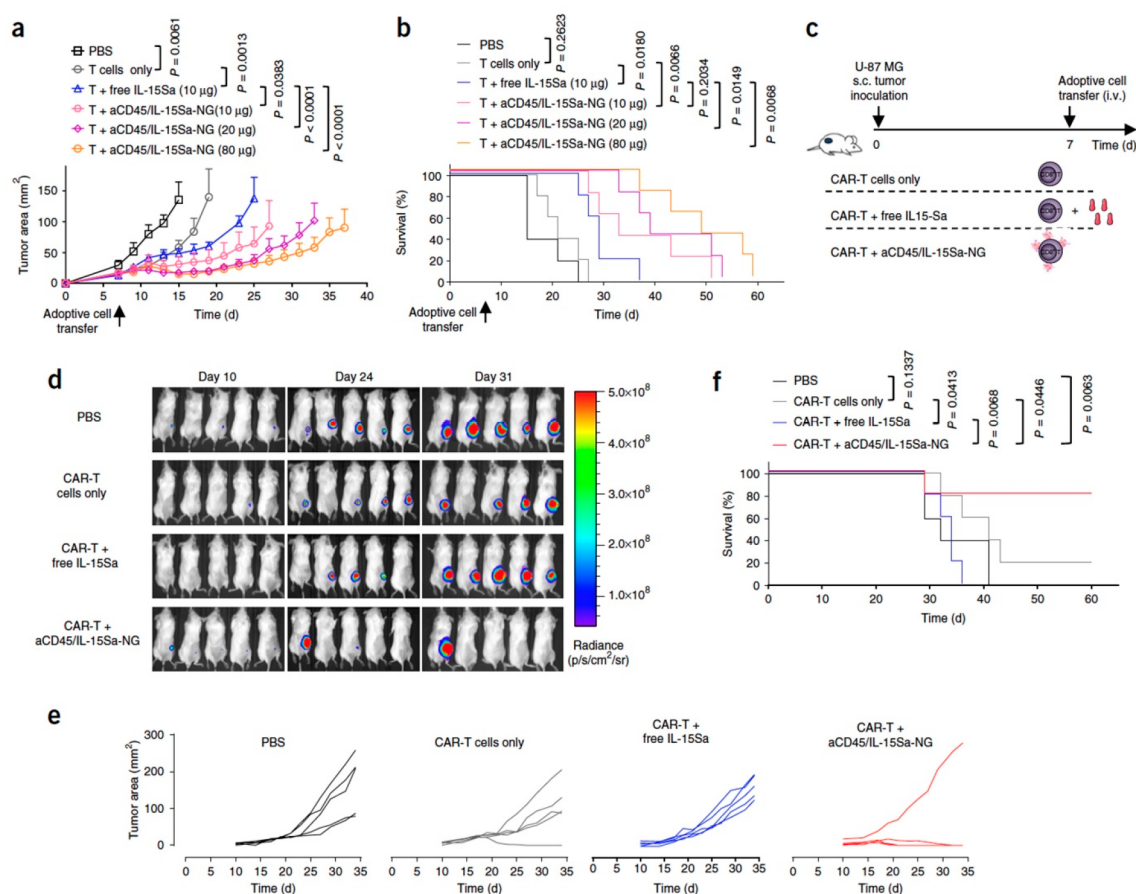


**Figure 11.** (a) Experimental timeline in which B16F10 melanoma tumor-bearing mice were sublethally lymphodepleted by irradiation and administered Thy1.1<sup>+</sup>CD8<sup>+</sup> T cells the next day either alone, with free interleukin-15 superagonist (IL-15Sa) or backpacked with protein nanogels carrying IL-15Sa and anchored by maleimide chemistry to T cell CD45 receptors (aCD45/IL-15Sa-NGs). Mice were sacrificed and tissues were processed and analyzed by flow cytometry 7 days later. (b) Flow cytometry graphs displaying the frequency of tumor-infiltrating T cells among all the lymphocytes for the different groups. (c–f) Number of adoptively transferred (ACT) and endogenous T cells in blood (c), nontumor draining lymph nodes (non-TDLNs, d), TDLNs (e), and tumors (f). (g) Ratio of counts of ACT T cells in the nanogel-treated group relative to the free IL-15Sa-treated group in the different tissues. (h–j) Counts of proliferation marker Ki67<sup>+</sup> (h), granzyme-B<sup>+</sup> (i), and polyfunctional (j) ACT T cells in tumors for the different treated groups. Reproduced with permission from ref 290. Copyright 2018 Nature Publishing Group.

Various types of organic and inorganic NMs have been loaded into monocytes/macrophages for their improved delivery to tumors. For instance, incorporating doxorubicin-containing PLGA NPs into monocytes significantly improved the biodistribution and reach of NPs to the tumor site in tumor-bearing mice, and the resulting complex was able to efficiently induce cocultured cancer-cell destruction.<sup>268</sup> In a similar study by Choi *et al.*, doxorubicin-containing liposomes were internalized within macrophages while preserving host activity and doxorubicin toxicity against tumor cells, and their subsequent administration in mice bearing lung metastasis xenograft tumors resulted in significant tumor growth inhibition.<sup>269</sup> Recently, intravenously injected chitosan-based micelles were shown to be selectively taken up by circulating monocytes in tumor-bearing mice and, upon the differentiation of these monocytes into macrophages, the micelles were exocytosed and subsequently internalized by the cancer cells.<sup>270</sup> In the context of inorganic NPs, doxorubicin-encapsulated graphene-oxide NPs were loaded in mouse macrophage-like cells, and the resulting construct exhibited improved homing toward a mouse prostate cancer model.<sup>271</sup> Upon irradiation with NIR light, doxorubicin was rapidly released into the TME, significantly inhibiting tumor growth.

In separate studies, gold nanoshell-loaded monocytes/macrophages were able to penetrate deep into the hypoxic centers of human breast tumor<sup>272</sup> and glioma cancer cell<sup>273</sup> spheroids and were further ablated by photothermal therapy upon irradiation with NIR light, exhibiting significant antitumor efficacy compared to the free nanoshells. Quantum dot hitchhiking onto macrophages is also being explored to label brain tumors preoperatively.<sup>274</sup>

Because internalization of NPs may lead to their endosomal degradation,<sup>275</sup> efforts have been made to avoid phagocytosis by monocytes and to attach particles to their cellular surface instead, although such a task has proven to be quite challenging due to the cells' phagocytic competence. One method that has shown promise is the use of anisotropic polymeric particles or "cellular backpacks (BPs)", which are fabricated *via* layer-by-layer assembly and are able to circumvent phagocytosis due to their size, disk-like shape, and flexibility.<sup>276,277</sup> Polak *et al.* were able to embed doxorubicin-containing echogenic liposomes into such BPs, which were then loaded to the surfaces of monocytes.<sup>278</sup> Although follow-up experiments showed no cytotoxic effects of the NP-BP construct on the monocytes, no additional *in vitro* or *in vivo* tests were performed to investigate the antitumor



efficacy of this system. In a separate study, BPs containing IONPs were conjugated onto the surfaces of monocytes without impairing cellular function, and the resulting construct exhibited effective targeting of skin and lung inflammation models *in vivo*.<sup>277</sup>

**6.1.3. Lymphocytes.** Besides monocytes and macrophages, the central role of lymphocytes, particularly T-cells, in adaptive immunity has been widely exploited to target and destroy cancer cells in the form of immunotherapy.<sup>279,280</sup> While their function to destroy infected cells (cytotoxic T-cells) or activate other immune cells (helper T-cells) renders them promising anticancer therapeutic tools, their attractiveness for cell-mediated drug delivery is mainly due to their natural ability to migrate toward either inflammation regions or lymphoid organs,<sup>281</sup> and consequently for the targeting of primary tumors or loose cancer cells that have reached the lymph nodes, respectively. The subsequent coupling of NPs to these lymphocytes serves to (1) improve the circulation and reach of the NPs to tumors and lymph nodes, and (2) enhance the proliferation and cytotoxicity of the reintroduced “adoptive” T-cells that are otherwise suppressed by the TME.<sup>282</sup>

As was performed with macrophages, photolithographic-patterning techniques have been used to design cellular BPs containing superparamagnetic IONPs (SPIONs) as well as a hyaluronic acid cell-adhesive component that binds to the surfaces of T-cells *via* the CD44 receptor.<sup>283</sup> The migration capacity of the resulting modified T-cells was then confirmed by their ability to migrate on substrates coated with ICAM-1, an adhesion ligand present on endothelial cells that binds to T-cell integrin LFA-1, for over 6 h until the BP detached. Efforts aimed at using B-cells for NP delivery have also used hyaluronic acid-mediated adhesion of the particles to the cell surface *via* polyelectrolyte multilayer (PEM) patches.<sup>283–285</sup> Besides surface adhesion with BPs, liposomes have been attached to T-cell surfaces reversibly *via* simple incubation without compromising the integrity of T-cell proliferation and cytotoxicity and with their *in vitro* release being triggered by the presence of glutathione.<sup>286</sup> In a separate study, lipid NPs loaded with topoisomerase I poison SN-38 and functionalized on T-cell surfaces were able to accumulate in the lymph nodes at levels 90-fold greater than a 10-fold higher dose of free SN-38 in a murine model of disseminated lymphoma, significantly reducing tumor burden and improving animal survival compared to SN-38-loaded NPs alone.<sup>287</sup>

In studies of adoptive T-cell therapy, T-cell surfaces have been functionalized with adjuvant-containing liposomes (interleukin-15 and -21) with the aim of circumventing TME immunosuppression and providing the cells with sustained pseudoautocrine stimulation in lung- and bone-metastasis models over a period of 7 days.<sup>288</sup> These modified T-cells retained 83% of their NP load as they transmigrated across endothelial layers and improved the efficacy of T-cells in eliminating metastases. In a follow-up study, T-cells were similarly modified to contain liposomes loaded with an inhibitor of Shp1 and Shp2, which downregulate lymphocyte receptor activation at the T-cell/cancer cell synapse during adoptive therapy.<sup>289</sup> These constructs were shown to increase T-cell proliferation in mice bearing advanced prostate cancer as well as improve survival by 14 days compared to animals treated with T-cells alone. Protein nanogels carrying an IL-15 superagonist complex were also hitchhiked onto T-cell surfaces and were shown to selectively release their cargoes upon T-cell

receptor activation (Figure 11).<sup>290</sup> These constructs improved the proliferation of T-cells at the tumor site by 16-fold as well as increased the maximum tolerated dose of cytokine without toxicity by 8-fold, compared to the administration of free cytokines. Epidermal growth factor receptor (EGFR)-targeting chimeric-antigen receptor (CAR)-T cells coupled with these backpacked nanogels significantly enhanced tumor clearance in mouse models of glioblastoma.

**6.1.4. Neutrophils.** Neutrophils function as the body's first line of defense by phagocytosing foreign agents. They are produced in the bone marrow and compose 50–70% of all leukocytes.<sup>291</sup> Despite their short circulation time, their abundance in the bloodstream and their large surface area that accommodates high quantities of NPs and drugs to be loaded onto their surface or cytosol render them promising delivery systems to tumors, particularly due to their added ability to migrate across endothelial barriers.<sup>292</sup> In the first of a series of studies, Chu *et al.* demonstrated this potential in a mouse model of acute lung inflammation, where they used intravital microscopy to show that intravenously injected albumin NPs are internalized by activated neutrophils, which in turn cross endothelial barriers to reach the inflammation site.<sup>293</sup> The enhanced neutrophil-mediated delivery of the NPs was further confirmed by their lower accumulation at the target site upon neutrophil depletion with anti-Gr-1. The prior inoculation of TA99, a monoclonal antibody that has been shown to enhance neutrophil recruitment to the tumor site in mice bearing melanoma was able to further increase NP accumulation in the tumor.<sup>291</sup> The subsequent photodynamic therapy by pyropheophorbide-a (Ppa)-loaded albumin NPs led to significant tumor growth inhibition and improved mouse survival compared to treatment with NP or TA99 alone. In a third follow-up study, gold nanorods were used instead of albumin NPs and were coated with anti-CD11 antibodies to further target activated neutrophils.<sup>294</sup> In fact, coating with anti-CD11 showed a 35-fold increase in tumor accumulation of the nanorods compared to those coated with PEG. Photosensitization and the subsequent photothermal therapy of the tumors by the neutrophil-mediated accumulation of the nanorods significantly inhibited tumor growth and enhanced mouse survival. Similar studies have also used magnetic NPs to show the ability of neutrophils to improve delivery to the tumor site.<sup>295</sup> Furthermore, the natural ability of neutrophils to cross the blood–brain barrier renders them promising delivery tools in the treatment of glioblastoma. For instance, in a mouse model of postoperative malignant glioma, the highly concentrated inflammatory signals in the brain that result from tumor resection drive the migration of neutrophils containing paclitaxel-loaded cationic liposomes to the inflammation site and trigger the release of the NPs from the cells *via* extracellular traps into the TME.<sup>296</sup> This neutrophil-mediated delivery was able to significantly hinder the recurrent growth of tumors and improve animal survival, although complete inhibition of tumor regrowth was not achieved.

**6.1.5. Stem Cells.** One remainder type of circulatory cell that has been heavily explored as a delivery vehicle for NPs is stem cells, namely adult stem cells. Unlike their embryonic counterparts that are derived from the blastocyst inner cell mass, adult stem cells are not as pluripotent but are rather tissue-specific cells that are only capable of differentiating into limited types of specialized cells. However, these stem cells have been shown to be less likely to promote tumor growth following transplantation.<sup>297</sup> More importantly, as is the case



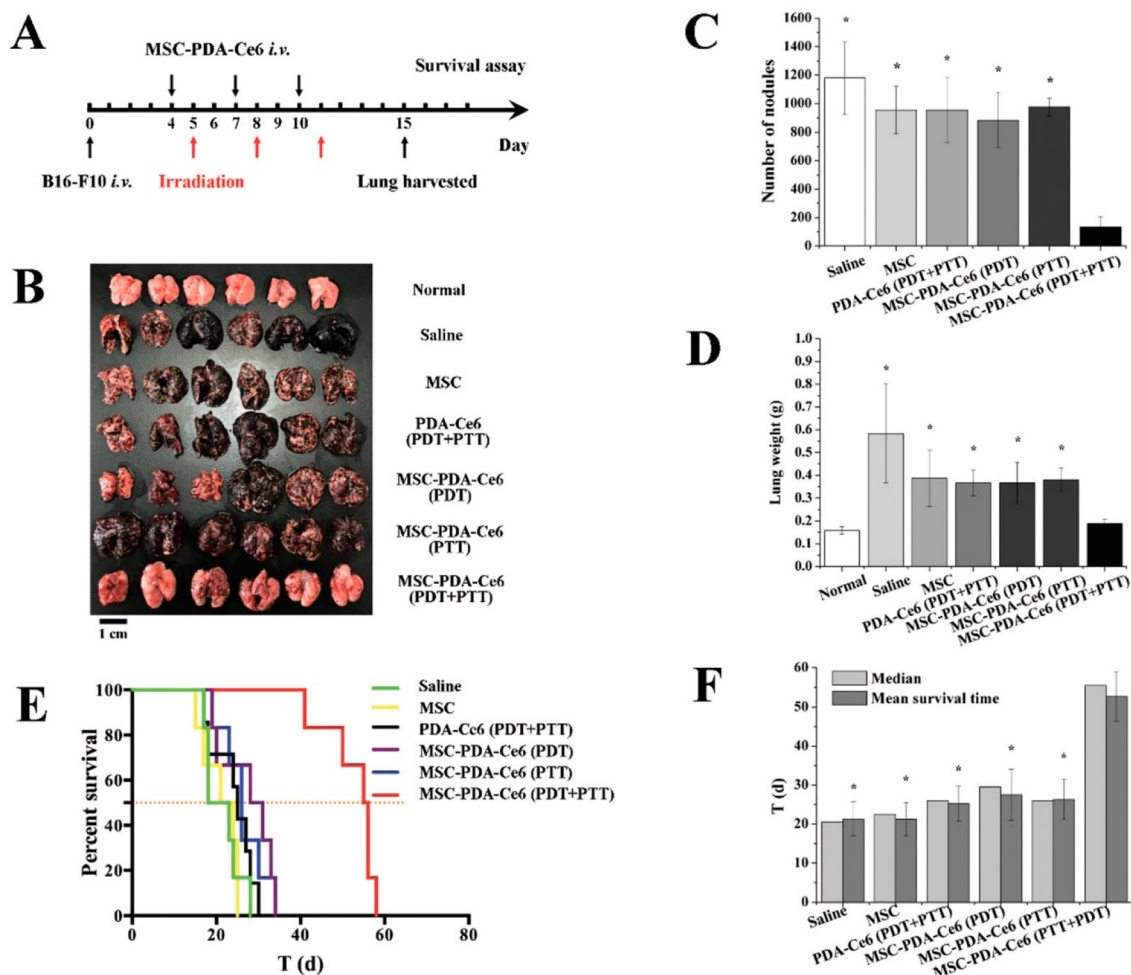


**Figure 12.** (A) Experimental setup for testing the *in vivo* effect of MSCs loaded with Ce6-grafted polydopamine NPs (PDA-Ce6) on tumor growth with or without irradiation with PDT/PTT. (B) Harvested lung tumors on day 15 post B16F10 murine melanoma injection. (C–F) Count of metastatic colonies (C), lung weights (D), Kaplan–Meier survival curves (E), and median survival times for each group (F). This figure has been reproduced with permission from ref 307. Copyright 2020 Royal Society of Chemistry.

with the aforementioned circulatory cells, they possess certain surface markers that provide them with tumorigenic properties, which render them attractive delivery tools in cancer therapy.

Mesenchymal stem cells (MSC) are derived from the bone marrow and are easily isolated and cultivated, although their translation to the clinic is limited as they have been associated with immunosuppressive properties that may promote tumor growth.<sup>298,299</sup> Some of the earlier studies that have exploited the tumorigenic ability of MSCs showed significant improvement in the delivery of organic NMs, including poly(lactic acid) NPs and lipid nanocapsules loaded with coumarin-6<sup>300</sup> as well as doxorubicin-loaded silica nanorattles,<sup>301</sup> to glioma mouse models without compromising the integrity and functionality of the MSCs nor the NMs. Paclitaxel<sup>302</sup> and docetaxel<sup>303</sup> containing PLGA NPs were also shown to significantly accumulate in mouse lung tumor models when hitchhiked onto MSCs compared to free NPs that exhibited nonspecific biodistribution. In a recent study by Wang *et al.*, they show that intravenously injected MSCs are trapped in the lung tissue after 12 h in rabbits and after 24 h in mice and monkeys and that loading these MSCs with docetaxel-containing PLGA NPs significantly inhibits tumor growth in mouse models of lung cancer.<sup>304</sup> Throughout their study, they also demonstrate the

dynamic transportation of the NPs from their carrier MSCs to the cancer cells *via* the imaging of cocultured 3D spheroids *in vitro* and lung tissue sections *in vivo*.

While the use of MSCs in cancer therapy has shown to improve the therapeutic index of drug-loaded organic NMs by enhancing their exposure to tumor cells, the incorporation of inorganic NMs into these cell-based regimens provides opportunities for combinatorial treatment with photothermal therapy. For instance, MSCs loaded with superparamagnetic iron oxide (SPION)-coated gold NPs that had homed toward hepatocellular carcinoma (HCC) tumors *in vivo* were irradiated with NIR light, generating local hyperthermia and successfully ablating surrounding cancer cells.<sup>305</sup> In a separate study, pH-sensitive gold NPs that tend to aggregate in the acidic environment of endosomes, thereby exhibiting higher photothermal effects upon irradiation with NIR light, were loaded onto MSCs and intravenously injected in mice.<sup>306</sup> These gold NP-laden MSCs revealed a 37-fold greater tumor-targeting efficiency and an 8.3 °C increase in hyperthermia generation compared to free NMs. Interestingly, metallic organic NPs have also been incorporated into MSCs for the photothermal and photodynamic therapy of cancers. In a recent study by Ouyang *et al.*, Ce6-grafted polydopamine NMs were internalized into MSCs, and within 72h of *in vitro*

cocultures, 60% of the NMs were shown to be exocytosed from the MSCs and subsequently endocytosed by the cancer cells.<sup>307</sup> When injected in mice bearing pulmonary melanoma, the NM-labeled MSCs in combination with low-dose photothermal and photodynamic therapy induced significant synergistic inhibition of tumor growth, confirmed by the lower number of nodules and lung weight as well as increased survival compared to either therapy alone or free NMs (Figure 12).

Neural stem cells (NSCs), on the other hand, are obtained from neurogenic areas in the brain and have been shown to also be tumorigenic and, unlike MSCs, nontumorigenic and marginally immunogenic,<sup>308</sup> although a recent study revealed the NSCs may promote glioblastoma formation.<sup>309</sup> Despite the complications associated with accessing NSCs for autologous transfer in the brain which has limited their use in the clinic in the past, some reports have shown that neural stem-like cells can be obtained from the bone marrow instead and can thus be used for delivery purposes.<sup>310</sup> A series of experiments by Mooney *et al.* in 2014 have been conducted that harness the tumorigenic properties of NSCs to deliver a variety of NMs to different tumor types.<sup>311–313</sup> In their first study, they functionalized large polystyrene NPs to the surface of NSCs and confirmed their ability to home toward glioma cells in the brain.<sup>311</sup> The use of large NPs, which when administered freely, are unable to cross the blood–brain barrier and migrate to tumor tissue, served as a control to ensure that any NP accumulation in the brain is due to mediation by NSCs. In a follow study, polymeric NPs were loaded with docetaxel and conjugated onto the surfaces of NSCs to improve NP delivery by intratumoral administration to mice bearing triple negative breast cancer (TNBC) and induce antitumor activity without compromising the integrity of the NSCs.<sup>312</sup> Finally, in the same tumor models of TNBC, NSCs loaded with gold nanorods were intratumorally injected in mice and irradiated with NIR light to induce local hyperthermia and improve the photothermal therapy of the tumors compared to free nanorods, significantly lowering tumor recurrence rates.<sup>313</sup>

#### 6.1.6. Cell-Surface-Binding vs Encapsulation of NPs.

In designing a hitchhiking system, the diversity in surface properties that arises from the various types of biomolecules present on the surfaces of different cellular carriers, such as proteins, lipids, and polysaccharides, can be exploited to functionalize NPs on the outer cell membranes using a variety of methods that can be subdivided into two categories, noncovalent and covalent. While covalent methods tend to result in sturdier bonds that render the construct highly stable, they are often less desirable as their associated high degree of molecular modification may cause significant alterations in cell properties, particularly at off-target sites. The simplest method of noncovalent attachment that requires the least modification of both the cell and NM is the adsorption of cationic or hydrophobic NPs to the cell surface. Functional groups found on biomolecules such as carboxylate, sialic acid, and phosphate render cellular membranes negatively charged, allowing cationic NPs to be passively and electrostatically adsorbed onto the surface.<sup>314</sup> At the same time, conclusions from studies evaluating the extent of protein adsorption onto the surface of NPs suggest that NP adsorption may also involve van der Waals and hydrogen bonds in cases where NPs are sufficiently hydrophobic.<sup>250,252</sup> Despite its simplicity and ability to maintain cellular and NP integrity, the strength of NP adsorption is difficult to establish, leading to the uncontrollable

detachment of NPs in biological systems that is often based on shear stress. Another method that requires minimal modification and has potential for successful *in vivo* translation exploits the presence of specific receptors on cellular surfaces onto which NP-bound ligands can be attached *via* ligand–receptor interactions. In such cases, however, ligand–receptors must be carefully selected to be sufficiently specific to the cell of choice, given that many receptors are often present on a variety of cell types and thus may be triggered by nonspecific binding and result in undesired biological responses, particularly upon early NP detachment in constructs containing low binding affinities. Examples of such an attachment are the aforementioned binding of hyaluronic acid on cellular BPs to CD44 receptors that are overexpressed on macrophages as well as T- and B-cells<sup>283–285</sup> and the formation of strong biotin–avidin bridges that have been shown to be resilient against denaturants such as fluctuations in pH, temperature, and buffer salts.<sup>315</sup> Lastly, in contrast to adsorption and ligand-induced conjugation, covalent coupling results in more stable constructs that circumvent the issue of off-target NP release, although additional release strategies are often required to be incorporated into the construct design to ensure the ability of the NPs to exert their intended effects. In this approach, NP surfaces can be modified with reactive compounds that covalently bind to the amine and thiol groups found abundantly on cellular surfaces.<sup>316,317</sup> Alternatively, cell surfaces can be functionalized with non-natural functional groups onto which the NPs can be covalently bound.<sup>318</sup>

Despite the efficacy and ease of functionalizing NPs to cell membranes, surface-bound NPs may uncontrollably detach from the cell surface at off-target sites due to shear-stress, while the exposure of the NPs to the extracellular environment may cause them to remain susceptible to recognition by the immune system. At the same time, the NPs may damage the intrinsic morphology and flexibility of the cells, thereby affecting their navigation through narrow vessels to reach tumor tissues. In attempt to circumvent these challenges *in vivo*, efforts have been made to internalize NPs into cells in a mechanism known as “Trojan Horse” using a variety of methods, including hypotonic dialysis, wherein hypotonic swelling of the cells creates transient pores in their membranes through which NPs are able to diffuse, and the subsequent isotonic resealing of the pores entraps the NPs within the cells.<sup>319</sup> Other methods involve the coupling of NPs to CPPs most commonly through disulfide linkages which are easily broken by the abundance of glutathione within the intracellular environment,<sup>320</sup> as well as receptor-mediated internalization as is the case with the coadministration or coupling of NPs with RGD peptides.<sup>321</sup> Additionally, the natural internalization of NPs can be achieved through phagocytosis, although this method is limited to cell types with natural phagocytic abilities such as neutrophils, macrophages, and monocytes.<sup>272</sup> Similarly to the cell surface binding of NPs, the encapsulation of NPs within cells is also accompanied by its own set of drawbacks, including the possible premature degradation of the NPs within the host cell as well as the need to incorporate a NP release strategy upon delivery to the target site.

#### 6.2. Biomimetic Cell Membrane-Coated NPs (MCNPs)

As previously discussed, the cell-mediated delivery of NPs is at times associated with a few drawbacks, such as the potential lysosomal degradation of internalized NPs and the uncontrolled release and immunomodulatory stimulation of surface-

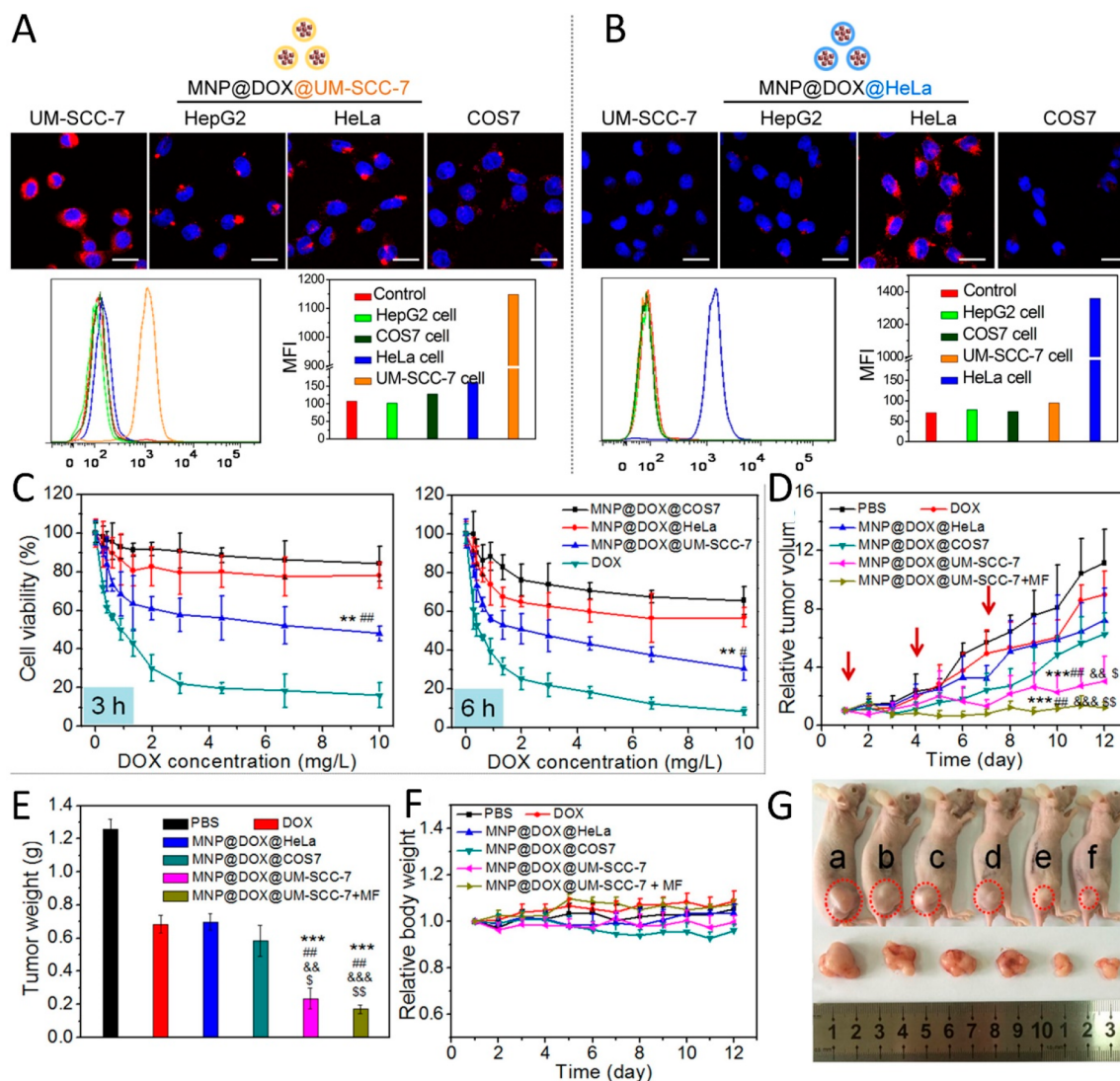


**Figure 13.** (A,B) Increased internalization of DOX-loaded magnetic iron oxide NPs (MNPs) coated with membrane fragments of UM-SCC-7 (A) and HeLa (B) cells in homotypic cancer cells compared to other cell lines. (C) Viability of UM-SCC-7 cells upon 3 and 6 h exposure to DOX-loaded MNPs coated with membranes obtained from different cell lines (UM-SCC-7, COS7, and HeLa). (D,F) Relative tumor volumes (D) and body weights (F) upon treatment of UM-SCC-7 tumor-bearing mice with variations of MNPs with or without targeting by application of an external magnetic field (MF) on days indicated by the red arrows. (E) Average tumor weight measured on day 12 post treatment. (G) Photograph of UM-SCC-7 tumor-bearing mice and tumors on day 12 post treatment for each of the different groups (a = PBS, b = DOX, c = @HeLa, d = @COS7, e = @UM-SCC-7, f = @UM-SCC-7 + MF). Reproduced with permission from ref 342. Copyright 2016 American Chemical Society.

bound NPs. Accordingly, progress made toward the circumvention of these challenges has led to the design of NPs coated with the membranes of the desired circulatory cells instead of hitchhiking or loading them into the cells. The resulting construct not only possesses the unique biomimetic qualities of these cells, such as increased circulation time, evasion by the immune and reticuloendothelial systems, and tumortropic tendencies, but it also retains the unique material properties of the NPs. Additionally, the nanosize of the coated particles allows them to more easily diffuse across endothelial barriers and reach deep within target tissues compared to the significantly larger cells.

### 6.2.1. Membranes from Normal Circulatory Cells.

Various NP types have been coated with membranes of the aforementioned circulatory cells and investigated for their improved blood circulation times compared to their non-membrane-coated counterparts, with RBC-coated organic and

inorganic NMs composing a large proportion of explored MCNPs. For instance, in a study by Piao *et al.*, coating gold nanocages with RBC membranes not only enhanced the *in vivo* blood retention of the NMs without affecting their structural integrity but it also increased the uptake of the nanocages in the tumors, thereby improving the efficacy of photothermal therapy and achieving 100% animal survival within a period of 45 days.<sup>322</sup> In a separate study, RBC membranes functionalized with tumor-targeting epithelial cell-adhesion molecule antibodies were coated onto paclitaxel-loaded gold nanocages, and the resulting constructs were shown to be effective for the chemo- and photothermal therapy of murine models of breast cancer *in vitro*.<sup>323</sup> Decreased phagocytic uptake of RBC-coated gold NPs due to surface CD47 expression has also been observed.<sup>324</sup> Besides gold NMs, upconversion NPs have been coated with RBC membranes and were shown to completely reduce protein corona adsorption upon exposure to human



plasma, while the additional functionalization of folic acid on the NP membranes significantly improved the tumor-targeting abilities of the NPs.<sup>325</sup> Organic NMs such as polymeric NPs have also been coated with RBC membranes and controlled drug release strategies were further incorporated into the nanoconstruct design. For instance, RBC-coated, pH-sensitive, and paclitaxel-loaded poly(L-γ-glutamylcarboxystein) NPs were developed to sustain NP blood circulation and release paclitaxel upon their successful delivery to the acidic TME. Accordingly, these constructs were able to circumvent uptake by macrophages and significantly inhibit tumor growth in mice bearing nonsmall cell lung cancer compared to their noncoated counterparts.<sup>326</sup> In a more recent study, Lin *et al.* were able to fine-tune the release kinetics of paclitaxel from RBC-coated PLA nanocarriers by altering the macromolecular stereochemistry of PLA, with increased stereocomplexation resulting in slower rates of release.<sup>327</sup>

Similarly to RBC-cloaked particles, leukocyte-MCNPs possess lengthy circulation times *in vivo* but also have the added advantage of homing to solid tumors as a result of the natural ability of leukocytes to migrate toward inflammatory regions. Specifically, macrophage- and monocyte-MCNPs are one of the most commonly explored leukocyte-coated constructs. Some of the first NPs of this kind were developed with a silica core, with the integrity of membrane surface functional groups such as CD45 and CD11a and glycans being preserved to circumvent potential phagocytosis.<sup>328</sup> In subsequent studies, enhanced cellular uptake in breast cancer cell lines *in vitro* was achieved using doxorubicin-loaded PLGA nanoghosts enclosed in monocyte membranes,<sup>329</sup> while macrophage-coated emtansine liposomes were capable of inhibiting lung metastasis in murine models of breast cancer *in vivo*.<sup>29</sup> Other tumor-targeting macrophage-MCNPs consisting of lanthanide-doped (upconversion NPs),<sup>330</sup> and gold<sup>331</sup> cores have been developed for the *in vivo* imaging and photothermal therapy of cancers, respectively. Interestingly, Wang *et al.* used grapefruit-derived nanovectors to explore the tumor-homing mechanism of leukocyte-MCNPs and found that blocking LFA1 or CXCR1 and CXCR2 inflammatory-related receptors on these membranes significantly reduces the tumortropic capabilities of these constructs.<sup>332</sup>

Besides RBC- and macrophage-MCNPs, there currently exists formulations with a wide variety of membrane–core combinations, resulting in improved tumor-homing, including membranes isolated from neutrophils and platelets. As in the case with monocytes, neutrophils<sup>333</sup> and platelets<sup>334</sup> have the intrinsic ability to bind circulating and premetastatic niche tumor cells and contribute to cancer progression. In a study by Kang *et al.*, neutrophil-membrane-coated PLGA NPs not only showed enhanced cellular uptake *in vitro* and circulating tumor cell (CTC) capturing efficiency *in vivo*, but when loaded with proteasome inhibitor carfilzomib, these particles were able to significantly reduce blood CTC count and inhibit both the onset of new and growth of existing metastases in breast cancer mouse models.<sup>335</sup> A similar effect was achieved using platelet-MCNPs loaded with tumor necrosis factor-related apoptosis inducing ligand (TRAIL) and doxorubicin in breast cancer tumor-bearing immunodeficient mice.<sup>336</sup> Other platelet-MCNPs consisting of a magnetic iron oxide core<sup>337</sup> and coencapsulated with immunogenic cell death (ICD)-inducing metformin and reactive oxygen species (ROS)-producing IR780<sup>338</sup> have been developed for the photothermal and photodynamic therapy of cancers, respectively. Some studies

have even coated NPs with hybrid membranes derived from different types of circulating cells with the aim of controlling the degree of a certain biological outcome. For instance, in designing strategies for the optimized detection and selective separation of CTCs from circulation, platelet-leukocyte hybrid-membrane coated immunomagnetic beads have been developed to exhibit the improved CTC-binding properties intrinsic to platelets while maintaining the purity of CTC isolation by reducing CTC–leukocyte interaction as a result of the tendency of leukocytes to evade homologous binding.<sup>328,339</sup>

**6.2.2. Use of Cancer Cell Membranes.** Finally, scientists have recently begun to exploit the ability of cancer cells to escape from the immune system<sup>340</sup> and bind homotypically to one another<sup>341</sup> by designing NPs encapsulated within cancer cell membranes. The resulting NPs are not only capable of circumventing immune clearance and remaining in circulation for longer periods of time, but they also exhibit homotypic cancer cell-specific binding due to the expression of certain proteins on the surface of their membranes. In a study by Zhu *et al.*, doxorubicin-loaded magnetic iron oxide NPs were coated with cell membranes derived from various cancer cell lines to confirm their high selectivity to the homologous tumor *in vivo*, even in the presence of a heterotypic tumor (Figure 13).<sup>342</sup> One of the earliest cancer-MCNPs consisting of a PLGA core were functionalized with toll-like receptor 4 (TLR-4) agonist monophosphoryl lipid A (MPLA) as an immunological adjuvant to boost tumor-specific immune responses during vaccine therapy.<sup>343</sup> In a similar tumor vaccination study, cancer-CMC PLGA NPs loaded with TLR-7 agonist imiquimod were further modified with mannose for the improved uptake by dendritic cells and associated antitumor response.<sup>344</sup> In combination with anti-PD-1 blockade immunotherapy, these NPs exhibited almost complete tumor progression inhibition in a mouse model of human melanoma *in vivo*, whereas treatment with immunotherapy alone led to rapid tumor progression after a few days. Tumor-targeted cancer-MCNPs have also been developed for the dual-modal imaging and photothermal therapy of cancers,<sup>345</sup> as well as for photodynamic and cancer starvation therapy, in which glucose oxidase and catalase are used to deplete intratumoral glucose.<sup>346</sup>

### 6.3. Use of Extracellular Vesicles

Extracellular vesicles (EV) are natural intercellular carriers of biomolecules that are able to transport themselves over both short and long ranges due to their lipid membrane protecting their cargoes from extracellular influences and their internal nutrient richness that mirrors intracellular environments. Accordingly, EVs are able to function as nanocarriers themselves with improved stability and biocompatibility compared to synthetic NMs and are similarly able to take advantage of the EPR effect by extravasating across the leaky tumor vasculature to reach deep within tumor tissue.<sup>347</sup> They can also be functionalized with similar ligands and coatings to NPs, such as CD47 stealth ligands and PEG, to further improve their targeted delivery. The most interesting aspect of using EVs as carriers, however, is that they have been shown to inherit the tropic properties of their parental cell due to the presence of certain surface integrins, and thus loading the EVs of preferred tropism with drugs allows the delivery of their cargo to target organs, rendering them promising delivery tools for cancer therapy. For instance, EVs isolated from cancer cells that have metastasized to specific organs have been shown to



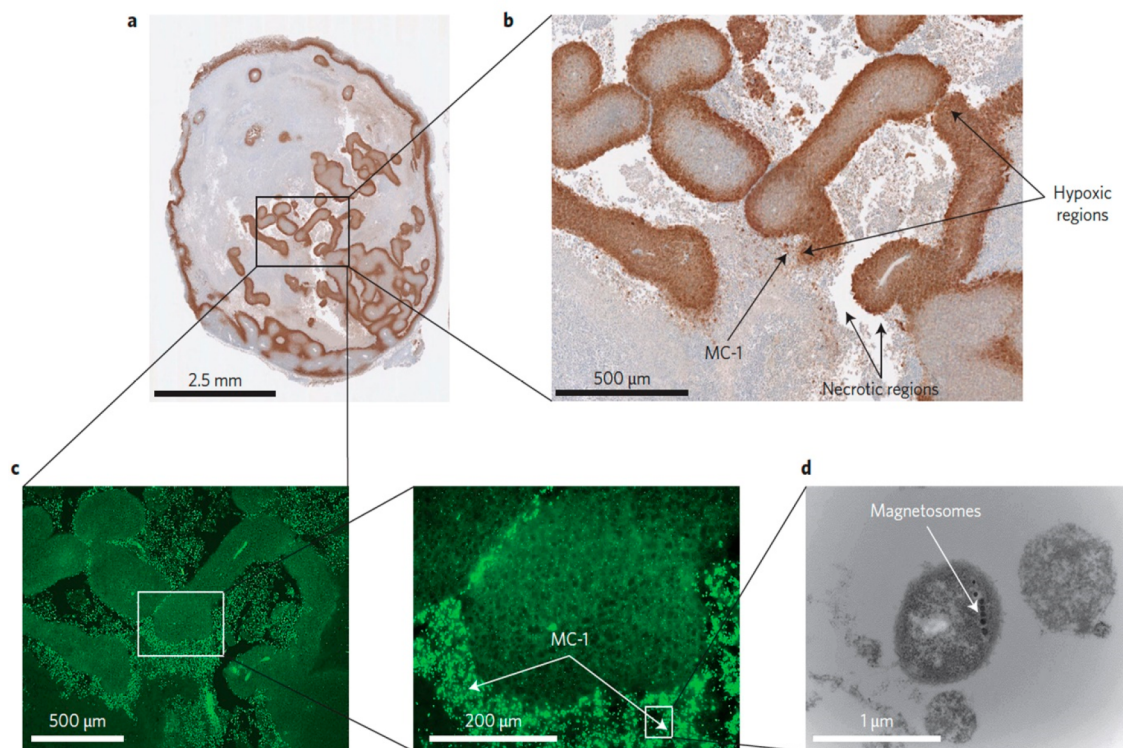


**Figure 14.** (a,b) Peritumorally injected MC-1 cells localize in hypoxic regions (brown islands) of mouse xenografts. (c) Fluorescent images of MC-1 bacteria stained with FITC-conjugated secondary antibodies in adjacent sections of the same xenografts. (d) TEM images of MC-1 bacteria highlighting the presence of magnetosomes. Reproduced with permission from ref 365. Copyright 2016 Nature Publishing Group.

display identical tropism to the cells from which they were secreted and to also reprogram the tropic properties of cancer cells toward organs that were not originally target sites of metastasis.<sup>348,349</sup> Similarly, EVs isolated from MSCs have been shown to naturally home toward inflammatory sites and tumors.<sup>350</sup> As such, EVs have been extensively investigated for the delivery of a wide variety of cargoes for cancer therapy, particularly small drugs and genetic material.<sup>351,352</sup> In a few cases, even NMs such as SPIONs<sup>353</sup> and curcumin-loaded silk NPs<sup>354</sup> have been internalized into MSC-derived EVs for their improved delivery to tumors, and the loading of EVs with SPIONs has shown to improve the ability of macrophages to migrate and degrade the extracellular matrix, thereby enhancing the immunoregulatory activity of EVs. As is the case with circulating cells, NMs have not only been loaded into EVs for Trojan Horse-like delivery, but they have also been coated with EV membranes to improve their biodistribution and tumor-tropic abilities.<sup>355</sup>

The process of EV formation also known as biogenesis can take place in one of three ways:<sup>356–358</sup> (1) Multivesicular bodies produced by endosomal invagination fuse with the cell membrane to form 30–100 nm-sized exosomes that over-express tetraspanins (*i.e.*, CD63, CD81, and CD9), (2) Microvesicles pinch out from cell membranes in sizes of 50–1000 nm containing high levels of Annexin A1, and (3) apoptotic bodies in the micrometer range form from cellular residues during the process of apoptosis with high expression of Annexin V. The heterogeneity within these types of EVs implies that their physicochemical properties are determined by multiple factors, including the parental cell, activation state, mechanism of formation and intracellular cargo sorting, level of enrichment, among others.<sup>356</sup> Common methods used for the

isolation of EVs include ultracentrifugation, size exclusion chromatography, ultrafiltration, and immunoaffinity capture, while NM loading into the vesicles are often performed by incubation with cells prior to EV secretion, or incubation, sonication, or electroporation with EVs post isolation.<sup>347,359</sup> These isolation procedures are, however, associated with low purity and yield, and when coupled with the low loading capacities of the EVs, these inefficiencies have so far limited the clinical translation of EVs as nanocarriers in cancer therapy.<sup>360</sup>

#### 6.4. Use of Attenuated (Nonimmunogenic) Bacteria

Nonimmunogenic bacteria have also been heavily explored as delivery vehicles for a wide range of drugs and NMs due to the diversity in their tropism that allows them to migrate along or against concentration gradients of a variety of signaling molecules. Specifically, oxygen gradients can be exploited to guide the movement of anaerobic bacteria toward hypoxic regions of the TME and can thus be utilized as carriers of NMs for cancer therapy. For instance, Luo *et al.* used *Bifidobacterium breve* and *Clostridium difficile* as tumor-tropic carriers of upconversion and gold nanorods for the bioimaging and photothermal therapy of lung adenocarcinoma xenografts and found that the administration of antibody-functionalized nanorods that target spore germination after the injection of bacterial spores into the mice actually led to the complete destruction of tumors with no signs of relapse.<sup>361</sup> A specific and diverse subgroup of nonimmunogenic microorganisms are magnetotactic bacteria (MTB), most of which are Gram-negative and are characterized by the presence of magnetosomes within their intracellular organelles that create strong magnetic dipole moments and provide them with the ability to navigate along the lines of the Earth's magnetic field in a mechanism known as magnetotaxis.<sup>362</sup> This taxis is in fact

assisted by the aerotactic preference of MTBs to migrate toward sites of low oxygen concentrations, and thus refines the three-dimensional aerotactic movement to a one-dimensional propulsion.<sup>363</sup> In their natural environment, MTBs commonly reside at the oxic–anoxic interface (OAI) of sediment water columns consisting of vertical chemical concentration gradients that serve as sustainable sources of energy and thus hotspots for adaptation including magneto-aerotaxis.<sup>364</sup> It was hypothesized by Felfoul *et al.* that a similar OAI is present in the tumor interstitium between the oxic angiogenic network and the anoxic sites of tumor necrosis that can be exploited to specifically drive MTBs to hypoxic solid tumors with the guided assistance of an externally applied magnetic field, thus allowing MTBs to be used as targeted carriers of drugs and NMs in cancer therapy (Figure 14).<sup>365</sup> Specifically in their study, they functionalized SN-38-loaded liposomes onto the surface of *Magnetococcus marinus* (MC-1) MTBs and found that 55% of the peritumorally injected NP-bacterial constructs were able to be magnetically guided through the complex angiogenic networks and interstitial areas of the hypoxic regions of the tumor. At the same time, the magnetosomes found in MTBs have been explored as nanocarriers themselves as they range from 35 to 120 nm, consist of a lipid bilayer membrane and magnetic iron mineral crystals in the form of magnetite (Fe<sub>3</sub>O<sub>4</sub>) or greigite (Fe<sub>3</sub>S<sub>4</sub>) chains, and do not exhibit any of the toxicities induced by their synthetic and magnetic NP counterparts such as SPIONs.<sup>366,367</sup> Additionally, the biosynthesis of magnetosomes from MTBs is highly controlled and results in particles with uniform size, shape, dispersion, and even magnetization, whereas magnetic NPs that are synthesized by chemical precipitation are often superparamagnetic and nonuniform with respect to the aforementioned parameters.<sup>368</sup>

## 7. TRANSLATIONAL VALUE

### 7.1. Difficulties Concerning Bionano Interaction Studies

Assays that are frequently performed to evaluate the effects of small prospective drugs such as their toxicity toward certain cell lines *in vitro* are often not suitable for NM testing and do not accurately reflect their potential behavior *in vivo*. For instance, in the case of cationic and large-sized NPs, their charge and larger gravitational pull respectively may lead to greater interaction with cell membranes in 2D cultures compared to their opposite counterparts, thereby amplifying any associated signals. Additionally, light-emitting inorganic NPs are capable of interfering with signals from viability assays that are based on fluorescence, absorbance, and luminescence, yielding false positives.<sup>369</sup> As a result, in addition to the fact that even the smallest differences in NM physicochemical properties such as size, coatings, synthesis methods, structural defects, concentrations, exposure times, *etc.* may significantly affect the degree of cell–nano interactions and associated NM toxicity, research groups are employing different methodologies in attempt to evaluate NM toxicity *in vitro*, leading to discrepancies in published data and irreproducible results.<sup>370</sup> NMs have also been shown to induce toxicity to different cell lines by a variety of mechanisms, either by ROS-mediated apoptosis (*via* mitochondrial membrane potential disruption, DNA damage, or activation of MAPK and p53 signaling pathways), endoplasmic reticulum-mediated apoptosis, autophagy, or necrosis, rendering it even more difficult to understand the critical factors involved in their toxicity and to

standardize assays, and calling for innovative solutions in the field of nanotoxicology.<sup>371</sup>

Over the years, novel “safe-by-design” strategies have been put forth to enhance the comparability and reproducibility of NM experimental results *in vitro*, including physicochemical characterization, high-throughput and -content screening, establishment of quantitative structure–activity relationships (QSARs), and determination of the nanoassociated molecular patterns (NAMPs), leading to adverse outcome pathways (AOPs).<sup>372</sup> Together, these modalities encompass the majority of NM safety end points and serve as checkpoints for NM progression to *in vivo* studies. With the growing importance of nanotoxicology, research groups have recognized the increasing need to use various characterization methods to determine parameters such as size, shape, charge, release and dissolution kinetics, band gap, and crystallinity of the NMs prior to conducting their experimental objectives, as each of these factors may significantly impact their biological effects.<sup>373</sup> For instance, with respect to NM size, transmission electron microscopy (TEM) is frequently used to measure the core size of the NM while dynamic light scattering (DLS) is commonly used to determine their hydrodynamic size. However, there exists inherent shortcomings with many popular techniques, and efforts are also being made to overcome such drawbacks by developing alternative modalities that would thereby allow a more accurate understanding of the mechanistic effects associated with altering NM physicochemical properties. Accordingly, NP tracking analysis (NTA) is an alternative technique to DLS that uses the Brownian motion of the NPs instead of the intensity of scattered light to measure their size and thus removes the bias toward large particles and concentrated samples that is associated with DLS.<sup>374</sup> Tunable resistive pulse sensing (TRPS) technology is another alternative to DLS that is gaining popularity as it generates size measurements of NPs and even NP aggregates with higher resolution and sensitivity by recording alterations in their ionic current.<sup>375</sup> In parallel to establishing particle characterization, the safety of NMs and their cellular interactions can be studied *in vitro* using high-throughput screening (HTS) and high-content imaging (HCI). The HTS approach developed by Nel and colleagues is a powerful tool for the rapid kinetic analysis of cell–nano interactions, although it requires limited numbers of cells and parameters per analysis to sustain fast data acquisition.<sup>376</sup> HCI, on the other hand, is able to conduct rapid multiparametric acquisitions and automated analyses of images consisting of thousands of cells per condition, generating large data sets that allow the quantitative comparison of the effects of even the smallest differences between NMs on their behavior in various cellular environments.<sup>370,377,378</sup> Cellular parameters evaluated using such techniques include viability, proliferation, oxidative stress, damage to cell membrane, mitochondria, lysosomes and DNA, autophagy, cell morphology and cytoskeletal rearrangements, endosomal network changes, among others. These large generated data sets can then be extensively analyzed using statistical tools such as *in silico* hazard ranking to understand their QSARs, based on which computational paradigms can be developed to predict the toxicological outcome of other NMs both *in vitro* and *in vivo*.<sup>379,380</sup> Lastly, AOP networks have been generated on collaborative platforms such as the publicly accessible AOP Knowledge Base to further understand the complex relationship between NAMPs and key events taking place in the development of adverse outcomes.<sup>381</sup>

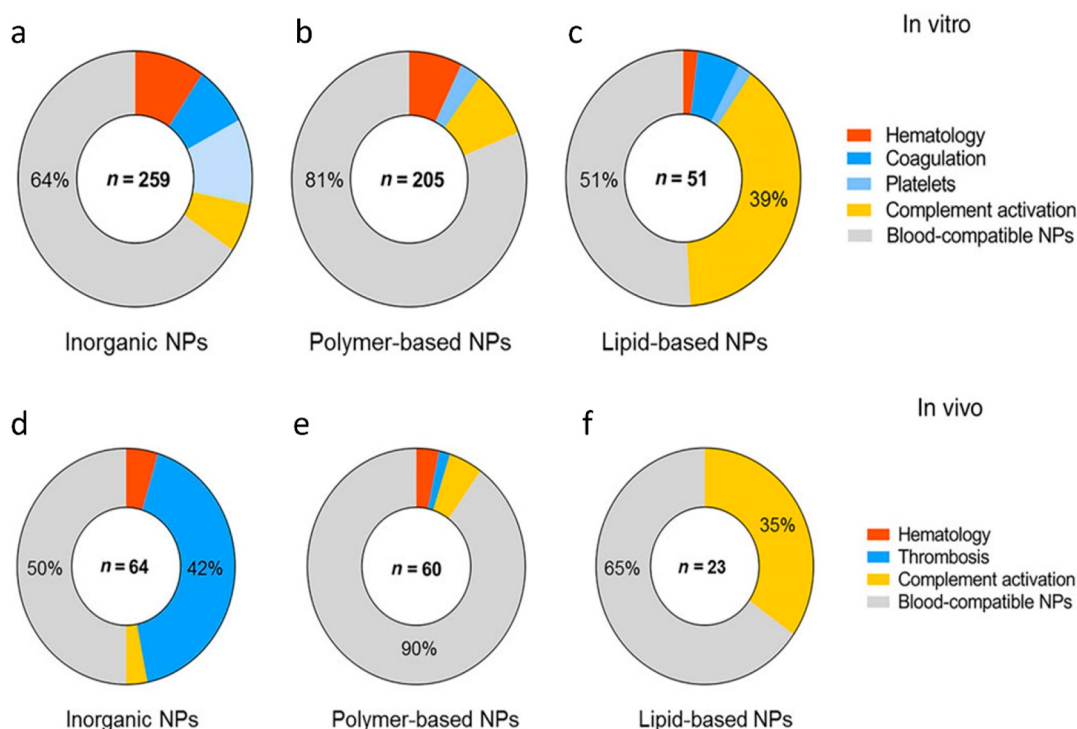


**Figure 15.** Number of publications reporting blood incompatibilities *in vivo* (a) and *in vitro* (b) for different types of nanomaterials. This image has been reproduced with permission from ref 383. Copyright 2019 Wiley-VCH.

## 7.2. In Vivo Translation of *In Vitro* Results

In an interesting publication by Dobrovolskaia and McNeil,<sup>382</sup> the authors conducted a meta-analysis of the available literature to identify the gaps in the effective *in vitro* translation of immunotoxicity testing of NMs to the *in vivo* stage. In their analysis, they found a good correlation between the *in vitro* and *in vivo* testing of hemolysis, coagulation, complement activation, opsonization, and phagocytosis, as well as a fair correlation in immunosuppression and thrombogenicity.<sup>382</sup> In a more recent study by Urbán *et al.*, the authors reviewed 515 publications and found that 30% of the NPs are blood-incompatible *in vitro* due to at least one of the aforementioned end points depending on the composition of the NM (Figure 15a–c).<sup>383</sup> For instance, while 64% of the inorganic NPs were found to be blood-compatible, the main adversity associated with these NPs was the combination of alterations on coagulation and platelets, which translate to thrombosis *in vivo*. With respect to lipid-based NPs, 39% were associated with complement activation, whereas polymer-based NPs showed low blood-incompatibility. In addition to the evaluation of these end points, another important test that should be conducted prior to *in vivo* testing and even before the *in vitro* immunotoxicity assays is endotoxin contamination, which is able to yield false assay results and has been found to be assessed in only 12.7% of the analyzed literature.<sup>384</sup> In fact, 30% of the NMs evaluated by the US NP Characterization Laboratory (USNCL) have failed during their preclinical assessments due to endotoxin contamination.<sup>382</sup> Endotoxins are components of Gram-negative bacteria cell walls and can easily bind to NPs due to their lipid and phosphate group constituents which have high affinities toward both hydrophobic and cationic surfaces of NPs. The exposure to even picogram concentrations of endotoxins in the body has been shown to induce pro-inflammatory, pro-coagulant, and

hemolytic effects, as well as the activation of the complement system, tissue damage, and septic shock, and thus may significantly affect the results of immunotoxicity tests.<sup>385</sup> Endotoxins have also been shown to be highly resistant against autoclaving and other sterilization techniques and that their levels of contamination can differ even between batches produced from the same laboratory, suggesting the need to perform thorough endotoxin contamination assays at the initial stages of NM development for their successful translation in the future.<sup>386</sup> Accordingly, in their review throughout which they examine the various methods of detection and elimination of NM-associated endotoxins, Li and Boraschi highlight that the use of endotoxin-free reagents and the optimization of certain synthesis procedures can significantly decrease the levels of endotoxins compared to purging contaminations at later stages of testing.<sup>387</sup> In addition to these safe-by-design strategies and immunotoxicity assays, various efforts have been made to further improve the translation of *in vitro* studies to the *in vivo* setting through the development of novel experimental models, including the use of lab- and organ-on-a-chip methods, *ex vivo* systems, and dynamic organoids.<sup>388</sup> The chick chorioallantoic membrane (CAM) model is another accessible approach that aims to minimize the costly use of rodents. It consists of intricate vascularization that represents the complex environments within biological organs in which NMs tend to get trapped.<sup>389</sup>

In the transition from the *in vitro* to *in vivo* setting, NM behavior tends to transform significantly as the variety of biomolecules and environments within biological systems are able to interfere with NM distribution, pharmacokinetics, cargo release, and even physicochemical characteristics. Therefore, conducting multiparametric evaluations of various NM behaviors *in vivo* is necessary for the advancement of nanomedicines to the clinic. In fact, one of the events that



take place upon NM exposure to the nutrient-rich environments in the body is the adsorption of biomolecules to the surfaces of the NMs, altering their size, shape, charge, and surface chemistry. The resulting “protein coronas” that form around the NPs are referred to as “hard” or “soft”, depending on whether adsorbed proteins are firmly bound to the NP surfaces or possess low binding affinities that result in dynamic and competitive exchanges in surface proteins.<sup>390</sup> The energetically favorable process of protein corona formation is highly complex and significantly impacts the original physicochemical properties of the particles, also known as their synthetic identity, by providing them with a new biological identity that governs their fate *in vivo*.<sup>391–393</sup> For instance, the shielding effect of the protein corona may interfere with the ability of active surface ligands that are functionalized on the NP surface to recognize certain receptors on cancer cells due to steric hindrance, thereby affecting their tumor-homing properties. Instead, it may weaken the EPR effect, guide the NPs to off-target sites, and promote clearance by the uptake by the mononuclear phagocytic system (MPS). NMs phagocytosed by macrophages tend to accumulate in MPS organs such as the liver and spleen, a phenomenon exhibited by a wide variety of materials, including quantum dots and polymeric and gold NPs.<sup>394–396</sup> In fact, high concentrations of adsorbed opsonins such as fibrinogens and immunoglobulins have been shown to enhance NP recognition and uptake by macrophages and reduce NP circulation time, requiring additional doses for effective anticancer activity that induce further off-target toxicity.<sup>397</sup> Protein corona formation has also been shown to stimulate the classical and lectin pathways leading to complement system activation, which in turn further induces the opsonization and modification of the NP surface.<sup>398</sup> Complement system activation may trigger inflammation, tumor growth, and in many cases, pseudoallergies involving complex networks of leukocytes and platelets that have led to the withdrawal of various NMs from the clinic, particularly IONPs.<sup>399,400</sup> In some instances, however, protein corona formation may enhance the targeting efficiency of NMs and prevent immunotoxicity.<sup>401,402</sup> The constituents of the protein coronas and the resulting biological identity of the NMs thus tend to vary between tumor types and even among patients, rendering it challenging to develop a universal strategy to control bionano interactions and suggesting the potential need for patient-specific designs of nanomedicines in cases where *in vivo* modifications of NMs are significant enough to impact safety and efficacy.<sup>403,404</sup> Accordingly, given the importance of the transformation of NM behavior due to protein corona formation, additional *in vitro* NM characterization should be performed after their exposure to biofluids to more accurately understand the bionano interactions. At the same time, the incorporation of dysopsonins into the NM design, including apolipoproteins, albumin, and polymeric coats such as PEG and PVP have proven to inhibit protein corona formation by reducing the reactivity and surface charge of the NMs.<sup>405</sup>

Besides opsonization, the interaction of NMs with circulating coagulation factors may disrupt the associated homeostatic balance through mechanisms such as platelet factor upregulation and damage to platelet membranes, which may result in disseminated intravascular coagulation causing abnormal hemorrhaging or intravascular thrombosis.<sup>385,406</sup> For instance, Oslakovic *et al.* found that cationic NPs reduced thrombin formation by binding to factors VII and IX, whereas

anionic NPs stimulated the intrinsic coagulation pathway.<sup>407</sup> Moreover, given that circulating tumor cells possess procoagulant phenotypes, additional procoagulant effects due to NM exposure may result in pro-tumoral activity.<sup>408</sup> In fact, in the study by Urbán *et al.*, the authors also analyzed the blood incompatibilities of NMs *in vivo* and found that 61% of the reported blood toxicities involve thrombosis, while the remaining 28% and 11% include complement activation and changes in hematology, respectively (Figure 15d–f).<sup>383</sup> In many cases of NP-drug constructs, the active pharmaceutical ingredient (API) may exhibit immunotoxic effects at levels greater than the administration of the drug alone as the NP causes the drug to accumulate in areas that are otherwise not exposed to such high levels of the API, such as the lymphatic system or spleen.<sup>409</sup> At the same time, the interaction of the nanocarrier with various biomolecules including opsonization may affect the kinetics of drug release and result in off-site targeting. For example, Abraxane and Caelyx are associated with higher rates of neuropathy and hand and foot syndrome, respectively, compared to free paclitaxel and doxorubicin.<sup>410,411</sup> As such, in addition to conducting *in vivo* immunotoxicity assays, the spatiotemporal behaviors of the nanocarrier and drug should be carefully studied both separately and jointly to obtain a holistic understanding of the potential clinical impact of the nanomedicine.

### 7.3. Clinical Translation

The clinical translation of (in)organic NMs is slowly expanding, driven by the vast number of outstanding preclinical results that have been obtained over the past few years. Their main biomedical application lies in cancer treatment, where, from an ideal point of view, NMs can be administered intravenously and are transported *via* the blood circulation to reach the tumor upon which they can be used for therapeutic and/or diagnostic purposes. However, some major obstacles are still unresolved and stand in the path of achieving their potential as therapeutic agents. One of these hindrances lies in the efficient targeting of the tumor tissue. A recent, extensive, meta-analysis of a wide array of NMs categorized according to similarities or differences in their physicochemical properties, performed by Wilhelm and colleagues,<sup>30</sup> demonstrated that currently the efficiency of NM delivery to solid tumors is very limited, reaching on average 0.7% of the injected dose. They further observed little added value from the use of classical active targeting strategies, such as conjugating the NMs with ligands that can bind selective tumor-associated epitopes. Another recent exhaustive study revealed that antibody or small molecule-coupled NMs show very poor tumor targeting, and more importantly, that only 2% of the cancer cells interact with the NMs at the tumor site. This was associated with the NMs being trapped in the ECM or being sequestered by TAMs.<sup>412</sup>

## 8. CONCLUSION

In conclusion,, all of these studies have shown possible improvements for the delivery of (in)organic NMs to solid tumors. However, these strategies have been developed as stand-alone methods and have not been studied adequately in order to make comparative studies possible. Furthermore, the potential impact of the methods used or even on the use of NMs in general must be studied carefully as illustrated by recent work. In particular, the finding that NM delivery to solid tumors by EPR may not be as influential as has been assumed

for the past decade may shift the focus of this research domain into different areas. Here, the biological methods using cellular strategies or methods to enhance NM transcytosis across the endothelial barrier may be essential to drive further progress. A proper combination of both strategies, focusing on a characterization of individual tumors in view of their perfusion and leakiness combined with the alternative targeting approaches seems like an optimal way forward.

## AUTHOR INFORMATION

### Corresponding Author

**Stefaan J. Soenen** – NanoHealth and Optical Imaging Group, Translational Cell and Tissue Research Unit, Department of Imaging and Pathology, KU Leuven, B3000 Leuven, Belgium; [orcid.org/0000-0003-2390-3133](https://orcid.org/0000-0003-2390-3133); Email: [s.soenen@kuleuven.be](mailto:s.soenen@kuleuven.be)

### Authors

**Mukaddes Izci** – NanoHealth and Optical Imaging Group, Translational Cell and Tissue Research Unit, Department of Imaging and Pathology, KU Leuven, B3000 Leuven, Belgium  
**Christy Maksoudian** – NanoHealth and Optical Imaging Group, Translational Cell and Tissue Research Unit, Department of Imaging and Pathology, KU Leuven, B3000 Leuven, Belgium; [orcid.org/0000-0001-8852-915X](https://orcid.org/0000-0001-8852-915X)  
**Bella B. Manshian** – Translational Cell and Tissue Research Unit, Department of Imaging and Pathology, KU Leuven, B3000 Leuven, Belgium; [orcid.org/0000-0002-3402-3927](https://orcid.org/0000-0002-3402-3927)

Complete contact information is available at:  
<https://pubs.acs.org/10.1021/acs.chemrev.0c00779>

### Author Contributions

M.I. and C.M. contributed equally to this work

### Notes

The authors declare no competing financial interest.

### Biographies

Mukaddes Izci is an FWO-SB awarded Ph.D. student, who in her work is focusing on developing and optimizing new methods to deliver nanomaterials to solid tumors in the most optimal way. She focuses on using high-throughput preclinical imaging methods for personalized tumor characterization, in combination with biological and pharmacological methods to enhance nanomaterial delivery to solid tumors.

Christy Maksoudian obtained her B.Sc. in Biomedical Sciences from New York University and M.Sc. in Drug Discovery and Development from Imperial College London, during which she worked extensively on the use of cell-penetrating peptides and gold nanoparticles in cancer therapy, respectively. She is currently pursuing her Ph.D. at KU Leuven, with her work mainly focusing on the optimization of nanoparticle delivery to solid tumors using a variety of biological methods, particularly cell-based therapy.

Bella B. Manshian is a group leader at the NanoHealth and Optical imaging group and focuses on the use of nanotherapeutics for a wide range of pathologies. Her current research interests lie in the development and optimization of nanomaterial-mediated delivery of pharmaceutical compounds across the blood–brain barrier or to specifically target inflammatory regions (cancer, infectious diseases,...). Dr. Manshian has over 60 publications and an h-index of 24.

Stefaan J. Soenen heads the NanoHealth and Optical Imaging Group at KU Leuven, Belgium, since January 2018. His main research interests lie in the use of nanomaterials for therapeutic and diagnostic purposes and on developing novel preclinical optical imaging methods. He has published over 75 manuscript with an h-index of 34 and received an ERC Starting Grant for his work on nanotherapeutics for cancer therapy.

## ACKNOWLEDGMENTS

We acknowledge financial support from the European Commission Horizon 2020 Research Framework (ERC starting grant no. 757398), FWO research project (G0B2919N), and KU Leuven BOF funding (C2 project 3M180306). I.M. is a recipient from an FWO-SB student fellowship. Nora Dekoning is acknowledged for her help with designing schematic illustrations.

## ABBREVIATIONS

**AMF** = Alternating magnetic field: An alternating magnetic field is a field in which the poles switch from one to the other side repeatedly. The switching of the magnetic field causes localized heating when magnetic NMs are present. This process is called magnetic hyperthermia.

**BBB** = Blood–brain barrier: A highly specialized structure from a tight monolayer of endothelial cells that only allows selective transport of compounds from the blood into the central nervous system.

**BPs** = Back packs: The “cargo” molecules loaded on the surface of a cell in order to avoid premature clearance and improve targeted delivery.

**CPP** = Cell penetrating peptide: Small peptides that facilitate cellular uptake of a variety of agents, going from small molecules to whole NMs.

**CPT** = Camptothecin: A natural compound isolated from specific trees (*Camptotheca acuminata* Decne) and potentially inhibits DNA-topoisomerase-I. Because of its low solubility, its clinical use has remained limited, but 4 CPT analogues have been approved and are used in cancer chemotherapy today: topotecan, irinotecan, belotecan, and trastuzumab deruxetecan.

**CSC** = Cancer stem cells: A small subpopulation of tumor cells that possess many features typically associated with stem cells, including self-renewal. These cells are often associated with higher therapeutic resistance and tumor relapse.

**DDS** = Drug delivery system: Any type of system (commonly a nanoparticle) that is used as a vessel to transport drugs from the site of administration to its intended target site and hereby prevents premature clearance or off-target effects.

**DOX** = Doxorubicin: Commonly used chemotherapeutic agent, clinically used for breast metastases treatment.

**DP** = Doxorubicin prodrug: An alternative form of doxorubicin which only becomes therapeutically active upon biological or chemical processing.

**DTX** = Docetaxel: Similar to PTX, a cytostatic chemotherapeutic agent used in breast, colorectal, lung, ovarian, prostate, liver, renal, gastric, and head and neck cancers and melanoma

**EC** = Endothelial cells: Cells that make up the inner lining of the blood vessels. They normally form close bounds (tight junctions) and control transport across blood vessel

walls. Immature vessels, such as sometimes present in tumors, can have gaps between the ECs.

ECM = Extracellular matrix: A dense fibrous network that provides structure and support to cells. In tumors, the ECM is often particularly dense and thick and can be seen as a barrier for delivery.

EGF = Epidermal growth factor: A protein stimulating cell growth and differentiation by binding to its receptor (EGFR). It is therefore used as a peptide for targeted NM delivery.

EGFR = Epidermal growth factor receptor: A receptor commonly overexpressed by tumor cells. It is often targeted by NMs for targeted delivery. It is also therapeutically targeted by clinically approved formulations (cetuximab and panitumumab).

EMT = Epithelial–mesenchymal transition: The process by which cells go from an epithelial to a more mesenchymal form. For cancer cells, this process is linked to going from an adherent to less adherent cell type, and is commonly associated with metastasis.

EPR = Enhanced permeability and retention: The classical view of nanoparticle delivery to solid tumors, please see [Chart 1](#).

EV = Extracellular vesicle: A lipid-coated particle that is naturally shed by a cell and serves as a means of intercellular communication.

FA = Folic acid, folate: A naturally occurring dietary compound (Vitamin B9 in US). Folic acid receptors are commonly overexpressed on many tumor types and folic acid is therefore frequently used as a peptide for targeted NM delivery.

FR = Folate receptor: The receptor for folic acid commonly overexpressed on many tumor types and therefore frequently used for targeted NM delivery.

FU = Fluorouracil: A cytostatic chemotherapeutic agent that inhibits tumor growth. It is clinically used in colon cancer, esophageal cancer, stomach cancer, pancreatic cancer, breast cancer, and cervical cancer.

GBM = Glioblastoma multiforme: The most common and highly malignant form of brain tumor.

HA = Hyaluronic acid: A glycosaminoglycan that is often present in connective tissue and makes part of the ECM. It naturally binds CD44, which is commonly overexpressed on cancer cells. Therefore, it is frequently used for targeted NM delivery.

HCC = Hepatocellular carcinoma: The most common type of primary liver cancer.

HER2 = Human epidermal growth factor receptor 2 (synonym: ErbB2): Cell surface receptor expressed by some, not all, breast or ovarian tumors. Can be targeted directly using Trastuzumab (Herceptin), a clinically approved antibody.

HPMA = *N*-(2-Hydroxypropyl) methacrylamide: A monomer that can be used to make polymeric nanoparticles for biomedical use

ICG = Indocyanine green: A near-infrared optical imaging agent with rapid renal clearance, can serve as contrast agent for optical or photoacoustic imaging. Can be used as photosensitizer in either photodynamic (ROS generation) or photothermal (temperature increase) therapy upon excitation with NIR light.

IFP = Interstitial fluid pressure: The interstitial space is the intercellular and extravascular compartment present in all

tissues. Fluids from the blood can reach tumors led by forces called interstitial fluid pressure. In tumors, the IFP is really high due to a very dense cell mass, poor perfusion, permeable vessels, and very poor lymphatic drainage (fluid outflow). This hardens the extravasation of NMs from the bloodstream against the IFP into the tumor tissue.

IONP = Iron oxide nanoparticle: Small iron oxide nanoparticles, see SPION.

MB = Microbubbles: Gas filled bubbles that are encapsulated by a polymeric or lipid layer and gives US contrast. The gas can be tuned to enable 19F MRI, or the MB can be loaded with therapeutic agents on the surface. *Via* sonoporation (see [Chart 1](#)), they release their cargo or transiently induce pores in blood vessels or cell membranes.

MCNPs = Biomimetic cell membrane-coated NPs: Nanomaterials that are overcoated with biological membranes to avoid immune recognition and clearance.

MDSC = Myeloid-derived suppressor cells: A myeloid derived cell that can be monocytic or granulocytic but which has potent immunosuppressive properties and helps the tumor to avoid immune clearance.

MDT = Magnetic drug targeting (a, active; p, passive): The process by which magnetic fields are used to promote drug delivery to the tissue of interest.

MHC = Major histocompatibility complex: A cluster of proteins involved in antigen presentation to T cells. There are 2 main types: MHC I and MHC II. MHC I is present on nearly all cells in the body, MHC II is present on specialized antigen-presenting cells.

m-NCs = Magnetic nanocapsules. A NM that serves as a vessel for transport of therapeutic molecules and also contains magnetic NMs for follow-up by imaging or magnetic guidance.

MNMs = Mitochondrial-targeted multifunctional NMs: NMs that are specifically targeted toward mitochondria.

MPI = Magnetic particle imaging: A more recent (pre)-clinical noninvasive imaging method that enables sensitive, quantitative and fast imaging of magnetic NMs to study functional parameters (e.g., inflammation, blood flow, perfusion, cell homing,...).

MRI = Magnetic resonance imaging: A (pre)clinical noninvasive imaging method.

MSC = Mesenchymal stem cell: An adult multipotent stem cell that can be isolated from bone marrow, fat, umbilical cord or amniotic fluid and that are important for making and repairing skeletal tissues, such as cartilage, bone, and the fat found in bone marrow.

MTB = Magnetotactic bacteria: A group of bacteria that naturally synthesize magnetic iron-containing minerals that enable them to respond to magnetic fields.

MTO = Mitoxantrone: A cytostatic agent used to limit tumor growth, it is primarily used in treating leukemia.

NC = Nanocarrier: A NM that serves as a vessel to transport therapeutically active molecules from the injection site to the target tissue.

NIR = Near-infrared: Light with wavelengths just above the spectrum visible for the human eye, typically with wavelengths ranging from 800 to 2500 nm.

NM = Nanomaterial: According to the EU definition: "A natural, incidental or manufactured material containing particles, in an unbound state or as an aggregate or as an agglomerate and where, for 50 % or more of the particles in the number size distribution, one or more external dimensions is in



the size range 1–100 nm.” In practice, this definition is not followed very strictly in academic research where polymeric or liposomal particles of around 200 nm diameter will still be called a nanomaterial.

NO = Nitric oxide: A type of ROS.

NP = Nanoparticle: Please see “nanomaterial (NM)”.

NSC = Neural stem cell: Multipotent cells which are able to self-renew and proliferate without limit, to produce progeny cells which terminally differentiate into neurons, astrocytes, or oligodendrocytes.

NRP-1 = Neuropilin-1: Transmembrane proteins involved in vascular development. Upon nutrient starvation, they enable a specific endocytosis pathway, which for tumor cells can result in direct transcytosis of components (including NMs) from the blood across the endothelial cells toward the tumor cells.

PDT = Photodynamic therapy: The therapeutic use of an agent (a photosensitizer) that upon activation by light of a specific wavelength, directly kills cancer cells or renders them more sensitive to other therapy. This often occurs by the light-induced generation of ROS.

PEG = Poly(ethylene glycol): A long, flexible polymer frequently employed to cover NMs in a brush-like manner. PEGylation of NMs increases their blood circulation times by reducing immune recognition, opsonisation (see Chart <sup>1</sup>) and clearance.

PET = Positron emission tomography: A (pre)clinical noninvasive imaging method based on the detection of radionuclides and commonly used for functional imaging (e.g., detection of tumors).

PLGA = Poly(lactic acid/glycolic acid): An FDA-approved polymer frequently employed for generating drug loaded NMs. The ratio of lactic versus glycolic acid can differ, influencing the solubility and drug release rates.

PTX = Paclitaxel: A natural compound derived from *Taxus brevifolia*. It exerts a potent anticancer effect and is classified as a cytostatic agent, inhibiting tumor growth, rather than inducing direct cell death. It is clinically used in a wide range of tumors, including ovarian cancer, breast cancer, lung cancer, Kaposi sarcoma, cervical cancer, and pancreatic cancer. Because of its low solubility, it is now also available as an albumin-bound nanoparticle (nAb-PTX).

RBC = Red blood cells: Also known as erythrocyte, transports oxygen in the blood.

rBV = Relative blood volume: The volume of blood in a particular tissue (tumor) or over a period of time, expressed as relative values (nonabsolute, but a % of a predefined starting point) and often measured using noninvasive methods.

RES = Reticulo-endothelial system: A cell system derived from phagocytic monocytes that enable the recognition and clearance of immune complexes (including immune factor-bound nanoparticles) from the blood. These cells are mainly located in the liver and spleen and are typically the major system where NMs end up after intravenous administration.

ROS = Reactive oxygen species: Highly reactive chemicals produced by electron acceptance by oxygen (O<sub>2</sub>). Various forms exist and they are key components in cellular signaling. Exaggerated levels of ROS, induced by NMs, can result in oxidative stress with wide ranging effects (DNA damage, cell death,...).

SOR = Sorafenib: A targeted anticancer therapeutic. It acts as a kinase inhibitor and is approved for clinical use against

advanced renal cell carcinoma, advanced primary liver cancer and thyroid cancer.

SPECT = Single photon emission computed tomography: A (pre)clinical noninvasive imaging method using specific radioactive tracers and detect single emitted photons.

SPIONs = Superparamagnetic iron oxide NMs: Small iron oxide NMs commonly used as MRI contrast agents. Because of their small size, they are no longer ferromagnetic, but become superparamagnetic, meaning that upon removal of an external magnetic field (e.g., MR scanner) they do not hold any remnant magnetism.

SPR = Surface plasmon resonance: The oscillation of conduction band electrons in resonance with the oscillating electric field of incident light. This typically occurs at the surface of metals and can be used to sensitively detect biomolecules binding to NMs (biosensors).

TAF = Tumor associated fibroblast: Fibroblasts that make up part of the TME. They mainly contribute to making a dense ECM and secrete factors that drive angiogenesis.

TAM = Tumor associated macrophage: Macrophage specifically linked to a tumor. From a classical perspective, there are two main types, M1 (pro-inflammatory), and M2, anti-inflammatory, but this distinction is not fully covering the wide range of subtle differences in macrophage types.

Tf = Transferrin: A natural compound involved in transport of iron in the blood. As transferrin receptors are commonly overexpressed on many tumor types, Tf is often used as a ligand for targeted NM delivery.

TNF $\alpha$  = Tumor necrosis factor-alpha: A cell signaling protein (cytokine) involved in a broad range of signaling pathways, commonly associated with pro-inflammatory signaling.

TME = Tumor microenvironment: The complete environment of a tumor, which apart from tumor cells, consists of a wide range of cell types, being immune cells (T cells, macrophage,...), fibroblasts, endothelial cells, and extracellular matrix components.

TPZ = Tirapazamine: An experimental anticancer drug that is only toxic in conditions of hypoxia (low oxygen).

US = Ultrasound: Sound of which the frequency is higher than the upper limit of human hearing. It is commonly employed as a noninvasive imaging method, where specific contrast can be generated using MBs.

VCAM-1 = Vascular cell adhesion molecule-1 (= CD106): A cytokine-inducible molecule predominantly expressed on endothelial cells. It links endothelial adhesion to signal transduction.

VEGF = Vascular endothelial growth factor: A potent angiogenic factor secreted by cells to promote the formation of new blood vessels (= angiogenesis). It is a crucial process in tumor formation and VEGF is therefore an actively studied therapeutic agent.

## REFERENCES

- (1) Fenton, O. S.; Olafson, K. N.; Pillai, P. S.; Mitchell, M. J.; Langer, R. *Advances in Biomaterials for Drug Delivery. Adv. Mater.* **2018**, *30*, e1705328.
- (2) Salata, O. *Applications of Nanoparticles in Biology and Medicine. J. Nanobiotechnol.* **2004**, *2*, 3.
- (3) Anselmo, A. C.; Mitragotri, S. *Nanoparticles in the Clinic: An Update. Bioeng. Transl. Med.* **2019**, *4*, e10143.
- (4) Anselmo, A. C.; Mitragotri, S. *An Overview of Clinical and Commercial Impact of Drug Delivery Systems. J. Controlled Release* **2014**, *190*, 15–28.

- (5) Torchilin, V. P. Multifunctional, Stimuli-Sensitive Nanoparticulate Systems for Drug Delivery. *Nat. Rev. Drug Discovery* **2014**, *13*, 813–827.
- (6) Min, Y.; Caster, J. M.; Eblan, M. J.; Wang, A. Z. Clinical Translation of Nanomedicine. *Chem. Rev.* **2015**, *115*, 11147–11190.
- (7) Wagner, V.; Dullaart, A.; Bock, A. K.; Zweck, A. The Emerging Nanomedicine Landscape. *Nat. Biotechnol.* **2006**, *24*, 1211–1217.
- (8) Kanasty, R.; Dorkin, J. R.; Vegas, A.; Anderson, D. Delivery Materials for SiRNA Therapeutics. *Nat. Mater.* **2013**, *12*, 967–977.
- (9) Whitehead, K. A.; Langer, R.; Anderson, D. G. Knocking Down Barriers: Advances in SiRNA Delivery. *Nat. Rev. Drug Discovery* **2009**, *8*, 129–138.
- (10) Petros, R. A.; DeSimone, J. M. Strategies in the Design of Nanoparticles for Therapeutic Applications. *Nat. Rev. Drug Discovery* **2010**, *9*, 615–627.
- (11) Peer, D.; Karp, J. M.; Hong, S.; Farokhzad, O. C.; Margalit, R.; Langer, R. Nanocarriers as an Emerging Platform for Cancer Therapy. *Nat. Nanotechnol.* **2007**, *2*, 751–760.
- (12) Maksoudian, C.; Saffarzadeh, N.; Hesemans, E.; Dekoning, N.; Buttiens, K.; Soenen, S. J. Role of Inorganic Nanoparticle Degradation in Cancer Therapy. *Nanoscale Adv.* **2020**, *2*, 3734–3763.
- (13) Anselmo, A. C.; Mitragotri, S. A Review of Clinical Translation of Inorganic Nanoparticles. *AAPS J.* **2015**, *17*, 1041–1054.
- (14) McCarthy, J. R.; Weissleder, R. Multifunctional Magnetic Nanoparticles for Targeted Imaging and Therapy. *Adv. Drug Delivery Rev.* **2008**, *60*, 1241–1251.
- (15) Sun, T.; Zhang, Y. S.; Pang, B.; Hyun, D. C.; Yang, M.; Xia, Y. Engineered Nanoparticles for Drug Delivery in Cancer Therapy. *Angew. Chem., Int. Ed.* **2014**, *53*, 12320–12364.
- (16) Wang, A. Z.; Langer, R.; Farokhzad, O. C. Nanoparticle Delivery of Cancer Drugs. *Annu. Rev. Med.* **2012**, *63*, 185–198.
- (17) Mura, S.; Nicolas, J.; Couvreur, P. Stimuli-Responsive Nanocarriers for Drug Delivery. *Nat. Mater.* **2013**, *12*, 991–1003.
- (18) Soenen, S. J.; Parak, W. J.; Rejman, J.; Manshian, B. (Intra)Cellular Stability of Inorganic Nanoparticles: Effects on Cytotoxicity, Particle Functionality, and Biomedical Applications. *Chem. Rev.* **2015**, *115*, 2109–2135.
- (19) Manshian, B. B.; Pokhrel, S.; Himmelreich, U.; Tamm, K.; Sikk, L.; Fernandez, A.; Rallo, R.; Tamm, T.; Madler, L.; Soenen, S. J. In Silico Design of Optimal Dissolution Kinetics of Fe-Doped ZnO Nanoparticles Results in Cancer-Specific Toxicity in a Preclinical Rodent Model. *Adv. Healthcare Mater.* **2017**, *6*, 1601379.
- (20) Naatz, H.; Manshian, B. B.; Rios Luci, C.; Tsikourkitoudi, V.; Deligiannakis, Y.; Birkenstock, J.; Pokhrel, S.; Madler, L.; Soenen, S. J. Model-Based Nanoengineered Pharmacokinetics of Iron-Doped Copper Oxide for Nanomedical Applications. *Angew. Chem., Int. Ed.* **2020**, *59*, 1828–1836.
- (21) Golombek, S. K.; May, J. N.; Theek, B.; Appold, L.; Drude, N.; Kiessling, F.; Lammers, T. Tumor Targeting Via EPR: Strategies to Enhance Patient Responses. *Adv. Drug Delivery Rev.* **2018**, *130*, 17–38.
- (22) Longmire, M.; Choyke, P. L.; Kobayashi, H. Clearance Properties of Nano-Sized Particles and Molecules as Imaging Agents: Considerations and Caveats. *Nanomedicine (London, U. K.)* **2008**, *3*, 703–717.
- (23) Suk, J. S.; Xu, Q.; Kim, N.; Hanes, J.; Ensign, L. M. Pegylation as a Strategy for Improving Nanoparticle-Based Drug and Gene Delivery. *Adv. Drug Delivery Rev.* **2016**, *99*, 28–51.
- (24) Gustafson, H. H.; Holt-Casper, D.; Grainger, D. W.; Ghandehari, H. Nanoparticle Uptake: The Phagocyte Problem. *Nano Today* **2015**, *10*, 487–510.
- (25) Ngoune, R.; Peters, A.; von Elverfeldt, D.; Winkler, K.; Putz, G. Accumulating Nanoparticles by EPR: A Route of No Return. *J. Controlled Release* **2016**, *238*, 58–70.
- (26) Tsoi, K. M.; MacParland, S. A.; Ma, X. Z.; Spetzler, V. N.; Echeverri, J.; Ouyang, B.; Fadel, S. M.; Sykes, E. A.; Goldaracena, N.; Kathis, J. M.; et al. Mechanism of Hard-Nanomaterial Clearance by the Liver. *Nat. Mater.* **2016**, *15*, 1212–1221.
- (27) Schubert, J.; Chanana, M. Coating Matters: Review on Colloidal Stability of Nanoparticles with Biocompatible Coatings in Biological Media, Living Cells and Organisms. *Curr. Med. Chem.* **2018**, *25*, 4553–4586.
- (28) Schöttler, S.; Becker, G.; Winzen, S.; Steinbach, T.; Mohr, K.; Landfester, K.; Mailänder, V.; Wurm, F. R. Protein Adsorption Is Required for Stealth Effect of Poly(Ethylene Glycol)- and Poly-(Phosphoester)-Coated Nanocarriers. *Nat. Nanotechnol.* **2016**, *11*, 372–377.
- (29) Cao, H.; Dan, Z.; He, X.; Zhang, Z.; Yu, H.; Yin, Q.; Li, Y. Liposomes Coated with Isolated Macrophage Membrane Can Target Lung Metastasis of Breast Cancer. *ACS Nano* **2016**, *10*, 7738–7748.
- (30) Wilhelm, S.; Tavares, A. J.; Dai, Q.; Ohta, S.; Audet, J.; Dvorak, H. F.; Chan, W. C. W. Analysis of Nanoparticle Delivery to Tumours. *Nat. Rev. Mater.* **2016**, *1*, 16014.
- (31) McNeil, S. E. Evaluation of Nanomedicines: Stick to the Basics. *Nat. Rev. Mater.* **2016**, *1*, 16073.
- (32) Price, L. S. L.; Stern, S. T.; Deal, A. M.; Kabanov, A. V.; Zamboni, W. C. A Reanalysis of Nanoparticle Tumor Delivery Using Classical Pharmacokinetic Metrics. *Science Adv.* **2020**, *6*, eaay9249.
- (33) Ouyang, B.; Poon, W.; Zhang, Y.-N.; Lin, Z. P.; Kingston, B. R.; Tavares, A. J.; Zhang, Y.; Chen, J.; Valic, M. S.; Syed, A. M.; et al. The Dose Threshold for Nanoparticle Tumor Delivery. *Nat. Mater.* **2020**, *19*, 1362–1371.
- (34) Wilhelm, S.; Tavares, A. J.; Chan, W. C. W. Reply to “Evaluation of Nanomedicines: Stick to the Basics”. *Nat. Rev. Mater.* **2016**, *1*, 16074.
- (35) Sykes, E. A.; Dai, Q.; Sarsons, C. D.; Chen, J.; Rocheleau, J. V.; Hwang, D. M.; Zheng, G.; Cramb, D. T.; Rinker, K. D.; Chan, W. C. Tailoring Nanoparticle Designs to Target Cancer Based on Tumor Pathophysiology. *Proc. Natl. Acad. Sci. U. S. A.* **2016**, *113*, E1142–1151.
- (36) Ojha, T.; Pathak, V.; Shi, Y.; Hennink, W. E.; Moonen, C. T. W.; Storm, G.; Kiessling, F.; Lammers, T. Pharmacological and Physical Vessel Modulation Strategies to Improve EPR-Mediated Drug Targeting to Tumors. *Adv. Drug Delivery Rev.* **2017**, *119*, 44–60.
- (37) Sonveaux, P.; Dessy, C.; Martinive, P.; Havaux, X.; Jordan, B. F.; Gallez, B.; Grégoire, V.; Balligand, J.-L.; Feron, O. Endothelin-1 Is a Critical Mediator of Myogenic Tone in Tumor Arterioles. *Cancer Res.* **2004**, *64*, 3209–3214.
- (38) Tracey, K. J.; Cerami, A. Tumor Necrosis Factor, Other Cytokines and Disease. *Annu. Rev. Cell Biol.* **1993**, *9*, 317–343.
- (39) Krajcnik, M.; Zyllicz, Z. Understanding Pruritus in Systemic Disease. *J. Pain Symptom Manage.* **2001**, *21*, 151–168.
- (40) Eggermont, A. M.; Schraffordt Koops, H.; Liénard, D.; Kroon, B. B.; van Geel, A. N.; Hoekstra, H. J.; Lejeune, F. J. Isolated Limb Perfusion with High-Dose Tumor Necrosis Factor-Alpha in Combination with Interferon-Gamma and Melphalan for Non-resectable Extremity Soft Tissue Sarcomas: A Multicenter Trial. *J. Clin. Oncol.* **1996**, *14*, 2653–2665.
- (41) Lejeune, F.; Liénard, D.; Eggermont, A.; Koops, H. S.; Rosenkaimer, F.; Gérard, J.; Klaase, J.; Kroon, B.; Vanderveken, J.; Schmitz, P. Rationale for Using Tnf $\alpha$  and Chemotherapy in Regional Therapy of Melanoma. *J. Cell. Biochem.* **1994**, *56*, 52–61.
- (42) Zhang, B.; Jiang, T.; Tuo, Y.; Jin, K.; Luo, Z.; Shi, W.; Mei, H.; Hu, Y.; Pang, Z.; Jiang, X. Captopril Improves Tumor Nanomedicine Delivery by Increasing Tumor Blood Perfusion and Enlarging Endothelial Gaps in Tumor Blood Vessels. *Cancer Lett.* **2017**, *410*, 12–19.
- (43) Jain, R. K. Normalization of Tumor Vasculature: An Emerging Concept in Antiangiogenic Therapy. *Science* **2005**, *307*, 58–62.
- (44) Batchelor, T. T.; Gerstner, E. R.; Emblem, K. E.; Duda, D. G.; Kalpathy-Cramer, J.; Snuderl, M.; Ancukiewicz, M.; Polaskova, P.; Pinho, M. C.; Jennings, D.; et al. Improved Tumor Oxygenation and Survival in Glioblastoma Patients Who Show Increased Blood Perfusion after Cediranib and Chemoradiation. *Proc. Natl. Acad. Sci. U. S. A.* **2013**, *110*, 19059–19064.
- (45) Cantelmo, A. R.; Conradi, L. C.; Brajic, A.; Goveia, J.; Kalucka, J.; Pircher, A.; Chaturvedi, P.; Hol, J.; Thienpont, B.; Teuwen, L. A.;

et al. Inhibition of the Glycolytic Activator Pfkfb3 in Endothelium Induces Tumor Vessel Normalization, Impairs Metastasis, and Improves Chemotherapy. *Cancer Cell* **2016**, *30*, 968–985.

(46) Chauhan, V. P.; Stylianopoulos, T.; Martin, J. D.; Popovic, Z.; Chen, O.; Kamoun, W. S.; Bawendi, M. G.; Fukumura, D.; Jain, R. K. Normalization of Tumor Blood Vessels Improves the Delivery of Nanomedicines in a Size-Dependent Manner. *Nat. Nanotechnol.* **2012**, *7*, 383–388.

(47) Jain, R. K.; Duda, D. G.; Clark, J. W.; Loeffler, J. S. Lessons from Phase III Clinical Trials on Anti-Vegf Therapy for Cancer. *Nat. Clin. Pract. Oncol.* **2006**, *3*, 24–40.

(48) Jain, R. K. Normalizing Tumor Microenvironment to Treat Cancer: Bench to Bedside to Biomarkers. *J. Clin. Oncol.* **2013**, *31*, 2205–2218.

(49) Satterlee, A. B.; Rojas, J. D.; Dayton, P. A.; Huang, L. Enhancing Nanoparticle Accumulation and Retention in Desmoplastic Tumors Via Vascular Disruption for Internal Radiation Therapy. *Theranostics* **2017**, *7*, 253–269.

(50) Beaugreard, D. A.; Thelwall, P. E.; Chaplin, D. J.; Hill, S. A.; Adams, G. E.; Brindle, K. M. Magnetic Resonance Imaging and Spectroscopy of Combretastatin A4 Prodrug-Induced Disruption of Tumor Perfusion and Energetic Status. *Br. J. Cancer* **1998**, *77*, 1761–1767.

(51) Lubner, M. G.; Brace, C. L.; Hinshaw, J. L.; Lee, F. T., Jr. Microwave Tumor Ablation: Mechanism of Action, Clinical Results, and Devices. *J. Vasc. Interv. Radiol.* **2010**, *21*, S192–203.

(52) Kurokohchi, K.; Watanabe, S.; Masaki, T.; Hosomi, N.; Funaki, T.; Arima, K.; Yoshida, S.; Miyauchi, Y.; Kuriyama, S. Combined Use of Percutaneous Ethanol Injection and Radiofrequency Ablation for the Effective Treatment of Hepatocellular Carcinoma. *Int. J. Oncol.* **2002**, *21*, 841–846.

(53) Hijnen, N. M.; Heijman, E.; Köhler, M. O.; Ylihautala, M.; Ehnholm, G. J.; Simonetti, A. W.; Grüll, H. Tumor Hyperthermia and Ablation in Rats Using a Clinical Mr-Hifu System Equipped with a Dedicated Small Animal Set-Up. *Int. J. Hyperthermia* **2012**, *28*, 141–155.

(54) Vujaskovic, Z.; Song, C. W. Physiological Mechanisms Underlying Heat-Induced Radiosensitization. *Int. J. Hyperthermia* **2004**, *20*, 163–174.

(55) Mohamed, F.; Marchettini, P.; Stuart, O. A.; Urano, M.; Sugarbaker, P. H. Thermal Enhancement of New Chemotherapeutic Agents at Moderate Hyperthermia. *Ann. Surg. Oncol.* **2003**, *10*, 463–468.

(56) Sato, I.; Umemura, M.; Mitsudo, K.; Fukumura, H.; Kim, J.-H.; Hoshino, Y.; Nakashima, H.; Kioi, M.; Nakakaji, R.; Sato, M.; et al. Simultaneous Hyperthermia-Chemotherapy with Controlled Drug Delivery Using Single-Drug Nanoparticles. *Sci. Rep.* **2016**, *6*, 24629.

(57) Schwickert, H. C.; Stiskal, M.; Roberts, T. P.; van Dijke, C. F.; Mann, J.; Muhler, A.; Shames, D. M.; Demsar, F.; Disston, A.; Brasch, R. C. Contrast-Enhanced Mr Imaging Assessment of Tumor Capillary Permeability: Effect of Irradiation on Delivery of Chemotherapy. *Radiology* **1996**, *198*, 893–898.

(58) Lammers, T.; Subr, V.; Peschke, P.; Kuhnlein, R.; Hennink, W. E.; Ulbrich, K.; Kiessling, F.; Heilmann, M.; Debus, J.; Huber, P. E.; et al. Image-Guided and Passively Tumor-Targeted Polymeric Nanomedicines for Radiochemotherapy. *Br. J. Cancer* **2008**, *99*, 900–910.

(59) Davies, C.; Lundstrom, L. M.; Frengen, J.; Eikenes, L.; Bruland, S. O.; Kaalhus, O.; Hjelstuen, M. H.; Brekken, C. Radiation Improves the Distribution and Uptake of Liposomal Doxorubicin (Caelyx) in Human Osteosarcoma Xenografts. *Cancer Res.* **2004**, *64*, 547–553.

(60) Erel-Akbaba, G.; Carvalho, L. A.; Tian, T.; Zinter, M.; Akbaba, H.; Obeid, P. J.; Chiocca, E. A.; Weissleder, R.; Kantarci, A. G.; Tannous, B. A. Radiation-Induced Targeted Nanoparticle-Based Gene Delivery for Brain Tumor Therapy. *ACS Nano* **2019**, *13*, 4028–4040.

(61) Lentacker, I.; De Cock, I.; Deckers, R.; De Smedt, S. C.; Moonen, C. T. Understanding Ultrasound Induced Sonoporation: Definitions and Underlying Mechanisms. *Adv. Drug Delivery Rev.* **2014**, *72*, 49–64.

(62) Theek, B.; Baues, M.; Ojha, T.; Möckel, D.; Veettil, S. K.; Steitz, J.; van Bloois, L.; Storm, G.; Kiessling, F.; Lammers, T. Sonoporation Enhances Liposome Accumulation and Penetration in Tumors with Low Epr. *J. Controlled Release* **2016**, *231*, 77–85.

(63) Henderson, B. W.; Bellnier, D. A.; Greco, W. R.; Sharma, A.; Pandey, R. K.; Vaughan, L. A.; Weishaupt, K. R.; Dougherty, T. J. An in Vivo Quantitative Structure-Activity Relationship for a Congeneric Series of Porphyrin Derivatives as Photosensitizers for Photodynamic Therapy. *Cancer Res.* **1997**, *57*, 4000–4007.

(64) Fingar, V. H.; Wieman, T. J.; Wiehle, S. A.; Cerrito, P. B. The Role of Microvascular Damage in Photodynamic Therapy: The Effect of Treatment on Vessel Constriction, Permeability, and Leukocyte Adhesion. *Cancer Res.* **1992**, *52*, 4914–4921.

(65) Roberts, W. G.; Hasan, T. Role of Neovasculature and Vascular Permeability on the Tumor Retention of Photodynamic Agents. *Cancer Res.* **1992**, *52*, 924–930.

(66) Chen, B.; Pogue, B. W.; Luna, J. M.; Hardman, R. L.; Hoopes, P. J.; Hasan, T. Tumor Vascular Permeabilization by Vascular-Targeting Photosensitization: Effects, Mechanism, and Therapeutic Implications. *Clin. Cancer Res.* **2006**, *12*, 917–923.

(67) Sporn, L. A.; Foster, T. H. Photofrin and Light Induces Microtubule Depolymerization in Cultured Human Endothelial Cells. *Cancer Res.* **1992**, *52*, 3443–3448.

(68) Snyder, J. W.; Greco, W. R.; Bellnier, D. A.; Vaughan, L.; Henderson, B. W. Photodynamic Therapy: A Means to Enhanced Drug Delivery to Tumors. *Cancer Res.* **2003**, *63*, 8126–8131.

(69) Paris, J. L.; Villaverde, G.; Gómez-Graña, S.; Vallet-Regí, M. Nanoparticles for Multimodal Antivascular Therapeutics: Dual Drug Release, Photothermal and Photodynamic Therapy. *Acta Biomater.* **2020**, *101*, 459–468.

(70) Vaupel, P.; Mayer, A. Hypoxia in Cancer: Significance and Impact on Clinical Outcome. *Cancer Metastasis Rev.* **2007**, *26*, 225–239.

(71) Muz, B.; de la Puente, P.; Azab, F.; Azab, A. K. The Role of Hypoxia in Cancer Progression, Angiogenesis, Metastasis, and Resistance to Therapy. *Hypoxia* **2015**, *3*, 83–92.

(72) Gao, M.; Liang, C.; Song, X.; Chen, Q.; Jin, Q.; Wang, C.; Liu, Z. Erythrocyte-Membrane-Enveloped Perfluorocarbon as Nanoscale Artificial Red Blood Cells to Relieve Tumor Hypoxia and Enhance Cancer Radiotherapy. *Adv. Mater.* **2017**, *29*, 1701429.

(73) Chen, Q.; Feng, L.; Liu, J.; Zhu, W.; Dong, Z.; Wu, Y.; Liu, Z. Intelligent Albumin-MnO<sub>2</sub> Nanoparticles as Ph-/H<sub>2</sub>O<sub>2</sub>-Responsive Dissociable Nanocarriers to Modulate Tumor Hypoxia for Effective Combination Therapy. *Adv. Mater.* **2016**, *28*, 7129–7136.

(74) Liu, L.-H.; Zhang, Y.-H.; Qiu, W.-X.; Zhang, L.; Gao, F.; Li, B.; Xu, L.; Fan, J.-X.; Li, Z.-H.; Zhang, X.-Z. Dual-Stage Light Amplified Photodynamic Therapy against Hypoxic Tumor Based on an O<sub>2</sub> Self-Sufficient Nanoplatform. *Small* **2017**, *13*, 1701621.

(75) Liu, P.; Xie, X.; Shi, X.; Peng, Y.; Ding, J.; Zhou, W. Oxygen-Self-Supplying and Hif-1 $\alpha$ -Inhibiting Core-Shell Nanosystem for Hypoxia-Resistant Photodynamic Therapy. *ACS Appl. Mater. Interfaces* **2019**, *11*, 48261–48270.

(76) Prasad, P.; Gordijo, C. R.; Abbasi, A. Z.; Maeda, A.; Ip, A.; Rauth, A. M.; DaCosta, R. S.; Wu, X. Y. Multifunctional Albumin-MnO<sub>2</sub> Nanoparticles Modulate Solid Tumor Microenvironment by Attenuating Hypoxia, Acidosis, Vascular Endothelial Growth Factor and Enhance Radiation Response. *ACS Nano* **2014**, *8*, 3202–3212.

(77) Zhu, W.; Dong, Z.; Fu, T.; Liu, J.; Chen, Q.; Li, Y.; Zhu, R.; Xu, L.; Liu, Z. Modulation of Hypoxia in Solid Tumor Microenvironment with MnO<sub>2</sub> Nanoparticles to Enhance Photodynamic Therapy. *Adv. Funct. Mater.* **2016**, *26*, 5490–5498.

(78) Scharping, N. E.; Menk, A. V.; Whetstone, R. D.; Zeng, X.; Delgoffe, G. M. Efficacy of Pd-1 Blockade Is Potentiated by Metformin-Induced Reduction of Tumor Hypoxia. *Cancer Immunol. Res.* **2017**, *5*, 9–16.

(79) Ashton, T. M.; Fokas, E.; Kunz-Schughart, L. A.; Folkes, L. K.; Anbalagan, S.; Huether, M.; Kelly, C. J.; Pirovano, G.; Buffa, F. M.; Hammond, E. M.; et al. The Anti-Malarial Atovaquone Increases



Radiosensitivity by Alleviating Tumour Hypoxia. *Nat. Commun.* **2016**, *7*, 12308.

(80) Yang, Z.; Chen, Q.; Chen, J.; Dong, Z.; Zhang, R.; Liu, J.; Liu, Z. Tumor-Ph-Responsive Dissociable Albumin-Tamoxifen Nano-complexes Enabling Efficient Tumor Penetration and Hypoxia Relief for Enhanced Cancer Photodynamic Therapy. *Small* **2018**, *14*, 1803262.

(81) Yu, W.; Liu, T.; Zhang, M.; Wang, Z.; Ye, J.; Li, C. X.; Liu, W.; Li, R.; Feng, J.; Zhang, X. Z. O<sub>2</sub> Economizer for Inhibiting Cell Respiration to Combat the Hypoxia Obstacle in Tumor Treatments. *ACS Nano* **2019**, *13*, 1784–1794.

(82) Song, X.; Feng, L.; Liang, C.; Yang, K.; Liu, Z. Ultrasound Triggered Tumor Oxygenation with Oxygen-Shuttle Nanoperfluorocarbon to Overcome Hypoxia-Associated Resistance in Cancer Therapies. *Nano Lett.* **2016**, *16*, 6145–6153.

(83) Jahanban-Esfahlan, R.; de la Guardia, M.; Ahmadi, D.; Yousefi, B. Modulating Tumor Hypoxia by Nanomedicine for Effective Cancer Therapy. *J. Cell. Physiol.* **2018**, *233*, 2019–2031.

(84) Liu, Y.; Liu, Y.; Bu, W.; Cheng, C.; Zuo, C.; Xiao, Q.; Sun, Y.; Ni, D.; Zhang, C.; Liu, J.; et al. Hypoxia Induced by Upconversion-Based Photodynamic Therapy: Towards Highly Effective Synergistic Bioreductive Therapy in Tumors. *Angew. Chem., Int. Ed.* **2015**, *54*, 8105–8109.

(85) Moellering, R. E.; Black, K. C.; Krishnamurty, C.; Baggett, B. K.; Stafford, P.; Rain, M.; Gatenby, R. A.; Gillies, R. J. Acid Treatment of Melanoma Cells Selects for Invasive Phenotypes. *Clin. Exp. Metastasis* **2008**, *25*, 411–425.

(86) Stubbs, M.; McSheehy, P. M.; Griffiths, J. R.; Bashford, C. L. Causes and Consequences of Tumour Acidity and Implications for Treatment. *Mol. Med. Today* **2000**, *6*, 15–19.

(87) Peretyazhko, T. S.; Zhang, Q.; Colvin, V. L. Size-Controlled Dissolution of Silver Nanoparticles at Neutral and Acidic Ph Conditions: Kinetics and Size Changes. *Environ. Sci. Technol.* **2014**, *48*, 11954–11961.

(88) Zhong, S.; Jeong, J.-H.; Chen, Z.; Chen, Z.; Luo, J.-L. Targeting Tumor Microenvironment by Small-Molecule Inhibitors. *Transl. Oncol.* **2020**, *13*, 57–69.

(89) Zhou, Y.; Chen, X.; Cao, J.; Gao, H. Overcoming the Biological Barriers in the Tumor Microenvironment for Improving Drug Delivery and Efficacy. *J. Mater. Chem. B* **2020**, *8*, 6765–6781.

(90) Luo, G.-F.; Chen, W.-H.; Hong, S.; Cheng, Q.; Qiu, W.-X.; Zhang, X.-Z. A Self-Transformable Ph-Driven Membrane-Anchoring Photosensitizer for Effective Photodynamic Therapy to Inhibit Tumor Growth and Metastasis. *Adv. Funct. Mater.* **2017**, *27*, 1702122.

(91) Provenzano, P. P.; Cuevas, C.; Chang, A. E.; Goel, V. K.; Von Hoff, D. D.; Hingorani, S. R. Enzymatic Targeting of the Stroma Ablates Physical Barriers to Treatment of Pancreatic Ductal Adenocarcinoma. *Cancer Cell* **2012**, *21*, 418–429.

(92) Netti, P. A.; Berk, D. A.; Swartz, M. A.; Grodzinsky, A. J.; Jain, R. K. Role of Extracellular Matrix Assembly in Interstitial Transport in Solid Tumors. *Cancer Res.* **2000**, *60*, 2497–2503.

(93) Haider, T.; Sandha, K. K.; Soni, V.; Gupta, P. N. Recent Advances in Tumor Microenvironment Associated Therapeutic Strategies and Evaluation Models. *Mater. Sci. Eng., C* **2020**, *116*, 111229.

(94) Yang, S.; Gao, H. Nanoparticles for Modulating Tumor Microenvironment to Improve Drug Delivery and Tumor Therapy. *Pharmacol. Res.* **2017**, *126*, 97–108.

(95) Jarvelainen, H.; Sainio, A.; Koulu, M.; Wight, T. N.; Penttinen, R. Extracellular Matrix Molecules: Potential Targets in Pharmacotherapy. *Pharmacol. Rev.* **2009**, *61*, 198–223.

(96) Frantz, C.; Stewart, K. M.; Weaver, V. M. The Extracellular Matrix at a Glance. *J. Cell Sci.* **2010**, *123*, 4195–4200.

(97) Zhang, B.; Jiang, T.; Shen, S.; She, X.; Tuo, Y.; Hu, Y.; Pang, Z.; Jiang, X. Cyclopamine Disrupts Tumor Extracellular Matrix and Improves the Distribution and Efficacy of Nanotherapeutics in Pancreatic Cancer. *Biomaterials* **2016**, *103*, 12–21.

(98) Stylianopoulos, T.; Jain, R. K. Combining Two Strategies to Improve Perfusion and Drug Delivery in Solid Tumors. *Proc. Natl. Acad. Sci. U. S. A.* **2013**, *110*, 18632–18637.

(99) Aziz, J.; Shezali, H.; Radzi, Z.; Yahya, N. A.; Abu Kassim, N. H.; Czernuszka, J.; Rahman, M. T. Molecular Mechanisms of Stress-Responsive Changes in Collagen and Elastin Networks in Skin. *Skin Pharmacol. Physiol.* **2016**, *29*, 190–203.

(100) Miao, L.; Lin, C. M.; Huang, L. Stromal Barriers and Strategies for the Delivery of Nanomedicine to Desmoplastic Tumors. *J. Controlled Release* **2015**, *219*, 192–204.

(101) Deryugina, E. I.; Quigley, J. P. Matrix Metalloproteinases and Tumor Metastasis. *Cancer Metastasis Rev.* **2006**, *25*, 9–34.

(102) Pickup, M. W.; Laklai, H.; Acerbi, I.; Owens, P.; Gorska, A. E.; Chytil, A.; Aakre, M.; Weaver, V. M.; Moses, H. L. Stromally Derived Lysyl Oxidase Promotes Metastasis of Transforming Growth Factor-Beta-Deficient Mouse Mammary Carcinomas. *Cancer Res.* **2013**, *73*, 5336–5346.

(103) Aluwihare, P.; Mu, Z.; Zhao, Z.; Yu, D.; Weinreb, P. H.; Horan, G. S.; Violette, S. M.; Munger, J. S. Mice That Lack Activity of Av $\beta$ 6- and Av $\beta$ 8-Integrins Reproduce the Abnormalities of < Em > Tgfb1</Em>- and < Em > Tgfb3</Em>-Null Mice. *J. Cell Sci.* **2009**, *122*, 227–232.

(104) Whatcott, C. J.; Han, H.; Posner, R. G.; Hostetter, G.; Von Hoff, D. D. Targeting the Tumor Microenvironment in Cancer: Why Hyaluronidase Deserves a Second Look. *Cancer Discovery* **2011**, *1*, 291–296.

(105) Liu, Y.; Jiang, P.; Capkova, K.; Xue, D.; Ye, L.; Sinha, S. C.; Mackman, N.; Janda, K. D.; Liu, C. Tissue Factor-Activated Coagulation Cascade in the Tumor Microenvironment Is Critical for Tumor Progression and an Effective Target for Therapy. *Cancer Res.* **2011**, *71*, 6492–6502.

(106) Nakahara, T.; Norberg, S. M.; Shalinsky, D. R.; Hu-Lowe, D. D.; McDonald, D. M. Effect of Inhibition of Vascular Endothelial Growth Factor Signaling on Distribution of Extravasated Antibodies in Tumors. *Cancer Res.* **2006**, *66*, 1434–1445.

(107) Nichols, J. W.; Bae, Y. H. Odyssey of a Cancer Nanoparticle: From Injection Site to Site of Action. *Nano Today* **2012**, *7*, 606–618.

(108) Chauhan, V. P.; Lanning, R. M.; Diop-Frimpong, B.; Mok, W.; Brown, E. B.; Padera, T. P.; Boucher, Y.; Jain, R. K. Multiscale Measurements Distinguish Cellular and Interstitial Hindrances to Diffusion in Vivo. *Biophys. J.* **2009**, *97*, 330–336.

(109) Zhang, B.; Jiang, T.; She, X.; Shen, S.; Wang, S.; Deng, J.; Shi, W.; Mei, H.; Hu, Y.; Pang, Z.; et al. Fibrin Degradation by Rtpa Enhances the Delivery of Nanotherapeutics to A549 Tumors in Nude Mice. *Biomaterials* **2016**, *96*, 63–71.

(110) Raeesi, V.; Chan, W. C. W. Improving Nanoparticle Diffusion through Tumor Collagen Matrix by Photo-Thermal Gold Nanorods. *Nanoscale* **2016**, *8*, 12524–12530.

(111) Lee, S.; Han, H.; Koo, H.; Na, J. H.; Yoon, H. Y.; Lee, K. E.; Lee, H.; Kim, H.; Kwon, I. C.; Kim, K. Extracellular Matrix Remodeling in Vivo for Enhancing Tumor-Targeting Efficiency of Nanoparticle Drug Carriers Using the Pulsed High Intensity Focused Ultrasound. *J. Controlled Release* **2017**, *263*, 68–78.

(112) Zhou, H.; Fan, Z.; Deng, J.; Lemons, P. K.; Arhontoulis, D. C.; Bowne, W. B.; Cheng, H. Hyaluronidase Embedded in Nanocarrier Peg Shell for Enhanced Tumor Penetration and Highly Efficient Antitumor Efficacy. *Nano Lett.* **2016**, *16*, 3268–3277.

(113) Magzoub, M.; Jin, S.; Verkman, A. S. Enhanced Macromolecule Diffusion Deep in Tumors after Enzymatic Digestion of Extracellular Matrix Collagen and Its Associated Proteoglycan Decorin. *FASEB J.* **2008**, *22*, 276–284.

(114) Kato, M.; Hattori, Y.; Kubo, M.; Maitani, Y. Collagenase-1 Injection Improved Tumor Distribution and Gene Expression of Cationic Lipoplex. *Int. J. Pharm.* **2012**, *423*, 428–434.

(115) Mardhian, D. F.; Storm, G.; Bansal, R.; Prakash, J. Nano-Targeted Relaxin Impairs Fibrosis and Tumor Growth in Pancreatic Cancer and Improves the Efficacy of Gemcitabine in Vivo. *J. Controlled Release* **2018**, *290*, 1–10.

- (116) Parodi, A.; Haddix, S. G.; Taghipour, N.; Scaria, S.; Taraballi, F.; Cevenini, A.; Yazdi, I. K.; Corbo, C.; Palomba, R.; Khaled, S. Z.; et al. Bromelain Surface Modification Increases the Diffusion of Silica Nanoparticles in the Tumor Extracellular Matrix. *ACS Nano* **2014**, *8*, 9874–9883.
- (117) Liu, J.; Liao, S.; Diop-Frimpong, B.; Chen, W.; Goel, S.; Naxerova, K.; Ancukiewicz, M.; Boucher, Y.; Jain, R. K.; Xu, L. Tgf-Beta Blockade Improves the Distribution and Efficacy of Therapeutics in Breast Carcinoma by Normalizing the Tumor Stroma. *Proc. Natl. Acad. Sci. U. S. A.* **2012**, *109*, 16618–16623.
- (118) Kanapathipillai, M.; Mammoto, A.; Mammoto, T.; Kang, J. H.; Jiang, E.; Ghosh, K.; Korin, N.; Gibbs, A.; Mannix, R.; Ingber, D. E. Inhibition of Mammary Tumor Growth Using Lysyl Oxidase-Targeting Nanoparticles to Modify Extracellular Matrix. *Nano Lett.* **2012**, *12*, 3213–3217.
- (119) Pinter, M.; Weinmann, A.; Wörns, M.-A.; Hucke, F.; Bota, S.; Marquardt, J. U.; Duda, D. G.; Jain, R. K.; Galle, P. R.; Trauner, M.; et al. Use of Inhibitors of the Renin–Angiotensin System Is Associated with Longer Survival in Patients with Hepatocellular Carcinoma. *United Eur. Gastroenterol. J.* **2017**, *5*, 987–996.
- (120) Hu, X.-X.; He, P.-P.; Qi, G.-B.; Gao, Y.-J.; Lin, Y.-X.; Yang, C.; Yang, P.-P.; Hao, H.; Wang, L.; Wang, H. Transformable Nanomaterials as an Artificial Extracellular Matrix for Inhibiting Tumor Invasion and Metastasis. *ACS Nano* **2017**, *11*, 4086–4096.
- (121) Matsuda, K.; Ohga, N.; Hida, Y.; Muraki, C.; Tsuchiya, K.; Kurosu, T.; Akino, T.; Shih, S. C.; Totsuka, Y.; Klagsbrun, M.; et al. Isolated Tumor Endothelial Cells Maintain Specific Character During Long-Term Culture. *Biochem. Biophys. Res. Commun.* **2010**, *394*, 947–954.
- (122) De Sanctis, F.; Ugel, S.; Facciponte, J.; Facciabene, A. The Dark Side of Tumor-Associated Endothelial Cells. *Semin. Immunol.* **2018**, *35*, 35–47.
- (123) Raza, A.; Franklin, M. J.; Dudek, A. Z. Pericytes and Vessel Maturation During Tumor Angiogenesis and Metastasis. *Am. J. Hematol.* **2010**, *85*, 593–598.
- (124) Lu, C.; Thaker, P. H.; Lin, Y. G.; Spanuth, W.; Landen, C. N.; Merritt, W. M.; Jennings, N. B.; Langley, R. R.; Gershenson, D. M.; Yancopoulos, G. D.; et al. Impact of Vessel Maturation on Antiangiogenic Therapy in Ovarian Cancer. *Am. J. Obstet. Gynecol.* **2008**, *198*, 477.
- (125) Reinmuth, N.; Liu, W.; Jung, Y. D.; Ahmad, S. A.; Shaheen, R. M.; Fan, F.; Bucana, C. D.; McMahon, G.; Gallick, G. E.; Ellis, L. M. Induction of Vegf in Perivascular Cells Defines a Potential Paracrine Mechanism for Endothelial Cell Survival. *FASEB J.* **2001**, *15*, 1239–1241.
- (126) Cabral, H.; Matsumoto, Y.; Mizuno, K.; Chen, Q.; Murakami, M.; Kimura, M.; Terada, Y.; Kano, M. R.; Miyazono, K.; Uesaka, M.; et al. Accumulation of Sub-100 Nm Polymeric Micelles in Poorly Permeable Tumours Depends on Size. *Nat. Nanotechnol.* **2011**, *6*, 815–823.
- (127) Meng, H.; Zhao, Y.; Dong, J.; Xue, M.; Lin, Y. S.; Ji, Z.; Mai, W. X.; Zhang, H.; Chang, C. H.; Brinker, C. J.; et al. Two-Wave Nanotherapy to Target the Stroma and Optimize Gemcitabine Delivery to a Human Pancreatic Cancer Model in Mice. *ACS Nano* **2013**, *7*, 10048–10065.
- (128) Weisshardt, P.; Trarbach, T.; Durig, J.; Paul, A.; Reis, H.; Tilki, D.; Miroschnick, I.; Ergun, S.; Klein, D. Tumor Vessel Stabilization and Remodeling by Anti-Angiogenic Therapy with Bevacizumab. *Histochem. Cell Biol.* **2012**, *137*, 391–401.
- (129) Loi, M.; Marchio, S.; Becherini, P.; Di Paolo, D.; Soster, M.; Curnis, F.; Brignole, C.; Pagnan, G.; Perri, P.; Caffa, I.; et al. Combined Targeting of Perivascular and Endothelial Tumor Cells Enhances Anti-Tumor Efficacy of Liposomal Chemotherapy in Neuroblastoma. *J. Controlled Release* **2010**, *145*, 66–73.
- (130) Guan, Y. Y.; Luan, X.; Xu, J. R.; Liu, Y. R.; Lu, Q.; Wang, C.; Liu, H. J.; Gao, Y. G.; Chen, H. Z.; Fang, C. Selective Eradication of Tumor Vascular Pericytes by Peptide-Conjugated Nanoparticles for Antiangiogenic Therapy of Melanoma Lung Metastasis. *Biomaterials* **2014**, *35*, 3060–3070.
- (131) Shiga, K.; Hara, M.; Nagasaki, T.; Sato, T.; Takahashi, H.; Takeyama, H. Cancer-Associated Fibroblasts: Their Characteristics and Their Roles in Tumor Growth. *Cancers* **2015**, *7*, 2443–2458.
- (132) Kalluri, R. The Biology and Function of Fibroblasts in Cancer. *Nat. Rev. Cancer* **2016**, *16*, 582–598.
- (133) Ji, T.; Ding, Y.; Zhao, Y.; Wang, J.; Qin, H.; Liu, X.; Lang, J.; Zhao, R.; Zhang, Y.; Shi, J.; et al. Peptide Assembly Integration of Fibroblast-Targeting and Cell-Penetration Features for Enhanced Antitumor Drug Delivery. *Adv. Mater.* **2015**, *27*, 1865–1873.
- (134) Hu, C.; Liu, X.; Ran, W.; Meng, J.; Zhai, Y.; Zhang, P.; Yin, Q.; Yu, H.; Zhang, Z.; Li, Y. Regulating Cancer Associated Fibroblasts with Losartan-Loaded Injectable Peptide Hydrogel to Potentiate Chemotherapy in Inhibiting Growth and Lung Metastasis of Triple Negative Breast Cancer. *Biomaterials* **2017**, *144*, 60–72.
- (135) Patel, K.; Doddapaneni, R.; Chowdhury, N.; Boakye, C. H.; Behl, G.; Singh, M. Tumor Stromal Disrupting Agent Enhances the Anticancer Efficacy of Docetaxel Loaded Pegylated Liposomes in Lung Cancer. *Nanomedicine (London, U. K.)* **2016**, *11*, 1377–1392.
- (136) Hu, K.; Miao, L.; Goodwin, T. J.; Li, J.; Liu, Q.; Huang, L. Quercetin Remodels the Tumor Microenvironment to Improve the Permeation, Retention, and Antitumor Effects of Nanoparticles. *ACS Nano* **2017**, *11*, 4916–4925.
- (137) Diop-Frimpong, B.; Chauhan, V. P.; Krane, S.; Boucher, Y.; Jain, R. K. Losartan Inhibits Collagen I Synthesis and Improves the Distribution and Efficacy of Nanotherapeutics in Tumors. *Proc. Natl. Acad. Sci. U. S. A.* **2011**, *108*, 2909–2914.
- (138) Miao, L.; Wang, Y.; Lin, C. M.; Xiong, Y.; Chen, N.; Zhang, L.; Kim, W. Y.; Huang, L. Nanoparticle Modulation of the Tumor Microenvironment Enhances Therapeutic Efficacy of Cisplatin. *J. Controlled Release* **2015**, *217*, 27–41.
- (139) Nam, J.; Son, S.; Park, K. S.; Zou, W.; Shea, L. D.; Moon, J. J. Cancer Nanomedicine for Combination Cancer Immunotherapy. *Nat. Rev. Mater.* **2019**, *4*, 398–414.
- (140) Jinushi, M.; Chiba, S.; Yoshiyama, H.; Masutomi, K.; Kinoshita, I.; Dosaka-Akita, H.; Yagita, H.; Takaoka, A.; Tahara, H. Tumor-Associated Macrophages Regulate Tumorigenicity and Anti-cancer Drug Responses of Cancer Stem/Initiating Cells. *Proc. Natl. Acad. Sci. U. S. A.* **2011**, *108*, 12425–12430.
- (141) Mantovani, A.; Marchesi, F.; Malesci, A.; Laghi, L.; Allavena, P. Tumour-Associated Macrophages as Treatment Targets in Oncology. *Nat. Rev. Clin. Oncol.* **2017**, *14*, 399–416.
- (142) Gabrilovich, D. I.; Ostrand-Rosenberg, S.; Bronte, V. Coordinated Regulation of Myeloid Cells by Tumours. *Nat. Rev. Immunol.* **2012**, *12*, 253–268.
- (143) Zhang, G.; Huang, H.; Zhu, Y.; Yu, G.; Gao, X.; Xu, Y.; Liu, C.; Hou, J.; Zhang, X. A Novel Subset of B7-H3(+)/Cd14(+)/Hla-Dr(-/Low) Myeloid-Derived Suppressor Cells Are Associated with Progression of Human Nscl. *Oncoimmunol.* **2015**, *4*, e977164.
- (144) Popovic, P. J.; Zeh, H. J., 3rd; Ochoa, J. B. Arginine and Immunity. *J. Nutr.* **2007**, *137*, 1681S–1686S.
- (145) Hu, C. E.; Gan, J.; Zhang, R. D.; Cheng, Y. R.; Huang, G. J. Up-Regulated Myeloid-Derived Suppressor Cell Contributes to Hepatocellular Carcinoma Development by Impairing Dendritic Cell Function. *Scand. J. Gastroenterol.* **2011**, *46*, 156–164.
- (146) Talmadge, J. E.; Gabrilovich, D. I. History of Myeloid-Derived Suppressor Cells. *Nat. Rev. Cancer* **2013**, *13*, 739–752.
- (147) Waldhauer, I.; Steinle, A. Nk Cells and Cancer Immun-surveillance. *Oncogene* **2008**, *27*, 5932–5943.
- (148) Buoncervello, M.; Gabriele, L.; Toschi, E. The Janus Face of Tumor Microenvironment Targeted by Immunotherapy. *Int. J. Mol. Sci.* **2019**, *20*, 4320.
- (149) Li, K.; Tian, H. Development of Small-Molecule Immune Checkpoint Inhibitors of Pd-1/Pd-L1 as a New Therapeutic Strategy for Tumour Immunotherapy. *J. Drug Target.* **2019**, *27*, 244–256.
- (150) Liu, D.; Chen, B.; Mo, Y.; Wang, Z.; Qi, T.; Zhang, Q.; Wang, Y. Redox-Activated Porphyrin-Based Liposome Remote-Loaded with Indoleamine 2,3-Dioxygenase (Ido) Inhibitor for Synergistic Photo-immunotherapy through Induction of Immunogenic Cell Death and Blockage of Ido Pathway. *Nano Lett.* **2019**, *19*, 6964–6976.

- (151) Lyons, Y. A.; Pradeep, S.; Wu, S. Y.; Haemmerle, M.; Hansen, J. M.; Wagner, M. J.; Villar-Prados, A.; Nagaraja, A. S.; Dood, R. L.; Previs, R. A.; et al. Macrophage Depletion through Colony Stimulating Factor 1 Receptor Pathway Blockade Overcomes Adaptive Resistance to Anti-Vegf Therapy. *Oncotarget* **2017**, *8*, 96496–96505.
- (152) Opperman, K. S.; Vandyke, K.; Clark, K. C.; Coulter, E. A.; Hewett, D. R.; Mrozik, K. M.; Schwarz, N.; Evdokiou, A.; Croucher, P. I.; Psaltis, P. J.; et al. Clodronate-Liposome Mediated Macrophage Depletion Abrogates Multiple Myeloma Tumor Establishment in Vivo. *Neoplasia* **2019**, *21*, 777–787.
- (153) Ngambenjawong, C.; Cieslewicz, M.; Schellinger, J. G.; Pun, S. H. Synthesis and Evaluation of Multivalent M2pep Peptides for Targeting Alternatively Activated M2Macrophages. *J. Controlled Release* **2016**, *224*, 103–111.
- (154) Shime, H.; Matsumoto, M.; Oshiumi, H.; Tanaka, S.; Nakane, A.; Iwakura, Y.; Tahara, H.; Inoue, N.; Seya, T. Toll-Like Receptor 3 Signaling Converts Tumor-Supporting Myeloid Cells to Tumoricidal Effectors. *Proc. Natl. Acad. Sci. U. S. A.* **2012**, *109*, 2066–2071.
- (155) Xu, C.; Yang, S.; Jiang, Z.; Zhou, J.; Yao, J. Self-Propelled Gemini-Like Lmwh-Scaffold Nanodrugs for Overall Tumor Micro-environment Manipulation Via Macrophage Reprogramming and Vessel Normalization. *Nano Lett.* **2020**, *20*, 372–383.
- (156) Chen, D.; Xie, J.; Fiskesund, R.; Dong, W.; Liang, X.; Lv, J.; Jin, X.; Liu, J.; Mo, S.; Zhang, T.; et al. Chloroquine Modulates Antitumor Immune Response by Resetting Tumor-Associated Macrophages toward M1 Phenotype. *Nat. Commun.* **2018**, *9*, 873.
- (157) Roode, L. E.; Brighton, H.; Bo, T.; Perry, J. L.; Parrott, M. C.; Kersey, F.; Luft, J. C.; Bear, J. E.; DeSimone, J. M.; Davis, I. J. Subtumoral Analysis of Print Nanoparticle Distribution Reveals Targeting Variation Based on Cellular and Particle Properties. *Nanomedicine* **2016**, *12*, 1053–1062.
- (158) Sato, K.; Sato, N.; Xu, B.; Nakamura, Y.; Nagaya, T.; Choyke, P. L.; Hasegawa, Y.; Kobayashi, H. Spatially Selective Depletion of Tumor-Associated Regulatory T Cells with near-Infrared Photo-immunotherapy. *Sci. Transl. Med.* **2016**, *8*, 352ra110.
- (159) Yu, H.; Lee, H.; Herrmann, A.; Buettner, R.; Jove, R. Revisiting Stat3 Signalling in Cancer: New and Unexpected Biological Functions. *Nat. Rev. Cancer* **2014**, *14*, 736–746.
- (160) Saeed, M.; Gao, J.; Shi, Y.; Lammers, T.; Yu, H. Engineering Nanoparticles to Reprogram the Tumor Immune Microenvironment for Improved Cancer Immunotherapy. *Theranostics* **2019**, *9*, 7981–8000.
- (161) Zhao, Y.; Huo, M.; Xu, Z.; Wang, Y.; Huang, L. Nanoparticle Delivery of Cddo-Me Remodels the Tumor Microenvironment and Enhances Vaccine Therapy for Melanoma. *Biomaterials* **2015**, *68*, 54–66.
- (162) Sasso, M. S.; Lollo, G.; Pitorre, M.; Solito, S.; Pinton, L.; Valpione, S.; Bastiat, G.; Mandruzzato, S.; Bronte, V.; Marigo, I.; et al. Low Dose Gemcitabine-Loaded Lipid Nanocapsules Target Monocytic Myeloid-Derived Suppressor Cells and Potentiate Cancer Immunotherapy. *Biomaterials* **2016**, *96*, 47–62.
- (163) Zhao, Y.; Cao, J.; Melamed, A.; Worley, M.; Gockley, A.; Jones, D.; Nia, H. T.; Zhang, Y.; Stylianopoulos, T.; Kumar, A. S.; et al. Losartan Treatment Enhances Chemotherapy Efficacy and Reduces Ascites in Ovarian Cancer Models by Normalizing the Tumor Stroma. *Proc. Natl. Acad. Sci. U. S. A.* **2019**, *116*, 2210–2219.
- (164) Maeda, H.; Bharate, G. Y.; Daruwalla, J. Polymeric Drugs for Efficient Tumor-Targeted Drug Delivery Based on Epr-Effect. *Eur. J. Pharm. Biopharm.* **2009**, *71*, 409–419.
- (165) Li, S. D.; Huang, L. Pharmacokinetics and Biodistribution of Nanoparticles. *Mol. Pharmaceutics* **2008**, *5*, 496–504.
- (166) Liu, D.; Mori, A.; Huang, L. Role of Liposome Size and Res Blockade in Controlling Biodistribution and Tumor Uptake of Gm1-Containing Liposomes. *Biochim. Biophys. Acta, Biomembr.* **1992**, *1104*, 95–101.
- (167) Zahr, A. S.; Davis, C. A.; Pishko, M. V. Macrophage Uptake of Core-Shell Nanoparticles Surface Modified with Poly(Ethylene Glycol). *Langmuir* **2006**, *22*, 8178–8185.
- (168) Zhang, J. S.; Liu, F.; Huang, L. Implications of Pharmacokinetic Behavior of Lipoplex for Its Inflammatory Toxicity. *Adv. Drug Delivery Rev.* **2005**, *57*, 689–698.
- (169) Campbell, R. B.; Fukumura, D.; Brown, E. B.; Mazzola, L. M.; Izumi, Y.; Jain, R. K.; Torchilin, V. P.; Munn, L. L. Cationic Charge Determines the Distribution of Liposomes between the Vascular and Extravascular Compartments of Tumors. *Cancer Res.* **2002**, *62*, 6831–6836.
- (170) Shehata, T.; Ogawara, K.; Higaki, K.; Kimura, T. Prolongation of Residence Time of Liposome by Surface-Modification with Mixture of Hydrophilic Polymers. *Int. J. Pharm.* **2008**, *359*, 272–279.
- (171) de Wolf, H. K.; Snel, C. J.; Verbaan, F. J.; Schifflers, R. M.; Hennink, W. E.; Storm, G. Effect of Cationic Carriers on the Pharmacokinetics and Tumor Localization of Nucleic Acids after Intravenous Administration. *Int. J. Pharm.* **2007**, *331*, 167–175.
- (172) Sihorkar, V.; Vyas, S. P. Potential of Polysaccharide Anchored Liposomes in Drug Delivery, Targeting and Immunization. *J. Pharm. Pharm. Sci.* **2001**, *4*, 138–158.
- (173) Ehling, J.; Theek, B.; Gremse, F.; Baetke, S.; Mockel, D.; Maynard, J.; Ricketts, S. A.; Grull, H.; Neeman, M.; Knuechel, R.; et al. Micro-Ct Imaging of Tumor Angiogenesis: Quantitative Measures Describing Micromorphology and Vascularization. *Am. J. Pathol.* **2014**, *184*, 431–441.
- (174) Theek, B.; Gremse, F.; Kunjachan, S.; Fokong, S.; Pola, R.; Pechar, M.; Deckers, R.; Storm, G.; Ehling, J.; Kiessling, F.; et al. Characterizing Epr-Mediated Passive Drug Targeting Using Contrast-Enhanced Functional Ultrasound Imaging. *J. Controlled Release* **2014**, *182*, 83–89.
- (175) Karageorgis, A.; Dufort, S.; Sancey, L.; Henry, M.; Hirsjarvi, S.; Passirani, C.; Benoit, J. P.; Gravier, J.; Texier, I.; Montigon, O.; et al. An Mri-Based Classification Scheme to Predict Passive Access of 5 to 50-Nm Large Nanoparticles to Tumors. *Sci. Rep.* **2016**, *6*, 21417.
- (176) Lammers, T.; Rizzo, L. Y.; Storm, G.; Kiessling, F. Personalized Nanomedicine. *Clin. Cancer Res.* **2012**, *18*, 4889–4894.
- (177) Chen, H.; Zhang, W.; Zhu, G.; Xie, J.; Chen, X. Rethinking Cancer Nanotheranostics. *Nat. Rev. Mater.* **2017**, *2*, 17024.
- (178) Lammers, T.; Aime, S.; Hennink, W. E.; Storm, G.; Kiessling, F. Theranostic Nanomedicine. *Acc. Chem. Res.* **2011**, *44*, 1029–1038.
- (179) Miller, M. A.; Arlauckas, S.; Weissleder, R. Prediction of Anti-Cancer Nanotherapy Efficacy by Imaging. *Nanotheranostics* **2017**, *1*, 296–312.
- (180) Lee, H.; Shields, A. F.; Siegel, B. A.; Miller, K. D.; Krop, I.; Ma, C. X.; LoRusso, P. M.; Munster, P. N.; Campbell, K.; Gaddy, D. F.; et al. (64)Cu-Mm-302 Positron Emission Tomography Quantifies Variability of Enhanced Permeability and Retention of Nanoparticles in Relation to Treatment Response in Patients with Metastatic Breast Cancer. *Clin. Cancer Res.* **2017**, *23*, 4190–4202.
- (181) Perez-Medina, C.; Abdel-Atti, D.; Tang, J.; Zhao, Y.; Fayad, Z. A.; Lewis, J. S.; Mulder, W. J. M.; Reiner, T. Nanoreporter Pet Predicts the Efficacy of Anti-Cancer Nanotherapy. *Nat. Commun.* **2016**, *7*, 11838.
- (182) Lee, H.; Gaddy, D.; Ventura, M.; Bernards, N.; de Souza, R.; Kirpotin, D.; Wickham, T.; Fitzgerald, J.; Zheng, J.; Hendriks, B. S. Companion Diagnostic (64)Cu-Liposome Positron Emission Tomography Enables Characterization of Drug Delivery to Tumors and Predicts Response to Cancer Nanomedicines. *Theranostics* **2018**, *8*, 2300–2312.
- (183) Sindhvani, S.; Syed, A. M.; Ngai, J.; Kingston, B. R.; Maiorino, L.; Rothschild, J.; MacMillan, P.; Zhang, Y.; Rajesh, N. U.; Hoang, T.; et al. The Entry of Nanoparticles into Solid Tumours. *Nat. Mater.* **2020**, *19*, 566–575.
- (184) Challenging Paradigms in Tumour Drug Delivery. *Nat. Mater.* **2020**, *19*, 477–477.
- (185) Peng, F.; Setyawati, M. I.; Tee, J. K.; Ding, X.; Wang, J.; Nga, M. E.; Ho, H. K.; Leong, D. T. Nanoparticles Promote in Vivo Breast Cancer Cell Intravasation and Extravasation by Inducing Endothelial Leakiness. *Nat. Nanotechnol.* **2019**, *14*, 279–286.
- (186) Manshian, B. B.; Poelmans, J.; Saini, S.; Pokhrel, S.; Grez, J. J.; Himmelreich, U.; Madler, L.; Soenen, S. J. Nanoparticle-Induced



Inflammation Can Increase Tumor Malignancy. *Acta Biomater.* **2018**, *68*, 99–112.

(187) Setyawati, M. I.; Tay, C. Y.; Chia, S. L.; Goh, S. L.; Fang, W.; Neo, M. J.; Chong, H. C.; Tan, S. M.; Loo, S. C.; Ng, K. W.; et al. Titanium Dioxide Nanomaterials Cause Endothelial Cell Leakiness by Disrupting the Homophilic Interaction of Ve-Cadherin. *Nat. Commun.* **2013**, *4*, 1673.

(188) Malinova, T. S.; Huveneers, S. Opening the Vascular Gate. *Nat. Nanotechnol.* **2019**, *14*, 195–196.

(189) Chiang, S. P.; Cabrera, R. M.; Segall, J. E. Tumor Cell Intravasation. *Am. J. Physiol. Cell Physiol.* **2016**, *311*, C1–C14.

(190) Langley, R. R.; Fidler, I. J. The Seed and Soil Hypothesis Revisited—the Role of Tumor-Stroma Interactions in Metastasis to Different Organs. *Int. J. Cancer* **2011**, *128*, 2527–2535.

(191) Dos Anjos Pultz, B.; Andres Cordero da Luz, F.; Socorro Faria, S.; Peixoto Ferreira de Souza, L.; Cristina Brigido Tavares, P.; Alonso Goulart, V.; Fontes, W.; Ricardo Goulart, L.; Jose Barbosa Silva, M. The Multifaceted Role of Extracellular Vesicles in Metastasis: Priming the Soil for Seeding. *Int. J. Cancer* **2017**, *140*, 2397–2407.

(192) Christen, S.; Lorendeau, D.; Schmieder, R.; Broekaert, D.; Metzger, K.; Veys, K.; Elia, I.; Buescher, J. M.; Orth, M. F.; Davidson, S. M.; et al. Breast Cancer-Derived Lung Metastases Show Increased Pyruvate Carboxylase-Dependent Anaplerosis. *Cell Rep.* **2016**, *17*, 837–848.

(193) Cully, M. Cancer: Tumour Vessel Normalization Takes Centre Stage. *Nat. Rev. Drug Discovery* **2017**, *16*, 87.

(194) Sugahara, K. N.; Teesalu, T.; Karmali, P. P.; Kotamraju, V. R.; Agemy, L.; Greenwald, D. R.; Ruoslahti, E. Coadministration of a Tumor-Penetrating Peptide Enhances the Efficacy of Cancer Drugs. *Science* **2010**, *328*, 1031–1035.

(195) Miao, H. Q.; Lee, P.; Lin, H.; Soker, S.; Klagsbrun, M. Neuropilin-1 Expression by Tumor Cells Promotes Tumor Angiogenesis and Progression. *FASEB J.* **2000**, *14*, 2532–2539.

(196) Kadonosono, T.; Yamano, A.; Goto, T.; Tsubaki, T.; Niibori, M.; Kuchimaru, T.; Kizaka-Kondoh, S. Cell Penetrating Peptides Improve Tumor Delivery of Cargos through Neuropilin-1-Dependent Extravasation. *J. Controlled Release* **2015**, *201*, 14–21.

(197) Ruoslahti, E. Access Granted: Irgd Helps Silicasome-Encased Drugs Breach the Tumor Barrier. *J. Clin. Invest.* **2017**, *127*, 1622–1624.

(198) Hu, C.; Yang, X.; Liu, R.; Ruan, S.; Zhou, Y.; Xiao, W.; Yu, W.; Yang, C.; Gao, H. Coadministration of Irgd with Multistage Responsive Nanoparticles Enhanced Tumor Targeting and Penetration Abilities for Breast Cancer Therapy. *ACS Appl. Mater. Interfaces* **2018**, *10*, 22571–22579.

(199) Wang, Y.; Xie, Y.; Li, J.; Peng, Z. H.; Sheinin, Y.; Zhou, J.; Oupický, D. Tumor-Penetrating Nanoparticles for Enhanced Anticancer Activity of Combined Photodynamic and Hypoxia-Activated Therapy. *ACS Nano* **2017**, *11*, 2227–2238.

(200) Ni, D.; Ding, H.; Liu, S.; Yue, H.; Bao, Y.; Wang, Z.; Su, Z.; Wei, W.; Ma, G. Superior Intratumoral Penetration of Paclitaxel Nanodots Strengthens Tumor Restriction and Metastasis Prevention. *Small* **2015**, *11*, 2518–2526.

(201) Liu, X.; Lin, P.; Perrett, I.; Lin, J.; Liao, Y. P.; Chang, C. H.; Jiang, J.; Wu, N.; Donahue, T.; Wainberg, Z.; et al. Tumor-Penetrating Peptide Enhances Transcytosis of Silicasome-Based Chemotherapy for Pancreatic Cancer. *J. Clin. Invest.* **2017**, *127*, 2007–2018.

(202) Zhang, J.; Hu, J.; Chan, H. F.; Skibba, M.; Liang, G.; Chen, M. Irgd Decorated Lipid-Polymer Hybrid Nanoparticles for Targeted Co-Delivery of Doxorubicin and Sorafenib to Enhance Anti-Hepatocellular Carcinoma Efficacy. *Nanomedicine* **2016**, *12*, 1303–1311.

(203) Ma, L.; Chen, Q.; Ma, P.; Han, M. K.; Xu, Z.; Kang, Y.; Xiao, B.; Merlin, D. Irgd-Functionalized Pegylated Nanoparticles for Enhanced Colon Tumor Accumulation and Targeted Drug Delivery. *Nanomedicine (London, U. K.)* **2017**, *12*, 1991–2006.

(204) Sugahara, K. N.; Scodeller, P.; Braun, G. B.; de Mendoza, T. H.; Yamazaki, C. M.; Kluger, M. D.; Kitayama, J.; Alvarez, E.; Howell,

S. B.; Teesalu, T.; et al. A Tumor-Penetrating Peptide Enhances Circulation-Independent Targeting of Peritoneal Carcinomatosis. *J. Controlled Release* **2015**, *212*, 59–69.

(205) Ren, Y.; Sagers, J. E.; Landegger, L. D.; Bhatia, S. N.; Stankovic, K. M. Tumor-Penetrating Delivery of Sirna against Tnfalpha to Human Vestibular Schwannomas. *Sci. Rep.* **2017**, *7*, 12922.

(206) King, A.; Ndifon, C.; Lui, S.; Widdows, K.; Kotamraju, V. R.; Agemy, L.; Teesalu, T.; Glazier, J. D.; Cellesi, F.; Tirelli, N.; et al. Tumor-Homing Peptides as Tools for Targeted Delivery of Payloads to the Placenta. *Sci. Adv.* **2016**, *2*, e1600349.

(207) Liu, X.; Braun, G. B.; Qin, M.; Ruoslahti, E.; Sugahara, K. N. In Vivo Cation Exchange in Quantum Dots for Tumor-Specific Imaging. *Nat. Commun.* **2017**, *8*, 343.

(208) Kim, D.; Kang, J.; Wang, T.; Ryu, H. G.; Zuidema, J. M.; Joo, J.; Kim, M.; Huh, Y.; Jung, J.; Ahn, K. H.; et al. Two-Photon in Vivo Imaging with Porous Silicon Nanoparticles. *Adv. Mater.* **2017**, *29*, 1703309.

(209) Wang, C. F.; Sarparanta, M. P.; Makila, E. M.; Hyvonen, M. L.; Laakkonen, P. M.; Salonen, J. J.; Hirvonen, J. T.; Airaksinen, A. J.; Santos, H. A. Multifunctional Porous Silicon Nanoparticles for Cancer Theranostics. *Biomaterials* **2015**, *48*, 108–118.

(210) Mantis, C.; Kandela, I.; Aird, F. Replication Study: Coadministration of a Tumor-Penetrating Peptide Enhances the Efficacy of Cancer Drugs. *eLife* **2017**, *6*, 17584.

(211) Doolittle, E.; Peiris, P. M.; Doron, G.; Goldberg, A.; Tucci, S.; Rao, S.; Shah, S.; Sylvestre, M.; Govender, P.; Turan, O.; et al. Spatiotemporal Targeting of a Dual-Ligand Nanoparticle to Cancer Metastasis. *ACS Nano* **2015**, *9*, 8012–8021.

(212) Tang, J.; Howard, C. B.; Mahler, S. M.; Thurecht, K. J.; Huang, L.; Xu, Z. P. Enhanced Delivery of Sirna to Triple Negative Breast Cancer Cells in Vitro and in Vivo through Functionalizing Lipid-Coated Calcium Phosphate Nanoparticles with Dual Target Ligands. *Nanoscale* **2018**, *10*, 4258–4266.

(213) Luo, W.; Wen, G.; Yang, L.; Tang, J.; Wang, J.; Wang, J.; Zhang, S.; Zhang, L.; Ma, F.; Xiao, L.; et al. Dual-Targeted and Ph-Sensitive Doxorubicin Prodrug-Microbubble Complex with Ultrasound for Tumor Treatment. *Theranostics* **2017**, *7*, 452–465.

(214) Zhang, J.; Xiao, X.; Zhu, J.; Gao, Z.; Lai, X.; Zhu, X.; Mao, G. Lactoferrin- and Rgd-Comodified, Temozolomide and Vincristine-Coloaded Nanostructured Lipid Carriers for Gliomatosis Cerebri Combination Therapy. *Int. J. Nanomed.* **2018**, *13*, 3039–3051.

(215) Gao, H.; Qian, J.; Cao, S.; Yang, Z.; Pang, Z.; Pan, S.; Fan, L.; Xi, Z.; Jiang, X.; Zhang, Q. Precise Glioma Targeting of and Penetration by Aptamer and Peptide Dual-Functioned Nanoparticles. *Biomaterials* **2012**, *33*, 5115–5123.

(216) Gao, H.; Xiong, Y.; Zhang, S.; Yang, Z.; Cao, S.; Jiang, X. Rgd and Interleukin-13 Peptide Functionalized Nanoparticles for Enhanced Glioblastoma Cells and Neovasculature Dual Targeting Delivery and Elevated Tumor Penetration. *Mol. Pharmaceutics* **2014**, *11*, 1042–1052.

(217) Zong, T.; Mei, L.; Gao, H.; Shi, K.; Chen, J.; Wang, Y.; Zhang, Q.; Yang, Y.; He, Q. Enhanced Glioma Targeting and Penetration by Dual-Targeting Liposome Co-Modified with T7 and Tat. *J. Pharm. Sci.* **2014**, *103*, 3891–3901.

(218) Chen, C.; Duan, Z.; Yuan, Y.; Li, R.; Pang, L.; Liang, J.; Xu, X.; Wang, J. Peptide-22 and Cyclic Rgd Functionalized Liposomes for Glioma Targeting Drug Delivery Overcoming Bbb and Bbtb. *ACS Appl. Mater. Interfaces* **2017**, *9*, 5864–5873.

(219) Levine, R. M.; Kokkoli, E. Dual-Ligand Alpha5beta1 and Alpha6beta4 Integrin Targeting Enhances Gene Delivery and Selectivity to Cancer Cells. *J. Controlled Release* **2017**, *251*, 24–36.

(220) Jing, F.; Li, D.; Xu, W.; Liu, Y.; Wang, K.; Sui, Z. Transferrin- and Folate-Modified, Double-Targeted Nanocarriers for Gene Delivery. *Pharm. Biol.* **2014**, *52*, 570–574.

(221) Fang, J. Y.; Liu, P. F.; Huang, C. M. Decreasing Systemic Toxicity Via Transdermal Delivery of Anticancer Drugs. *Curr. Drug Metab.* **2008**, *9*, 592–597.

- (222) Cheng, M.; Gao, X.; Wang, Y.; Chen, H.; He, B.; Li, Y.; Han, J.; Zhang, Z. Synthesis of Liver-Targeting Dual-Ligand Modified Gcga/5-Fu Nanoparticles and Their Characteristics in Vitro and in Vivo. *Int. J. Nanomed.* **2013**, *8*, 4265–4276.
- (223) Chen, F.; Zeng, Y.; Qi, X.; Chen, Y.; Ge, Z.; Jiang, Z.; Zhang, X.; Dong, Y.; Chen, H.; Yu, Z. Targeted Salinomycin Delivery with Egfr and Cd133 Aptamers Based Dual-Ligand Lipid-Polymer Nanoparticles to Both Osteosarcoma Cells and Cancer Stem Cells. *Nanomedicine* **2018**, *14*, 2115–2127.
- (224) Tan, S.; Wang, G. Lung Cancer Targeted Therapy: Folate and Transferrin Dual Targeted, Glutathione Responsive Nanocarriers for the Delivery of Cisplatin. *Biomed. Pharmacother.* **2018**, *102*, 55–63.
- (225) Jang, C.; Lee, J. H.; Sahu, A.; Tae, G. The Synergistic Effect of Folate and Rgd Dual Ligand of Nanographene Oxide on Tumor Targeting and Photothermal Therapy in Vivo. *Nanoscale* **2015**, *7*, 18584–18594.
- (226) Xu, Q.; Liu, Y.; Su, S.; Li, W.; Chen, C.; Wu, Y. Anti-Tumor Activity of Paclitaxel through Dual-Targeting Carrier of Cyclic Rgd and Transferrin Conjugated Hyperbranched Copolymer Nanoparticles. *Biomaterials* **2012**, *33*, 1627–1639.
- (227) Peiris, P. M.; He, F.; Covarrubias, G.; Raghunathan, S.; Turan, O.; Lorkowski, M.; Gnanasambandam, B.; Wu, C.; Schiemann, W. P.; Karathanasis, E. Precise Targeting of Cancer Metastasis Using Multi-Ligand Nanoparticles Incorporating Four Different Ligands. *Nanoscale* **2018**, *10*, 6861–6871.
- (228) Chen, Z.; Zhang, L.; Song, Y.; He, J.; Wu, L.; Zhao, C.; Xiao, Y.; Li, W.; Cai, B.; Cheng, H.; et al. Hierarchical Targeted Hepatocyte Mitochondrial Multifunctional Chitosan Nanoparticles for Anticancer Drug Delivery. *Biomaterials* **2015**, *52*, 240–250.
- (229) Xia, Q.-s.; Ding, H.-m.; Ma, Y.-q. Can Dual-Ligand Targeting Enhance Cellular Uptake of Nanoparticles? *Nanoscale* **2017**, *9*, 8982–8989.
- (230) Colombo, M.; Fiandra, L.; Alessio, G.; Mazzucchelli, S.; Nebuloni, M.; De Palma, C.; Kantner, K.; Pelaz, B.; Rotem, R.; Corsi, F.; Parak, W. J.; Prosperi, D. Tumour Homing and Therapeutic Effect of Colloidal Nanoparticles Depend on the Number of Attached Antibodies. *Nat. Commun.* **2016**, *7*, 13818.
- (231) Liu, Y.; Hui, Y.; Ran, R.; Yang, G. Z.; Wibowo, D.; Wang, H. F.; Middelberg, A. P. J.; Zhao, C. X. Synergetic Combinations of Dual-Targeting Ligands for Enhanced in Vitro and in Vivo Tumor Targeting. *Adv. Healthcare Mater.* **2018**, *7*, 1800106.
- (232) Bai, J.; Wang, J. T.; Rubio, N.; Protti, A.; Heidari, H.; Elgogary, R.; Southern, P.; Al-Jamal, W. T.; Sosabowski, J.; Shah, A. M.; et al. Triple-Modal Imaging of Magnetically-Targeted Nanocapsules in Solid Tumours in Vivo. *Theranostics* **2016**, *6*, 342–356.
- (233) Al-Jamal, K. T.; Bai, J.; Wang, J. T.-W.; Protti, A.; Southern, P.; Bogart, L.; Heidari, H.; Li, X.; Cakebread, A.; Asker, D.; et al. Magnetic Drug Targeting: Preclinical in Vivo Studies, Mathematical Modeling, and Extrapolation to Humans. *Nano Lett.* **2016**, *16*, 5652–5660.
- (234) Bai, J.; Wang, J. T.; Mei, K. C.; Al-Jamal, W. T.; Al-Jamal, K. T. Real-Time Monitoring of Magnetic Drug Targeting Using Fibered Confocal Fluorescence Microscopy. *J. Controlled Release* **2016**, *244*, 240–246.
- (235) Mei, K. C.; Bai, J.; Lorio, S.; Wang, J. T.; Al-Jamal, K. T. Investigating the Effect of Tumor Vascularization on Magnetic Targeting In vivo Using Retrospective Design of Experiment. *Biomaterials* **2016**, *106*, 276–285.
- (236) Nigam, S.; Bahadur, D. Doxorubicin-Loaded Dendritic-Fe<sub>3</sub>O<sub>4</sub> Supramolecular Nanoparticles for Magnetic Drug Targeting and Tumor Regression in Spheroid Murine Melanoma Model. *Nanomedicine* **2018**, *14*, 759–768.
- (237) Yang, Y.; Liu, Y.; Cheng, C.; Shi, H.; Yang, H.; Yuan, H.; Ni, C. Rational Design of Go-Modified Fe<sub>3</sub>O<sub>4</sub>/SiO<sub>2</sub> Nanoparticles with Combined Rhenium-188 and Gambogic Acid for Magnetic Target Therapy. *ACS Appl. Mater. Interfaces* **2017**, *9*, 28195–28208.
- (238) Alev, M.; Egenberger, L.; Mühleisen, L.; Weigel, B.; Frey, B.; Friedrich, R. P.; Pöttler, M.; Alexiou, C.; Janko, C. Targeting of Drug-Loaded Nanoparticles to Tumor Sites Increases Cell Death and Release of Danger Signals. *J. Controlled Release* **2018**, *285*, 67–80.
- (239) Janko, C.; Durr, S.; Munoz, L. E.; Lyer, S.; Chaurio, R.; Tietze, R.; Lohneisen, S.; Schorn, C.; Herrmann, M.; Alexiou, C. Magnetic Drug Targeting Reduces the Chemotherapeutic Burden on Circulating Leukocytes. *Int. J. Mol. Sci.* **2013**, *14*, 7341–7355.
- (240) Tietze, R.; Lyer, S.; Dürr, S.; Struffert, T.; Engelhorn, T.; Schwarz, M.; Eckert, E.; Göen, T.; Vasylyev, S.; Peukert, W.; et al. Efficient Drug-Delivery Using Magnetic Nanoparticles-Biodistribution and Therapeutic Effects in Tumour Bearing Rabbits. *Nanomedicine* **2013**, *9*, 961–971.
- (241) Krukemeyer, M. G.; Krenn, V.; Jakobs, M.; Wagner, W. Magnetic Drug Targeting in a Rhabdomyosarcoma Rat Model Using Magnetite-Dextran Composite Nanoparticle-Bound Mitoxantrone and 0.6 T Extracorporeal Magnets - Sarcoma Treatment in Progress. *J. Drug Target.* **2012**, *20*, 185–193.
- (242) Roeth, A. A.; Slabu, I.; Baumann, M.; Alizai, P. H.; Schmeding, M.; Guentherodt, G.; Schmitz-Rode, T.; Neumann, U. P. Establishment of a Biophysical Model to Optimize Endoscopic Targeting of Magnetic Nanoparticles for Cancer Treatment. *Int. J. Nanomed.* **2017**, *12*, 5933–5940.
- (243) Zhang, X.; Le, T.-A.; Yoon, J. Development of a Real Time Imaging-Based Guidance System of Magnetic Nanoparticles for Targeted Drug Delivery. *J. Magn. Magn. Mater.* **2017**, *427*, 345–351.
- (244) Su, Y.; Xie, Z.; Kim, G. B.; Dong, C.; Yang, J. Design Strategies and Applications of Circulating Cell-Mediated Drug Delivery Systems. *ACS Biomater. Sci. Eng.* **2015**, *1*, 201–217.
- (245) Chessa, L.; Leuzzi, V.; Plebani, A.; Soresina, A.; Micheli, R.; D'Agnano, D.; Venturi, T.; Molinaro, A.; Fazzi, E.; Marini, M.; et al. Intra-Erythrocyte Infusion of Dexamethasone Reduces Neurological Symptoms in Ataxia Teleangiectasia Patients: Results of a Phase 2 Trial. *Orphanet J. Rare Dis.* **2014**, *9*, 5.
- (246) Muzykantov, V. R. Drug Delivery by Red Blood Cells: Vascular Carriers Designed by Mother Nature. *Expert Opin. Drug Delivery* **2010**, *7*, 403–427.
- (247) Rodriguez, P. L.; Harada, T.; Christian, D. A.; Pantano, D. A.; Tsai, R. K.; Discher, D. E. Minimal "Self" Peptides That Inhibit Phagocytic Clearance and Enhance Delivery of Nanoparticles. *Science (Washington, DC, U. S.)* **2013**, *339*, 971–975.
- (248) Hu, C.-M. J.; Fang, R. H.; Luk, B. T.; Chen, K. N. H.; Carpenter, C.; Gao, W.; Zhang, K.; Zhang, L. Marker-of-Self Functionalization of Nanoscale Particles through a Top-Down Cellular Membrane Coating Approach. *Nanoscale* **2013**, *5*, 2664–2668.
- (249) Pasini, E. M.; Kirkegaard, M.; Mortensen, P.; Lutz, H. U.; Thomas, A. W.; Mann, M. In-Depth Analysis of the Membrane and Cytosolic Proteome of Red Blood Cells. *Blood* **2006**, *108*, 791–801.
- (250) Chambers, E.; Mitragotri, S. Prolonged Circulation of Large Polymeric Nanoparticles by Non-Covalent Adsorption on Erythrocytes. *J. Controlled Release* **2004**, *100*, 111–119.
- (251) Chambers, E.; Mitragotri, S. Long Circulating Nanoparticles Via Adhesion on Red Blood Cells: Mechanism and Extended Circulation. *Exp. Biol. Med.* **2007**, *232*, 958–966.
- (252) Anselmo, A. C.; Gupta, V.; Zern, B. J.; Pan, D.; Zakrewsky, M.; Muzykantov, V.; Mitragotri, S. Delivering Nanoparticles to Lungs While Avoiding Liver and Spleen through Adsorption on Red Blood Cells. *ACS Nano* **2013**, *7*, 11129–11137.
- (253) Brenner, J. S.; Pan, D. C.; Myerson, J. W.; Marcos-Contreras, O. A.; Villa, C. H.; Patel, P.; Hekierski, H.; Chatterjee, S.; Tao, J. Q.; Parhiz, H.; et al. Red Blood Cell-Hitchhiking Boosts Delivery of Nanocarriers to Chosen Organs by Orders of Magnitude. *Nat. Commun.* **2018**, *9*, 2684.
- (254) Wang, C.; Sun, X.; Cheng, L.; Yin, S.; Yang, G.; Li, Y.; Liu, Z. Multifunctional Theranostic Red Blood Cells for Magnetic-Field-Enhanced in Vivo Combination Therapy of Cancer. *Adv. Mater.* **2014**, *26*, 4794–4802.
- (255) Wu, Z.; Li, T.; Li, J.; Gao, W.; Xu, T.; Christianson, C.; Gao, W.; Galarnyk, M.; He, Q.; Zhang, L.; et al. Turning Erythrocytes into Functional Micromotors. *ACS Nano* **2014**, *8*, 12041–12048.



- (256) Wang, P.; Wang, X.; Luo, Q.; Li, Y.; Lin, X.; Fan, L.; Zhang, Y.; Liu, J.; Liu, X. Fabrication of Red Blood Cell-Based Multimodal Theranostic Probes for Second near-Infrared Window Fluorescence Imaging-Guided Tumor Surgery and Photodynamic Therapy. *Theranostics* **2019**, *9*, 369–380.
- (257) Zhu, D. M.; Wu, L.; Suo, M.; Gao, S.; Xie, W.; Zan, M. H.; Liu, A.; Chen, B.; Wu, W. T.; Ji, L. W.; et al. Engineered Red Blood Cells for Capturing Circulating Tumor Cells with High Performance. *Nanoscale* **2018**, *10*, 6014–6023.
- (258) Sun, X.; Wang, C.; Gao, M.; Hu, A.; Liu, Z. Remotely Controlled Red Blood Cell Carriers for Cancer Targeting and near-Infrared Light-Triggered Drug Release in Combined Photothermal–Chemotherapy. *Adv. Funct. Mater.* **2015**, *25*, 2386–2394.
- (259) Zhao, Z.; Ukidve, A.; Gao, Y.; Kim, J.; Mitragotri, S. Erythrocyte Leveraged Chemotherapy (Elect): Nanoparticle Assembly on Erythrocyte Surface to Combat Lung Metastasis. *Sci. Adv.* **2019**, *5*, eaax9250.
- (260) Zelepukin, I. V.; Yaremenko, A. V.; Shipunova, V. O.; Babenyshev, A. V.; Balalaeva, I. V.; Nikitin, P. I.; Deyev, S. M.; Nikitin, M. P. Nanoparticle-Based Drug Delivery Via Rbc-Hitchhiking for the Inhibition of Lung Metastases Growth. *Nanoscale* **2019**, *11*, 1636–1646.
- (261) Pan, D. C.; Myerson, J. W.; Brenner, J. S.; Patel, P. N.; Anselmo, A. C.; Mitragotri, S.; Muzykantov, V. Nanoparticle Properties Modulate Their Attachment and Effect on Carrier Red Blood Cells. *Sci. Rep.* **2018**, *8*, 1615.
- (262) Gajewski, T. F.; Schreiber, H.; Fu, Y. X. Innate and Adaptive Immune Cells in the Tumor Microenvironment. *Nat. Immunol.* **2013**, *14*, 1014–1022.
- (263) Griffiths, L.; Binley, K.; Iqbal, S.; Kan, O.; Maxwell, P.; Ratcliffe, P.; Lewis, C.; Harris, A.; Kingsman, S.; Naylor, S. The Macrophage - a Novel System to Deliver Gene Therapy to Pathological Hypoxia. *Gene Ther.* **2000**, *7*, 255–262.
- (264) Shi, C.; Pamer, E. G. Monocyte Recruitment During Infection and Inflammation. *Nat. Rev. Immunol.* **2011**, *11*, 762–774.
- (265) Murdoch, C.; Giannoudis, A.; Lewis, C. E. Mechanisms Regulating the Recruitment of Macrophages into Hypoxic Areas of Tumors and Other Ischemic Tissues. *Blood* **2004**, *104*, 2224–2234.
- (266) Perry, V. H.; Anthony, D. C.; Bolton, S. J.; Brown, H. C. The Blood-Brain Barrier and the Inflammatory Response. *Mol. Med. Today* **1997**, *3*, 335–341.
- (267) Kelly, P. M.; Davison, R. S.; Bliss, E.; McGee, J. O. Macrophages in Human Breast Disease: A Quantitative Immunohistochemical Study. *Br. J. Cancer* **1988**, *57*, 174–177.
- (268) Allavena, P.; Palmioli, A.; Avigni, R.; Sironi, M.; La Ferla, B.; Maeda, A. Plga Based Nanoparticles for the Monocyte-Mediated Anti-Tumor Drug Delivery System. *J. Biomed. Nanotechnol.* **2020**, *16*, 212–223.
- (269) Choi, J.; Kim, H. Y.; Ju, E. J.; Jung, J.; Park, J.; Chung, H. K.; Lee, J. S.; Lee, J. S.; Park, H. J.; Song, S. Y.; et al. Use of Macrophages to Deliver Therapeutic and Imaging Contrast Agents to Tumors. *Biomaterials* **2012**, *33*, 4195–4203.
- (270) Yang, X.; Lian, K.; Tan, Y.; Zhu, Y.; Liu, X.; Zeng, Y.; Yu, T.; Meng, T.; Yuan, H.; Hu, F. Selective Uptake of Chitosan Polymeric Micelles by Circulating Monocytes for Enhanced Tumor Targeting. *Carbohydr. Polym.* **2020**, *229*, 115435.
- (271) Qiang, L.; Cai, Z.; Jiang, W.; Liu, J.; Tai, Z.; Li, G.; Gong, C.; Gao, S.; Gao, Y. A Novel Macrophage-Mediated Biomimetic Delivery System with Nir-Triggered Release for Prostate Cancer Therapy. *J. Nanobiotechnol.* **2019**, *17*, 83.
- (272) Choi, M.-R.; Stanton-Maxey, K. J.; Stanley, J. K.; Levin, C. S.; Bardhan, R.; Akin, D.; Badve, S.; Sturgis, J.; Robinson, J. P.; Bashir, R.; et al. A Cellular Trojan Horse for Delivery of Therapeutic Nanoparticles into Tumors. *Nano Lett.* **2007**, *7*, 3759–3765.
- (273) Madsen, S. J.; Baek, S. K.; Makkouk, A. R.; Krasieva, T.; Hirschberg, H. Macrophages as Cell-Based Delivery Systems for Nanoshells in Photothermal Therapy. *Ann. Biomed. Eng.* **2012**, *40*, 507–515.
- (274) Popescu, M. A.; Toms, S. A. In Vivo Optical Imaging Using Quantum Dots for the Management of Brain Tumors. *Expert Rev. Mol. Diagn.* **2006**, *6*, 879–890.
- (275) van Apeldoorn, A. A.; van Manen, H. J.; Bezemer, J. M.; de Bruijn, J. D.; van Blitterswijk, C. A.; Otto, C. Raman Imaging of Plga Microsphere Degradation inside Macrophages. *J. Am. Chem. Soc.* **2004**, *126*, 13226–13227.
- (276) Doshi, N.; Swiston, A. J.; Gilbert, J. B.; Alcaraz, M. L.; Cohen, R. E.; Rubner, M. F.; Mitragotri, S. Cell-Based Drug Delivery Devices Using Phagocytosis-Resistant Backpacks. *Adv. Mater.* **2011**, *23*, H105–H109.
- (277) Anselmo, A. C.; Gilbert, J. B.; Kumar, S.; Gupta, V.; Cohen, R. E.; Rubner, M. F.; Mitragotri, S. Monocyte-Mediated Delivery of Polymeric Backpacks to Inflamed Tissues: A Generalized Strategy to Deliver Drugs to Treat Inflammation. *J. Controlled Release* **2015**, *199*, 29–36.
- (278) Polak, R.; Lim, R. M.; Beppu, M. M.; Pitombo, R. N.; Cohen, R. E.; Rubner, M. F. Liposome-Loaded Cell Backpacks. *Adv. Healthcare Mater.* **2015**, *4*, 2832–2841.
- (279) Rosenberg, S. A.; Restifo, N. P.; Yang, J. C.; Morgan, R. A.; Dudley, M. E. Adoptive Cell Transfer: A Clinical Path to Effective Cancer Immunotherapy. *Nat. Rev. Cancer* **2008**, *8*, 299–308.
- (280) June, C. H.; Adoptive, T. Cell Therapy for Cancer in the Clinic. *J. Clin. Invest.* **2007**, *117*, 1466–1476.
- (281) Luster, A. D.; Alon, R.; von Andrian, U. H. Immune Cell Migration in Inflammation: Present and Future Therapeutic Targets. *Nat. Immunol.* **2005**, *6*, 1182–1190.
- (282) Viguier, M.; Lemaitre, F.; Verola, O.; Cho, M. S.; Gorochev, G.; Dubertret, L.; Bachelez, H.; Kourilsky, P.; Ferradini, L. Foxp3 Expressing Cd4+Cd25(High) Regulatory T Cells Are Overrepresented in Human Metastatic Melanoma Lymph Nodes and Inhibit the Function of Infiltrating T Cells. *J. Immunol.* **2004**, *173*, 1444–1453.
- (283) Swiston, A. J.; Cheng, C.; Um, S. H.; Irvine, D. J.; Cohen, R. E.; Rubner, M. F. Surface Functionalization of Living Cells with Multilayer Patches. *Nano Lett.* **2008**, *8*, 4446–4453.
- (284) Vasconcellos, F. C.; Swiston, A. J.; Beppu, M. M.; Cohen, R. E.; Rubner, M. F. Bioactive Polyelectrolyte Multilayers: Hyaluronic Acid Mediated B Lymphocyte Adhesion. *Biomacromolecules* **2010**, *11*, 2407–2414.
- (285) Gilbert, J. B.; O'Brien, J. S.; Suresh, H. S.; Cohen, R. E.; Rubner, M. F. Orientation-Specific Attachment of Polymeric Microtubules on Cell Surfaces. *Adv. Mater.* **2013**, *25*, 5948–5952.
- (286) Wayteck, L.; Dewitte, H.; De Backer, L.; Breckpot, K.; Demeester, J.; De Smedt, S. C.; Raemdonck, K. Hitchhiking Nanoparticles: Reversible Coupling of Lipid-Based Nanoparticles to Cytotoxic T Lymphocytes. *Biomaterials* **2016**, *77*, 243–254.
- (287) Huang, B.; Abraham, W. D.; Zheng, Y.; Bustamante López, S. C.; Luo, S. S.; Irvine, D. J. Active Targeting of Chemotherapy to Disseminated Tumors Using Nanoparticle-Carrying T Cells. *Sci. Transl. Med.* **2015**, *7*, 291ra294.
- (288) Stephan, M. T.; Moon, J. J.; Um, S. H.; Bershteyn, A.; Irvine, D. J. Therapeutic Cell Engineering with Surface-Conjugated Synthetic Nanoparticles. *Nat. Med.* **2010**, *16*, 1035–1041.
- (289) Stephan, M. T.; Stephan, S. B.; Bak, P.; Chen, J.; Irvine, D. J. Synapse-Directed Delivery of Immunomodulators Using T-Cell-Conjugated Nanoparticles. *Biomaterials* **2012**, *33*, 5776–5787.
- (290) Tang, L.; Zheng, Y.; Melo, M. B.; Mabardi, L.; Castaño, A. P.; Xie, Y.-Q.; Li, N.; Kudchodkar, S. B.; Wong, H. C.; Jeng, E. K.; et al. Enhancing T Cell Therapy through Tcr-Signaling-Responsive Nanoparticle Drug Delivery. *Nat. Biotechnol.* **2018**, *36*, 707–716.
- (291) Chu, D.; Zhao, Q.; Yu, J.; Zhang, F.; Zhang, H.; Wang, Z. Nanoparticle Targeting of Neutrophils for Improved Cancer Immunotherapy. *Adv. Healthcare Mater.* **2016**, *5*, 1088–1093.
- (292) Kolaczowska, E.; Kubes, P. Neutrophil Recruitment and Function in Health and Inflammation. *Nat. Rev. Immunol.* **2013**, *13*, 159–175.
- (293) Chu, D.; Gao, J.; Wang, Z. Neutrophil-Mediated Delivery of Therapeutic Nanoparticles across Blood Vessel Barrier for Treatment of Inflammation and Infection. *ACS Nano* **2015**, *9*, 11800–11811.



- (294) Chu, D.; Dong, X.; Zhao, Q.; Gu, J.; Wang, Z. Photosensitization Priming of Tumor Microenvironments Improves Delivery of Nanotherapeutics Via Neutrophil Infiltration. *Adv. Mater.* **2017**, *29*, 1701021.
- (295) Naumenko, V.; Nikitin, A.; Garanina, A.; Melnikov, P.; Vodopyanov, S.; Kapitanova, K.; Potashnikova, D.; Vishnevskiy, D.; Alieva, I.; Ilyasov, A.; et al. Neutrophil-Mediated Transport Is Crucial for Delivery of Short-Circulating Magnetic Nanoparticles to Tumors. *Acta Biomater.* **2020**, *104*, 176–187.
- (296) Xue, J.; Zhao, Z.; Zhang, L.; Xue, L.; Shen, S.; Wen, Y.; Wei, Z.; Wang, L.; Kong, L.; Sun, H.; et al. Neutrophil-Mediated Anticancer Drug Delivery for Suppression of Postoperative Malignant Glioma Recurrence. *Nat. Nanotechnol.* **2017**, *12*, 692–700.
- (297) Corsten, M. F.; Shah, K. Therapeutic Stem-Cells for Cancer Treatment: Hopes and Hurdles in Tactical Warfare. *Lancet Oncol.* **2008**, *9*, 376–384.
- (298) Uccelli, A.; Moretta, L.; Pistoia, V. Mesenchymal Stem Cells in Health and Disease. *Nat. Rev. Immunol.* **2008**, *8*, 726–736.
- (299) Karnoub, A. E.; Dash, A. B.; Vo, A. P.; Sullivan, A.; Brooks, M. W.; Bell, G. W.; Richardson, A. L.; Polyak, K.; Tubo, R.; Weinberg, R. A. Mesenchymal Stem Cells within Tumour Stroma Promote Breast Cancer Metastasis. *Nature* **2007**, *449*, 557–563.
- (300) Roger, M.; Clavreul, A.; Venier-Julienne, M.-C.; Passirani, C.; Sindji, L.; Schiller, P.; Montero-Menei, C.; Menei, P. Mesenchymal Stem Cells as Cellular Vehicles for Delivery of Nanoparticles to Brain Tumors. *Biomaterials* **2010**, *31*, 8393–8401.
- (301) Li, L.; Guan, Y.; Liu, H.; Hao, N.; Liu, T.; Meng, X.; Fu, C.; Li, Y.; Qu, Q.; Zhang, Y.; et al. Silica Nanorattle-Doxorubicin-Anchored Mesenchymal Stem Cells for Tumor-Tropic Therapy. *ACS Nano* **2011**, *5*, 7462–7470.
- (302) Sadhukha, T.; O'Brien, T. D.; Prabha, S. Nano-Engineered Mesenchymal Stem Cells as Targeted Therapeutic Carriers. *J. Controlled Release* **2014**, *196*, 243–251.
- (303) Zhao, Y.; Tang, S.; Guo, J.; Alahdal, M.; Cao, S.; Yang, Z.; Zhang, F.; Shen, Y.; Sun, M.; Mo, R.; et al. Targeted Delivery of Doxorubicin by Nano-Loaded Mesenchymal Stem Cells for Lung Melanoma Metastases Therapy. *Sci. Rep.* **2017**, *7*, 44758.
- (304) Wang, X.; Chen, H.; Zeng, X.; Guo, W.; Jin, Y.; Wang, S.; Tian, R.; Han, Y.; Guo, L.; Han, J.; et al. Efficient Lung Cancer-Targeted Drug Delivery Via a Nanoparticle/Msc System. *Acta Pharm. Sin. B* **2019**, *9*, 167–176.
- (305) Zhao, J.; Vykoukal, J.; Abdelsalam, M.; Recio-Boiles, A.; Huang, Q.; Qiao, Y.; Singhana, B.; Wallace, M.; Avritscher, R.; Melancon, M. P. Stem Cell-Mediated Delivery of Spio-Loaded Gold Nanoparticles for the Theranosis of Liver Injury and Hepatocellular Carcinoma. *Nanotechnology* **2014**, *25*, 405101.
- (306) Kang, S.; Bhang, S. H.; Hwang, S.; Yoon, J. K.; Song, J.; Jang, H. K.; Kim, S.; Kim, B. S. Mesenchymal Stem Cells Aggregate and Deliver Gold Nanoparticles to Tumors for Photothermal Therapy. *ACS Nano* **2015**, *9*, 9678–9690.
- (307) Ouyang, X.; Wang, X.; Kraatz, H.-B.; Ahmadi, S.; Gao, J.; Lv, Y.; Sun, X.; Huang, Y. A Trojan Horse Biomimetic Delivery Strategy Using Mesenchymal Stem Cells for Pdt/Ptt Therapy against Lung Melanoma Metastasis. *Biomater. Sci.* **2020**, *8*, 1160–1170.
- (308) Aboody, K. S.; Brown, A.; Rainov, N. G.; Bower, K. A.; Liu, S.; Yang, W.; Small, J. E.; Herrlinger, U.; Ourednik, V.; Black, P. M.; et al. Neural Stem Cells Display Extensive Tropism for Pathology in Adult Brain: Evidence from Intracranial Gliomas. *Proc. Natl. Acad. Sci. U. S. A.* **2000**, *97*, 12846–12851.
- (309) Wang, J.; Liu, J.; Meng, H.; Guan, Y.; Yin, Y.; Zhao, Z.; Sun, G.; Wu, A.; Chen, L.; Yu, X. Neural Stem Cells Promote Glioblastoma Formation in Nude Mice. *Clin. Transl. Oncol.* **2019**, *21*, 1551–1560.
- (310) Yuan, X.; Hu, J.; Belladonna, M. L.; Black, K. L.; Yu, J. S. Interleukin-23-Expressing Bone Marrow-Derived Neural Stem-Like Cells Exhibit Antitumor Activity against Intracranial Glioma. *Cancer Res.* **2006**, *66*, 2630–2638.
- (311) Mooney, R.; Weng, Y.; Tirughana-Sambandan, R.; Valenzuela, V.; Aramburo, S.; Garcia, E.; Li, Z.; Gutova, M.; Annala, A. J.; Berlin, J. M.; et al. Neural Stem Cells Improve Intracranial Nanoparticle Retention and Tumor-Selective Distribution. *Future Oncol.* **2014**, *10*, 401–415.
- (312) Mooney, R.; Weng, Y.; Garcia, E.; Bhojane, S.; Smith-Powell, L.; Kim, S. U.; Annala, A. J.; Aboody, K. S.; Berlin, J. M. Conjugation of Ph-Responsive Nanoparticles to Neural Stem Cells Improves Intratumoral Therapy. *J. Controlled Release* **2014**, *191*, 82–89.
- (313) Mooney, R.; Roma, L.; Zhao, D.; Van Haute, D.; Garcia, E.; Kim, S. U.; Annala, A. J.; Aboody, K. S.; Berlin, J. M. Neural Stem Cell-Mediated Intratumoral Delivery of Gold Nanorods Improves Photothermal Therapy. *ACS Nano* **2014**, *8*, 12450–12460.
- (314) Weiss, L.; Zeigel, R. Cell Surface Negativity and the Binding of Positively Charged Particles. *J. Cell. Physiol.* **1971**, *77*, 179–186.
- (315) Dundas, C. M.; Demonte, D.; Park, S. Streptavidin-Biotin Technology: Improvements and Innovations in Chemical and Biological Applications. *Appl. Microbiol. Biotechnol.* **2013**, *97* (21), 9343–9353.
- (316) Ulmschneider, M. B.; Sansom, M. S. P. Amino Acid Distributions in Integral Membrane Protein Structures. *Biochim. Biophys. Acta, Biomembr.* **2001**, *1512*, 1–14.
- (317) Sahaf, B.; Heydari, K.; Herzenberg, L. A.; Herzenberg, L. A. Lymphocyte Surface Thiol Levels. *Proc. Natl. Acad. Sci. U. S. A.* **2003**, *100*, 4001–4005.
- (318) Prescher, J. A.; Bertozzi, C. R. Chemistry in Living Systems. *Nat. Chem. Biol.* **2005**, *1* (1), 13–21.
- (319) Gutiérrez Millán, C.; Zarzuelo Castañeda, A.; Sayalero Mariner, M. L.; Lanao, J. M. Factors Associated with the Performance of Carrier Erythrocytes Obtained by Hypotonic Dialysis. *Blood Cells, Mol. Dis.* **2004**, *33*, 132–140.
- (320) He, H.; Ye, J.; Wang, Y.; Liu, Q.; Chung, H. S.; Kwon, Y. M.; Shin, M. C.; Lee, K.; Yang, V. C. Cell-Penetrating Peptides Mediated Encapsulation of Protein Therapeutics into Intact Red Blood Cells and Its Application. *J. Controlled Release* **2014**, *176*, 123–132.
- (321) Katsamakas, S.; Chatzisideri, T.; Thysiadis, S.; Sarli, V. Rgd-Mediated Delivery of Small-Molecule Drugs. *Future Med. Chem.* **2017**, *9*, 579–604.
- (322) Piao, J.-G.; Wang, L.; Gao, F.; You, Y.-Z.; Xiong, Y.; Yang, L. Erythrocyte Membrane Is an Alternative Coating to Polyethylene Glycol for Prolonging the Circulation Lifetime of Gold Nanocages for Photothermal Therapy. *ACS Nano* **2014**, *8*, 10414–10425.
- (323) Zhu, D. M.; Xie, W.; Xiao, Y. S.; Suo, M.; Zan, M. H.; Liao, Q. Q.; Hu, X. J.; Chen, L. B.; Chen, B.; Wu, W. T.; et al. Erythrocyte Membrane-Coated Gold Nanocages for Targeted Photothermal and Chemical Cancer Therapy. *Nanotechnology* **2018**, *29*, No. 084002.
- (324) Gao, W.; Hu, C.-M. J.; Fang, R. H.; Luk, B. T.; Su, J.; Zhang, L. Surface Functionalization of Gold Nanoparticles with Red Blood Cell Membranes. *Adv. Mater.* **2013**, *25*, 3549–3553.
- (325) Rao, L.; Meng, Q. F.; Bu, L. L.; Cai, B.; Huang, Q.; Sun, Z. J.; Zhang, W. F.; Li, A.; Guo, S. S.; Liu, W.; et al. Erythrocyte Membrane-Coated Upconversion Nanoparticles with Minimal Protein Adsorption for Enhanced Tumor Imaging. *ACS Appl. Mater. Interfaces* **2017**, *9*, 2159–2168.
- (326) Gao, L.; Wang, H.; Nan, L.; Peng, T.; Sun, L.; Zhou, J.; Xiao, Y.; Wang, J.; Sun, J.; Lu, W.; et al. Erythrocyte Membrane-Wrapped Ph Sensitive Polymeric Nanoparticles for Non-Small Cell Lung Cancer Therapy. *Bioconjugate Chem.* **2017**, *28*, 2591–2598.
- (327) Lin, Y.-N.; Elsabahy, M.; Khan, S.; Zhang, F.; Song, Y.; Dong, M.; Li, R.; Smolen, J.; Letteri, R. A.; Su, L.; et al. Erythrocyte-Membrane-Camouflaged Nanocarriers with Tunable Paclitaxel Release Kinetics Via Macromolecular Stereocomplexation. *ACS Mater. Lett.* **2020**, *2*, 595–601.
- (328) Parodi, A.; Quattrocchi, N.; van de Ven, A. L.; Chiappini, C.; Evangelopoulos, M.; Martinez, J. O.; Brown, B. S.; Khaled, S. Z.; Yazdi, I. K.; Enzo, M. V.; et al. Synthetic Nanoparticles Functionalized with Biomimetic Leukocyte Membranes Possess Cell-Like Functions. *Nat. Nanotechnol.* **2013**, *8*, 61–68.
- (329) Krishnamurthy, S.; Gnanasamandhan, M. K.; Xie, C.; Huang, K.; Cui, M. Y.; Chan, J. M. Monocyte Cell Membrane-Derived Nanoghosts for Targeted Cancer Therapy. *Nanoscale* **2016**, *8*, 6981–6985.

- (330) Rao, L.; He, Z.; Meng, Q.-F.; Zhou, Z.; Bu, L.-L.; Guo, S.-S.; Liu, W.; Zhao, X.-Z. Effective Cancer Targeting and Imaging Using Macrophage Membrane-Camouflaged Upconversion Nanoparticles. *J. Biomed. Mater. Res., Part A* **2017**, *105*, 521–530.
- (331) Xuan, M.; Shao, J.; Dai, L.; Li, J.; He, Q. Macrophage Cell Membrane Camouflaged Au Nanoshells for in Vivo Prolonged Circulation Life and Enhanced Cancer Photothermal Therapy. *ACS Appl. Mater. Interfaces* **2016**, *8*, 9610–9618.
- (332) Wang, Q.; Ren, Y.; Mu, J.; Egilmez, N. K.; Zhuang, X.; Deng, Z.; Zhang, L.; Yan, J.; Miller, D.; Zhang, H. G. Grapefruit-Derived Nanovectors Use an Activated Leukocyte Trafficking Pathway to Deliver Therapeutic Agents to Inflammatory Tumor Sites. *Cancer Res.* **2015**, *75*, 2520–2529.
- (333) Swierczak, A.; Mouchemore, K. A.; Hamilton, J. A.; Anderson, R. L. Neutrophils: Important Contributors to Tumor Progression and Metastasis. *Cancer Metastasis Rev.* **2015**, *34*, 735–751.
- (334) Nash, G. F.; Turner, L. F.; Scully, M. F.; Kakkar, A. K. Platelets and Cancer. *Lancet Oncol.* **2002**, *3*, 425–430.
- (335) Kang, T.; Zhu, Q.; Wei, D.; Feng, J.; Yao, J.; Jiang, T.; Song, Q.; Wei, X.; Chen, H.; Gao, X.; et al. Nanoparticles Coated with Neutrophil Membranes Can Effectively Treat Cancer Metastasis. *ACS Nano* **2017**, *11*, 1397–1411.
- (336) Hu, Q.; Sun, W.; Qian, C.; Wang, C.; Bomba, H. N.; Gu, Z. Anticancer Platelet-Mimicking Nanovehicles. *Adv. Mater.* **2015**, *27*, 7043–7050.
- (337) Rao, L.; Bu, L.-L.; Meng, Q.-F.; Cai, B.; Deng, W.-W.; Li, A.; Li, K.; Guo, S.-S.; Zhang, W.-F.; Liu, W.; et al. Antitumor Platelet-Mimicking Magnetic Nanoparticles. *Adv. Funct. Mater.* **2017**, *27*, 1604774.
- (338) Mai, X.; Zhang, Y.; Fan, H.; Song, W.; Chang, Y.; Chen, B.; Shi, J.; Xin, X.; Teng, Z.; Sun, J.; et al. Integration of Immunogenic Activation and Immunosuppressive Reversion Using Mitochondrial-Respiration-Inhibited Platelet-Mimicking Nanoparticles. *Biomaterials* **2020**, *232*, 119699.
- (339) Rao, L.; Meng, Q.-F.; Huang, Q.; Wang, Z.; Yu, G.-T.; Li, A.; Ma, W.; Zhang, N.; Guo, S.-S.; Zhao, X.-Z.; et al. Platelet–Leukocyte Hybrid Membrane-Coated Immunomagnetic Beads for Highly Efficient and Highly Specific Isolation of Circulating Tumor Cells. *Adv. Funct. Mater.* **2018**, *28*, 1803531.
- (340) Zou, W. Immunosuppressive Networks in the Tumor Environment and Their Therapeutic Relevance. *Nat. Rev. Cancer* **2005**, *5*, 263–274.
- (341) Glinsky, V. V.; Glinsky, G. V.; Glinskii, O. V.; Huxley, V. H.; Turk, J. R.; Mossine, V. V.; Deutscher, S. L.; Pienta, K. J.; Quinn, T. P. Intravascular Metastatic Cancer Cell Homotypic Aggregation at the Sites of Primary Attachment to the Endothelium. *Cancer Res.* **2003**, *63*, 3805–3811.
- (342) Zhu, J. Y.; Zheng, D. W.; Zhang, M. K.; Yu, W. Y.; Qiu, W. X.; Hu, J. J.; Feng, J.; Zhang, X. Z. Preferential Cancer Cell Self-Recognition and Tumor Self-Targeting by Coating Nanoparticles with Homotypic Cancer Cell Membranes. *Nano Lett.* **2016**, *16*, 5895–5901.
- (343) Fang, R. H.; Hu, C. M.; Luk, B. T.; Gao, W.; Copp, J. A.; Tai, Y.; O'Connor, D. E.; Zhang, L. Cancer Cell Membrane-Coated Nanoparticles for Anticancer Vaccination and Drug Delivery. *Nano Lett.* **2014**, *14*, 2181–2188.
- (344) Yang, R.; Xu, J.; Xu, L.; Sun, X.; Chen, Q.; Zhao, Y.; Peng, R.; Liu, Z. Cancer Cell Membrane-Coated Adjuvant Nanoparticles with Mannose Modification for Effective Anticancer Vaccination. *ACS Nano* **2018**, *12*, 5121–5129.
- (345) Chen, Z.; Zhao, P.; Luo, Z.; Zheng, M.; Tian, H.; Gong, P.; Gao, G.; Pan, H.; Liu, L.; Ma, A.; et al. Cancer Cell Membrane–Biomimetic Nanoparticles for Homologous-Targeting Dual-Modal Imaging and Photothermal Therapy. *ACS Nano* **2016**, *10*, 10049–10057.
- (346) Li, S. Y.; Cheng, H.; Xie, B. R.; Qiu, W. X.; Zeng, J. Y.; Li, C. X.; Wan, S. S.; Zhang, L.; Liu, W. L.; Zhang, X. Z. Cancer Cell Membrane Camouflaged Cascade Bioreactor for Cancer Targeted Starvation and Photodynamic Therapy. *ACS Nano* **2017**, *11*, 7006–7018.
- (347) Yong, T.; Wang, D.; Li, X.; Yan, Y.; Hu, J.; Gan, L.; Yang, X. Extracellular Vesicles for Tumor Targeting Delivery Based on Five Features Principle. *J. Controlled Release* **2020**, *322*, 555–565.
- (348) Hoshino, A.; Costa-Silva, B.; Shen, T. L.; Rodrigues, G.; Hashimoto, A.; Tesic Mark, M.; Molina, H.; Kohsaka, S.; Di Giannatale, A.; Ceder, S.; et al. Tumour Exosome Integrins Determine Organotropic Metastasis. *Nature* **2015**, *527*, 329–335.
- (349) Nogués, L.; Benito-Martin, A.; Hergueta-Redondo, M.; Peinado, H. The Influence of Tumour-Derived Extracellular Vesicles on Local and Distal Metastatic Dissemination. *Mol. Aspects Med.* **2018**, *60*, 15–26.
- (350) Kalluri, R.; LeBleu, V. S. The Biology, Function, and Biomedical Applications of Exosomes. *Science* **2020**, *367*, eaau6977.
- (351) O'Brien, K.; Lowry, M. C.; Corcoran, C.; Martinez, V. G.; Daly, M.; Rani, S.; Gallagher, W. M.; Radomski, M. W.; MacLeod, R. A.; O'Driscoll, L. Mir-134 in Extracellular Vesicles Reduces Triple-Negative Breast Cancer Aggression and Increases Drug Sensitivity. *Oncotarget* **2015**, *6*, 32774–32789.
- (352) Piffoux, M.; Silva, A. K. A.; Wilhelm, C.; Gazeau, F.; Taresté, D. Modification of Extracellular Vesicles by Fusion with Liposomes for the Design of Personalized Biogenic Drug Delivery Systems. *ACS Nano* **2018**, *12*, 6830–6842.
- (353) Mulens-Arias, V.; Nicolás-Boluda, A.; Silva, A. K. A.; Gazeau, F. Theranostic Iron Oxide Nanoparticle Cargo Defines Extracellular Vesicle-Dependent Modulation of Macrophage Activation and Migratory Behavior. *Adv. Biosystems* **2018**, *2*, 1800079.
- (354) Perteghella, S.; Crivelli, B.; Catenacci, L.; Sorrenti, M.; Bruni, G.; Necchi, V.; Viganì, B.; Sorlini, M.; Torre, M. L.; Chlapanidas, T. Stem Cell-Extracellular Vesicles as Drug Delivery Systems: New Frontiers for Silk/Curcumin Nanoparticles. *Int. J. Pharm.* **2017**, *520*, 86–97.
- (355) Cheng, G.; Li, W.; Ha, L.; Han, X.; Hao, S.; Wan, Y.; Wang, Z.; Dong, F.; Zou, X.; Mao, Y.; et al. Self-Assembly of Extracellular Vesicle-Like Metal–Organic Framework Nanoparticles for Protection and Intracellular Delivery of Biofunctional Proteins. *J. Am. Chem. Soc.* **2018**, *140*, 7282–7291.
- (356) de Jong, O. G.; Kooijmans, S. A. A.; Murphy, D. E.; Jiang, L.; Evers, M. J. W.; Sluijter, J. P. G.; Vader, P.; Schiffelers, R. M. Drug Delivery with Extracellular Vesicles: From Imagination to Innovation. *Acc. Chem. Res.* **2019**, *52*, 1761–1770.
- (357) Vader, P.; Mol, E. A.; Pasterkamp, G.; Schiffelers, R. M. Extracellular Vesicles for Drug Delivery. *Adv. Drug Delivery Rev.* **2016**, *106*, 148–156.
- (358) Nasiri Kenari, A.; Cheng, L.; Hill, A. F. Methods for Loading Therapeutics into Extracellular Vesicles and Generating Extracellular Vesicles Mimetic-Nanovesicles. *Methods* **2020**, *177*, 103–113.
- (359) Busatto, S.; Vilanilam, G.; Ticer, T.; Lin, W. L.; Dickson, D. W.; Shapiro, S.; Bergese, P.; Wolfram, J. Tangential Flow Filtration for Highly Efficient Concentration of Extracellular Vesicles from Large Volumes of Fluid. *Cells* **2018**, *7*, 273.
- (360) Piffoux, M.; Silva, A. K. A.; Lugagne, J.-B.; Hersen, P.; Wilhelm, C.; Gazeau, F. Extracellular Vesicle Production Loaded with Nanoparticles and Drugs in a Trade-Off between Loading, Yield and Purity: Towards a Personalized Drug Delivery System. *Adv. Biosystems* **2017**, *1*, 1700044.
- (361) Luo, C. H.; Huang, C. T.; Su, C. H.; Yeh, C. S. Bacteria-Mediated Hypoxia-Specific Delivery of Nanoparticles for Tumors Imaging and Therapy. *Nano Lett.* **2016**, *16*, 3493–3499.
- (362) Lefevre, C. T.; Bazylinski, D. A. Ecology, Diversity, and Evolution of Magnetotactic Bacteria. *Microbiol. Mol. Biol. Rev.* **2013**, *77*, 497–526.
- (363) Lefevre, C. T.; Bennet, M.; Landau, L.; Vach, P.; Pignol, D.; Bazylinski, D. A.; Frankel, R. B.; Klumpp, S.; Faivre, D. Diversity of Magneto-Aerotactic Behaviors and Oxygen Sensing Mechanisms in Cultured Magnetotactic Bacteria. *Biophys. J.* **2014**, *107*, 527–538.

- (364) Brune, A.; Frenzel, P.; Cypionka, H. Life at the Oxidative–Anoxic Interface: Microbial Activities and Adaptations. *FEMS Microbiol. Rev.* **2000**, *24*, 691–710.
- (365) Felfoul, O.; Mohammadi, M.; Taherkhani, S.; de Lanauze, D.; Zhong Xu, Y.; Loghin, D.; Essa, S.; Jancik, S.; Houle, D.; Lafleur, M.; et al. Magneto-Aerotactic Bacteria Deliver Drug-Containing Nanoliposomes to Tumour Hypoxic Regions. *Nat. Nanotechnol.* **2016**, *11*, 941–947.
- (366) Józefczak, A.; Leszczyński, B.; Skumiel, A.; Hornowski, T. A Comparison between Acoustic Properties and Heat Effects in Biogenic (Magnetosomes) and Abiotic Magnetite Nanoparticle Suspensions. *J. Magn. Magn. Mater.* **2016**, *407*, 92–100.
- (367) Wahajuddin; Arora, S. Superparamagnetic Iron Oxide Nanoparticles: Magnetic Nanoplatfoms as Drug Carriers. *Int. J. Nanomed.* **2012**, *7*, 3445–3471.
- (368) Hu, L. L.; Zhang, F.; Wang, Z.; You, X. F.; Nie, L.; Wang, H. X.; Song, T.; Yang, W. H. Comparison of the  $^1\text{H}$  NMR Relaxation Enhancement Produced by Bacterial Magnetosomes and Synthetic Iron Oxide Nanoparticles for Potential Use as Molecular Probes. *IEEE Trans. Appl. Supercond.* **2010**, *20*, 822–825.
- (369) Leong, H. S.; Butler, K. S.; Brinker, C. J.; Azzawi, M.; Conlan, S.; Dufes, C.; Owen, A.; Rannard, S.; Scott, C.; Chen, C.; et al. On the Issue of Transparency and Reproducibility in Nanomedicine. *Nat. Nanotechnol.* **2019**, *14*, 629–635.
- (370) Maksoudian, C.; Soenen, S. J.; Susumu, K.; Oh, E.; Medintz, I. L.; Manshian, B. B. A Multiparametric Evaluation of Quantum Dot Size and Surface-Grafted Peptide Density on Cellular Uptake and Cytotoxicity. *Bioconjugate Chem.* **2020**, *31*, 1077–1087.
- (371) Chen, L.; Wu, L. Y.; Yang, W. X. Nanoparticles Induce Apoptosis Via Mediating Diverse Cellular Pathways. *Nanomedicine (London, U. K.)* **2018**, *13*, 2939–2955.
- (372) Liu, X.; Tang, I.; Wainberg, Z. A.; Meng, H. Safety Considerations of Cancer Nanomedicine—A Key Step toward Translation. *Small* **2020**, *16*, 2000673.
- (373) Fadeel, B.; Fornara, A.; Toprak, M. S.; Bhattacharya, K. Keeping It Real: The Importance of Material Characterization in Nanotoxicology. *Biochem. Biophys. Res. Commun.* **2015**, *468*, 498–503.
- (374) Wu, L. P.; Wang, D.; Parhamifar, L.; Hall, A.; Chen, G. Q.; Moghimi, S. M. Poly(3-Hydroxybutyrate-Co-R-3-Hydroxyhexanoate) Nanoparticles with Polyethylenimine Coat as Simple, Safe, and Versatile Vehicles for Cell Targeting: Population Characteristics, Cell Uptake, and Intracellular Trafficking. *Adv. Healthcare Mater.* **2014**, *3*, 817–824.
- (375) Pal, A. K.; Aalaei, I.; Gadde, S.; Gaines, P.; Schmidt, D.; Demokritou, P.; Bello, D. High Resolution Characterization of Engineered Nanomaterial Dispersions in Complex Media Using Tunable Resistive Pulse Sensing Technology. *ACS Nano* **2014**, *8*, 9003–9015.
- (376) George, S.; Xia, T.; Rallo, R.; Zhao, Y.; Ji, Z.; Lin, S.; Wang, X.; Zhang, H.; France, B.; Schoenfeld, D.; et al. Use of a High-Throughput Screening Approach Coupled with in Vivo Zebrafish Embryo Screening to Develop Hazard Ranking for Engineered Nanomaterials. *ACS Nano* **2011**, *5*, 1805–1817.
- (377) Manshian, B. B.; Moyano, D. F.; Corthout, N.; Munck, S.; Himmelreich, U.; Rotello, V. M.; Soenen, S. J. High-Content Imaging and Gene Expression Analysis to Study Cell–Nanomaterial Interactions: The Effect of Surface Hydrophobicity. *Biomaterials* **2014**, *35*, 9941–9950.
- (378) Manshian, B. B.; Munck, S.; Agostinis, P.; Himmelreich, U.; Soenen, S. J. High Content Analysis at Single Cell Level Identifies Different Cellular Responses Dependent on Nanomaterial Concentrations. *Sci. Rep.* **2015**, *5*, 13890.
- (379) Burello, E.; Worth, A. P. Qsar Modeling of Nanomaterials. *Wiley Interdiscip. Rev.: Nanomed. Nanobiotechnol.* **2011**, *3*, 298–306.
- (380) Zhang, H.; Ji, Z.; Xia, T.; Meng, H.; Low-Kam, C.; Liu, R.; Pokhrel, S.; Lin, S.; Wang, X.; Liao, Y.-P.; et al. Use of Metal Oxide Nanoparticle Band Gap to Develop a Predictive Paradigm for Oxidative Stress and Acute Pulmonary Inflammation. *ACS Nano* **2012**, *6*, 4349–4368.
- (381) Gerloff, K.; Landesmann, B.; Worth, A.; Munn, S.; Palosaari, T.; Whelan, M. The Adverse Outcome Pathway Approach in Nanotoxicology. *Comput. Toxicol.* **2017**, *1*, 3–11.
- (382) Dobrovolskaia, M. A.; McNeil, S. E. Understanding the Correlation between in Vitro and in Vivo Immunotoxicity Tests for Nanomedicines. *J. Controlled Release* **2013**, *172*, 456–466.
- (383) Urbán, P.; Liptrott, N. J.; Bremer, S. Overview of the Blood Compatibility of Nanomedicines: A Trend Analysis of in Vitro and in Vivo Studies. *Wiley Interdiscip. Rev.: Nanomed. Nanobiotechnol.* **2019**, *11*, e1546.
- (384) Li, Y.; Fujita, M.; Boraschi, D. Endotoxin Contamination in Nanomaterials Leads to the Misinterpretation of Immunotoxicity Results. *Front. Immunol.* **2017**, *8*, 472.
- (385) Hannon, G.; Lysaght, J.; Liptrott, N. J.; Prina-Mello, A. Immunotoxicity Considerations for Next Generation Cancer Nanomedicines. *Adv. Sci. (Weinh)* **2019**, *6*, 1900133.
- (386) Oostingh, G. J.; Casals, E.; Italiani, P.; Colognato, R.; Stritzinger, R.; Ponti, J.; Pfaller, T.; Kohl, Y.; Ooms, D.; Favilli, F.; et al. Problems and Challenges in the Development and Validation of Human Cell-Based Assays to Determine Nanoparticle-Induced Immunomodulatory Effects. *Part. Fibre Toxicol.* **2011**, *8*, 8.
- (387) Li, Y.; Boraschi, D. Endotoxin Contamination: A Key Element in the Interpretation of Nanosafety Studies. *Nanomedicine (London, U. K.)* **2016**, *11*, 269–287.
- (388) Osman, N. M.; Sexton, D. W.; Saleem, I. Y. Toxicological Assessment of Nanoparticle Interactions with the Pulmonary System. *Nanotoxicology* **2020**, *14*, 21–58.
- (389) Vu, B. T.; Shahin, S. A.; Croissant, J.; Fatieiev, Y.; Matsumoto, K.; Le-Hoang Doan, T.; Yik, T.; Simargi, S.; Conteras, A.; Ratliff, L.; et al. Chick Chorioallantoic Membrane Assay as an in Vivo Model to Study the Effect of Nanoparticle-Based Anticancer Drugs in Ovarian Cancer. *Sci. Rep.* **2018**, *8*, 8524.
- (390) Liu, W.; Rose, J.; Plantevin, S.; Auffan, M.; Bottero, J. Y.; Vidaud, C. Protein Corona Formation for Nanomaterials and Proteins of a Similar Size: Hard or Soft Corona? *Nanoscale* **2013**, *5*, 1658–1668.
- (391) Tenzer, S.; Docter, D.; Kuharev, J.; Musyanovych, A.; Fetz, V.; Hecht, R.; Schlenk, F.; Fischer, D.; Kiouptsi, K.; Reinhardt, C.; et al. Rapid Formation of Plasma Protein Corona Critically Affects Nanoparticle Pathophysiology. *Nat. Nanotechnol.* **2013**, *8*, 772–781.
- (392) Ke, P. C.; Lin, S.; Parak, W. J.; Davis, T. P.; Caruso, F. A Decade of the Protein Corona. *ACS Nano* **2017**, *11*, 11773–11776.
- (393) Caracciolo, G.; Farokhzad, O. C.; Mahmoudi, M. Biological Identity of Nanoparticles in Vivo: Clinical Implications of the Protein Corona. *Trends Biotechnol.* **2017**, *35*, 257–264.
- (394) Ye, L.; Yong, K.-T.; Liu, L.; Roy, I.; Hu, R.; Zhu, J.; Cai, H.; Law, W.-C.; Liu, J.; Wang, K.; et al. A Pilot Study in Non-Human Primates Shows No Adverse Response to Intravenous Injection of Quantum Dots. *Nat. Nanotechnol.* **2012**, *7*, 453–458.
- (395) De Jong, W. H.; Hagens, W. I.; Krystek, P.; Burger, M. C.; Sips, A. J.; Geertsma, R. E. Particle Size-Dependent Organ Distribution of Gold Nanoparticles after Intravenous Administration. *Biomaterials* **2008**, *29*, 1912–1919.
- (396) Fonge, H.; Huang, H.; Scollard, D.; Reilly, R. M.; Allen, C. Influence of Formulation Variables on the Biodistribution of Multifunctional Block Copolymer Micelles. *J. Controlled Release* **2012**, *157*, 366–374.
- (397) Song, G.; Petschauer, J. S.; Madden, A. J.; Zamboni, W. C. Nanoparticles and the Mononuclear Phagocyte System: Pharmacokinetics and Applications for Inflammatory Diseases. *Curr. Rheumatol. Rev.* **2014**, *10*, 22–34.
- (398) Banda, N. K.; Mehta, G.; Chao, Y.; Wang, G.; Inturi, S.; Fossati-Jimack, L.; Botto, M.; Wu, L.; Moghimi, S. M.; Simberg, D. Mechanisms of Complement Activation by Dextran-Coated Superparamagnetic Iron Oxide (Spio) Nanoworms in Mouse Versus Human Serum. *Part. Fibre Toxicol.* **2014**, *11*, 64.



- (399) Shah, A.; Dobrovolskaia, M. A. Immunological Effects of Iron Oxide Nanoparticles and Iron-Based Complex Drug Formulations: Therapeutic Benefits, Toxicity, Mechanistic Insights, and Translational Considerations. *Nanomedicine* **2018**, *14*, 977–990.
- (400) Halamoda-Kenzaoui, B.; Bremer-Hoffmann, S. Main Trends of Immune Effects Triggered by Nanomedicines in Preclinical Studies. *Int. J. Nanomed.* **2018**, *13*, 5419–5431.
- (401) Peng, Q.; Mu, H. The Potential of Protein-Nanomaterial Interaction for Advanced Drug Delivery. *J. Controlled Release* **2016**, *225*, 121–132.
- (402) Landgraf, L.; Christner, C.; Storck, W.; Schick, I.; Krumbein, I.; Dähring, H.; Haedicke, K.; Heinz-Herrmann, K.; Teichgräber, U.; Reichenbach, J. R.; et al. A Plasma Protein Corona Enhances the Biocompatibility of Au@Fe<sub>3</sub>O<sub>4</sub> Janus Particles. *Biomaterials* **2015**, *68*, 77–88.
- (403) Colapicchioni, V.; Tilio, M.; Digiacomo, L.; Gambini, V.; Palchetti, S.; Marchini, C.; Pozzi, D.; Occhipinti, S.; Amici, A.; Caracciolo, G. Personalized Liposome-Protein Corona in the Blood of Breast, Gastric and Pancreatic Cancer Patients. *Int. J. Biochem. Cell Biol.* **2016**, *75*, 180–187.
- (404) Hajipour, M. J.; Laurent, S.; Aghaie, A.; Rezaee, F.; Mahmoudi, M. Personalized Protein Coronas: A “Key” Factor at the Nanobiointerface. *Biomater. Sci.* **2014**, *2*, 1210–1221.
- (405) Nguyen, V. H.; Lee, B. J. Protein Corona: A New Approach for Nanomedicine Design. *Int. J. Nanomed.* **2017**, *12*, 3137–3151.
- (406) Jones, C. F.; Campbell, R. A.; Brooks, A. E.; Assemi, S.; Tadjiki, S.; Thiagarajan, G.; Mulcock, C.; Weyrich, A. S.; Brooks, B. D.; Ghandehari, H.; et al. Cationic Pamam Dendrimers Aggressively Initiate Blood Clot Formation. *ACS Nano* **2012**, *6*, 9900–9910.
- (407) Oslakovic, C.; Cedervall, T.; Linse, S.; Dahlback, B. Polystyrene Nanoparticles Affecting Blood Coagulation. *Nanomedicine* **2012**, *8*, 981–986.
- (408) Lima, L. G.; Monteiro, R. Q. Activation of Blood Coagulation in Cancer: Implications for Tumour Progression. *Biosci. Rep.* **2013**, *33*, No. e00064.
- (409) Brand, W.; Noorlander, C. W.; Giannakou, C.; De Jong, W. H.; Kooi, M. W.; Park, M. V.; Vandebriel, R. J.; Bosselaers, I. E.; Scholl, J. H.; Geertsma, R. E. Nanomedicinal Products: A Survey on Specific Toxicity and Side Effects. *Int. J. Nanomed.* **2017**, *12*, 6107–6129.
- (410) Peng, L.; Bu, Z.; Ye, X.; Zhou, Y.; Zhao, Q. Incidence and Risk of Peripheral Neuropathy with Nab-Paclitaxel in Patients with Cancer: A Meta-Analysis. *Eur. J. Cancer Care (Engl.)* **2017**, *26*, e12407.
- (411) O’Brien, M. E.; Wigler, N.; Inbar, M.; Rosso, R.; Grischke, E.; Santoro, A.; Catane, R.; Kieback, D. G.; Tomczak, P.; Ackland, S. P.; et al. Reduced Cardiotoxicity and Comparable Efficacy in a Phase Iii Trial of Pegylated Liposomal Doxorubicin Hcl (Caelyx/Doxil) Versus Conventional Doxorubicin for First-Line Treatment of Metastatic Breast Cancer. *Ann. Oncol.* **2004**, *15*, 440–449.
- (412) Dai, Q.; Wilhelm, S.; Ding, D.; Syed, A. M.; Sindhwani, S.; Zhang, Y.; Chen, Y. Y.; MacMillan, P.; Chan, W. C. W. Quantifying the Ligand-Coated Nanoparticle Delivery to Cancer Cells in Solid Tumors. *ACS Nano* **2018**, *12*, 8423–8435.
- (413) Yang, Y.; Chen, Q.; Li, S.; Ma, W.; Yao, G.; Ren, F.; Cai, Z.; Zhao, P.; Liao, G.; Xiong, J.; et al. Irgd-Mediated and Enzyme-Induced Precise Targeting and Retention of Gold Nanoparticles for the Enhanced Imaging and Treatment of Breast Cancer. *J. Biomed. Nanotechnol.* **2018**, *14*, 1396–1408.
- (414) Chen, F.; Hong, H.; Shi, S. X.; Goel, S.; Valdovinos, H. F.; Hernandez, R.; Theuer, C. P.; Barnhart, T. E.; Cai, W. B. Engineering of Hollow Mesoporous Silica Nanoparticles for Remarkably Enhanced Tumor Active Targeting Efficacy. *Sci. Rep.* **2015**, *4*, 5080.
- (415) Chen, F.; Nayak, T. R.; Goel, S.; Valdovinos, H. F.; Hong, H.; Theuer, C. P.; Barnhart, T. E.; Cai, W. B. In Vivo Tumor Vasculature Targeted Pet/Nirx Imaging with Trc105(Fab)-Conjugated, Dual-Labeled Mesoporous Silica Nanoparticles. *Mol. Pharmaceutics* **2014**, *11*, 4007–4014.
- (416) Chen, F.; Hong, H.; Zhang, Y.; Valdovinos, H. F.; Shi, S.; Kwon, G. S.; Theuer, C. P.; Barnhart, T. E.; Cai, W. In Vivo Tumor Targeting and Image-Guided Drug Delivery with Antibody-Conjugated, Radiolabeled Mesoporous Silica Nanoparticles. *ACS Nano* **2013**, *7*, 9027–9039.
- (417) Chen, F.; Hong, H.; Goel, S.; Graves, S. A.; Orbay, H.; Ehlerding, E. B.; Shi, S. X.; Theuer, C. P.; Nickles, R. J.; Cai, W. B. In Vivo Tumor Vasculature Targeting of Cus@Msn Based Theranostic Nanomedicine. *ACS Nano* **2015**, *9*, 3926–3934.
- (418) Hong, H.; Wang, F.; Zhang, Y.; Graves, S. A.; Eddine, S. B. Z.; Yang, Y. A.; Theuer, C. P.; Nickles, R. J.; Wang, X. D.; Cai, W. B. Red Fluorescent Zinc Oxide Nanoparticle: A Novel Platform for Cancer Targeting. *ACS Appl. Mater. Interfaces* **2015**, *7*, 3373–3381.
- (419) Guo, J. T.; Hong, H.; Chen, G. J.; Shi, S. X.; Zheng, Q. F.; Zhang, Y.; Theuer, C. P.; Barnhart, T. E.; Cai, W. B.; Gong, S. Q. Image-Guided and Tumor-Targeted Drug Delivery with Radiolabeled Unimolecular Micelles. *Biomaterials* **2013**, *34*, 8323–8332.
- (420) Shi, S. X.; Yang, K.; Hong, H.; Valdovinos, H. F.; Nayak, T. R.; Zhang, Y.; Theuer, C. P.; Barnhart, T. E.; Liu, Z.; Cai, W. B. Tumor Vasculature Targeting and Imaging in Living Mice with Reduced Graphene Oxide. *Biomaterials* **2013**, *34*, 3002–3009.
- (421) Hong, H.; Yang, K.; Zhang, Y.; Engle, J. W.; Feng, L. Z.; Yang, Y. A.; Nayak, T. R.; Goel, S.; Bean, J.; Theuer, C. P.; et al. In Vivo Targeting and Imaging of Tumor Vasculature with Radiolabeled, Antibody-Conjugated Nanographene. *ACS Nano* **2012**, *6*, 2361–2370.
- (422) Hong, H.; Zhang, Y.; Engle, J. W.; Nayak, T. R.; Theuer, C. P.; Nickles, R. J.; Barnhart, T. E.; Cai, W. In Vivo Targeting and Positron Emission Tomography Imaging of Tumor Vasculature with (66)Ga-Labeled Nano-Graphene. *Biomaterials* **2012**, *33*, 4147–4156.
- (423) Han, X. P.; Li, Z. B.; Sun, J.; Luo, C.; Li, L.; Liu, Y. H.; Du, Y. Q.; Qiu, S. H.; Ai, X. Y.; Wu, C. N.; et al. Stealth Cd44-Targeted Hyaluronic Acid Supramolecular Nanoassemblies for Doxorubicin Delivery: Probing the Effect of Uncovalent Pegylation Degree on Cellular Uptake and Blood Long Circulation. *J. Controlled Release* **2015**, *197*, 29–40.
- (424) Guo, X.; Shi, C. L.; Wang, J.; Di, S. B.; Zhou, S. B. Ph-Triggered Intracellular Release from Actively Targeting Polymer Micelles. *Biomaterials* **2013**, *34*, 4544–4554.
- (425) Tang, T.; Wei, Y. S.; Yang, Q. L.; Yang, Y.; Sailor, M. J.; Pang, H. B. Rapid Chelator-Free Radiolabeling of Quantum Dots for in Vivo Imaging. *Nanoscale* **2019**, *11*, 22248–22254.
- (426) Quan, Q. M.; Xie, J.; Gao, H. K.; Yang, M.; Zhang, F.; Liu, G.; Lin, X.; Wang, A.; Eden, H. S.; Lee, S.; et al. Hsa Coated Iron Oxide Nanoparticles as Drug Delivery Vehicles for Cancer Therapy. *Mol. Pharmaceutics* **2011**, *8*, 1669–1676.
- (427) Bibby, D. C.; Talmadge, J. E.; Dalal, M. K.; Kurz, S. G.; Chytil, K. M.; Barry, S. E.; Shand, D. G.; Steiert, M. Pharmacokinetics and Biodistribution of Rgd-Targeted Doxorubicin-Loaded Nanoparticles in Tumor-Bearing Mice. *Int. J. Pharm.* **2005**, *293*, 281–290.
- (428) Qhattal, H. S. S.; Hye, T.; Alali, A.; Liu, X. L. Hyaluronan Polymer Length, Grafting Density, and Surface Poly(Ethylene Glycol) Coating Influence in Vivo Circulation and Tumor Targeting of Hyaluronan-Grafted Liposomes. *ACS Nano* **2014**, *8*, 5423–5440.
- (429) Yang, J.; Lu, W. F.; Xiao, J. L.; Zong, Q.; Xu, H. X.; Yin, Y. H.; Hong, H.; Xu, W. J. A Positron Emission Tomography Image-Guidable Unimolecular Micelle Nanoplatform for Cancer Theranostic Applications. *Acta Biomater.* **2018**, *79*, 306–316.
- (430) Ma, Y.; Sadoqi, M.; Shao, J. Biodistribution of Indocyanine Green-Loaded Nanoparticles with Surface Modifications of Peg and Folic Acid. *Int. J. Pharm.* **2012**, *436*, 25–31.
- (431) Dam, D. H. M.; Culver, K. S. B.; Kandela, I.; Lee, R. C.; Chandra, K.; Lee, H.; Mantis, C.; Ugolokov, A.; Mazar, A. P.; Odom, T. W. Biodistribution and in Vivo Toxicity of Aptamer-Loaded Gold Nanostars. *Nanomedicine* **2015**, *11*, 671–679.
- (432) Sykes, E. A.; Chen, J.; Zheng, G.; Chan, W. C. W. Investigating the Impact of Nanoparticle Size on Active and Passive Tumor Targeting Efficiency. *ACS Nano* **2014**, *8*, 5696–5706.

- (433) Park, J. H.; von Maltzahn, G.; Zhang, L. L.; Derfus, A. M.; Simberg, D.; Harris, T. J.; Ruoslahti, E.; Bhatia, S. N.; Sailor, M. J. Systematic Surface Engineering of Magnetic Nanoworms for in Vivo Tumor Targeting. *Small* **2009**, *5*, 694–700.
- (434) Zhong, Y. N.; Zhang, J.; Cheng, R.; Deng, C.; Meng, F. H.; Xie, F.; Zhong, Z. Y. Reversibly Crosslinked Hyaluronic Acid Nanoparticles for Active Targeting and Intelligent Delivery of Doxorubicin to Drug Resistant Cd44+Human Breast Tumor Xenografts. *J. Controlled Release* **2015**, *205*, 144–154.
- (435) Sun, B. F.; Deng, C.; Meng, F. H.; Zhang, J.; Zhong, Z. Y. Robust, Active Tumor-Targeting and Fast Bioresponsive Anticancer Nanotherapeutics Based on Natural Endogenous Materials. *Acta Biomater.* **2016**, *45*, 223–233.
- (436) Lee, H.; Fonge, H.; Hoang, B.; Reilly, R. M.; Allen, C. The Effects of Particle Size and Molecular Targeting on the Intratumoral and Subcellular Distribution of Polymeric Nanoparticles. *Mol. Pharmaceutics* **2010**, *7*, 1195–1208.
- (437) Mamot, C.; Drummond, D. C.; Noble, C. O.; Kallab, V.; Guo, Z. X.; Hong, K. L.; Kirpotin, D. B.; Park, J. W. Epidermal Growth Factor Receptor-Targeted Immunoliposomes Significantly Enhance the Efficacy of Multiple Anticancer Drugs in Vivo. *Cancer Res.* **2005**, *65*, 11631–11638.
- (438) Chattopadhyay, N.; Fonge, H.; Cai, Z. L.; Scollard, D.; Lechtman, E.; Done, S. J.; Pignol, J. P.; Reilly, R. M. Role of Antibody-Mediated Tumor Targeting and Route of Administration in Nanoparticle Tumor Accumulation in Vivo. *Mol. Pharmaceutics* **2012**, *9*, 2168–2179.
- (439) Lee, H.; Zheng, J.; Gaddy, D.; Orcutt, K. D.; Leonard, S.; Geretti, E.; Hesterman, J.; Harwell, C.; Hoppin, J.; Jaffray, D. A.; et al. A Gradient-Loadable Cu-64-Chelator for Quantifying Tumor Deposition Kinetics of Nanoliposomal Therapeutics by Positron Emission Tomography. *Nanomedicine* **2015**, *11*, 155–165.
- (440) Hainfeld, J. F.; O'Connor, M. J.; Dilmannian, F. A.; Slatkin, D. N.; Adams, D. J.; Smilowitz, H. M. Micro-Ct Enables Micro-localisation and Quantification of Her2-Targeted Gold Nanoparticles within Tumour Regions. *Br. J. Radiol.* **2011**, *84*, 526–533.
- (441) Kirpotin, D. B.; Drummond, D. C.; Shao, Y.; Shalaby, M. R.; Hong, K. L.; Nielsen, U. B.; Marks, J. D.; Benz, C. C.; Park, J. W. Antibody Targeting of Long-Circulating Lipidic Nanoparticles Does Not Increase Tumor Localization but Does Increase Internalization in Animal Models. *Cancer Res.* **2006**, *66*, 6732–6740.
- (442) Liang, M.; Liu, X.; Cheng, D.; Liu, G.; Dou, S.; Wang, Y.; Rusckowski, M.; Hnatowich, D. J. Multimodality Nuclear and Fluorescence Tumor Imaging in Mice Using a Streptavidin Nanoparticle. *Bioconjugate Chem.* **2010**, *21*, 1385–1388.
- (443) Zolata, H.; Abbasi Davani, F.; Afarideh, H. Synthesis, Characterization and Theranostic Evaluation of Indium-111 Labeled Multifunctional Superparamagnetic Iron Oxide Nanoparticles (Vol 42, Pg 164, 2015). *Nucl. Med. Biol.* **2015**, *42*, 164–170.
- (444) Lee, J. H.; Huh, Y. M.; Jun, Y.; Seo, J.; Jang, J.; Song, H. T.; Kim, S.; Cho, E. J.; Yoon, H. G.; Suh, J. S.; et al. Artificially Engineered Magnetic Nanoparticles for Ultra-Sensitive Molecular Imaging. *Nat. Med.* **2007**, *13*, 95–99.
- (445) DeNardo, S. J.; DeNardo, G. L.; Miers, L. A.; Natarajan, A.; Foreman, A. R.; Gruettner, C.; Adamson, G. N.; Ivkov, R. Development of Tumor Targeting Bioprobes (in-111-Chimeric L6Monoclonal Antibody Nanoparticles) for Alternating Magnetic Field Cancer Therapy. *Clin. Cancer Res.* **2005**, *11*, 7087s–7092s.
- (446) DeNardo, S. J.; DeNardo, G. L.; Natarajan, A.; Miers, L. A.; Foreman, A. R.; Gruettner, C.; Adamson, G. N.; Ivkov, R. Thermal Dosimetry Predictive of Efficacy of in-111-Chl6 Nanoparticle Amf-Induced Thermoablative Therapy for Human Breast Cancer in Mice. *J. Nucl. Med.* **2007**, *48*, 437–444.
- (447) Chauhan, R. P.; Mathur, R.; Singh, G.; Bag, N.; Singh, S.; Chuttani, K.; Kumar, B. S. H.; Agrawal, S. K.; Mishra, A. K. Evaluation of Biotinylated Magnetic Nanoparticles for Tumour Imaging. *J. Mater. Sci.* **2013**, *48*, 3913–3925.
- (448) Cheng, K.; Kothapalli, S. R.; Liu, H. G.; Koh, A. L.; Jokerst, J. V.; Jiang, H.; Yang, M.; Li, J. B.; Levi, J.; Wu, J. C.; et al. Construction and Validation of Nano Gold Tripods for Molecular Imaging of Living Subjects. *J. Am. Chem. Soc.* **2014**, *136*, 3560–3571.
- (449) Yang, X. Q.; Hong, H.; Grailer, J. J.; Rowland, I. J.; Javadi, A.; Hurley, S. A.; Xiao, Y. L.; Yang, Y. A.; Zhang, Y.; Nickles, R.; et al. Crgd-Functionalized, Dox-Conjugated, and Cu-64-Labeled Superparamagnetic Iron Oxide Nanoparticles for Targeted Anticancer Drug Delivery and Pet/Mr Imaging. *Biomaterials* **2011**, *32*, 4151–4160.
- (450) Chakravarty, R.; Goel, S.; Hong, H.; Chen, F.; Valdovinos, H. F.; Hernandez, R.; Barnhart, T. E.; Cai, W. B. Hollow Mesoporous Silica Nanoparticles for Tumor Vasculature Targeting and Pet Image-Guided Drug Delivery. *Nanomedicine* **2015**, *10*, 1233–1246.
- (451) Lee, J.; Lee, T. S.; Ryu, J.; Hong, S.; Kang, M.; Im, K.; Kang, J. H.; Lim, S. M.; Park, S.; Song, R. Rgd Peptide-Conjugated Multimodal Nagdf4:Yb3+/Er3+ Nanophosphors for Upconversion Luminescence, Mr, and Pet Imaging of Tumor Angiogenesis. *J. Nucl. Med.* **2013**, *54*, 96–103.
- (452) Cai, W. B.; Chen, K.; Li, Z. B.; Gambhir, S. S.; Chen, X. Y. Dual-Function Probe for Pet and near-Infrared Fluorescence Imaging of Tumor Vasculature. *J. Nucl. Med.* **2007**, *48*, 1862–1870.
- (453) Liu, Z.; Cai, W. B.; He, L. N.; Nakayama, N.; Chen, K.; Sun, X. M.; Chen, X. Y.; Dai, H. J. In Vivo Biodistribution and Highly Efficient Tumour Targeting of Carbon Nanotubes in Mice. *Nat. Nanotechnol.* **2007**, *2*, 47–52.
- (454) Chen, Q.; Wang, H.; Liu, H.; Wen, S. H.; Peng, C.; Shen, M. W.; Zhang, G. X.; Shi, X. Y. Multifunctional Dendrimer-Entrapped Gold Nanoparticles Modified with Rgd Peptide for Targeted Computed Tomography/Magnetic Resonance Dug-Modal Imaging of Tumors. *Anal. Chem.* **2015**, *87*, 3949–3956.
- (455) Gao, J. H.; Chen, K.; Xie, R. G.; Xie, J.; Yan, Y. J.; Cheng, Z.; Peng, X. G.; Chen, X. Y. In Vivo Tumor-Targeted Fluorescence Imaging Using near-Infrared Non-Cadmium Quantum Dots. *Bioconjugate Chem.* **2010**, *21*, 604–609.
- (456) Wang, J.; Zhao, H.; Zhou, Z. G.; Zhou, P.; Yan, Y. P.; Wang, M. W.; Yang, H.; Zhang, Y. J.; Yang, S. P. Mr/Spect Imaging Guided Photothermal Therapy of Tumor-Targeting Fe@Fe3o4 Nanoparticles in Vivo with Low Mononuclear Phagocyte Uptake. *ACS Appl. Mater. Interfaces* **2016**, *8*, 19872–19882.
- (457) Fang, Y.; Jiang, Y.; Zou, Y.; Meng, F. H.; Zhang, J.; Deng, C.; Sun, H. L.; Zhong, Z. Y. Targeted Glioma Chemotherapy by Cyclic Rgd Peptide-Functionalized Reversibly Core-Crosslinked Multifunctional Poly(Ethylene Glycol)-B-Poly (Epsilon-Caprolactone) Micelles. *Acta Biomater.* **2017**, *50*, 396–406.
- (458) Cui, L. L.; Xiong, C. Y.; Zhou, M.; Shi, S. X.; Chow, D. S. L.; Li, C. Integrin Alpha V Beta 3-Targeted [Cu-64]Cus Nanoparticles for Pet/Ct Imaging and Photothermal Ablation Therapy. *Bioconjugate Chem.* **2018**, *29*, 4062–4071.
- (459) Yan, H. H.; Wang, L.; Wang, J. Y.; Weng, X. F.; Lei, H.; Wang, X. X.; Jiang, L.; Zhu, J. H.; Lu, W. Y.; Wei, X. B.; et al. Two-Order Targeted Brain Tumor Imaging by Using an Optical/Paramagnetic Nanoprobe across the Blood Brain Barrier. *ACS Nano* **2012**, *6*, 410–420.
- (460) Rangger, C.; Helbok, A.; Sosabowski, J.; Kremser, C.; Koehler, G.; Prassl, R.; Andreae, F.; Virgolini, I. J.; von Guggenberg, E.; Decristoforo, C. Tumor Targeting and Imaging with Dual-Peptide Conjugated Multifunctional Liposomal Nanoparticles. *Int. J. Nanomed.* **2013**, *8*, 4659–4670.
- (461) Arora, G.; Dubey, P.; Shukla, J.; Ghosh, S.; Bandopadhyaya, G. Evaluation of Cytotoxic and Tumor Targeting Capability of Lu-177-Dotatate-Nanoparticles: A Trailblazing Strategy in Peptide Receptor Radionuclide Therapy. *Ann. Nucl. Med.* **2016**, *30*, 334–345.
- (462) Goel, S.; Chen, F.; Hong, H.; Valdovinos, H. F.; Hernandez, R.; Shi, S. X.; Barnhart, T. E.; Cai, W. B. Vegf(121)-Conjugated Mesoporous Silica Nanoparticle: A Tumor Targeted Drug Delivery System. *ACS Appl. Mater. Interfaces* **2014**, *6*, 21677–21685.
- (463) Chen, K.; Li, Z. B.; Wang, H.; Cai, W. B.; Chen, X. Y. Dual-Modality Optical and Positron Emission Tomography Imaging of Vascular Endothelial Growth Factor Receptor on Tumor Vasculature Using Quantum Dots. *Eur. J. Nucl. Med. Mol. Imaging* **2008**, *35*, 2235–2244.

- (464) Shi, S. X.; Yang, K.; Hong, H.; Chen, F.; Valdovinos, H. F.; Goel, S.; Barnhart, T. E.; Liu, Z.; Cai, W. B. Vegfr Targeting Leads to Significantly Enhanced Tumor Uptake of Nanographene Oxide in Vivo. *Biomaterials* **2015**, *39*, 39–46.
- (465) Meyers, J. D.; Cheng, Y.; Broome, A. M.; Agnes, R. S.; Schluchter, M. D.; Margevicius, S.; Wang, X. N.; Kenney, M. E.; Burda, C.; Basilion, J. P. Peptide-Targeted Gold Nanoparticles for Photodynamic Therapy of Brain Cancer. *Part. Part. Syst. Char.* **2015**, *32*, 448–457.
- (466) de Wolf, H. K.; Snel, C. J.; Verbaan, F. J.; Schifflers, R. M.; Hennink, W. E.; Storm, G. Effect of Cationic Carriers on the Pharmacokinetics and Tumor Localization of Nucleic Acids after Intravenous Administration. *Int. J. Pharm.* **2007**, *331*, 167–175.
- (467) Kafa, H.; Wang, J. T. W.; Rubio, N.; Klippstein, R.; Costa, P. M.; Hassan, H. A. F. M.; Sosabowski, J. K.; Bansal, S. S.; Preston, J. E.; Abbott, N. J.; et al. Translocation of Lrp1 Targeted Carbon Nanotubes of Different Diameters across the Blood-Brain Barrier in Vitro and in Vivo. *J. Controlled Release* **2016**, *225*, 217–229.
- (468) Choi, C. H. J.; Alabi, C. A.; Webster, P.; Davis, M. E. Mechanism of Active Targeting in Solid Tumors with Transferrin-Containing Gold Nanoparticles. *Proc. Natl. Acad. Sci. U. S. A.* **2010**, *107*, 1235–1240.
- (469) Ding, M. M.; Song, N. J.; He, X. L.; Li, J. H.; Zhou, L. J.; Tan, H.; Fu, Q.; Gu, Q. Toward the Next-Generation Nanomedicines: Design of Multifunctional Multiblock Polyurethanes for Effective Cancer Treatment. *ACS Nano* **2013**, *7*, 1918–1928.
- (470) Melancon, M. P.; Lu, W.; Yang, Z.; Zhang, R.; Cheng, Z.; Elliot, A. M.; Stafford, J.; Olson, T.; Zhang, J. Z.; Li, C. In Vitro and in Vivo Targeting of Hollow Gold Nanoshells Directed at Epidermal Growth Factor Receptor for Photothermal Ablation Therapy. *Mol. Cancer Ther.* **2008**, *7*, 1730–1739.
- (471) Yang, M.; Cheng, K.; Qi, S. B.; Liu, H. G.; Jiang, Y. X.; Jiang, H.; Li, J. B.; Chen, K.; Zhang, H. M.; Cheng, Z. Affibody Modified and Radiolabeled Gold-Iron Oxide Hetero-Nanostructures for Tumor PET, Optical and MR Imaging. *Biomaterials* **2013**, *34*, 2796–2806.
- (472) Gainkam, L. O. T.; Huang, L.; Cavellers, V.; Keyaerts, M.; Hernot, S.; Vaneycken, I.; Vanhove, C.; Revets, H.; De Baetselier, P.; Lahoutte, T. Comparison of the Biodistribution and Tumor Targeting of Two Tc-99m-Labeled Anti-Egfr Nanobodies in Mice, Using Pinhole Spect/Micro-Ct. *J. Nucl. Med.* **2008**, *49*, 788–795.
- (473) Karmani, L.; Labar, D.; Valembos, V.; Bouchat, V.; Nagaswaran, P. G.; Bol, A.; Gillart, J.; Leveque, P.; Bouzin, C.; Bonifazi, D.; et al. Antibody-Functionalized Nanoparticles for Imaging Cancer: Influence of Conjugation to Gold Nanoparticles on the Biodistribution of 89zr-Labeled Cetuximab in Mice. *Contrast Media Mol. Imaging* **2013**, *8*, 402–408.
- (474) Benezra, M.; Penate-Medina, O.; Zanzonico, P. B.; Schaer, D.; Ow, H.; Burns, A.; DeStanchina, E.; Longo, V.; Herz, E.; Iyer, S.; et al. Multimodal Silica Nanoparticles Are Effective Cancer-Targeted Probes in a Model of Human Melanoma. *J. Clin. Invest.* **2011**, *121*, 2768–2780.
- (475) Lu, W.; Xiong, C. Y.; Zhang, G. D.; Huang, Q.; Zhang, R.; Zhang, J. Z.; Li, C. Targeted Photothermal Ablation of Murine Melanomas with Melanocyte-Stimulating Hormone Analog-Conjugated Hollow Gold Nanospheres. *Clin. Cancer Res.* **2009**, *15*, 876–886.
- (476) Chakravarty, R.; Chakraborty, S.; Guleria, A.; Kumar, C.; Kunwar, A.; Nair, K. V. V.; Sarma, H. D.; Dash, A. Clinical Scale Synthesis of Intrinsically Radiolabeled and Cyclic Rgd Peptide Functionalized Au-198 Nanoparticles for Targeted Cancer Therapy. *Nucl. Med. Biol.* **2019**, *72–73*, 1–10.
- (477) Zou, Y.; Fang, Y.; Meng, H.; Meng, F. H.; Deng, C.; Zhang, J.; Zhong, Z. Y. Self-Crosslinkable and Intracellularly Decrosslinkable Biodegradable Micellar Nanoparticles: A Robust, Simple and Multifunctional Nanoplatform for High-Efficiency Targeted Cancer Chemotherapy. *J. Controlled Release* **2016**, *244*, 326–335.
- (478) Herringson, T. P.; Altin, J. G. Effective Tumor Targeting and Enhanced Anti-Tumor Effect of Liposomes Engrafted with Peptides Specific for Tumor Lymphatics and Vasculature. *Int. J. Pharm.* **2011**, *411*, 206–214.
- (479) Tang, L.; Tong, R.; Coyle, V. J.; Yin, Q.; Pondenis, H.; Borst, L. B.; Cheng, J. J.; Fan, T. M. Targeting Tumor Vasculature with Aptamer-Functionalized Doxorubicin - Polylactide Nanoconjugates for Enhanced Cancer Therapy. *ACS Nano* **2015**, *9*, 5072–5081.
- (480) Ganesh, S.; Iyer, A. K.; Gattacceca, F.; Morrissey, D. V.; Amiji, M. M. In Vivo Biodistribution of Sirna and Cisplatin Administered Using Cd44-Targeted Hyaluronic Acid Nanoparticles. *J. Controlled Release* **2013**, *172*, 699–706.
- (481) Huang, H. T.; Yue, T.; Xu, K.; Golzarian, J.; Yu, J. H.; Huang, J. Fabrication and Evaluation of Tumor-Targeted Positive Mri Contrast Agent Based on Ultrasmall Mno Nanoparticles. *Colloids Surf., B* **2015**, *131*, 148–154.
- (482) Khemtong, C.; Kessinger, C. W.; Ren, J. M.; Bey, E. A.; Yang, S. G.; Guthi, J. S.; Boothman, D. A.; Sherry, A. D.; Gao, J. M. In Vivo Off-Resonance Saturation Magnetic Resonance Imaging of Alpha-(V)Beta(3)-Targeted Superparamagnetic Nanoparticles. *Cancer Res.* **2009**, *69*, 1651–1658.
- (483) Zhang, C. F.; Xie, X.; Liang, S.; Li, M. L.; Liu, Y. J.; Gu, H. C. Mono-Dispersed High Magnetic Resonance Sensitive Magnetite Nanocluster Probe for Detection of Nascent Tumors by Magnetic Resonance Molecular Imaging. *Nanomedicine* **2012**, *8*, 996–1006.
- (484) Huang, X. H.; Peng, X. H.; Wang, Y. Q.; Wang, Y. X.; Shin, D. M.; El-Sayed, M. A.; Nie, S. M. A Reexamination of Active and Passive Tumor Targeting by Using Rod-Shaped Gold Nanocrystals and Covalently Conjugated Peptide Ligands. *ACS Nano* **2010**, *4*, 5887–5896.
- (485) Ming, H.; Fang, L.; Gao, J. M.; Li, C. X.; Ji, Y. H.; Shen, Y. M.; Hu, Y. M.; Li, N.; Chang, J.; Li, W.; et al. Antitumor Effect of Nanoparticle I-131-Labeled Arginine-Glycine-Aspartate-Bovine Serum Albumin-Polycaprolactone in Lung Cancer. *AJR, Am. J. Roentgenol.* **2017**, *208*, 1116–1126.
- (486) Li, S. D.; Chen, Y. C.; Hackett, M. J.; Huang, L. Tumor-Targeted Delivery of Sirna by Self-Assembled Nanoparticles. *Mol. Ther.* **2008**, *16*, 163–169.
- (487) Kim, J. H.; Kim, Y.; Bae, K. H.; Park, T. G.; Lee, J. H.; Park, K. Tumor-Targeted Delivery of Paclitaxel Using Low Density Lipoprotein-Mimetic Solid Lipid Nanoparticles. *Mol. Pharmaceutics* **2015**, *12*, 1230–1241.
- (488) Liu, C. W.; Lin, W. J. Polymeric Nanoparticles Conjugate a Novel Heptapeptide as an Epidermal Growth Factor Receptor-Active Targeting Ligand for Doxorubicin. *Int. J. Nanomed.* **2012**, *7*, 4749–4767.
- (489) Gao, J. H.; Chen, K.; Miao, Z.; Ren, G.; Chen, X. Y.; Gambhir, S. S.; Cheng, Z. Affibody-Based Nanoprobes for Her2-Expressing Cell and Tumor Imaging. *Biomaterials* **2011**, *32*, 2141–2148.
- (490) Gao, J. H.; Chen, K.; Luong, R.; Bouley, D. M.; Mao, H.; Qiao, T. C.; Gambhir, S. S.; Cheng, Z. A Novel Clinically Translatable Fluorescent Nanoparticle for Targeted Molecular Imaging of Tumors in Living Subjects. *Nano Lett.* **2012**, *12*, 281–286.
- (491) Wang, X.; Yang, C. C.; Zhang, Y. J.; Zhen, X.; Wu, W.; Jiang, X. Q. Delivery of Platinum(IV) Drug to Subcutaneous Tumor and Lung Metastasis Using Bradykinin-Potentiating Peptide-Decorated Chitosan Nanoparticles. *Biomaterials* **2014**, *35*, 6439–6453.
- (492) Yang, C. C.; Wang, X.; Yao, X. K.; Zhang, Y. J.; Wu, W.; Jiang, X. Q. Hyaluronic Acid Nanogels with Enzyme-Sensitive Cross-Linking Group for Drug Delivery. *J. Controlled Release* **2015**, *205*, 206–217.
- (493) Xu, C.; Sun, Y.; Yu, Y.; Hu, M.; Yang, C.; Zhang, Z. A Sequentially Responsive and Structure-Transformable Nanoparticle with a Comprehensively Improved 'Capir Cascade' for Enhanced Antitumor Effect. *Nanoscale* **2019**, *11*, 1177–1194.
- (494) Urnauer, S.; Klutz, K.; Grunwald, G. K.; Morys, S.; Schwenk, N.; Zach, C.; Gildehaus, F. J.; Rodl, W.; Ogris, M.; Wagner, E.; Spitzweg, C. Systemic Tumor-Targeted Sodium Iodide Symporter (Nis) Gene Therapy of Hepatocellular Carcinoma Mediated by B6 Peptide Polyplexes. *J. Gene Med.* **2017**, *19*, e2957.



- (495) Qi, W. W.; Yu, H. Y.; Guo, H.; Lou, J.; Wang, Z. M.; Liu, P.; Sapin-Minet, A.; Maincent, P.; Hong, X. C.; Hu, X. M.; et al. Doxorubicin-Loaded Glycyrhretinic Acid Modified Recombinant Human Serum Albumin Nanoparticles for Targeting Liver Tumor Chemotherapy. *Mol. Pharmaceutics* **2015**, *12*, 675–683.
- (496) Polyak, A.; Hajdu, I.; Bodnar, M.; Trencsenyi, G.; Postenyi, Z.; Haasz, V.; Janoki, G.; Janoki, G. A.; Balogh, L.; Borbely, J. Tc-99m-Labelled Nanosystem as Tumour Imaging Agent for Spect and Spect/Ct Modalities. *Int. J. Pharm.* **2013**, *449*, 10–17.
- (497) Hu, H.; Masarapu, H.; Gu, Y. N.; Zhang, Y. F.; Yu, X.; Steinmetz, N. F. Physalis Mottle Virus-Like Nanoparticles for Targeted Cancer Imaging. *ACS Appl. Mater. Interfaces* **2019**, *11*, 18213–18223.
- (498) Azad, B. B.; Banerjee, S. R.; Pullambhatla, M.; Lacerda, S.; Foss, C. A.; Wang, Y. C.; Ivkov, R.; Pomper, M. G. Evaluation of a PsmA-Targeted Bnf Nanoparticle Construct. *Nanoscale* **2015**, *7*, 4432–4442.
- (499) Wong, P.; Li, L.; Chea, J.; Delgado, M. K.; Poku, E.; Szpikowska, B.; Bowles, N.; Minnix, M.; Colcher, D.; Wong, J. Y. C.; et al. Synthesis, Positron Emission Tomography Imaging, and Therapy of Diabody Targeted Drug Lipid Nanoparticles in a Prostate Cancer Murine Model. *Cancer Biother. Radiopharm.* **2017**, *32*, 247–257.
- (500) Gu, F.; Zhang, L.; Teply, B. A.; Mann, N.; Wang, A.; Radovic-Moreno, A. F.; Langer, R.; Farokhzad, O. C. Precise Engineering of Targeted Nanoparticles by Using Self-Assembled Biointegrated Block Copolymers. *Proc. Natl. Acad. Sci. U. S. A.* **2008**, *105*, 2586–2591.
- (501) Gormley, A. J.; Malugin, A.; Ray, A.; Robinson, R.; Ghandehari, H. Biological Evaluation of Rgd-fk-Gold Nanorod Conjugates for Prostate Cancer Treatment. *J. Drug Target.* **2011**, *19*, 915–924.
- (502) Zhang, R.; Xiong, C. Y.; Huang, M.; Zhou, M.; Huang, Q.; Wen, X. X.; Liang, D.; Li, C. Peptide-Conjugated Polymeric Micellar Nanoparticles for Dual Spect and Optical Imaging of Ephb4 Receptors in Prostate Cancer Xenografts. *Biomaterials* **2011**, *32*, 5872–5879.
- (503) Zhong, J. P.; Wen, L. W.; Yang, S. H.; Xiang, L. Z.; Chen, Q.; Xing, D. Imaging-Guided High-Efficient Photoacoustic Tumor Therapy with Targeting Gold Nanorods. *Nanomedicine* **2015**, *11*, 1499–1509.
- (504) Lu, W.; Zhang, G. D.; Zhang, R.; Flores, L. G.; Huang, Q.; Gelovani, J. G.; Li, C. Tumor Site-Specific Silencing of Nf-Kappa B P65 by Targeted Hollow Gold Nanosphere-Mediated Photothermal Transfection. *Cancer Res.* **2010**, *70*, 3177–3188.
- (505) Gary, D. J.; Lee, H.; Sharma, R.; Lee, J. S.; Kim, Y.; Cui, Z. Y.; Jia, D.; Bowman, V. D.; Chipman, P. R.; Wan, L.; et al. Influence of Nano-Carrier Architecture on in Vitro Sirna Delivery Performance and in Vivo Biodistribution: Polyplexes Vs Micelleplexes. *ACS Nano* **2011**, *5*, 3493–3505.
- (506) Gao, W.; Li, S. S.; Liu, Z. H.; Sun, Y. H.; Cao, W. H.; Tong, L. L.; Cui, G. W.; Tang, B. Targeting and Destroying Tumor Vasculature with a near-Infrared Laser-Activated “Nanobomb” for Efficient Tumor Ablation. *Biomaterials* **2017**, *139*, 1–11.
- (507) Hu, H.; Dai, A. T.; Sun, J.; Li, X. Y.; Gao, F. H.; Wu, L. Z.; Fang, Y.; Yang, H.; An, L.; Wu, H. X.; et al. Aptamer-Conjugated Mn<sub>3</sub>O<sub>4</sub>@SiO<sub>2</sub> Core-Shell Nanoparticles for Targeted Magnetic Resonance Imaging. *Nanoscale* **2013**, *5*, 10447–10454.
- (508) Xu, Z. H.; Gu, W. W.; Huang, J.; Sui, H.; Zhou, Z. H.; Yang, Y. X.; Yan, Z.; Li, Y. P. In Vitro and in Vivo Evaluation of Actively Targetable Nanoparticles for Paclitaxel Delivery. *Int. J. Pharm.* **2005**, *288*, 361–368.
- (509) Zhang, H. J.; Hou, L.; Jiao, X. J.; Ji, Y. D.; Zhu, X. L.; Zhang, Z. Z. Transferrin-Mediated Fullerenes Nanoparticles as Fe<sup>2+</sup>-Dependent Drug Vehicles for Synergistic Anti-Tumor Efficacy. *Biomaterials* **2015**, *37*, 353–366.
- (510) Sunoqrot, S.; Bugno, J.; Lantvit, D.; Burdette, J. E.; Hong, S. Prolonged Blood Circulation and Enhanced Tumor Accumulation of Folate-Targeted Dendrimer-Polymer Hybrid Nanoparticles. *J. Controlled Release* **2014**, *191*, 115–122.
- (511) Nakamura, T.; Kawano, K.; Shiraiishi, K.; Yokoyama, M.; Maitani, Y. Folate-Targeted Gadolinium-Lipid-Based Nanoparticles as a Bimodal Contrast Agent for Tumor Fluorescent and Magnetic Resonance Imaging. *Biol. Pharm. Bull.* **2014**, *37*, 521–527.
- (512) Chauhan, R. P.; Mathur, R.; Singh, G.; Kaul, A.; Bag, N.; Singh, S.; Kumar, H.; Patra, M.; Mishra, A. K. Evaluation of Folate Conjugated Superparamagnetic Iron Oxide Nanoparticles for Scintigraphic/Magnetic Resonance Imaging. *J. Biomed. Nanotechnol.* **2013**, *9*, 323–334.
- (513) Bae, Y.; Nishiyama, N.; Kataoka, K. In Vivo Antitumor Activity of the Folate-Conjugated Ph-Sensitive Polymeric Micelle Selectively Releasing Adriamycin in the Intracellular Acidic Compartments. *Bioconjugate Chem.* **2007**, *18*, 1131–1139.
- (514) Rossin, R.; Pan, D. P. J.; Qi, K.; Turner, J. L.; Sun, X. K.; Wooley, K. L.; Welch, M. J. Cu-64-Labeled Folate-Conjugated Shell Cross-Linked Nanoparticles for Tumor Imaging and Radiotherapy: Synthesis, Radiolabeling, and Biologic Evaluation. *J. Nucl. Med.* **2005**, *46*, 1210–1218.
- (515) Kukowska-Latalo, J. F.; Candido, K. A.; Cao, Z. Y.; Nigavekar, S. S.; Majoros, I. J.; Thomas, T. P.; Balogh, L. P.; Khan, M. K.; Baker, J. R. Nanoparticle Targeting of Anticancer Drug Improves Therapeutic Response in Animal Model of Human Epithelial Cancer. *Cancer Res.* **2005**, *65*, 5317–5324.
- (516) Dijkgraaf, I.; Rijnders, A. Y.; Soede, A.; Dechesne, A. C.; van Esse, G. W.; Brouwer, A. J.; Corstens, F. H. M.; Boerman, O. C.; Rijkers, D. T. S.; Liskamp, R. M. J. Synthesis of Folate-Conjugated Multivalent Cyclic-Rgd Peptide Dendrimers Via 1,3-Dipolar Cycloaddition and Their Biological Evaluation: Implications for Tumor Targeting and Tumor Imaging Purposes. *Org. Biomol. Chem.* **2007**, *5*, 935–944.
- (517) Takara, K.; Hatakeyama, H.; Kibria, G.; Ohga, N.; Hida, K.; Harashima, H. Size-Controlled, Dual-Ligand Modified Liposomes That Target the Tumor Vasculature Show Promise for Use in Drug-Resistant Cancer Therapy. *J. Controlled Release* **2012**, *162*, 225–232.
- (518) Miyajima, Y.; Nakamura, H.; Kuwata, Y.; Lee, J. D.; Masunaga, S.; Ono, K.; Maruyama, K. Transferrin-Loaded Nido-Carborane Liposomes: Tumor-Targeting Boron Delivery System for Neutron Capture Therapy. *Bioconjugate Chem.* **2006**, *17*, 1314–1320.
- (519) Shi, H.; Sun, Y. D.; Yan, R. Q.; Liu, S. L.; Zhu, L.; Liu, S.; Feng, Y. Z.; Wang, P.; He, J.; Zhou, Z. Y.; et al. Magnetic Semiconductor Gd-Doping Cus Nanoparticles as Activatable Nanoparticles for Bimodal Imaging and Targeted Photothermal Therapy of Gastric Tumors. *Nano Lett.* **2019**, *19*, 937–947.
- (520) Zhang, C. L.; Li, C.; Liu, Y. L.; Zhang, J. P.; Bao, C. C.; Liang, S. J.; Wang, Q.; Yang, Y.; Fu, H. L.; Wang, K.; et al. Gold Nanoclusters-Based Nanoparticles for Simultaneous Fluorescence Imaging and Targeted Photodynamic Therapy with Superior Penetration and Retention Behavior in Tumors. *Adv. Funct. Mater.* **2015**, *25*, 1314–1325.
- (521) Xu, J.; Gattacceca, F.; Amiji, M. Biodistribution and Pharmacokinetics of Egrf-Targeted Thiolated Gelatin Nanoparticles Following Systemic Administration in Pancreatic Tumor-Bearing Mice. *Mol. Pharmaceutics* **2013**, *10*, 2031–2044.
- (522) Qian, X. M.; Peng, X. H.; Ansari, D. O.; Yin-Goen, Q.; Chen, G. Z.; Shin, D. M.; Yang, L.; Young, A. N.; Wang, M. D.; Nie, S. M. In Vivo Tumor Targeting and Spectroscopic Detection with Surface-Enhanced Raman Nanoparticle Tags. *Nat. Biotechnol.* **2008**, *26*, 83–90.
- (523) Elias, A.; Crayton, S. H.; Warden-Rothman, R.; Tsourkas, A. Quantitative Comparison of Tumor Delivery for Multiple Targeted Nanoparticles Simultaneously by Multiplex Icp-MS. *Sci. Rep.* **2015**, *4*, 5840.
- (524) Negi, L. M.; Talegaonkar, S.; Jaggi, M.; Verma, A. K.; Verma, R.; Dobhal, S.; Kumar, V. Surface Engineered Nanostructured Lipid Carriers for Targeting Mdr Tumor: Part II. In Vivo Biodistribution, Pharmacodynamic and Hematological Toxicity Studies. *Colloids Surf, B* **2014**, *123*, 610–615.